Experimental and thermodynamical study of water injection at the intake of an automotive Diesel engine for in-cylinder emission reduction

Samiur Rahman Shah

Ecole Centrale de Nantes

ÉCOLE DOCTORALE

ED SPIGA

Année 2011. N° B.U. :

Thèse de DOCTORAT

Spécialité : DYNAMIQUE DES FLUIDES ET DES TRANSFERTS

Présentée et soutenue publiquement par :

SAMIUR RAHMAN SHAH

le 21 Octobre 2011
à L'Ecole Centrale de Nantes

ÉTUDE EXPERIMENTALE ET THERMODYNAMIQUE DE L'INJECTION D'EAU A L'ADMISSION D'UN MOTEUR DIESEL AUTOMOBILE POUR LA REDUCTION A LA SOURCE DES EMISSIONS POLLUANTES

JURY

Rapporteurs :	M. DESMET Bernard	Professeur - Université de Valenciennes / ENSIAME, Laboratoire TEMPO/DF2T Le Mont Houy, 59313 Valenciennes Cedex 9…….
	M DESCOMBES Georges	Professeur - CNAM – Chaire de Turbomachines, 292 rue St Martin – 75141 Paris Cedex 3
Examinateurs :	M. STOUFFS Pascal	Professeur - IUT des Pays de l'Adour Avenue de l'Université 64000 PAU
	M. TAUZIA Xavier	Maître de Conférences - HDR - Laboratoire de Mécanique des Fluides, UMR CNRS 6598 Ecole Centrale de Nantes BP 92101 44321 Nantes Cedex
	M. MAIBOOM Alain	Maître de Conférences - Laboratoire de Mécanique des Fluides, UMR CNRS 6598 Ecole Centrale de Nantes BP 92101 44321 Nantes Cedex

Directeur de thèse : M. TAUZIA Xavier
Laboratoire : Laboratoire de Mécanique des Fluides, UMR CNRS 6598, Ecole Centrale de Nantes
Co-encadrant : M. MAIBOOM Alain
Laboratoire : Laboratoire de Mécanique des Fluides, UMR CNRS 6598, Ecole Centrale de Nantes N° ED 498-193

à Nuzhat

Dedication

The work on this thesis was carried out with the research team of Internal Combustion Engine Energetics at the Laboratory of Fluid Mechanics at the Ecole Centrale – Nantes. I had the pleasure of working here for over four years. I joined the team during my Masters in Applied Thermodynamics and Propulsion and continued to work with the same team for over 3 years as a PhD laureate.

First of all, I would like to thank Messrs Pascal Stouffs, Bernard Desmet and Georges Descombes for participating as jury members during my defence of thesis. I was greatly encouraged by their remarks and observations on my work. I would like to especially thank them for their efforts in finding a convenient defence date and making the journey from their respective cities for my defence.

This work would not have been possible without the help and abundance of knowledge of Professor Jean-François Hetet, Dr. Xavier Tauzia and Dr. Alain Maiboom. Their combined knowledge and guidance have helped me to no end in producing the doctoral work that I have presented in this thesis. I wish to thank Dr. Pascal Chesse as well in addition to Professor Hetet, Dr. Tauzia and Dr. Maiboom for the confidence he showed in me to develop my test bench and perform my experiments in absolute liberty, all the while staying up to date with what I was doing.

During my stay in France, I came to know people who have have been a very important part of my life in France Thanks to them I have been able to learn about the rich culture and integrate with great ease into the daily life in France. Alexandre, Adrien, Hani, David, Cyril, Jean-Louis, Michel, Thierry, Thibault, Dominique and Aline. I would like to thank Aline for all her help she gave me in administrative matters. We would almost everyday get together for a cup of coffee in the morning, and discuss all things French or otherwise. I would especially like to thank Jean-Louis, Michel and Thibault for their help in technical matters over the course of my research work.

I would like to thank Mme Anna Maneta and Mme Cecile Chaumier of SFERE for their help in my integration into the French education system and other aspects related to my stay in France. They were always very helpful in solving matters related to scholarship and related legal issues. I would like to especially thank Mme Somia Ashraf for her help above and

beyond of what was demanded of her in Pakistan and in France along with her husband Dr. Sajid Yaqub, who helped me out a great deal on a personal level.

A very special thank you to a great visionary, Professor Atta-ur-Rehman of the Higher Education Commission of Pakistan who had the determination and vision to conceive a scholarship program that caters to such a wide base of disciplines both in the sciences and the arts, inspite of so many hurdles and criticisms. I would personally like to thank the Pakistani people who have helped to pay my way through higher education and I hope to one day give a part of what's been given to me back to my nation.

Most importantly, this effort is dedicated to my father and mother; who have invested all of their lives into our upbringing, training and studies. It is due to their unwavering trust, farsightedness and determination that I have been able to leave my homeland and pursue my goals in a far away country.

Dr. Samiur Rahman Shah

Table of contents

Nomenclature

Variable	Meaning
ASI	After Start of Injection
A/F_x	Air/Fuel ratio
AHRR	Average Heat Release Rate
A_x	Area
BMEP	Brake Mean Effective Pressure
BSFC	Brake Specific Fuel Consumption
BSN	Bosch Smoke Number
BSNOx	Brake Specific Nitrogen Oxides
CA	Crank Angle
CHR	Cumulative Heat Release
CO	Carbon Monoxide
CO_2	Carbon Dioxide
COD	Coefficient of Discharge
C_x	Specific heat
DI	Direct Injection
DOC	Diesel Oxidising Catalyst
DPF	Diesel Particulate Filter
Dr	Dilution ratio
D_x	Diameter
ECR	Exhaust Closing Retard
ECU	Electronic Control Unit
EGR	Exhaust Gas Recirculation
FAP	Filtre à Particules (French translation for DPF)
FSN	Filter Smoke Number
HAM	Humid Air Motor
HAT	Humid Air Turbine
HC	Hydrocarbons
HLB	Hydrophilic / Lipophilic Fractions
h_{loss}	heat transfer coefficient
HPEGR	High Pressure Exhaust Gas Recirculation
HR	Hrumidity Ratio
HSDI	High Speed Direct Injection
H_x	Enthalpy
h_x	Specific Enthalpy
ID	Ignition Delay
IMEP	Indicated Mean Effective Pressure
IOA	Intake Opening Advance
IOD	Injector Opening Delay
K_x	Rate constant
LH	latent heat
LHV	Lower Heating Value
LPEGR	Low Pressure Exhaust Gas Recirculation
L_x	Lift
m_x	mass
M_x	Molar mass

$\dot{m}_x$	mass flow rate
N	Engine speed in revolutions per unit time
N/C	Normally Closed
N/O	Normally Open
NO	Nitrogen Oxide
NO_2	Nitrogen Dioxide
NOx	Nitrogen Oxides
n_x	number of moles
O/W	Oil / Water
OF	overlap factor
OH	Hydroxyl ions
PAH	Polycyclic Aromatic Hydrocarbons
PM	Particulate Matter
PV	Piston Velocity
P_x	Pressure
q	specific heat transfer
Q	Heat
RH	Relative Humidity
ROHR	Rate Of Heat Release
RPM	Revolutions Per Minute
RTWI	Real Time Water Injection
R_x	Gas constant
SH	Specific Humidity
SOC	Start Of Combustion
SOF	Soluble Organic Fractions
SOI	Start Of Injection
TC	Turbocharger
U	Internal energy
u	specific internal energy
UHC	Unburnt Hydro Carbons
v	specific volume
V_x	Volume
$\dot{V}_x$	Volume flow rate
w	specific work
W	Work
W/O	Water / Oil
WI	Water Injection
x	uncertainty of function
X_x	Molar ratio
γ	ratio of specific heats
ε	relative error
θ	angle
λ	Ratio of actual and stoichiometric air/fuel ratio
ρx	density
□	equivalence ratio

Introduction

Depuis une vingtaine d'années la réduction des émissions polluantes est devenue un enjeu majeur pour les moteurs à combustion interne, notamment ceux utilisés pour la propulsion des automobiles. Ainsi les normes qui se succèdent fixent des niveaux maximum autorisés toujours plus bas dans les pays industrialisés et, plus récemment, dans les pays émergents. En Europe, pour les moteurs Diesel, les niveaux de NOx et PM ont été respectivement divisés par environ 4 et 30 entre les normes euro 1 (1993) et euro 5 (actuelle). En outre, les objectifs en termes de réduction des émissions de gaz à effet de serre font que la dépollution ne doit pas se faire au détriment de la consommation.

Si le moteur Diesel dispose d'un avantage dans ce domaine par rapport au moteur à essence, sa dépollution est plus délicate. En effet, alors que le post-traitement s'est imposé pour le moteur à essence avec le catalyseur 3 voies, pour les moteurs Diesel les systèmes disponibles pour traiter les NOx (SCR, pièges à NOx) et les PM (Filtre à Particules) restent couteux et complexes à mettre en œuvre. C'est pourquoi la réduction à la source a été la voie privilégiée jusqu'ici. Pour ce faire, la technique la plus répandue est la recirculation de gaz d'échappement (EGR), généralement refroidis. Cependant, les possibilités de recirculation sont limitées, en particulier lorsque la charge augmente par le manque d'air et l'augmentation des émissions de particules.

L'injection d'eau, par différentes voies (dans le circuit d'admission, directement dans la chambre de combustion avec un injecteur séparé ou en émulsion avec le carburant,...) est un moyen utilisé sur les turbines à gaz et certains moteurs Diesel industriels, par exemple en propulsion navale, pour réduire les émissions de NOx par abaissement de la température de combustion. La tendance actuelle à la réduction de cylindrée des moteurs (« down-sizing ») pour réduire la consommation conduit à une augmentation de la charge moyenne et il semble donc pertinent d'évaluer le potentiel de l'injection d'eau comme moyen de dépollution à la source en propulsion automobile, comme alternative ou en complément de l'EGR.

Dans cette perspective, une étude bibliographique est tout d'abord menée pour rappeler les connaissances actuelles en matière de combustion Diesel et d'émissions polluantes, puis pour recenser les travaux existants sur l'injection d'eau comme moyen de dépollution des moteurs Diesel.

Le deuxième chapitre présente ensuite le dispositif expérimental développé et utilisé pour l'étude, ainsi que les éléments de thermodynamique nécessaires à l'interprétation des résultats.

Puis, dans le chapitre trois, ces éléments sont utilisés pour évaluer les conditions thermodynamiques (température, état de l'eau) dans le circuit d'admission du moteur après l'injection d'eau, puis dans le cylindre pendant les phases d'admission et de compression.

Enfin, les résultats des essais expérimentaux font l'objet du chapitre quatre. L'influence de l'injection d'eau sur la combustion, les émissions et le fonctionnement global du moteur est décrite, analysée, et comparée à l'influence de l'EGR.

Finalement, les principales conclusions de l'étude sont données, et des perspectives sont proposées.

For over twenty years, the reduction of pollutant emissions has become a major issue for internal combustion engines, especially those used for on-highway applications. As such, successive emissions standards define ever decreasing emissions limits in developed countries, and recently, in emerging economies as well. For diesel engines, in Europe, the permissible NOx and PM levels have been divided by between 4 and 30 between Euro 1 (1993) and Euro 5 (in use) standards. In addition to this, the objectives of reduction of greenhouse gas production means that the emissions controls cannot be performed to the detriment of fuel consumption.

If a diesel engine has anything to give away to a spark ignition engine, is that diesel engine emissions controls are much more complicated. While after treatment in spark ignition engines has been imposed for quite a long time with 3-way catalytic converters, the systems used in diesel engines for reduction of NOx (NOx Trap and SCR) and PM (Particulate Filters) remain expensive and difficult to implement. This is why at-the-source reduction of pollutant emissions has been favoured till now. EGR (Exhaust Gas Recirculation), generally cooled, is the most widely used technique for this. All the same, the possibilities of recirculation are limited since, more so when engine load is increased since fresh air is already limited and there is a increase in particulate matter emissions.

Water injection, by different means (in the intake system, directly into the combustion chamber via a separate injector, emulsion or stratification) is a method used on gas turbines and certain industrial diesel engine, for example in naval propulsion, for the reduction of NOx by reducing the peak combustion temperatures. The present trend of down sizing of engines implies an increase in average engine load over a driving cycle, and it would seem pertinent to study the potential of water injection as a means of in-cylinder pollutant emissions reduction in automotive propulsion, as an alternative or as a complement to EGR.

It is in this vein, that a bibliographic research was performed to recount the present know-how and research that has been performed in the field diesel combustion and pollutant emissions, and then to list the present work on water injection as a means of pollutant emissions reduction in diesel engines.

The second chapter then presents the experimental setup which was developed and used for the study, and thermodynamic relations that are necessary for the interpretation of the results.

In the third chapter, these elements are used to determine the thermodynamics states (temperature, state of water) in the intake system after water injection, and then in the cylinder during the intake and compression stages.

In the end, the results from experiments performed make up the fourth chapter. The different influences of water injection on combustion, emissions and overall functioning of the engine are described, analysed and compared to those observed in the case of EGR.

Finally, the principal conclusions are drawn from the study and future perspectives are proposed.

1. CHAPTER 1: Bibliographical survey

La combustion Diesel met en œuvre de nombreux processus physico-chimiques : injection du carburant liquide, développement d'un spray turbulent qui pénètre dans la chambre de combustion, entraîne de l'air, s'évapore. Lorsque l'avancement des réactions chimiques est suffisant l'auto-allumage a lieu sous l'effet de la pression et de la température, puis la combustion se déroule pour partie en pré-mélange et pour partie en diffusion. Elle s'accompagne en outre de la production d'espèces polluantes, notamment des NOx et des particules solides. La complexité des différents phénomènes et la difficulté à mener des études expérimentales dans un milieu confiné et instationnaire font que les connaissances dans le domaine restent encore incomplètes, même si elles ont beaucoup progressé.

Compte tenu des objectifs de la thèse énoncés en introduction, l'examen bibliographique qui suit se décompose en deux parties principales :

- ✓ *La première partie fait un point sur l'état de l'art en matière de combustion Diesel et sur les mécanismes physiques et chimiques à l'origine des émissions polluantes.*
- ✓ *La deuxième partie porte sur l'utilisation de l'eau pour réduire les émissions en combustion Diesel. Les différentes technologies existantes sont passées en revue : injection d'eau à l'admission du moteur, injection d'eau directement dans la chambre de combustion, et injection d'eau en émulsion avec le carburant. Les travaux antérieurs décrivant les effets de l'eau sur la combustion et les émissions sont analysés en détail et synthétisés.*

Diesel combustion combines a multitude of physical chemistry processes; injection of liquid fuel, development of a turbulent spray jet that penetrates into the combustion chamber, which mixes with air and then evaporates. When the chemical reactions have proceeded to a suitable limit, auto-ignition takes place under the combined effects of pressure and temperature, the combustion then proceeds in part as premixed and in part in diffusion. Combustion is accompanied by the production of pollutants, most of which are NOx and solid particles. The complexity of the different phenomena taking part and the difficulty in performing experimental studies of a process that takes place in a confined and unsteady environment means that knowledge on the subject remains incomplete, even though it has progressed a lot.

Taking into account the stated aim of this thesis, the following bibliographic study is divided into two main parts:

- ✓ *The first part brings the reader up to date on combustion in general and its physical and chemical reactions that lead to the pollutant emissions.*
- ✓ *The second part concerns the use of water injection for the reduction of pollutant emissions in diesel engines. Different existing technologies are reviewed; intake water injection, direct water injection into the combustion chamber, and water injection via emulsion. The past studies that describe the effects of water injection on combustion and pollutant emissions are analysed in detail and synthesised.*

1.1. Diesel engine combustion

Internal combustion engine basics:

An internal combustion engine utilises the thermal energy generated by combustion of fuel to do mechanical work. This mechanical work is obtained by making use of the increase in pressure and temperature of the working fluid (air). This conversion of thermal energy to mechanical energy is done by expansion of the working fluid. For automotive applications, generally a reciprocating piston engine is used. Reasons for this are relatively low cost of manufacture, high reliability and relatively high mechanical efficiency.

Reciprocating engines use one of two thermodynamic cycles to convert chemical energy to mechanical output. These two cycles depend on the type of fuel being used and the mode of combustion. The cycles are:

1. Otto cycle (the basic operating principles of the cycle are also attributed to Alphonse Beau de Rochas – thus de cycle is also known as the Beau de Rochas) [1]

2. Diesel cycle

Working under the Otto cycle: By thermodynamic definition, the Otto cycle is composed of four processes. These four processes are cyclic, and may be used an infinite number of times. The processes are:

1. Compression of working fluid

2. Addition of heat

3. Expansion and work

4. Release of heat

The combustion in an Otto cycle engine is started using an electric spark – it is therefore also known as a Spark Ignition engine. Physically, it is not possible to distinguish between the combustion and expansion phase in the practical Otto cycle. The two processes are intermixed and the duration and intensity of the combustion depends on various factors, such as the mixture density, temperature dilution and spark angle.

As stated earlier, Beau de Rochas outlined various operating conditions of the Beau de Rochas (or Otto) cycle to maximise fuel efficiency which were:

1. The largest possible cylinder volume to the minimum boundary surface area

2. The greatest possible working speed

3. The greatest possible expansion ratio

4. The greatest possible pressure at the beginning of the expansion stroke.

The first two conditions dictate the minimisation of heat losses from the combustion chamber. The third condition recognizes that the greater the post combustion expansion, the greater the work obtained from the charge. The fourth condition recognizes the fact that the greater the initial pressure of the expanding charge, the greater the average pressure throughout the cycle and thus greater the work obtained from the expansion process. Although Beau de Rochas'

unpublished work predates Otto's, the fact that he never practically make a working engine gives Otto the credit of being the first inventor of the internal combustion engine as it is known today [1].

This theoretical cycle can be translated physically into four processes:

1. Intake of fresh air / fuel charge
2. Compression of the air / fuel charge
3. Combustion and expansion of the air / fuel charge
4. Exhaust of the combustion products

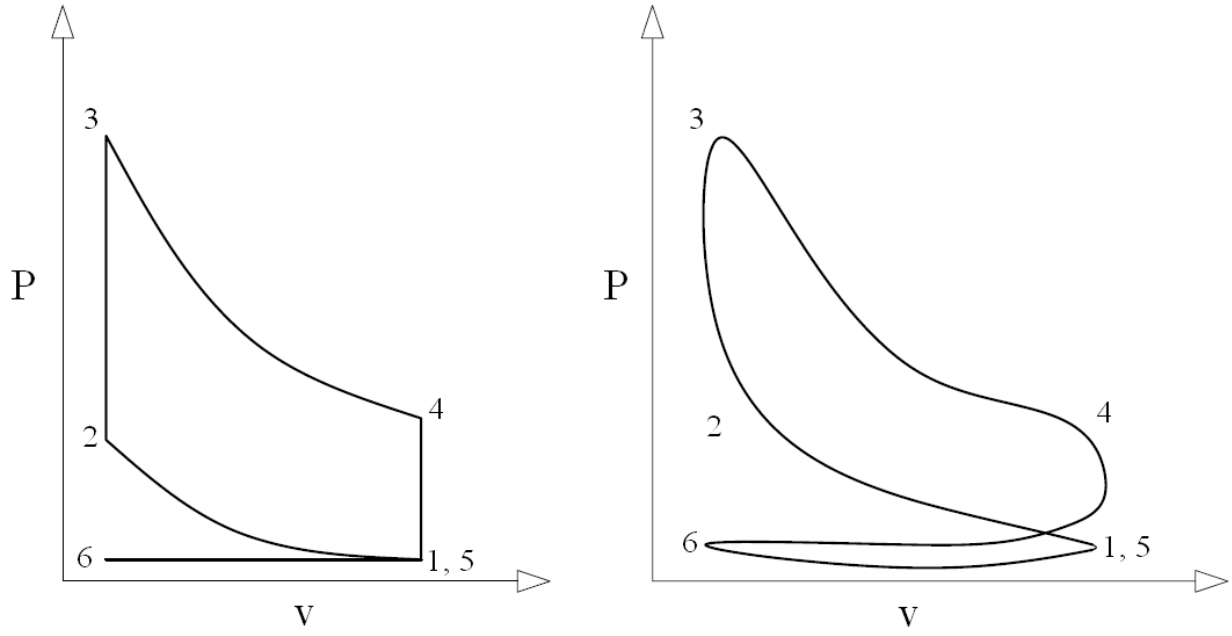

Figure 1. Theoretical and actual Otto cycle Pressure – Volume diagram traces

Comparing the theoretical and physical Otto cycles, the following table is presented

Theoretical Otto cycle	Practical Otto cycle
Compression (point 1-2)	Compression (point 1-2)
Addition of heat (point 2-3)	Combustion of air / fuel charge (point 2-3)
Expansion and work (point 3-4)	Expansion of combusted air / fuel charge (point 3-4)
Release of heat (point 4-5)	Exhaust (point 4-6)
Gas exchange (point 5-6-1)	Intake of fresh air / fuel charge (point 6-1)

Table 1. Comparison of theoretical and real Otto cycle phases

Working under the Diesel cycle: The main difference between the Otto and Diesel cycle engines can be found in the combustion phase and to a lesser extent in the intake phase:

1. Intake of fresh air / fuel charge
2. Compression of the air charge
3. Fuel injection near TDC, subsequent combustion and expansion of the air / fuel charge
4. Exhaust of the combustion products

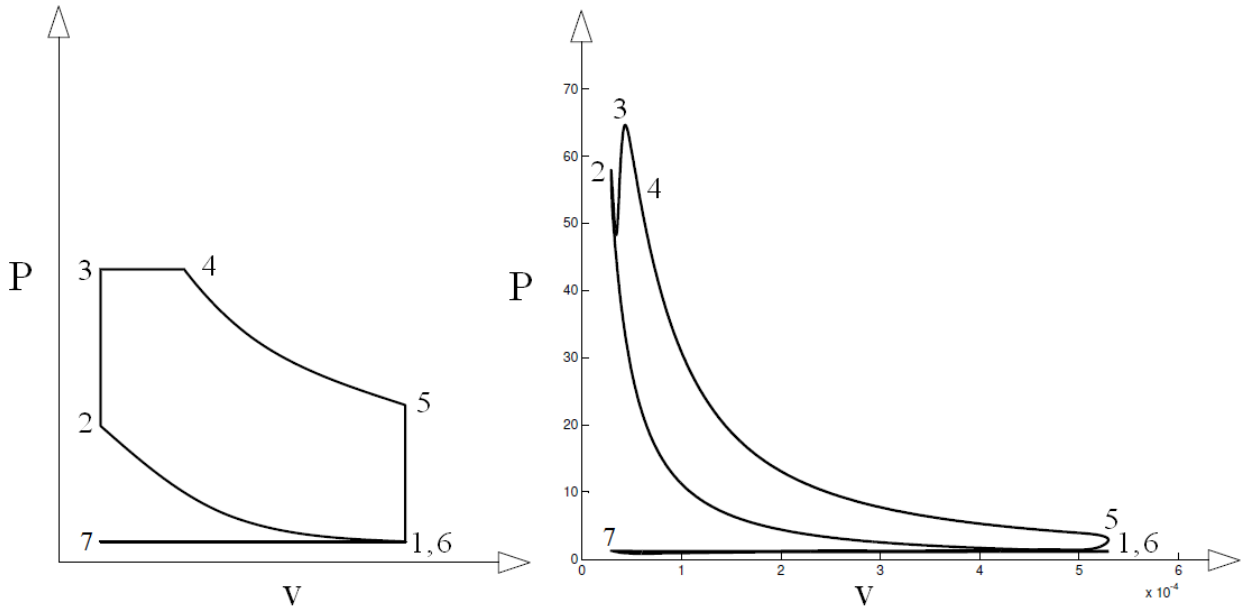

Figure 2. Theoretical and actual measured Diesel cycle pressure-volume diagram traces

Theoretical Diesel cycle	Practical Diesel cycle
Compression (point 1-2)	Compression (point 1-2)
Addition of heat (point 2-4)	Combustion of air / fuel charge (point 2-4)
Expansion and work (point 4-5)	Expansion of combusted air / fuel charge (point 4-5)
Release of heat (point 5-6)	Exhaust (point 5-6)
Gas exchange (point 6-7-1)	Intake of fresh air / fuel charge (point 6-7-1)

Table 2. Comparison of theoretical and real Diesel cycle phases

Traditional diesel engine combustion is characterised by lean global air/fuel ratios, an initial pre-mixed combustion followed by a diffusive combustion. If the time taken for the fuel jet to burn (ignition delay) is shorter than the injection duration, the combustion is termed as diffusive combustion.

For ignition and subsequent combustion, there are two basic requirements, a flammable fuel vapour / air mixture and an energy source. In a spark ignition engine, the spark is the energy source. In a compression-ignition engine however, the energy is supplied by the compression of air entrapped in the cylinder which raises its temperature sufficiently to cause auto-inflammation. The necessary temperatures of the order of 500°C and higher are obtained with compression ratios ranging from 12:1 to 23:1 depending on cylinder size, combustion chamber shape and whether the engine is supercharged or naturally-aspirated.

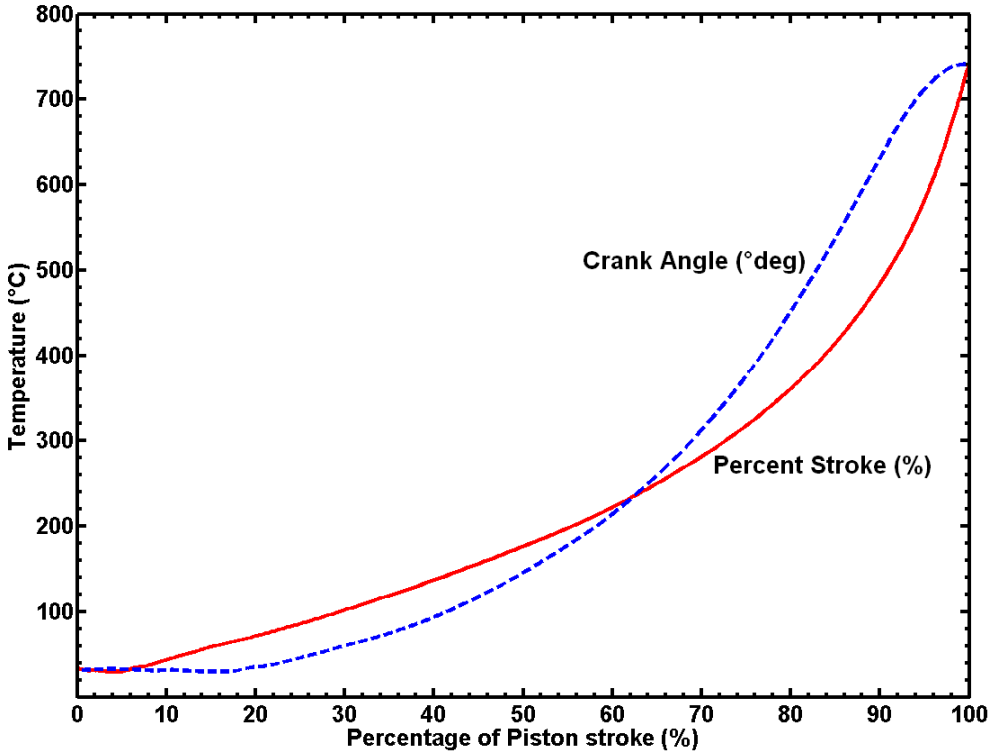

Figure 3. Rise in in-cylinder air charge temperature with respect to piston stroke in percent of movement from BDC to TDC [2]

The curves shown in the **Figure 3** are calculated from an actual pressure measurement during the compression stroke [22]. The full line in the above figure shows the relationship between the piston stroke and the rise in temperature. While the dashed line shows the relationship between the crank angle and the temperature rise. The crank angle is defined as a a percentage of 0° to 180° with 0° being BDC and 180° being TDC. We can see from the crank angle history, that the last 10% or so of the temperature rise take place in the last 10% or so of the crank angle movement (18°) or 10% of the total time to compress the mixture. For chemical reaction, the temperature rise / time history is important.

As an example, a Rate of Heat Release (ROHR) diagram is presented [1]. This diagram is for a direct injection diesel engine. The fuel injection profile is presented in **Figure 4**. A curve defining the rate of burning is shown in the bottom part of the figure for each slice of the injected fuel amount.

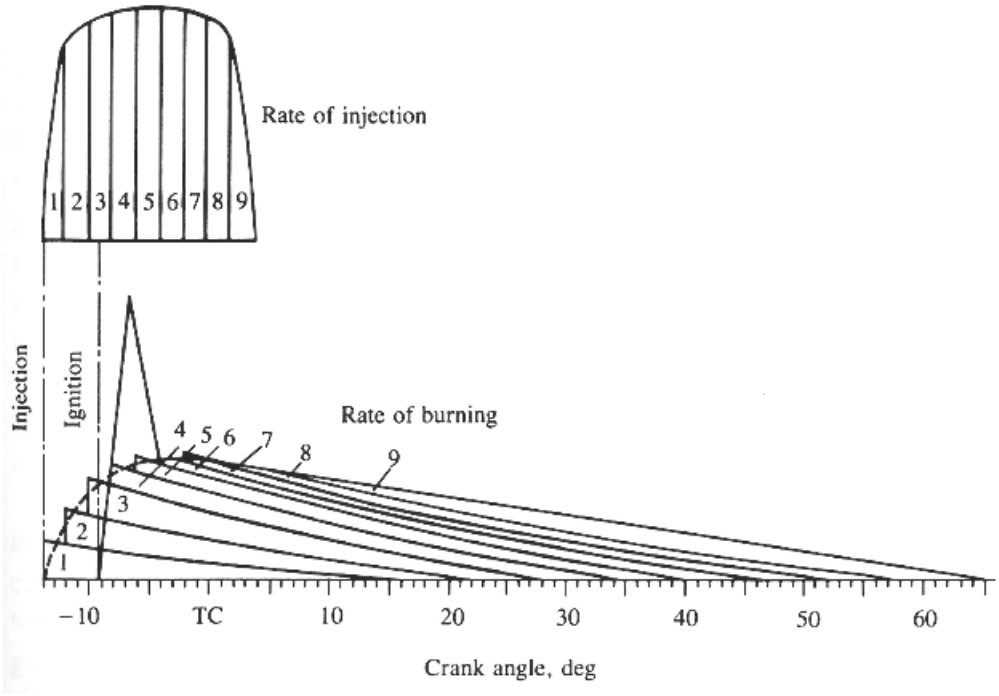

Figure 4. Injection rate for a DI diesel engine without pre-injection [1]

For the same period of injection, the ROHR curve is shown in **Figure 5**. In this please note that 180° and TC are the same reference points in the two figures.

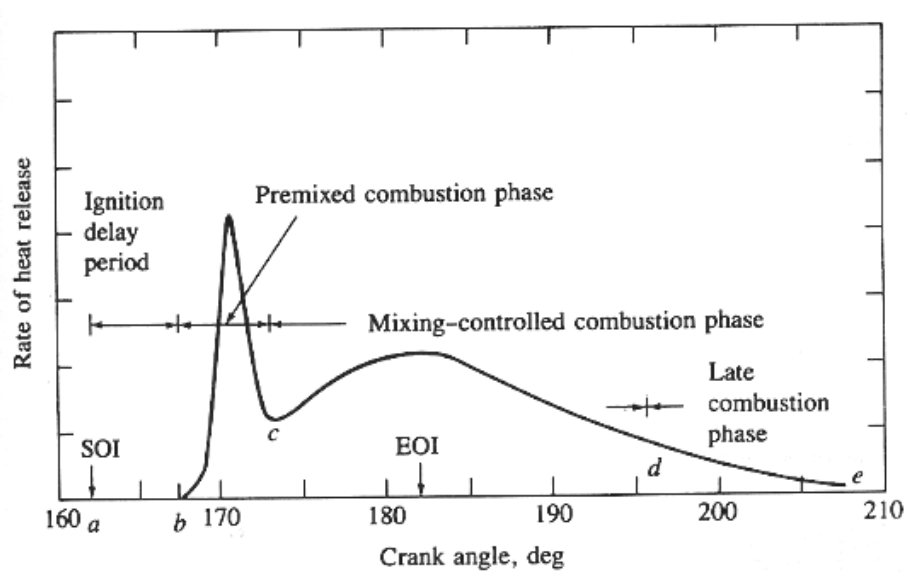

Figure 5. Rate of heat release for a direct injection diesel engine [1]

The combustion process can be divided into four stages;

a. The first stage where the fuel is injected into the combustion chamber. The fuel injector injects fuel at high pressure into the heated air charge. The high relative velocity of the fuel jet – or jets, for a multi-orifice injector – against the air charge causes the fuel droplets to atomise. This atomisation also aids in the mixing of the fuel droplets with the air, evaporating the fuel in the process. These evaporating droplets start to move away from the core of the jets. An air / fuel mixture has thus started to form and the high temperature encourages the reaction of the mixture even though no appreciable energy is

released. Ignition eventually starts to take place between the core and the outer fringes of the fuel jet / vapour envelope and the pressure in the cylinder thus starts to increase above the compression line. The first phase of combustion thus ends. This phase is known as the ignition delay (ID).

b. In the second phase of combustion, the fuel that was injected burns quickly and a relatively large amount of heat is released. This can be seen in **Figure 5** between points ***b*** and ***c***. in the first half, the fuel / air mixture burns quickly and then the intensity tapers off. This is known as the pre-mixed combustion phase.

c. In the third phase of combustion is the mixing-controlled combustion or diffusion combustion. Here, the combustion rate is controlled by the fuel injection itself. This can be seen in **Figure 5** between the points ***c*** and ***d***.

d. The fourth phase of combustion continues well into the expansion stroke. This combustion phase may be a result of partially unburned fuel. A part of the fuel energy is present in the fuel-rich combustion products and soot which is released as better mixing takes place during the expansion stroke. The reaction processes taking place during this phase are much slower as the charge temperature falls. In **Figure 5**, the combustion curve from point ***d*** to ***e*** is characteristic of this late combustion phase.

Dec et al. [5, 6] have developed a conceptual model depicting the physical conditions of fuel in the injected fuel jet. The shape of the developing fuel jet is depicted in **Figure 6** in a conceptual diagram:

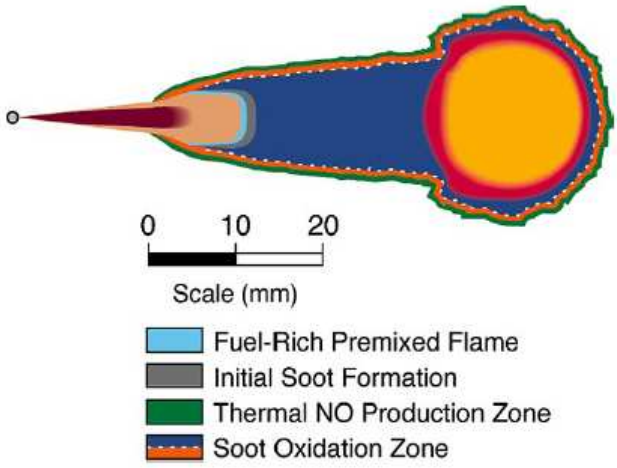

Figure 6. Dec's conceptual model of combustion of a fuel jet [5, 6]

This model has been developed using laser imaging and is a qualitative in nature. A few details on the optical-access test engine: It is a single-cylinder 4-stroke engine based on a Cummins N-series DI diesel engine with a 140mm stroke and a 152mm bore. The cylinder head is the original cylinder head that came with the engine to keep the flow characteristics as unchanged as possible. The piston is a classis, extended-piston design with a piston-crown window. Additional windows are added around the top of the cylinder wall to provide the orthogonal optical access necessary for the 2-D laser imaging. These windows allow the laser sheet to enter the combustion chamber horizontally (along the axis of the fuel jet). Details of the installation may be seen in the figure shown below:

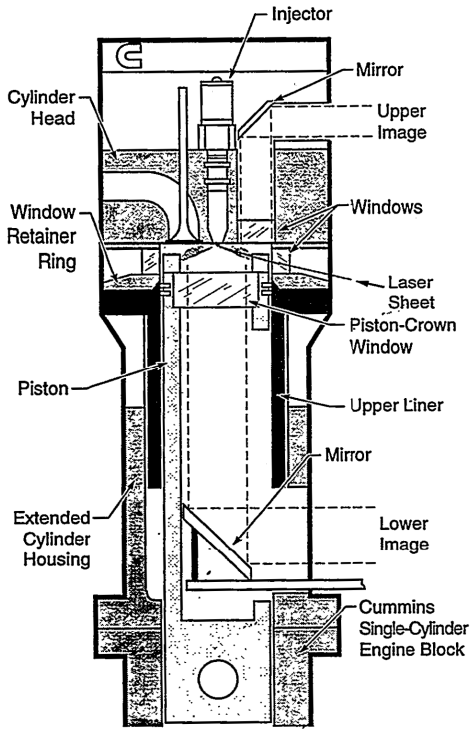

Figure 7. Test engine used for investigation of fuel jet combustion [5, 6]

The engine is made to run at 1200 rpm, with a motored TDC temperature of 992K and pressure of 50 bars, before the test was conducted, the engine was heater to 368K. The fuel load is relatively low of $\Phi = 0.25$ [6]. With reference to **Figure 8**, we see that the injection nozzle needle lift and Average Heat Release Rate (AHRR) are given.

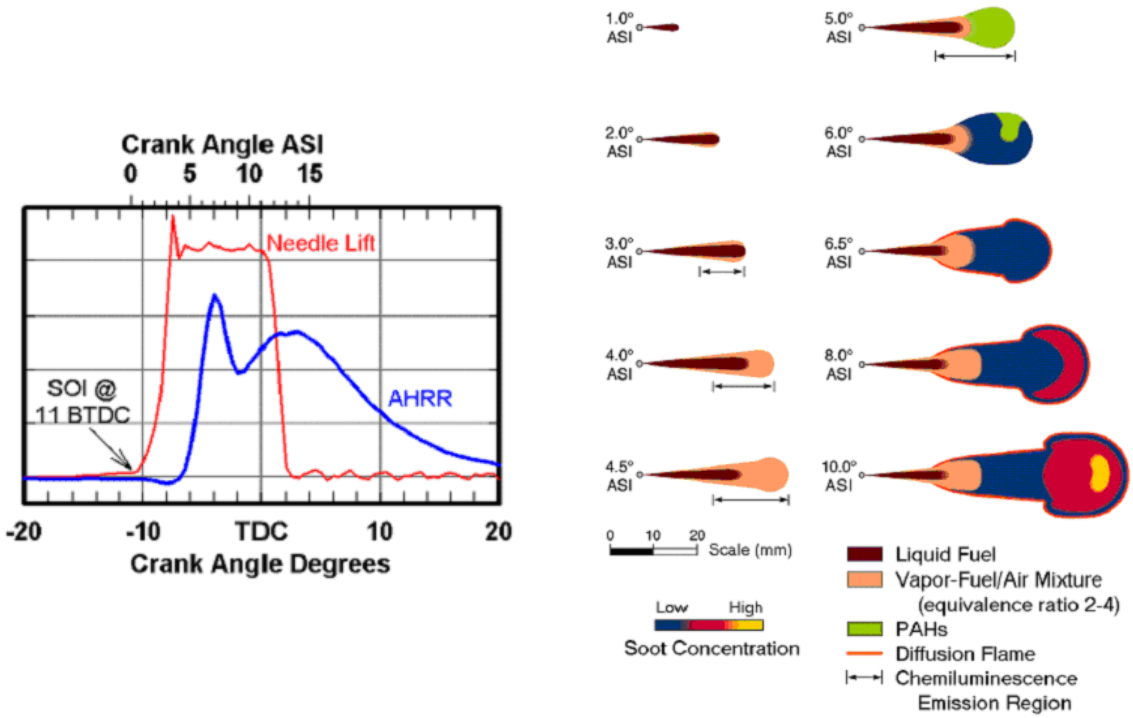

Figure 8. Time-based evolution of combustion of a fuel jet [5]

As the fuel is injected, the hot / compressed air entrapped in the combustion chamber is entrained by the fuel jet. This continuous entrainment of air into the fuel jet increases its temperature, and imparts heat energy to help the fuel vaporise. This vaporised fuel exists as an

envelope around the fuel jet and the temperature starts to rise to 750 K [5] and basic chemical reactions start to take place. Heat produced from these reactions and the further entrainment of hot air into the fuel jet increases the temperature to around 825 K [5]. At these temperatures, basic oxidation reactions commence. According to Dec et al. [5], the chemical products at this stage are largely composed of C_2H_2, C_2H_4, C_3H_3, CO and H_2O. The short-chain fuel components are the basic building blocks of polycyclic aromatic hydrocarbons (PAH) that lead to the production of soot. During these reactions, the temperature in the fuel jet increases to around 1600 K. These hot combustion products are pushed out by the fuel jet and then re-entrained in to the jet with the hot air in the cylinder. This has an effect of stabilising the fuel jet similar to the one shown in the second frame of **Figure 8**. In this case the stabilised fuel jet / combustion plume is obtained at 10° After Start of Injection (ASI).

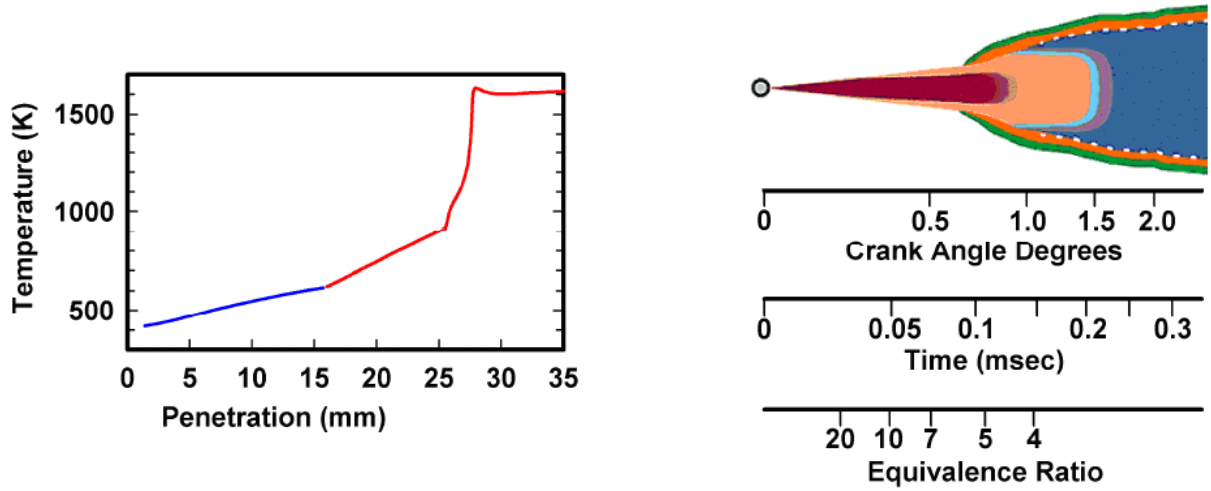

Figure 9. State of the fuel jet during development and quasi-stabilisation [5]

Figure 9 shows the development of the fuel jet as it heats up and subsequently stabilises [5, 7]. The first frame shows the rise in temperature of the fuel jet and entrained air in the combustion chamber. The second frame shows additional information on the fuel jet using three axes. The first axis correlates the length of the spray with the crank angle, the second axis shows the evolution of the fuel jet in terms of time in milliseconds and the third axis shows the average equivalence ratio estimated from mixing correlations [5]. These values are calculated using Siebers jet mixing correlations [7]. In the quasi-steady state, the temperature of the fuel jet rises from around 350 K to 650 K. This increase in the temperature is due to the direct transfer of heat from the hot compressed air to the fuel jet. As the higher temperatures are reached, exothermic reactions start to take place and the temperature in the fuel jet starts to rise to around 825 K. At this point, rapid oxidation of the fuel components starts and the temperature rises. The energy of the low temperature oxidation is sufficient to raise the temperature of the rich air fuel mixture in the jet to above 1150 K. At this temperature level, the speed of the combustion reactions increases rapidly leading to the consumption of all available oxygen in the fuel-rich region. The heat produced by these reactions increases the temperature in the jet and entrained air to around 1600 K.

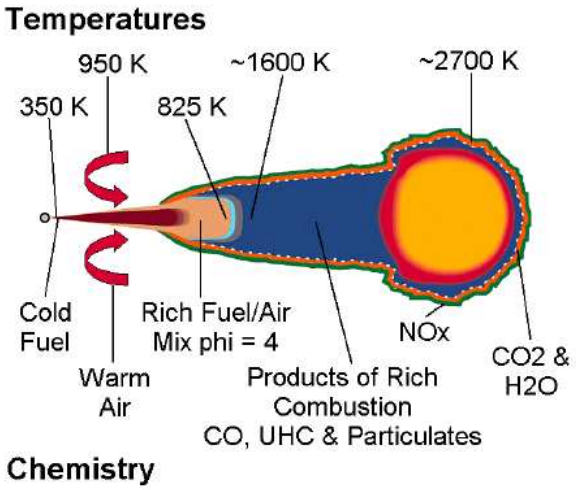

Figure 10. Evolution of temperature and chemical composition in a flame plume [5, 6]

Figure 10 provides a comprehensive look into the thermal and chemical makeup of an air/fuel spray jet. Surrounding the burning plume, a thin layer or envelope of diffusion flame is formed where oxidation takes place and products of combustion are formed. In this diffusion flame envelope, particulate matter and fuel fragments are converted to CO_2 and water vapour. In this region, temperatures are high, providing ideal conditions for NOx production. Inside the hot envelope, we find a rich premixed combustion zone. The products of the rich combustion are oxidised at the diffusion flame surface.

Siebers et al. [60] have performed a correlation between the flame lift-off length and oxygen concentration of the air charge. In general, the lift-off length is defined as the distance between the surface of the injector nozzle tip (or hole) and the point where combustion takes place in the air / fuel jet. The test apparatus consists of a constant volume combustion vessel of 108mm length per side. The fuel injector is mounted in one of the walls of the combustion chamber while each of the other walls has a 105mm diameter sapphire port for visualisation.

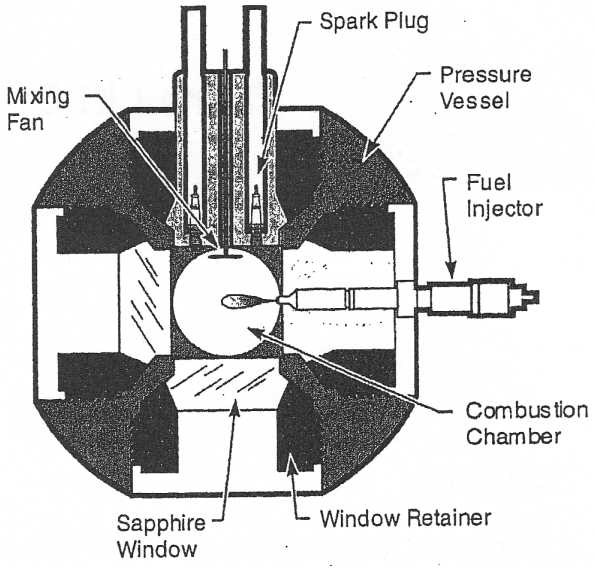

Figure 11. Cross section schematic of the combustion vessel [60]

The temperature, density and composition of the gas charge in the combustion vessel can be varied. The possible ranges of temperature and density at the time of fuel injection are 600 to

1400 K and 3.6 to 60 kg/m^3, respectively. Some tests performed on the apparatus show the following results

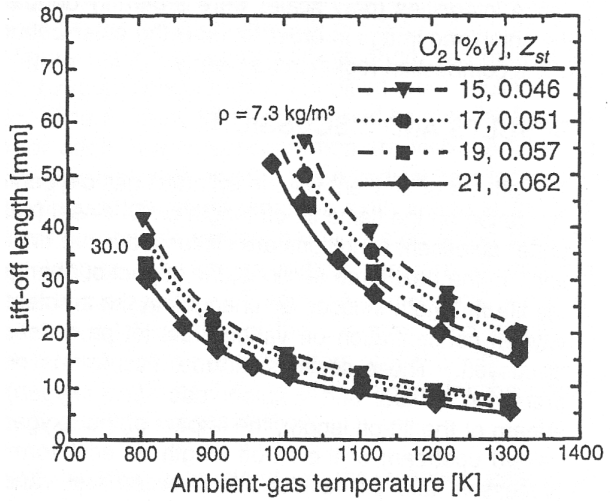

Lift off length versus ambient gas temperature for four gas oxygen concentrations. Ambient gas densities of 7.3 and 30 kg / m^3

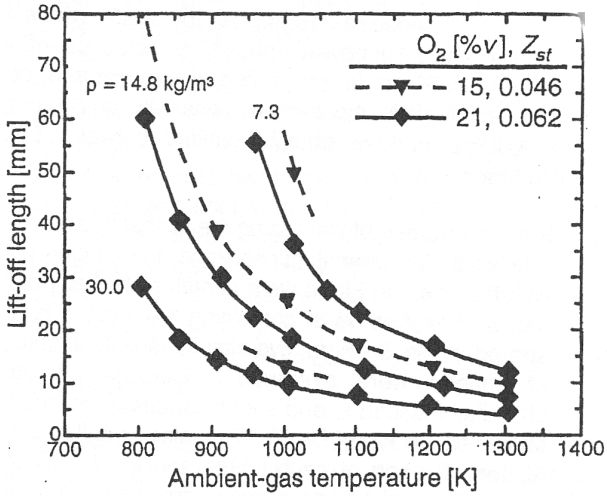

Lift off length versus ambient gas temperature for two gas oxygen concentrations and three ambient densities.

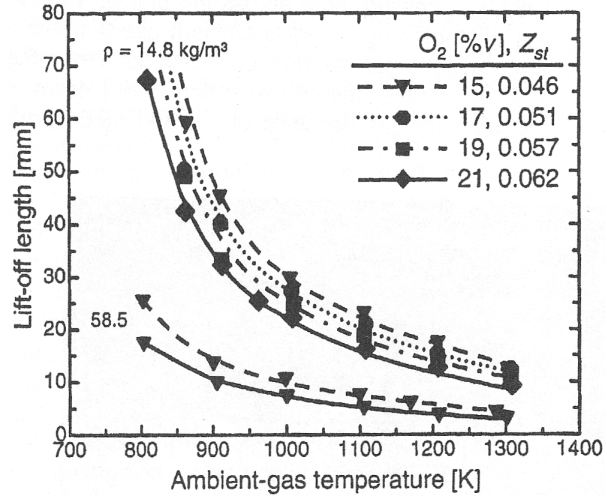

Lift off length versus ambient gas temperature for four gas oxygen concentrations – where ambient density is 14.8 kg/m^3 and for oxygen concentrations of 15% and 21% at a density of 58.5 kg/m^3

Figure 12. Lift off length comparison for different densities and oxygen concentrations [60].

Conclusions drawn from the research are as follows:

1. Lift off length is inversely proportional to the ambient gas oxygen concentration, increasing as the oxygen concentration decreases [60].

2. Due to two cancelling effects, the total amount of oxygen entrained upstream of the lift off length does not change with the ambient oxygen concentration. The two effects that cancel each other out are the reducing oxygen entrainment rate due to a smaller fraction of oxygen in the entrained gas, and the increase in lift off length that allows for more total ambient gas – and thus oxygen – to be entrained upstream of the lift off length. This however does result in the dilution of the air / fuel jet due to increase in diluent in the ambient gas [60].

3. Soot formation reduces as the amount of premixing between fuel and ambient gas increases, becoming negligible when the oxygen entrainment is sufficient to reduce the cross sectional average equivalence ratio in the air fuel jet to below a value of approximately two, at the lift off length [60].

4. As the ambient gas oxygen concentration decreases, the lift off length increases in relation to the liquid length. This trend indicates a reduction of interaction between combustion and fuel evaporation processes as the ambient gas oxygen concentration decreases [60].

5. The regions in a fuel jet where combustion and soot formation occurs is pushed along the fuel jet further away and stretched out as oxygen concentration in the ambient gas decreases. These trends are due to the increases in lift off length and decreasing rate of oxygen entrainment per length of jet length with decreasing ambient oxygen concentration. This in turn decreases the local combustion rate, increases the length of the fuel jet and the time required to complete the combustion process [60].

1.2. PM and NOx production in diesel engines:

1.2.1. Health effects of PM and NOx emissions

Nitrogen Oxides:

As for PM, the evidence of effects of NO_2 on health comes from different sources of information. These sources include observational epidemiology (study of factors affecting health of populations), controlled exposures of humans to the pollutants in question and animal toxicology tests. The observational data are derived from studies outdoors where NO_2 is one element of the complex mixture of pollutant emissions found in ambient air. This is in addition to studies of NO_2 exposure indoors where its sources include un-vented combustion appliances.

Interpretation of evidence on outdoors NO_2 exposures is complicated by the fact that in most urban locations, the nitrogen oxides that form NO_2 are primarily emitted by motor vehicles, making it a strong indicator of vehicle emissions (including other unmeasured emitted pollutants). NO_2 (and other nitrogen oxides) is also a precursor for a number of harmful secondary air pollutants including nitric acid, the nitrate part of secondary inorganic aerosols and photo oxidants (including ozone). The situation is also complicated by the fact that photochemical reactions take some time (depending on the composition of the atmosphere and meteorological parameters) and air can travel some distance before secondary pollutants are generated. These relationships are shown schematically in **Figure 13**.

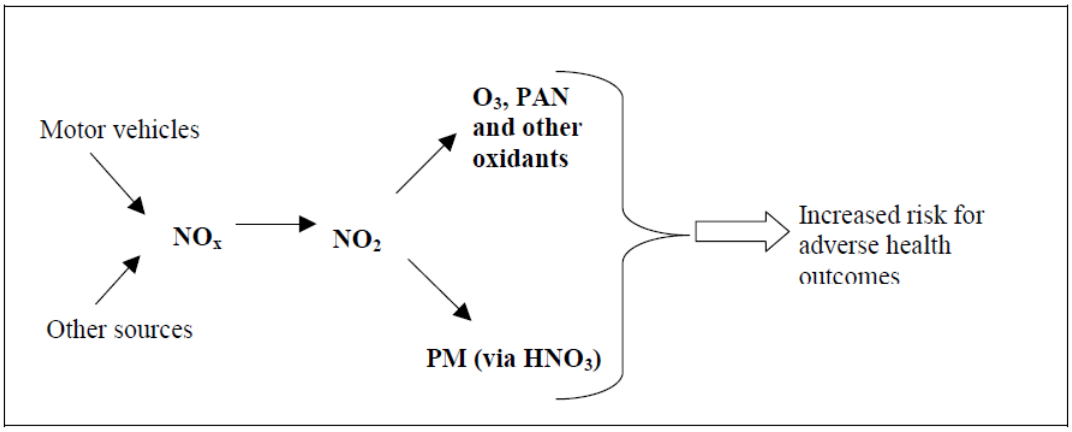

Figure 13. Simplified relationship of Nitrogen Oxides (NOx) emissions with formation of NO2 and other harmful reaction products

Health risks from nitrogen oxides may potentially result from NO_2 itself or its reaction products including O_3 and secondary particles. Epidemiological studies of NO_2 exposures from outdoor air are limited in being able to separate these effects. Evidence of the health effects of NO_2 by itself thus comes largely from toxicological studies and from observational studies on NO_2 exposure indoors.

PM:

Airborne Particulate Matter (PM) represents a complex mixture of organic and inorganic substances, whose mass and composition in urban environments can be divided into two classification groups – coarse particles and fine particles. The limit between these two types of particulates lies in between 1 and 2.5 µm (microns). For general cases however, the limit is

set at 2.5 µm, in aerodynamic diameter (Aerodynamic diameter is an expression of a particle's aerodynamic behaviour as if it were a perfect sphere with unit-density and diameter equal to the aerodynamic diameter. Such a model has the same terminal settling velocity) as $PM_{2.5}$ for measurement purposes. The smaller particles contain combustion particles, secondary aerosols (gas to particle conversion) and re-condensed organic and metal vapours. The larger particles usually consist of earth crust materials and dust from roads and industries. Most of the acidity (Hydrogen ion) and the mutagenic capacity of particle matter is present in the fine fraction. Whereas most of the mass is found in the fine fraction (between 100nm and 2.5 µm), the largest number of particles is present is found in the very small sizes, i.e. below 100 nm. As anticipated from the relationship of particle volume with mass, these ultra-fine particles often contribute to over 90% of the particle count while being only a few % of the total particulate matter mass [4].

PM air pollution is a mixture of solid, liquid or solid and liquid mixture suspended in air. These suspended particles vary in size, composition and origin. It has been considered convenient to classify these particles in terms of their aerodynamic properties, since it allows us to: (a) govern transport and removal of PM from air; (b) govern their deposition in the respiratory tract and (c) they are associated with the chemical composition and source of these particles. These properties are summarised by their aerodynamic diameter. Particles are thus sampled according to their aerodynamic diameters, usually simply called the particle size. The sizes of these suspended particles vary over four orders of magnitude, from a few nanometres to tens of micrometers. The largest particles, called the coarse fraction, are mechanically produced by the break-up of larger solid particles. Dust from agricultural processes, dirt, mining operations, particles from evaporation of sea-spray, pollen grains, mould spores, and plant and insect parts all come under the coarse particle range [4].

The amount of energy required to break these particles into smaller sizes increases as the size decreases, which effectively establishes a lower limit for the production of these coarse particles, the limit of which is of approximately 1 µm. Smaller particles, called the fine fraction or fine mode, are for the most part formed from gases. The smallest particles, less than 0.1 µm, are formed by nucleation, that is, condensation of low-vapour-pressure substances formed by high-temperature vaporization or by chemical reactions in the atmosphere to form new particles (nuclei). Four major classes of sources with equilibrium pressures low enough to form nuclei mode particles can yield PM: (a) heavy metals (vaporized during combustion); (b) elemental carbon (from short Carbon molecules generated by combustion); (c) organic carbon and (d) sulphates and nitrates [4].

Particles in this nucleation range or mode grow by coagulation, that is, the combination of two or more particles to form a larger particle, or by condensation, that is, condensation of gas or vapour molecules on the surface of existing particles. Coagulation is most efficient for large numbers of particles, and condensation is most efficient for large surface areas. Therefore the efficiency of both coagulation and condensation decreases as particle size increases, which effectively produces an upper limit such that particles do not grow by these processes beyond approximately 1 µm. Thus particles tend to “accumulate” between 0.1 and 1 µm, the so-called accumulation range [4].

Sub micrometre-sized particles can be produced by the condensation of metals or organic compounds that are vaporized in high-temperature combustion processes. They can also be produced by condensation of gases that have been converted in atmospheric reactions to low-vapour-pressure substances. For example, sulphur dioxide is oxidized in the atmosphere to form sulphuric acid (H_2SO_4), which can be neutralized by NH_3 to form ammonium sulphate.

Nitrogen dioxide (NO_2) is oxidized to nitric acid (HNO_3), which in turn can react with ammonia (NH_3) to form ammonium nitrate (NH_4NO_3). The particles produced by the intermediate reactions of gases in the atmosphere are called *secondary particles*. Secondary sulphate and nitrate particles are usually the dominant component of fine particles. Combustion of fossil fuels such as coal, oil and petrol can produce coarse particles from the release of non-combustible materials, i.e. fly ash, fine particles from the condensation of materials vaporized during combustion, and secondary particles through the atmospheric reactions of sulphur oxides and nitrogen oxides initially released as gases [4].

Sulphate and organic matter are the two main contributors to the annual average PM_{10} and $PM_{2.5}$ mass concentrations, except at kerbside sites where mineral dust (including trace elements) is also a main contributor to PM_{10}. On days when $PM_{10} > 50$ $\mu g/m^3$, nitrate becomes also a main contributors to PM_{10} and $PM_{2.5}$. Black carbon contributes 5 – 10% to $PM_{2.5}$ and somewhat less to PM_{10} at all sites, including the natural background sites. Its contribution increases to 15–20% at some of the kerbside sites [4].

Because of its complexity and the importance of particle size in determining exposure and human dose, numerous terms are used to describe PM. Some are derived from and defined by sampling and/or analytic methods, for example, “suspended particulate matter”, “total suspended particulates”, “black smoke”. Others refer more to the site of deposition in the respiratory tract, e.g. “inhalable particles”, which pass into the upper airways (nose and mouth) of the respiratory system, and “thoracic particles”, which deposit within the lower respiratory tract, and “respirable particles”, which penetrate into the gas-exchange region of the lungs (alveoli). Other terms, such as “PM_{10}”, have both physiological and sampling connotations [4].

Exhaust gases emitted from diesel engines are composed of different constituents. Carbon particles, organic and inorganic compounds, ash etc. of the gases / vapours emitted, the main constituents are O_2, N_2, water, CO_2, NOx, PM, UHC and CO.

Diesel engine combustion is characterised by lean overall air / fuel ratios. It is for this reason that UHC and CO production rates are relatively low as compared to SI engine. These are relatively easy to oxidise using Diesel Oxidising Catalysts. Hence most efforts are focused on PM and NOx control.

1.2.2. Particulate Matter production

“Particulate Matter” (PM) consists of all the chemical species existing in the exhaust gases after cooling. Particulates are suspected to cause respiratory problems in human beings. PM can be divided into three groups in general [1, 2 and 4]:

a. Soot: These are solid carbonaceous particles. They are composed of spherical carbon aggregates

b. The Soluble Organic Fraction (SOF): These include heavy organic components, such as unburnt Hydrocarbons (UHC), oxygenated derivatives (ketones, esters, aldehydes, organic acids) as well as Polycyclic Aromatic Hydrocarbons (PAHs) and their oxygenated and nitrated derivatives.

c. Non-organic residue: These consist of mineral residues that may be present in the fuel itself or in the lubricating oil. Nitrates and Sulphates are the most common form of non-organic particulates as well as ash.

1.2.2.1. Fundamental mechanisms of Particulate Matter production:

According to studies done by Dec et al. [5], particulate formation follows the path as described in the following paragraph.

The products obtained by the early stages of combustion are small. These products are as described earlier, composed of partially burnt fractions of hydrocarbons of C_4 or smaller. Generally, C_2H_2, C_2H_4 and C_3H_3 combine to form PAHs that are considered to be soot precursors. The temperature reached during this partial oxidation of fuel is of the order of 1600 K. This high temperature coupled with the absence of oxygen is considered to be favourable for the formation and agglomeration of Carbon particles.

The appearance of small particulates in the combusting air/fuel plume has been indicated by various diagnostics performed by Dec et al. the size of the particles appears to increase as the particles move along the air/fuel spray plume.

The overall chemical and thermodynamics analysis allows the speculation on local conditions in the air/fuel spray plume such as temperature, oxygen/fuel ratios, and the energy or heat release rate in different zones of the flame.

Figure 14 shows a potential evolution of chemical reactions in an air/fuel spray plume. Temperature, cumulative heat release, soot production, oxygen and NOx concentrations are shown. The time scale at the bottom of the graph shows the relative time taken by one molecule of fuel from its injection into the hot air charge until it is fully consumed. These times are of the order of .3 to 2 milliseconds.

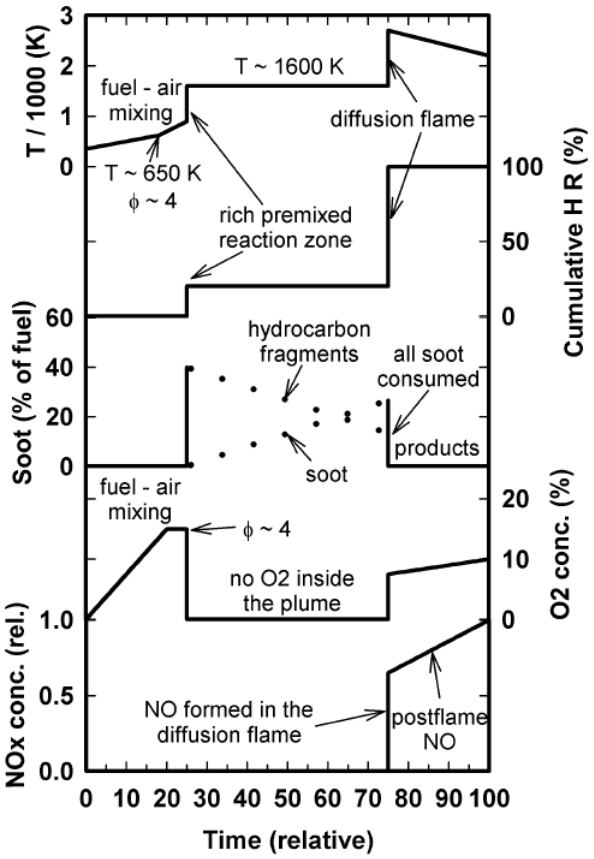

Figure 14. Speculation on the types of reactions present in the air/fuel spray plume [5]

As shown in the figure, the fuel enters the air charge at a relatively modest temperature. This fuel is then heated by the entrained air. The initial chemical reactions start to take place and the temperature steadily starts to rise to 650 K. At this point, no significant chemical reactions have taken place, and the rise in temperature of the fuel is due to the mixing with the hot compressed air present in the combustion chamber. The rise in temperature at this point is governed by the degree of mixing and the initial temperatures of the air and that of the fuel.

Inside the diffusion flame sheath where the temperature of the air/fuel mixture increases rapidly, temperatures of 825 to 850 K are observed. At these temperatures, chemical reactions start to break down the fuel components into smaller chains that use up all of the available oxygen to form CO, CO_2, and H_2O. As a result of these chemical reactions, the temperature of this mixture of combustion products reaches 1600K.

As the half-reacted fuel fragments travel towards the flame sheath, the convective and radiative heat transfer from the flame sheath causes the temperatures of these fragments to increase. The flame sheath itself is a very thin reaction zone. This thinness owes to the fact that the local reaction rates are very high. Local temperatures of 2500 K are observed and these combustion reactions accelerate markedly above 2000 K.

Referring to the cumulative Heat Release diagram, we see that only 10 to 15 percent of the total heat is released in the primary reaction zone. The rest of the heat is released at the diffusion flame interface. This can be referenced using the relative time frame shown at the bottom of **Figure 14**.

Speculations [5] have been made concerning the production of Particulate Matter in that they could be a result of the fuel passing from the fuel injector directly to the flame plume without

being oxidised. The resulting pyrolysis of the fuel molecule may result in the formation of soot particles. It has been seen however that the resulting structure of the soot molecules is different to that typically obtained from diesel fumes.

There are six processes that are well defined for soot generation processes, and they are listed as follows:

a. Oxidation
b. Pyrolysis
c. Nucleation
d. Coalescence
e. Surface growth
f. Agglomeration

The first process, oxidation, can happen at any time in the air/fuel flame plume converting hydrocarbons to CO, CO_2, and H_2O.

Oxidation: Oxidation is the conversion of HC to CO, CO_2 and H_2O. Once carbon has been partially oxidised to form CO, its will no longer influence the production of soot. It has been stated in a review by Tree & Svensson [8] that the soot oxidation starts from 1300 K onwards. The structure of soot is graphite-like and hard to oxidise. Generally, the oxidation process of small carbon particles is believed to consist of oxygen molecules being absorbed by the carbon on the surface, and then desorption of these molecules combined with the carbon. OH radicals are responsible for oxidation in rich and stoichiometric conditions, while a mixture of O_2 and OH radicals will dominate for lean combustion conditions [8].

Pyrolysis: Pyrolysis is defined as the changing of chemical structure under the influence of heat without oxidation. In general, pyrolytic reactions are endothermic and their rates of reaction depend on the temperature and reactant concentration levels. Pyrolysis reactions generate soot precursors or building blocks. The generation of soot precursors is a competition between the oxidation rates and the pyrolytic reactions. As temperature rises, both pyrolysis reactions and oxidation reactions speed up, although the rate of reaction for the oxidation reactions speed up faster as temperature rises. This fact may explain that both premixed and diffusion flames produce less soot as their temperatures are increased. All fuels undergo pyrolysis and produce essentially the same types of species; PAHs, unsaturated hydrocarbons, polyacetylenes and acetylene.

Nucleation: Nucleation is the process by which particles are formed from gas-phase reactants. It is generally believed [8] that the nucleation process consists of radical addition of small aliphatic HCs to large PAHs at temperatures between 1300 and 1600 K. These particle nuclei do not directly contribute to the soot mass, but provide sites for particle growth. Nucleation sites are generally restricted to a region near the primary reaction zone where temperature and radical concentrations are the highest.

The presence of a general fuel-independent soot formation mechanism [8] is indicated which has different routes to intermediate species. These routes are affected by the initial fuel type and temperatures. The tendency to soot is thus dependent on the initial formation of the first and second ring structures. Soot nucleation and growth are similar for all fuels and these processes are faster than the formation of the first ring structures. Thus, the relatively slow

initial ring formation process determines the soot formation rate, which in turn determines the amount of soot formed. Two propynyl radicals, C_3H_3 are likely to form the first ring. This aromatic ring absorbs alkyl radicals and develops into a PAH structure. This PAH structure grows in the presence of acetylene and other vapour-phase soot precursors. At some point in time, the PAH is large enough to develop into a particle nuclei, which at this point contains large amounts of Hydrogen.

Surface growth: Surface growth is the process by which mass is added to the surface of a nucleated soot particle. There is no clear distinction between the end of nucleation and the start of the surface growth. During surface growth, the hot surfaces of the soot particles easily accept gas-phase radicals, usually acetylenes. An increase in soot mass is thus encountered without an increase in the number of particles. The majority of the soot mass is added during surface growth and thus the residence time in the zone of surface growth has a large influence on the total soot mass. Surface growth rates are higher for smaller particles than for larger ones as smaller particles have more reactive radical sites.

Coalescence and agglomeration: Coalescence and agglomeration are both processes by which particles join together and combine. Coalescence occurs when particles collide and coalesce, thus reducing the number of particles while maintaining the soot mass. Typically, agglomeration leads to string-like structures being formed. It has however been noted in some cases that the agglomerate clumps together.

1.2.2.2. Physical parameters and their effects on soot formation

It is of interest to see how physical operating parameters like stoichiometric ratio, pressure, temperature etc. affect the soot formation process. By nature, diesel engine combustion consists of a turbulent flame that burns in part in premix and in part in diffusion. This variation in operating conditions makes it a very difficult combustion system to analyse and model. Researchers have however, tried to resolve these issues by studying these flames in controlled laboratory environments in combustion chambers where physical parameters and fuel compositions can be closely controlled. A summary of these studies is presented here.

Temperature: Temperature has, of all the known physical parameters, the greatest effect on the soot formation mechanism. Temperature has the tendency to increase the rates of all types of reactions in the soot formation process. It has been generally noted that soot inception begins around 1400 K while soot burn-off ceases below 1300 K [8]. As temperature increases, the rate of oxidation increases faster than the rate of formation of soot. In a well-mixed combustion reactor, where the oxidation and formation reactions are occurring at the same time, the highest rate for soot formation is in the region of 1500 to 1700 K [8]. In the case of premixed flames higher temperatures decrease net soot formation. In the case of diffusion flames however, the soot formation rates increase with increasing temperature. On tests performed in an optically-accessible constant-volume combustion chamber Siebers et al. [9] have studied the effects of injection pressure, ambient density (or pressure, indirectly) and ambient temperature on flame lift-off and soot formation characteristics. Their studies have shown that while a rise in temperature decreases the lift-off length, similar ambient pressure i.e. density dictates that the equivalence ratio at lift-off length is higher. This would lead to an increase in soot formation rate as well.

Pressure: Pressure changes in the gases enclosed in a combustion chamber cause changes in the flame structure, propagation velocity, temperature and thermal diffusivity. Isolating the effects of pressure changes alone can thus be difficult. For premixed flames, an increase in the

tendency to soot as the pressure is increased is noted [8]. In the case of diffusion flames, the increase in pressure decreases the thermal diffusivity and changes the flame structure. It has been seen that the soot volume increases with an increase in the charge pressure. The variation of soot formation volume with respect to pressure increase varies between $P^{1.2}$ and $P^{2.0}$ [8] depending on combustion conditions. Higher pressures have also yielded larger particles, lower peak flame temperatures and a greater particle number density. Siebers et al. [9] state that as a general trend, for the same temperature, increasing the ambient pressure or density forces the lift-off length to become shorter. The local equivalence ratio at the lift-off length also increases as the ambient pressure is increased. This would increase the propensity of the fuel jet to soot. The soot processes also come nearer to the injector nozzle as the ambient pressure increases. As a side note, it has been noted that as the equivalence ratio at lift-off length approaches 2.0 or below, no soot is detectable in the fuel jet [9].

Stoichiometry: The effects of stoichiometry on soot formation are complex. Oxygen can be added to the fuel either via mixing with air, or by changing the composition of fuel such that it incorporates oxygen as a part of the chemical structure. For diesel engines, generally, only premixing effects with air are considered. In general, addition of oxygen quantity in the premixed mixture decreases the quantity of soot formed. This however, is not always the case as oxygen also has the effect of speeding up the combustion reactions and increasing temperatures. It can thus be very difficult to separate effects of oxygen from the effects of temperature change due to oxygen. Results presented in [8] show that in different air/fuel jets, as the quantity of oxygen is increased, the rate of soot formation increases as well. This soot formation rate increases to a maximum level after which it drops down to zero at the critical sooting equivalence ratio. It was concluded from these tests that the initial increase in sooting is due to the fact that oxygen molecules favour an increase in the reaction zone temperature leading to increased intensity of pyrolysis reactions. These pyrolysis reactions as discussed earlier, give rise to soot precursors. Eventually, a peak in soot formation rate is reached where the oxidation reactions and the pyrolysis reactions are in equilibrium, after which, the oxidation reactions become much more significant as the temperature rises. These phenomena are much more pertinent to diesel engine combustion as the equivalence ratios are between 2 and 10, where most fuels tend to soot the most. In addition to this, it is not necessary to decrease equivalence ratio to stoichiometric to eliminate sooting as it is only required to convert carbon molecules to CO and they can no longer take part in the soot formation reactions.

1.2.2.3. Modelling of soot processes:

Seeing that the soot formation processes are so complex, a large number of models have been proposed that try to explain the effect of different parameters on the soot formation rates. In general, these models divide the overall soot formation rate into two steps: soot generation, and soot oxidation. The difference between these two rates determines the overall soot formation rate. An example model originally proposed by Jung and Assanis [12][18] is presented below:

$$\frac{dm_{sf}}{dt} = A_f m_{f,ev} P^{0.5} \exp\left(-\frac{E_{sf}}{RT}\right) \quad \textbf{1}$$

$$\frac{dm_{sb}}{dt} = A_b m_s \frac{P_{O_2}}{P} P^{1.8} \exp\left(-\frac{E_{sb}}{RT}\right) \quad \textbf{2}$$

Where:

m_{sf}, m_{sb}	:	Mass of soot formed and burnt respectively
m_s	:	Mass of soot
$m_{f,ev}$	:	Mass of evaporated fuel
P	:	Cylinder pressure
Po_2	:	Partial pressure of oxygen
T	:	Temperature
R	:	Perfect gas constant
A_f, A_b	:	Constants that are used to calibrate the measured and calculated values of soot
E_{sf}, E_{sb}	:	Energies of activation of soot formation and soot burning respectively with values of E_{sf} = 1.25 x 10^4 cal/mol, E_{sb} = 1.40 x 10^4 cal/mol

The net soot formation rate can then be expressed as:

$$\frac{dm_s}{dt} = \frac{dm_{sf}}{dt} - \frac{dm_{sb}}{dt} \quad \textbf{3}$$

Another soot formation model is the Nagle and Strickland-Constable oxidation model. This model is based on experiments of oxidation of graphite in an O_2 environment over a range of partial pressures. In this model, the oxidation occurs by two mechanisms whose rates depend on the surface chemistry involving more reactive "***A***" sites and less reactive "***B***" sites. The chemical reactions are:

$$A + O_2 \leftrightarrow A + 2CO \quad \textbf{4}$$

$$B + O_2 \leftrightarrow A + 2CO \quad \textbf{5}$$

$$A \leftrightarrow B \quad \textbf{6}$$

The NSC soot oxidation rate as implemented in **Eq. 3** is given as:

$$\frac{dm_{sb}}{dt} = \frac{M_c}{\rho_s d_s} m_s w \quad \textbf{7}$$

Where M_c is the carbon molecular weight (12 g/mole), ρ_s is the soot density (2.0 g/cm^3) and d_s is the soot diameter (4.5 x 10^{-9} m). The term w in **Eq. 7** is the net reaction rate of reactions as given in **Eqs. 4** to **6**, and is defined as:

$$w = \left(\frac{K_a P_{O_2}}{1 + K_z P_{O_2}} \right) x + K_b P_{O_2} (1 - x) \quad \textbf{8}$$

Where Po_2 is the partial pressure of oxygen given in atmospheres and the proportion "***x***" of A sites is given by:

$$x = \frac{P_{O_2}}{P_{O_2} + (K_t / K_b)} \quad \textbf{9}$$

The rate constants used in the NSC oxidation model are given in **Table 3** below:

Rate Constant	Value	Units
K_a	20 exp(-15100/T)	g-C/cm^2.s.atm
K_b	4.46 x 10^{-3} exp(-7640/T)	g-C/cm^2.s.atm
K_t	1.51 x 10^5 exp(-48800/T)	g-C/cm^2.s
K_z	20 exp(-15100/T)	atm^{-1}

Table 3. Table giving the rate constants and their values for use in the NSC soot oxidation model [21]

1.2.3. Nitrogen Oxides production

Nitrogen oxides group two types of chemical products together, NO and NO_2. In general, internal combustion engines produce more NO than NO_2 as a product of combustion. In spark ignition engines, NO_2/NO ratio is very low. In the case of diesel engines however, this ratio can be as high as 30% [1].

1.2.3.1. Fundamental mechanisms of NO production:

The main source of production of NO in internal combustion engines is atmospheric Nitrogen. This atmospheric Nitrogen, under the effect of high temperatures and chemical reactions, combines with oxygen in the air to form Nitrogen Oxides. For the most part, four sources of NO from internal combustion engines have been identified:

a. Nitrogen Oxides formed as a result of the reaction between atmospheric Nitrogen and Oxygen at high temperatures is called **Thermal NO**.

b. Nitrogen Oxides formed as a result of the "fast" conversion of atmospheric Nitrogen and Oxygen in the flame front during combustion is called **Prompt NO**.

c. Nitrogen Oxides formed as a result of an intermediate reaction of N_2O production is called **Nitrous NO**.

d. Nitrogen Oxide can also be formed by the Nitrogenous content in fuel and is called the **Fuel NO**.

Thermal NO: The mechanism of Nitrogen Oxide formation from atmospheric Nitrogen and Oxygen has been studied extensively. The production of NO takes place both in the flame front and in the hot post combustion gases. In the case of the internal combustion engine however, the combustion occurs at very high pressures, so the reaction zone were the combustion process takes place is very thin. Thus the residence time in the flame is very short. In addition to this, the cylinder pressure rises during the process of combustion. Thus the pressures and temperatures that are encountered by gases are greater than during or before combustion. It is for this reason that the quantity produced of **Thermal NO** is greater than **Prompt NO** [1]. In the case of near-stoichiometric air/fuel mixtures, the principal reactions governing the formation and destruction of Nitrogen Oxides from molecular Nitrogen are as follows and were proposed by Zeldovich [1]:

$$O + N_2 = NO + N \quad \textbf{10}$$

$$N + O_2 = NO + O \quad \textbf{11}$$

To further improve the quality of the Zeldovich model, Lavoie et al. [1] proposed an additional reaction to the mechanism which contributes significantly:

$$N + OH = NO + H \qquad \textbf{12}$$

For reference the rates of reaction for each reaction are given in **Table 4**:

Reaction	Rate constant, $cm^3/mol.s$	Temperature range, K	Uncertainty factor of or %
(1) $O + N_2 \rightarrow NO + N$	7.6 x 10^{13}exp(-38000/T)	2000-5000	2
(-1) $NO + N \rightarrow O + N_2$	1.6 x 10^{13}	300-5000	±20% at 300 K 2 at 2000-5000 K
(2) $N + O_2 \rightarrow NO + O$	6.4 x 10^{9}exp(-3150/T)	300-3000	±30% 300-1500 K 2 at 3000 K
(-2) $NO + O \rightarrow N + O_2$	1.5 x 10^{9}exp(-19500/T)	1000-3000	±30% at 1000 K 2 at 3000 K
(3) $N + OH \rightarrow NO + H$	4.1 x 10^{13}	300-2500	±80%
(-3) $NO + H \rightarrow N + OH$	2.0 x 10^{14}exp(-23650/T)	2200-4500	2

Table 4. Rate constants for the Nitrogen Oxides formation mechanism [1]

As can be seen from the table above, the reaction energies are relatively high for NO formation. It is for this reason that NO production rates are insignificant until at least 1900 – 2000 K [1]. The rate of formation of NO via reactions as detailed in **Eq. 10** to **12** is given by:

$$\frac{d[NO]}{dt} = k_1^+[O][N_2] + k_2^+[N][O_2] + k_3^+[N][OH] - k_1^-[NO][N] - k_2^-[NO][O] - k_3^-[NO][H] \qquad \textbf{13}$$

Where [] denotes the species concentrations in moles per cubic centimetre when k_i have the values as given in **Table 4**. The forward rate constants for **Eq. 10** and **11** have large activation energies which results in a strong temperature dependence of NO formation rates. A similar relation to **Eq. 13** may be written as under:

$$\frac{d[N]}{dt} = k_1^+[O][N_2] - k_2^+[N][O_2] - k_3^+[N][OH] - k_1^-[NO][N] + k_2^-[NO][O] + k_3^-[NO][H] \qquad \textbf{14}$$

Since [N] is much less than the concentrations of other species of interest (~10^{-8} mole fraction), the steady state approximation is appropriate: d[N]/dt is set equal to zero and **Eq. 14** is used to eliminate [N]. The NO formation rate then becomes:

$$\frac{d[NO]}{dt} = 2k_1^+[O][N_2]\frac{1-[NO]^2/(K[N_2][O_2])}{1+k_1^-[NO]/(k_2^+[O_2]+k_3^+[OH])} \qquad \textbf{15}$$

Where $K = (k_1^+/k_1^-)(k_2^+/k_2^-)$

As detailed earlier, due to high pressures, the combustion reactions happen in a very thin zone and the residence time being short, the majority of the NO produced is in the post flame zone of hot gases. It is thus appropriate to assume that the combustion and NO processes are decoupled and to approximate the molar concentrations of O_2, O, OH, H and N_2 by their equilibrium values at the local pressure and equilibrium temperature.

To introduce this equilibrium assumption, we may use the notation $R_1 = k_1^+[O]_e[N_2]_e = k_1^-[NO]_e[N]_e$, where $[]_e$ denotes the equilibrium concentration, for the one-way equilibrium rate for reaction given by **Eq. 10**, with similar definitions for

$R_2 = k_2^+[N]_e[O_2]_e = k_2^-[NO]_e[O]_e$ and $R_3 = k_3^+[N]_e[OH]_e = k_3^-[NO]_e[H]_e$. Substituting $[O]_e$, $[O_2]_e$, $[OH]_e$, $[H]_e$ and $[N_2]_e$ in **Eq. 15**, we have,

$$\frac{d[NO]}{dt} = \frac{2R_1\left\{1-([NO]/[NO]_e)^2\right\}}{1+([NO]/[NO]_e)R_1/(R_2+R_3)} \qquad \textbf{16}$$

Typical values of R_1, R_1/R_2 and $R_1/(R_2+R_3)$ are given in **Table 5**. As can be seen, the difference between the second and third terms gives an idea of the importance of the reaction given by **Eq. 12** when added to the mechanism.

Equivalence Ratio	R_1‡	R_1/R_2	$R_1/(R_2+R_3)$
0.8	5.8×10^{-5}	1.2	0.33
1.0	2.8×10^{-5}	2.5	0.26
1.2	7.6×10^{-6}	9.1	0.14

Table 5. typical values of R_1, R_1/R_2 and $R_1/(R_2+R_3)$ [1]

The strong temperature dependence of the NO formation rate can be demonstrated by considering the initial value of d[NO]/dt when $[NO]/[NO]_e << 1$. Then from **Eq. 16**,

$$\frac{d[NO]}{dt} = 2R_1 = 2k_1^+[O]_e[N_2]_e \qquad \textbf{17}$$

At equilibrium, the oxygen atom concentration is given by

$$[O]_e = \frac{K_{p(O)}[O_2]_e^{1/2}}{\left(\tilde{R}T\right)^{1/2}} \qquad \textbf{18}$$

Where $K_{p(O)}$ is the equilibrium equation for the reaction

$$\tfrac{1}{2}O_2 = O$$

And is given by

$$K_{p(O)} = 3.6\times10^3 \exp\left(\frac{-31090}{T}\right) \quad atm^{1/2} \qquad \textbf{19}$$

The initial NO formation rate may then be written by combining **Eq. 17** to **19** using k_1^+ from **Table 4** as:

$$\frac{d[NO]}{dt} = \frac{6\times10^{16}}{T^{1/2}}\exp\left(\frac{-69090}{T}\right)[O_2]_e^{1/2}[N_2]_e \quad mol/cm^3\cdot s \qquad \textbf{20}$$

The strong dependence of the NO formation rate on the temperature in the exponential term is evident. High temperature and high oxygen concentrations result in the production of high NO formation rates. **Figure 15** shows us the NO formation rate with respect to the post-combustion gas temperature and equivalence ratio. The inclusion of the equivalence ratio gives an indication of the composition of the post-combustion gases. Also shown is a curve giving the adiabatic flame temperature given by combustion of an air/fuel mixture initially at 700 K and 15 bars of constant pressure. The curve shows the variation in final temperature for different air/fuel equivalence ratios. As can be seen from the graph, the NO formation rate peaks at stoichiometric air/fuel ratios and diminishes on either the lean or rich side. This is of course only true if the combustion is performed in adiabatic conditions. In a system where heat transfer is pronounced between the fluid and the walls, this assumption may not hold true.

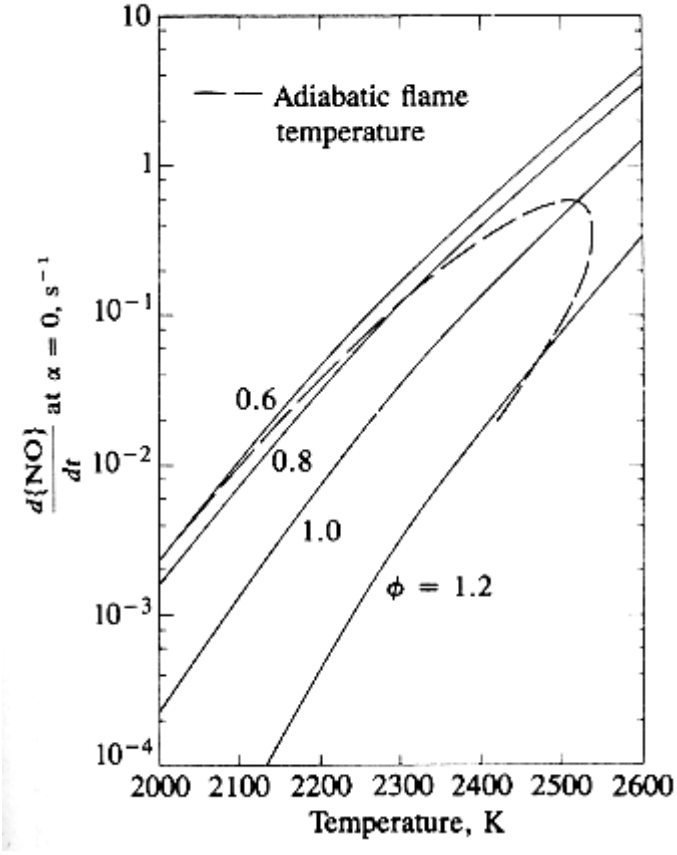

Figure 15. Variation of NO formation rate with temperature and equivalence ratio [1]

A characteristic time τ_{NO} for the NO formation rate can be defined as follows:

$$\tau_{NO}^{-1} = \frac{1}{[NO]_e}\frac{d[NO]}{dt} \quad \textbf{21}$$

$[NO]_e$ can be obtained from the equilibrium constant

$$K_{NO} = 20.3\times\exp(-21650/T) \quad \textbf{22}$$

For the reaction

$$O_2 + N_2 = 2NO \quad \textbf{23}$$

As $[NO]_e = \left(K_{NO}[O_2]_e[N_2]_e\right)^{1/2}$. **Eq. 21** and **22** can be combined to give

$$\tau_{NO} = \frac{8\times10^{-16}T\exp(58300/T)}{p^{1/2}} \quad \textbf{24}$$

Where τ_{NO} is in seconds, T is in Kelvin, p is in atmospheres. It is assumed at this juncture that the molar ratio of Nitrogen is 0.71. For engine operation conditions, τ_{NO} is comparable to, or longer than the time durations that are characteristic of changes in engine conditions. Therefore, the formation process is kinetically controlled. For near-stoichiometric conditions, however, at maximum pressures and temperatures, τ_{NO} is comparable to typical combustion times of 1 ms and thus equilibrium NO concentrations may be obtained.

Prompt NO: Of the total NO production during combustion in engines, a part is produced in the active flame front [12]. Here, the thermal NOx has not had sufficient residence time to

form. A small amount of the prompt NOx is produced via the Zeldovich mechanism, in regions where the O and OH radical concentrations are higher than equilibrium concentrations.

Various numerical analyses [12] have shown that the formation of Prompt NO is linked principally to the reaction between N_2 and radicals produced during the combustion process, such as CH_2, CH and C to produce H_2CN, HCN and CN. Going by the reactions, we get;

$$CH + N_2 \leftrightarrow HCN + N \quad \textbf{25}$$

$$CH_2 + N_2 \leftrightarrow HCN + NH \quad \textbf{26}$$

$$CH_2 + N_2 \leftrightarrow H_2CN + N \quad \textbf{27}$$

$$C + N_2 \leftrightarrow CN + N \quad \textbf{28}$$

The species H_2CN, HCN and CN are formed in the rich flame regions; afterwards, these are transformed into NCO, HNCO or NHx to form NO. Of the reaction noted above, the reactions given by **Eqs. 25** and **28** are much stronger than those given by **Eqs. 26** and **27** [12]. Thus, it can be said that the Prompt NOx formation reactions take place in the following zones:

a. In the rich zones in pre-mixed flames

b. In the fuel-rich zone in diffusion flames, where there is a simultaneous destruction and production of reactive chemical species.

As it stands, the formation rate for Prompt NO stays inferior to that of Thermal NO for combustion temperatures below 2500 K [12]. It should be noted however, that the prompt NO reactions are invariably linked to those of Thermal NO formation, most notably, the inverse form of the reaction given by **Eq. 10** where a part of the Prompt NO is converted to N_2;

$$NO + N = O + N_2 \quad \textbf{29}$$

From the previous section on Thermal NO, it was said that for simplifying the combustion analysis, the reactions leading to the formation of the Thermal NO could be treated separately to the reactions for combustion. In the case of the Prompt NO however, the reactions for combustion and the reactions which define Prompt NO formation are closely linked and can not be treated separately. This makes it relatively complicated to model numerically. For the most part, most authors [12] neglect Prompt NO reactions for the following reasons;

a. The premixed combustion being too rich for the formation of Prompt NO. According to Fenimore et al. [12], the optimum Prompt NO formation rate is obtained at an equivalence ratio of 1.4.

b. Seeing that the zone where the diffusion combustion is very thin, the residence time of reactants in this zone is too short for any noticeable formation of Prompt NO. The resulting formation rate of NO is then much smaller than that of Thermal NO.

Nitrous NO: According to Mellor et al. [13], NO formation can also take place via a reaction that introduces an production of N_2O. Considering high pressure combustion reactions at temperatures of higher than 2400 K, the reaction rates of this mechanism are found to be the same or only slightly lower than those of Thermal NO formation reactions. Malte and Pratt introduced, in 1974, a mechanism that consists of four reactions;

$$N_2O + O \leftrightarrow 2NO \quad \textbf{30}$$

$$O + N_2 + M \leftrightarrow N_2O + M \quad \textbf{31}$$

$$N_2O + H \leftrightarrow N_2 + OH \quad \textbf{32}$$

$$N_2O + O \leftrightarrow N_2 + O_2 \quad \textbf{33}$$

According to Mellor et al. [13] the results presented by Malte and Pratt were obtained from low pressure combustion analyses. And it is possible to take only the **Eq. 30** and **31** if we consider the combustion to take place at high pressure. It will be necessary however to add the following reaction [13];

$$N_2O + H \leftrightarrow NO + NH \ldots \rightarrow 2NO \quad \textbf{34}$$

While the following equation has been added to their model for N_2O modelling;

$$O_2 + M \leftrightarrow 2O + M \quad \textbf{35}$$

Eq. 31 is a tri-molecular reaction, which is more sensitive to pressure changes than bi-molecular reactions.

In the following **Table 6**, Mellor et al. [13] present the influence of pressure and temperature on the different NO formation mechanisms;

Combustion Temp. (K)	Pressure (atm)	Significant NO formation pathway	Secondary NO formation pathway	Negligible NO formation pathway
Low (~1800)	1	N_2O	Zeldovich & Prompt	---
High (~2400)	1	Zeldovich	N_2O and Prompt	---
Low (~1800)	10 to 30	N_2O	Zeldovich	Prompt
High (~2400)	10 to 30	Zeldovich	N_2O	Prompt

Table 6. Table giving the importance of different mechanisms for NO formation [1]

With reference to the table above, it can be seen that according to Mellor et al., in the case of the high pressure diesel combustion, the Prompt NO formation reaction is always negligible as compared to the other formation reactions. Contrary to this, at lower temperatures, the N_2O reaction (Nitrous NO) becomes more significant.

Fraction	Average Nitrogen, wt. %	Range, wt. %
Crude	0.65	-
Heavy distillates	1.40	0.60-2.15
Light distillates	0.07	0.00-0.60

Table 7. Typical Nitrogen content in different petroleum distillates [1]

Fuel NO: Fuel Nitrogen is also a source of NO formation during combustion. **Table 7** shows a selection of some fuels and their Nitrogenous content. During the distillation process, the heavier distillates retain higher Nitrogen content. The Nitrogen can exist as amines and ring compounds. During combustion, it is likely that these compounds are subjected to thermal decomposition processes prior to entering the combustion zone. The precursors to NO formation are therefore likely to be low molecular weight Nitrogen compounds such as NH_3, HCN and CN. Oxidation to NO is usually rapid, occurring on a time scale comparable to that of the combustion reactions. The amount of NO produced is sensitive to the air/fuel equivalence ratio. As the equivalence ratio is decreased to stoichiometric or even lean conditions, the NO yield approaches 100 percent, in the case of rich mixtures however, the NO yield is limited. Fuel NO formation is very weakly dependent on temperature, unlike NO formation linked to atmospheric Nitrogen [1].

1.2.3.2. Formation of NO2:

Chemical equilibrium considerations indicate that for unburned gases at typical flame temperatures; NO/NO_2 ratios should be relatively small. While experimental data shows this is true for spark-ignition engines, in diesels, NO_2 may contribute up to 30% of the total NOx emission [1]. Presented below is a plausible NO to NO_2 conversion:

$$NO + HO_2 \rightarrow NO_2 + OH \quad \textbf{36}$$

Subsequently, the conversion of this NO_2 to NO may proceed as follows:

$$NO_2 + O \rightarrow NO + O_2 \quad \textbf{37}$$

The reaction outlined in **Eq. 37** can take place only if the reaction outlined in **Eq. 36** is not quenched by mixing with a cooler fluid. This explanation is consistent with the highest NO_2/NO ratios occurring at light load in diesel engines, where cooler regions which could quench the conversion back to NO conversion are widespread.

As a reference, a graph is given for a diesel engine Nitrogen Oxide emissions as a ratio of NO_2/NO [1].

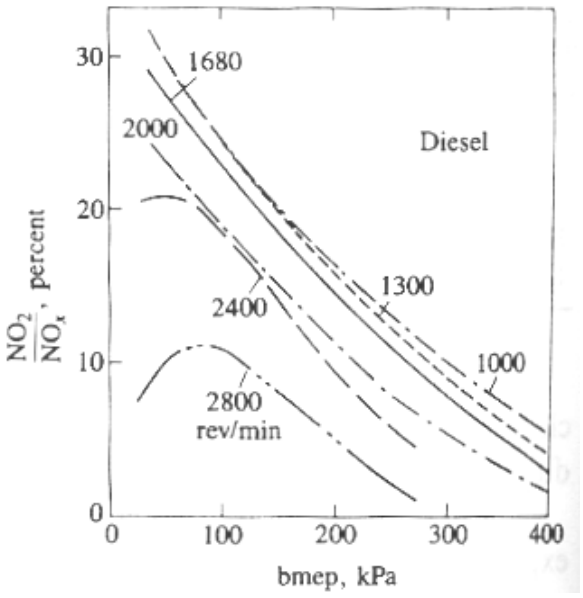

Figure 16. Variation of NO_2/NO with respect to diesel engine operating conditions [1]

1.3. Water Injection and its effects on Engine Emissions and Performance

Water injection was introduced during the Second World War for use as thrust augmentation in gas turbines. It was also used in Spark-Ignition engines to decrease the tendency of the fuel to knock. This enabled higher boost pressures to be run allowing higher power outputs to be obtained.

It was later that it was discovered that the Water Injection could also modify combustion and reduce pollutant emission, most notably Nitrogen Oxides. Much research has been done on these aspects of the Water Injection on both reciprocating engines and turbines [14]. For the purpose of this thesis, we shall be concentrating on the applications of the Water Injection system to the diesel engine. The effects on pollutant emissions, engine performance etc shall be studied.

1.3.1. Types of Water Injection:

In general for diesel engines, water injection has been divided into two distinct types. One in which water is introduced into the engine as a mixture with the fuel, and one in which water is introduced separately into the charge air in liquid or vapour form. Going by references of other researchers, the following water injection methodologies have been studied [20]:

a. Water / Fuel emulsion injection

b. Combustion chamber water injection

c. Stratified water injection

d. Intake manifold water injection

1.3.1.1. Water / Fuel emulsion injection:

Water / Fuel emulsions have been commercialised over a period of time as a measure of reducing NOx and PM emissions in diesel engines. These products were marketed under the trade name of PuriNOx by the Lubrizol Corporation, Proformix (Chevron), Aquadiesel (Shell), Aspira (BP), GECAM (Cam Technologie) and Aquazole (TotalFinaElf). In general, water / fuel emulsions consist of the fuel, water, and an emulsifier. The nature of the emulsifier depends on the type of mix desired. The **Bancroft rule** states:

"The phase in which an emulsifier is more soluble constitutes the continuous phase."

This means that the type of emulsion, i.e., Water in Oil (W/O) or Oil in Water (O/W) is determined by the Hydrophilic-Lipophilic Balance (HLB) of the surfactant in question used. In the case of a W/O emulsion, a surfactant with a high value of HLB will be employed whereas a low HLB value surfactant shall be used for an O/W emulsion. In general, surfactants with HLB values of higher than 11 are considered to be water soluble, while those having HLB values of lower than 9 are considered to be oil soluble. The HLB scale was developed in the late 1940's by William C. Griffin of the Atlas Powder Company. In general for petroleum oils, an HLB value of 10 is required [15]. The requisite HLB value can be, if required, obtained from the weighted average of two different types of surfactants.

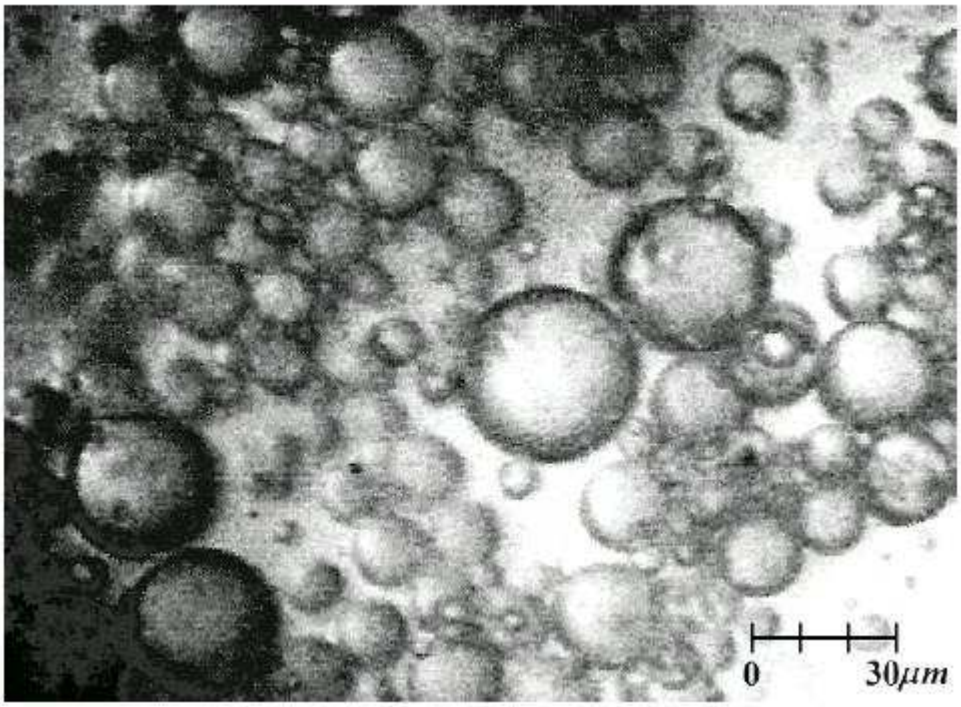

Figure 17. Liquid structure of a 40% W/O diesel emulsion [16]

Figure 17 shows a microscopic photograph of a W/O emulsion having 40% water by mass. This fuel was used in a Rapid Compression and Expansion Machine (RCEM) to evaluate the change in combustion performance with varying levels of W/O mix ratios. Subsequently, correlations were developed to correlate the change in NOx and PM formation levels [16].

It is evident that as the ratio of water to fuel is increased, the volume of mixture to be injected increases. To compensate, the injection pressure may be raised to obtain the same injection duration as in the case of the pure diesel fuel, or the injection duration may be increased to inject the same quantity of fuel. The subsequent effects of both of these scenarios are discussed later in this document.

1.3.1.2. Combustion chamber water injection:

Water can be introduced into the air / fuel spray mixture inside the combustion chamber. Referring to systems already in use, there seem to be two systems, one in which a second water injector is installed in the cylinder head, while the second setup changes the injector to one which has two needles – one to control the fuel flow, and the second one to control the water flow. In both cases, high pressure water supply and metering systems are needed. Much higher in pressure than the ones used in stratified fuel injection. In comparison with the emulsion injection, the ratio of water/fuel can be changed. In addition, the injection timing of water can be adjusted. An example of a fuel/water injector is shown in **Figure 18**.

Figure 18. Wartsila's direct water injection fuel injector [17, 18]

1.3.1.3. Stratified Water Injection:

In addition to the first two methods of water injection, we may inject water into the cylinder by mixing it with the fuel in the injector prior to injection. This can be achieved via special injectors that incorporate an inlet for high pressure water in addition to that of diesel. A system developed by Mitsubishi Heavy Industries is shown in **Figure 19**. Here, the injector is charged with a pre-determined quantity of water by a distribution system during the time the injector is not pressurised. The surplus diesel fuel in the injector is pushed into the spill circuit. When the injector is pressurised by the injector pump, the higher pressure diesel closes the water supply check valve and the water is injected into the combustion chamber in as a spray via the fuel injector. The advantages of stratified injection as compared to emulsion injection are:

a. More precise control of water / fuel mix ratio.

b. Ability to vary water / fuel mix ratio variably

c. Ability to start and stop on neat diesel fuel without need for a second fuel source

d. Combustion delay is shorter than for emulsion injection as the first part of the injection is pure diesel

As compared to the emulsion injection, the cost associated is much higher as a separate high pressure water metering system is required.

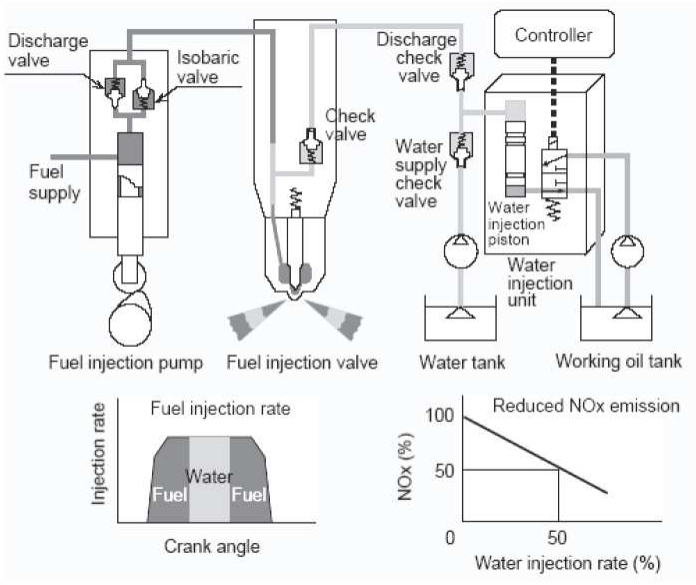

Figure 19. Mitsubishi Heavy Industries Stratified Water Injection [18]

1.3.1.4. Intake manifold Water Injection:

Here, water may be injected in liquid or vapour form into the intake manifold of an engine. Water injection may take place before or after the compressor. In case of liquid water injection, the injection may be continuous, or it may be pulsed. Water injection may be achieved via a single injector or via multiple injectors to ensure proper distribution from cylinder to cylinder.

In the case of the vapour injection, certain manufacturers have been working with unheated or heated water sprays in a large chamber through which intake air is passed. One example of such a system is presented below in **Figure 20**. Details are outlined in the figure.

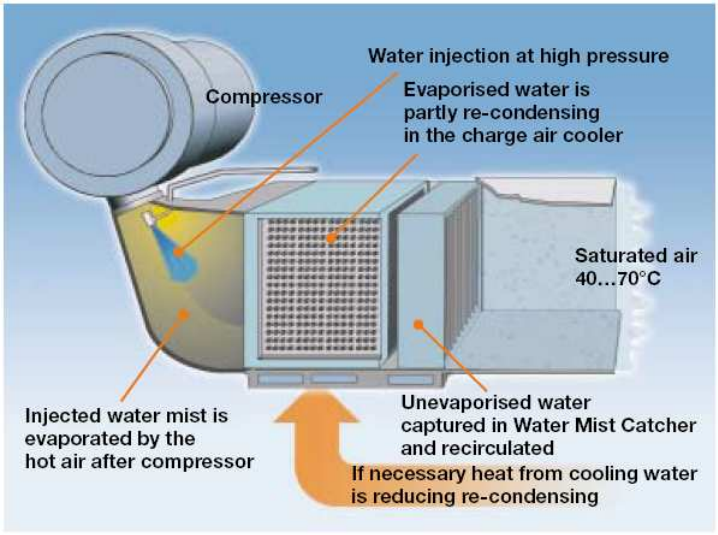

Figure 20. Wartsila's Combustion Air Saturation System (CASS) [17, 18]

Another example of this type of system, but using a humidification tower is proposed by Pielstick/Man and is a part of their Humid Air Motor (HAM) system. This system uses water heated by either the exhaust or by the cooling system. Humidification ratios of up to 140 g/kg dry air are obtained using this system. The system works off of seawater, and is presented below.

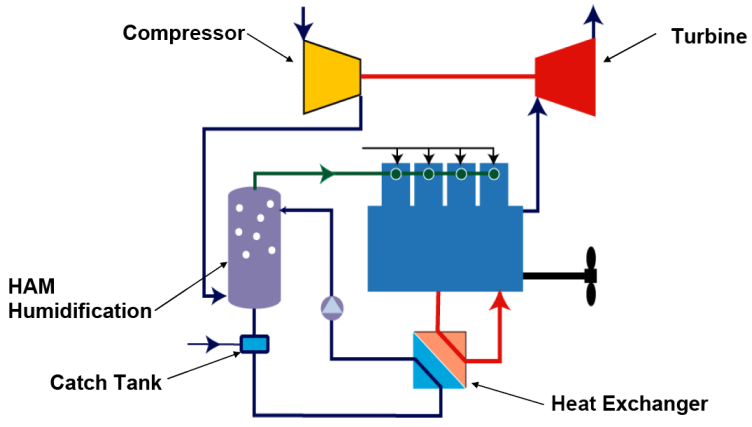

Figure 21. Pielstick / Man HAM system, using heated seawater to humidify intake air [19]

Now that we have outlined the main types of Water Injection systems, a study is presented on the perceived effects of Water Injection on the formation of NOx and PM, as well as the change in engine parameters, and the change in formation rates of other pollutants such as HC

and CO. These would give an idea of the quality of combustion of fuel. That is to say in general, poor combustion gives rise to an increase in production of CO and HC.

1.3.2. Comparison of results obtained from different W/I systems:

In the following section, results from diverse tests performed by different researchers and research groups are presented. Seeing that there are different ways of injecting water into the combustion chamber, comparisons are also made on the same testbenches for the different water injection strategies.

- Ladommatos et al. [22] did some tests on a Ford 2.5 litre DI diesel naturally aspirated engine. Engine load was kept at 40% with an Air / Fuel (A/F) ratio of 44.6:1 and injection at 10° BTDC. Water vapour injection was used in such a manner that only oxygen in the air was substituted. For 3% injection, the NOx production rate drops from 560 ppmv to 150 ppmv, HC rises from 220 ppmv to 300 ppmv and the particulate emissions rise from 2.6 to 5.6 g/kg of fuel.

- Samec et al. [26] have run tests on a 7.1 litre TAM 4 cylinder DI diesel air cooled engine. Two different W/I setups have been used. The first system "WS1" is used to inject water as liquid in front of each intake port, while the "WS2" system injects water at the inlet of the compressor. It has been found that the result for NOx and PM production rates are relatively similar for both systems. Thermal loading on the engine however was different for each system. Cylinder and head temperatures were lower for the WS1 system as compared to the WS2 system. This could be traced back to the fact that the latent heat of vaporisation of water serves to cool down more effectively. At maximum power (150 kW) and 2150 RPM, the NOx reduction rate was a maximum of 32% for a 45% Water/Fuel rate. For a second operating point of 1300 RPM and BMEP varying from 7.5 to 14 Bar, the NOx reduction rate was given as follows in **Figure 22**:

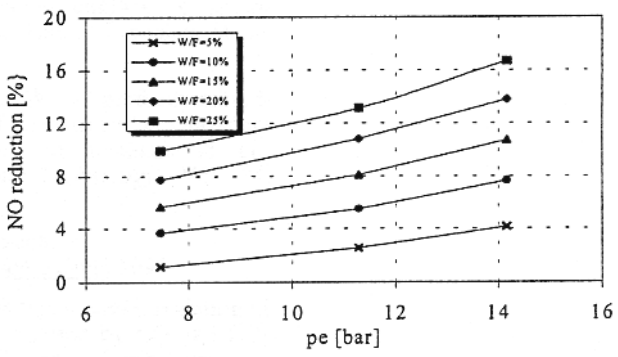

Figure 22. Reduction of NOx production rate for various W/F ratios. [26]

In **Figure 23**, we see the soot production rate at maximum torque and 1300 RPM. We can see that initially the soot production rate rises, which may be due to reduction in equivalence ratio, resulting in the decrease of available oxygen. And then the soot production rate has a tendency to decrease. This may be due to the fact that the proportion of fuel that is injected into the cylinder burns in premixed combustion and burns at a cooler temperature, thus the production of soot is limited [26].

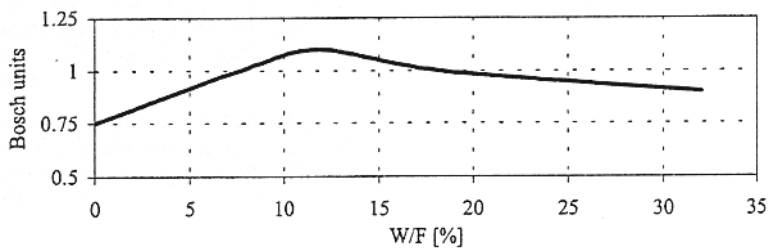

Figure 23. Variation of Soot production with varying water injection rate [26]

- Hountalas et al. [3] have investigated effects of water injection as an emulsion and in mist form in the intake air using a simulation model. The model was modified to take into account the injection of water with the fuel and the intake air. The simulated engine was considered to be a heavy-duty direct injection diesel engine running at 1800 RPM. The engine is considered to have a 150 mm stroke and a 130 mm bore with a compression ratio of 18. Engine loads have been varied from part to full load and three different water percentages of 10%, 20% and 30% have been examined. The simulation model consists of the following engine subsystems:

  1. Engine Cylinder System
  2. Fuel Injection System
  3. Gas Exchange System

  The model used is of a three-dimensional multi zone type. The pressure inside the engine is considered to be uniform. The first law of thermodynamics and the conversation equations for mass and momentum are used for the calculation of conditions inside each zone.

  For calculation of soot formation rate, the Hiroyasu model is used, according to which, the rate of soot formation and burnout depend on the local temperature and mean cylinder pressure. The rate of soot yield considers the local fuel evaporated mass while the rate of soot oxidation rate depends on the local concentration of soot and partial pressure of oxygen. Consideration has been made for the inclusion of OH radicals in the calculation of soot oxidation as it has been known to affect the soot destruction process [3]. For the effect of water injection on the NOx mechanism, the extended Zeldovich mechanism was used. The formation of NOx being considered to be affected mainly by temperature in this mechanism, the main effect of cooling due to water injection was considered.

  The simulation model was calibrated and validated with a production engine of the characteristics as noted earlier. After the verification process is completed, model constants are retained constant for the entire engine operating field with and without water injection. The model constants are calibrated for one operating condition, that is 1800 rpm and full load, and then the constants are kept constant. It was shown that the agreement of values of NOx and PM production and the engine performance between the measured values and the values predicted by the model was good.

  The water injection was performed via two methods, the first being water injection in emulsion form. In this injection strategy, the fuel injection timing was kept similar as for pure diesel injection. The water percentage as noted earlier was varied from 0% to 30% in 10% steps. As water content was increased, the injection duration was increased as well to compensate for the power loss incurred due to the reduction in quantity of the diesel fuel.

Engine Mode	Engine Speed (RPM)	Engine Load (%)	Water (%)	Injection Duration (°CA)	Inlet Pressure (bar)	Injection Pressure (bar)	Injection Advanced (°ATDC)
B25	1800	25	0	11	1.90	900	-2
			10	12			
			20	13			
			30	14			
B50		50	0	17	2.35	1200	-3
			10	18			
			20	20			
			30	23			
B75		75	0	23	2.77	1300	-4
			10	26			
			20	29			
			30	33			
B100		100	0	31	3.18	1400	-4
			10	34			
			20	48			
			30	45			

Table 8. Operating points for the test engine with emulsion injection [3]

In this case, a general trend of soot reduction is seen for increasing quantity of water injection at low and medium loads. This is attributed to the increase in air entrainment rate which increases the rate of oxidation of soot. At higher load rates however, the increase in injection duration is said to be responsible for the increase in the soot production rate as the production of soot is too late to be properly oxidised. As concerns the BSFC, at low loads, a decrease in BSFC is observed while at high loads, an increase in BSFC is observed. This has been attributed to increased dissociation of water, an increase in the energy transfer to evaporation and an increase in duration of injection, which causes combustion during the expansion stroke.

As for NOx production, in general, when quantity of water injected is increased, the reduction of NOx production rate is observed. At high water injection rates, the rate of reduction of NOx production is reduced.

BSFC is reduced slightly at low load as water/fuel ratio is increased, at high loads however; the BSFC has a tendency to increase for higher water/fuel ratios. NOx emissions drop as the ratio of water/fuel is increased. A maximum drop of 40% in NOx production rate was noted for the 30% emulsion at 75% and 100% load. Particulate Matter production is most visibly reduced when the engine load is low, i.e. 25% where the relative reduction is of the order of 35%. This has been attributed to the increase in entrainment rate due to the increase in the volume of liquid in the spray. At high load however, and at 30% water/fuel ratio, the soot production increases, since the injection duration becomes very long. These results may be seen on the accompanying graphical representations:

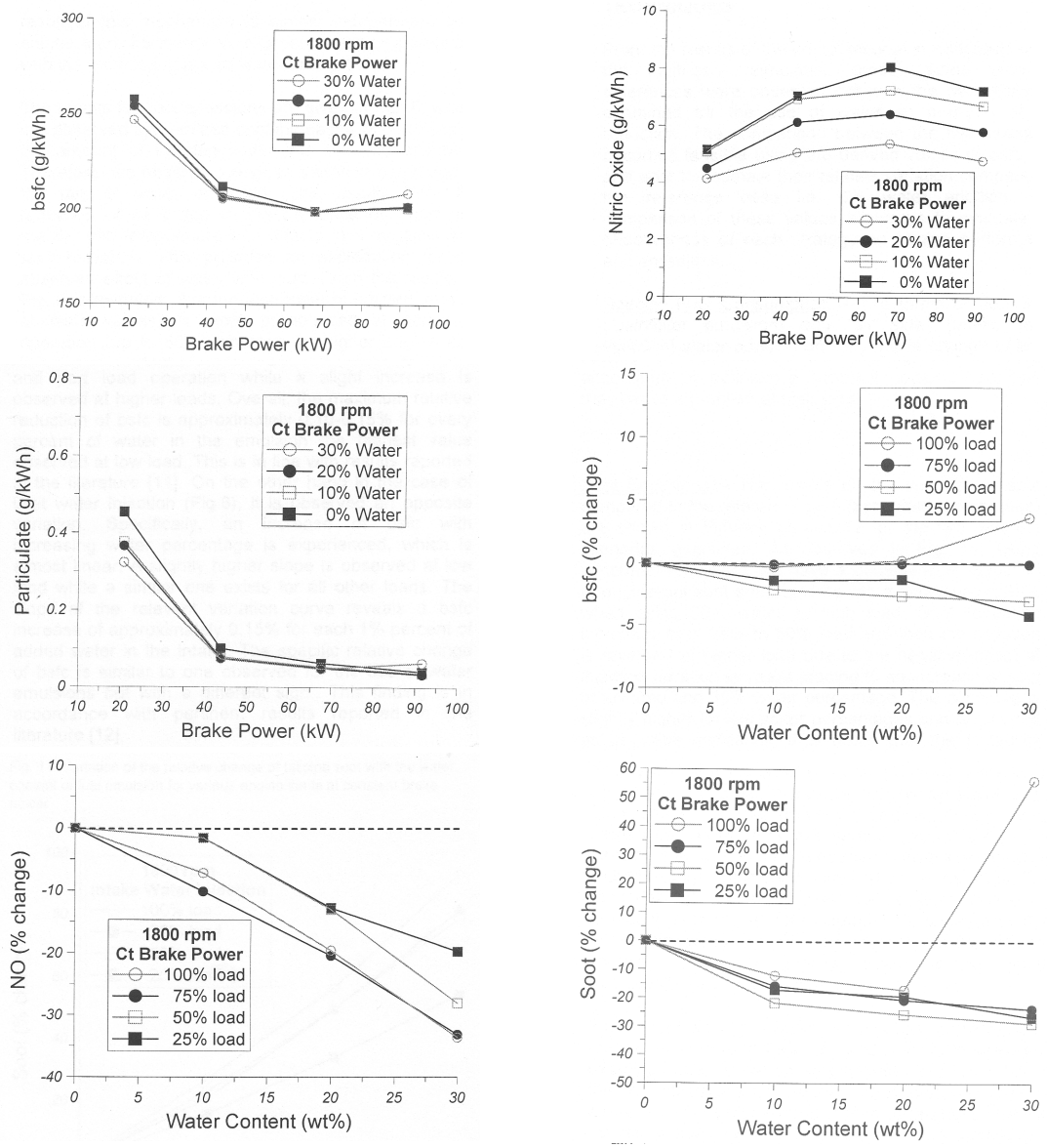

Figure 24. Graphical representation of results obtained for Emulsion water injection [3]

In the case of the intake manifold water injection, the water injection rate was changed between 0 and 30% in 10% steps. **Table 8** gives the operating conditions for the engine for intake manifold water injection as well. Fuel injection duration will however remain constant for the given engine load level. It has been seen that the maximum increase in BSFC with a 30% water/fuel ratio is around 8% at 25% load and around 5% at high load. In the case of the NOx production rate, we see a drop of 25% for a 30% water/fuel injection rate at 25% load, to a drop of 27.5% at high and full load. In the case of PM production rate, we see an increase of 35% at 25% load. At 50 and 75% load, we see a rise of around 50%, while for full load; we see a rise of around 40%. The above presented values are shown in **Figure 25** in graphical form:

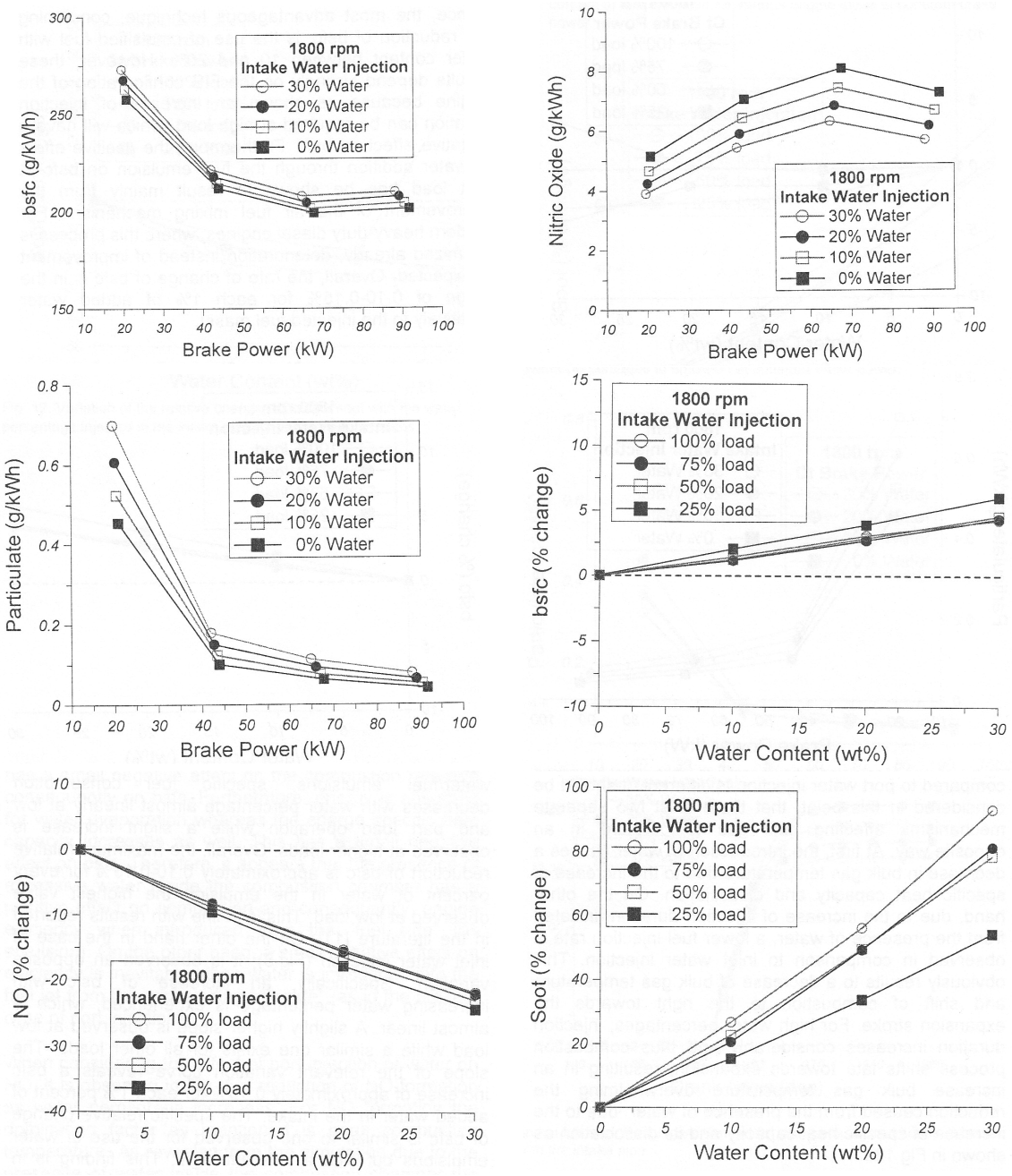

Figure 25. Graphical representation of results obtained for intake manifold water injection [3]

The authors have presented a few hypotheses concerning the effect of water injection on the combustion processes and the production of NOx and soot emissions.

The effect of the two types of water injection, namely emulsion injection and intake manifold injection are rather different as concerns the evolution of bulk gas temperature in the cylinder. In the case of the emulsion injection, the temperature at the initial part of the combustion process is lower and at the final part of the combustion is higher. This tendency increases for higher water injection rates. The decrease in the gas bulk temperature comes about by two methods; the first is that the presence of water in the fuel jet decreases the local temperature due to the evaporation and dissociation of water. Secondly, assuming injection at constant pressure, the fuel injection rate is decreased which offsets the combustion such as to make it retarded. This would also reduce the bulk gas temperature due to the presence of a greater amount of diluent.

In the case of the manifold injection however, as the quantity of water is increased in the intake charge, its influence on the bulk gas temperature increases as well as during the evolution of combustion in the fuel jet. This is due to the fact that the water, being premixed with the intake air charge, is progressively entrained into the fuel jet as combustion takes place on the downstroke and thus the effect of water on the bulk gas temperature increases progressively.

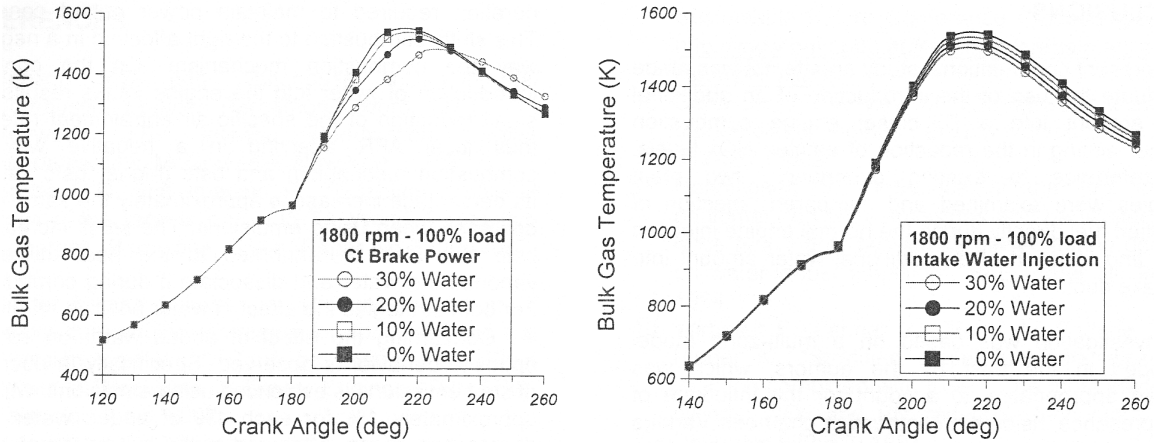

Figure 26. Computed temperature profile for water / fuel ratios of 0, 10, 20 and 30 % [3]

In **Figure 26**, the computed bulk gas temperatures are presented. As discussed above, in the case of the emulsion injection, the temperature initially drops more as water injection quantity is increased, however, the temperature near the end of the expansion increases.

Here, the model is used to calculate the NO and PM emissions production rates. The next two figures show the effect of water injection on the NO production rate in the cylinder. It is observed that with increasing water injection rate as shown in **Figure 27**, the NO production rate decreases both for emulsion water injection and the manifold water injection. Going by the results shown in the graphs, the effectiveness of the emulsion water injection is much greater as compared to the intake manifold water injection. This is a result of the previously explained effect of water percentage on the bulk gas temperature. Therefore, as already stated, the most important parameter affecting the NO emissions is the peak combustion temperature. The reduction of the local peak combustion temperature reveals a reduction of the peak local combustion temperature due to the increased specific heat capacity of the cylinder content and the energy consumed for water evaporation and dissociation.

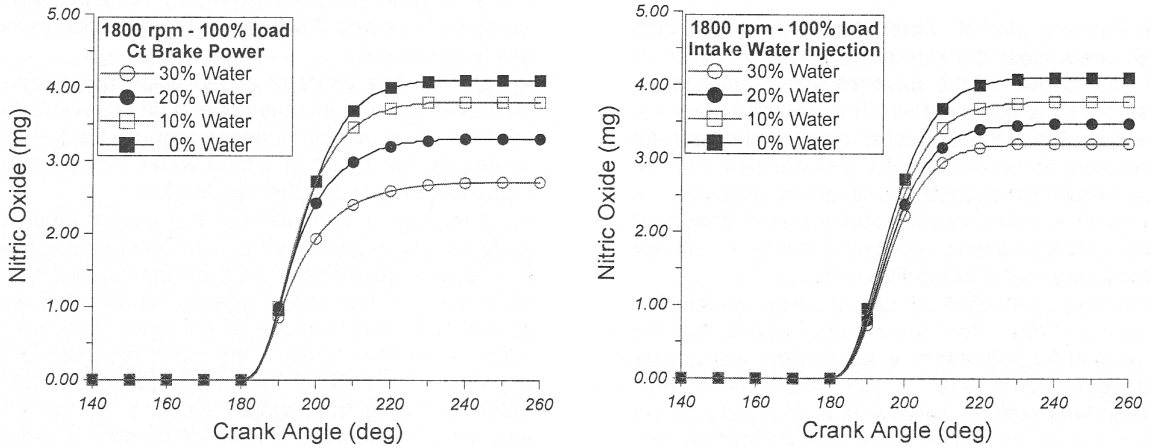

Figure 27. Effect of water injection on calculated NO formation history at 1800 RPM and Full Load using emulsion injection and intake manifold injection [3]

Finally, the authors come to a discussion of soot emissions. Referencing to **Figure 28** In the case of the emulsion water injection, they observe a reduction of the soot emissions rate as the water injection rate is increased. It is noted that an improvement in the mixing of the air and the fuel is the result of a reduction in soot formation rate. Even though the presence of water in the fuel jet has a tendency to reduce the temperature in the combustion zone, the reduction in the oxidation rate is more than compensated by a decrease in the formation rate, and the tailpipe soot emissions are reduced up until a 20% water injection rate. At the 30% water injection rate however, it is seen that the soot formation / oxidation curve has been shifted to the right, and the overall tailpipe soot emissions are much higher than for the 20% water injection case. This is attributed to the fact that the presence of the high quantity of water in the fuel jet has increased the ignition delay to such an extent as to shift the combustion mechanism noticeably to the right. Even though the soot formation is reduced by the similar air / fuel mixing improvements as in the 20% emulsion case, the fact that the oxidation of the soot happens more in the expanding portion of the cycle means that the oxidation is compromised and there is a net increase in the tailpipe soot emissions.

In the case of the manifold water injection, as the water injection rate is increased, the PM emissions also increase (see Figure 28). We can see from the PM emissions calculations, the formation rate increases progressively with an increasing water injection rate. This increase in the formation rate is due to the decrease in the air / fuel ratio. This decrease in the air / fuel ratio is due to the water vapour occupying space in the combustion chamber and displacing the fresh air charge. The reduction in the PM oxidation rate is due to the decrease in temperature which is in turn due to an increase in specific heat capacity of the fresh air charge. Both of these effects combined lead to an increase in the tailpipe soot emissions. It was noted that the soot formation rate did not increase appreciably from 10% to 30%, however, the soot oxidation rate increase by a large amount. It may be surmised that in this case, the increase in the soot emissions rate is due to the decrease of the gas temperature.

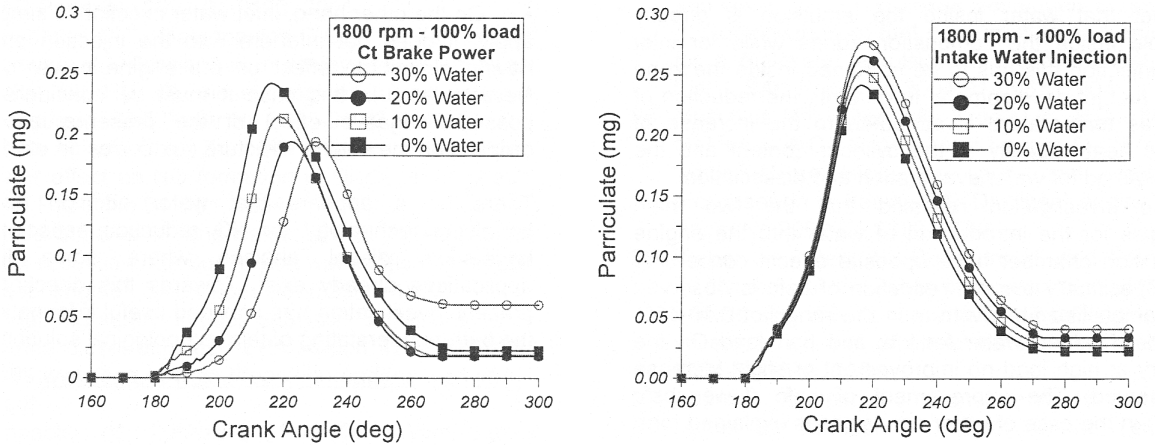

Figure 28. Effect of water injection on calculated soot formation history at 1800 RPM and Full Load using emulsion injection and intake manifold injection [3]

- Hountalas et al. [32] have done test on a 6-cylinder direct injection supercharged diesel engine with a bore of 130mm and a stroke of 150mm. It has direct injection with an injection pressure of 1600 bars. The tests performed are at 25%, 50%, 75% and 100% load. The engine speed is kept constant at 1800 RPM. Contrary to the previous case [3] here it was aimed to reduce the NOx production rate by 10%, 20% and 30%. To do this, different levels of EGR, intake manifold water injection and emulsion injection were performed. The settings were thus:

Engine Speed (RPM)	Engine Load (%)	NOx Reduction (%)	EGR (%)	Water Injection (% Water)	Emulsion (% Water)
1800	25	10	8.8	15.0	11.0
		20	11.4	33.0	16.0
		30	13.8	54.0	24.0
1800	50	10	6.9	12.0	10.0
		20	8.8	26.0	16.0
		30	11.1	42.0	22.5
1800	75	10	6.1	11.0	8.0
		20	8.0	24.0	13.0
		30	9.9	38.0	18.0
1800	100	10	5.8	10.0	7.0
		20	7.5	21.0	12.0
		30	9.1	33.0	18.8

Table 9. Table giving NOx reduction ratios in relation to EGR and W/I rates [32]

Each pollutant reduction technique was used in isolation. This was to give a comparative conclusion of the different effects of the different diluents on the emission rates of NOx and PM.

In conclusion we see that as far as reduction of NOx is concerned, referring to **Table 9**, Emulsion is more or less twice as effective at reducing the NOx emissions rates all load ranges for higher NOx reduction rates. At lower injection rates, the NOx reduction rates are relatively similar. As concerns PM emissions, we see a general reduction of around 40 – 50% across the load range.

- Chadwell et al. [33] have done some tests on a Volvo D-12 heavy-duty on-road diesel engine of 11.7 litres and six cylinders. A High-Pressure EGR loop was added to the engine and a VGT turbocharger was added as well. A custom-designed Real Time Water Injection (RTWI) system was designed that was used to inject water with the fuel as a fuel/water stratified injection. The quantity of water injected varies between 0 and 30% in 10% steps. The change in opacity was considered as a homologue of change in the production in PM. It has been seen that if EGR rate is to be increased while keeping the level of opacity the same, the rate of WI is to be increased. The reason being that increasing WI rate in itself reduces opacity.

  The author in the introduction to the article has compared the RTWI to fuel / emulsion injection. The advantage of a Real Time Water Injection system is that the water /fuel ratio may be varied as a function of engine load to minimize HC / CO production at low load conditions. In comparison to emulsion injection, the author notes that even though CO and HC emissions may be a problem at low load conditions with the Water Injection, at high and medium load, it does not seem to affect it too much as combustion is more stable.

  As concerns the BSNOx (Brake Specific NOx) reduction rates, three means of reduction were tested; Retarded SOI (Start Of Injection), EGR (Exhaust Gas Recirculation) and RTWI(Real-Time Water Injection). The results of the tests are presented in the **Table 10**:

BSNOx Reduction Technique	BSNOx g/kW-hr	Change %	BSFC g/kW-hr	Change %	BSNOx per BSFC %
Baseline	5.38	-	201.8	-	-
Retard SOI	3.20	-40.5	235.0	16.5	-2.5
EGR	1.87	-65.2	219.2	8.6	-7.6
RTWI	3.12	-42.0	206.1	2.1	-20.0

Table 10. Tabulated results for various BSNOx reduction strategies [33]

Data from the test engines are presented in graphical form as noted below:

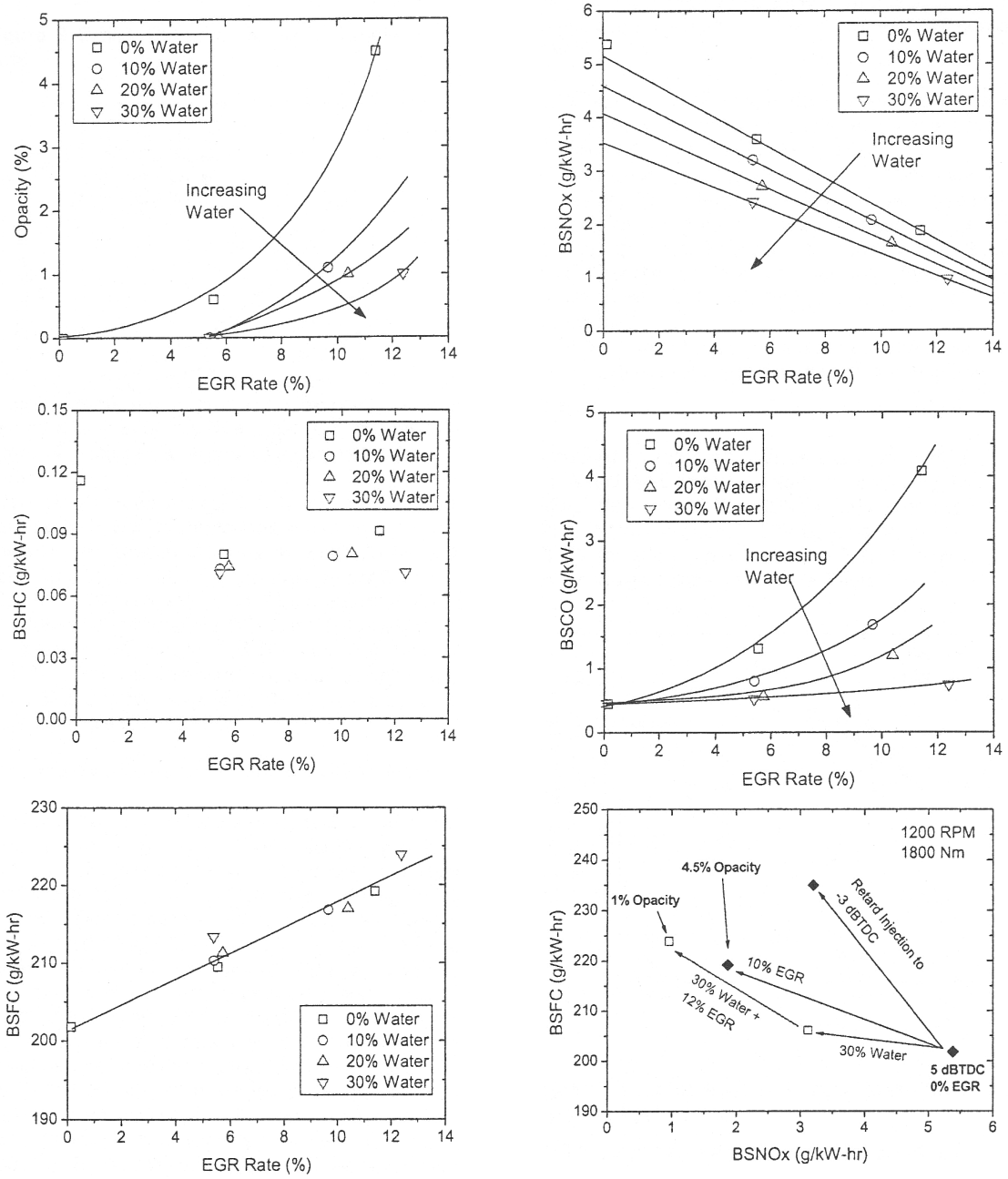

Figure 29. Test data presented in tabulated form for the test engine as described in Chadwell et al. [33]

Water injection can in this case allow the use of higher rated of EGR in keeping PM production rates under limits. As an example, at 1% opacity limit on diesel fuel alone, the

EGR rate could not exceed 6%. However, using water injection of 30%, the EGR rate could be increased to more than 12%. This increase in EGR and W/I corresponds to a decrease in NOx production of 82%.

Being that NOx and PM production rates are of the highest importance as far as emissions controls are concerned. The HC and CO production rates are generally so low that they are not often targeted for reduction since they are generally oxidised in the DOC. The situation changes however, if a production of HC and CO is increased due to HCCI or low temperature combustion modes since the temperature of the oxidation catalysts may also be lowered. The figures for CO and HC production rates show that HC and CO production increases at low engine loads. At high loads, the increase of HC / CO production is not significant. With increasing injection rate, HC production is left rather unaffected, CO emissions on the other hand are reduced as water injection rate is increased. The CO and PM production rates are considered to be closely linked for normal lean-burn diesel combustion. According to the authors, the mechanism that oxidises PM is also potentially responsible for the oxidation of CO.

Regarding effects on BSFC, the authors note a slight increase in BSFC as water injection rate is increased; around 2% increase for a 30% water injection rate. They propose the following potential competing effects that may influence the fuel consumption of the engine:

- Water in small concentrations has a tendency to increase combustion efficiency because of a more complete oxidation of CO and PM
- There is an increase in the work done to compress and inject the fuel and water into the engine. The supplementary work done to pressurise water has been taken into account.
- With the inclusion of water in the injection, the injection duration is increased for the same mass of fuel injected. This retards the centroid of injection, which consequently leads to a retarded combustion and reduced combustion efficiency. Although it is physically possible to re-adjust timing to achieve iso-centroid injection, it was not done during the test for this article.
- The energy required to evaporate water in the injected fuel plume will reduce the in-cylinder temperature, thus reducing the pressure acting on the piston.
- Phase change of water to vapour will increase the pressure in the cylinder available for utilisation by the piston.

All these effects act against each other so that in the end, in comparison to EGR, for the same BSNOx reduction, it is better to use RTWI as compared to EGR in as far as fuel consumption is concerned. The last two graphs in **Figure 29** show the relative changes in BSFC referenced to RTWI, EGR and injection timing retardation.

- Taking a break from internal combustion reciprocating engines, Chen et al. [36] have performed tests on turbine engines. The gas turbine runs what is known as a HAT (Humid Air Turbine) cycle using liquid fuel at combustion chamber pressures of up to 6.9 bars and inlet air temperatures of up to 733K. The advantage of the HAT cycle is the reduction in NOx production rates when compared to the base cycle. A typical diagram of the HAT cycle is presented thus:

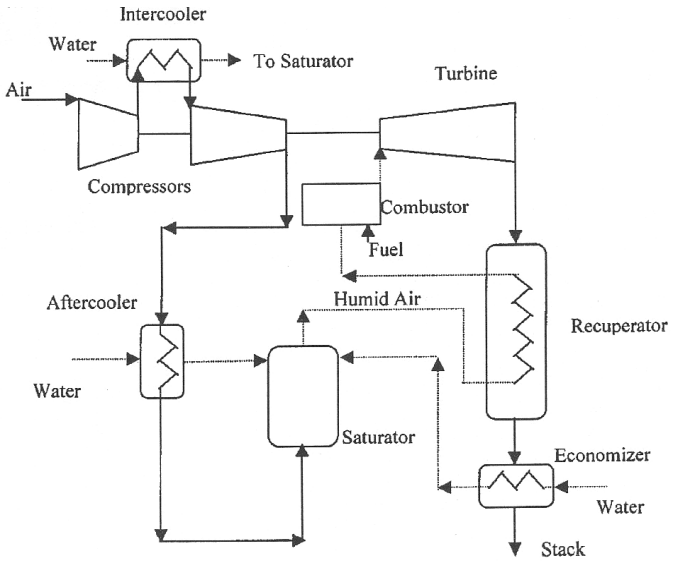

Figure 30. Schematic of a HAT cycle [36]

Results conducted on the combustor were grouped into three categories:

- CO and NOx production relative to equivalence ratio and combustion chamber pressures of 3.45 bars and 6.9 bars (50 and 100 psi)
- CO and NOx production rates relative to equivalence ratio and dry air or air mixed with 10% steam
- CO and NOx production rates relative to the adiabatic flame temperature and dry air or air mixed with 10% steam

The minima for the CO and NOx production rates for each of these cases are presented in the tables below:

Case	Equiv. Ratio (ratio)	Chamber Press. (bars)	Vapour (%)	Flame temp. (K)	CO (ppm)
1a	0.475	3.45	0		50
1b	0.425	6.9	0		10
2a	0.525	6.9	10		10
2b	0.415	6.9	0		10
3a		6.9	10	1750	10
3b		6.9	0	1750	10

Table 11. Tabulated results for CO production [36]

Case	Equiv. Ratio (ratio)	Chamber Press. (bars)	Vapour (%)	Flame temp. (K)	NOx (ppm)
1a	0.43	3.45	0		50
1b	0.33	6.9	0		150
2a	0.475	6.9	10		15
2b	0.33	6.9	0		110
3a		6.9	10	1600	15
3b		6.9	0	1520	110

Table 12. Tabulated results for NOx production [36]

The test results are shown graphically below:

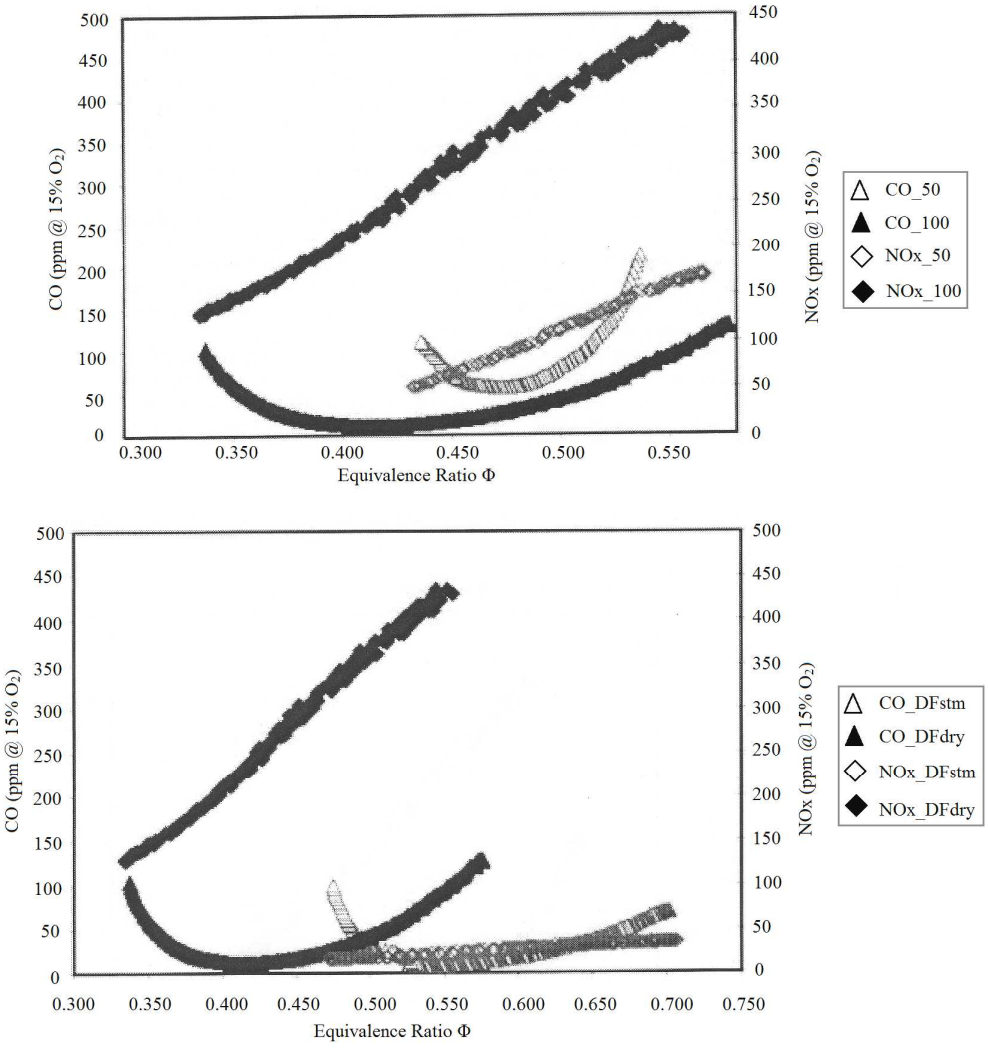

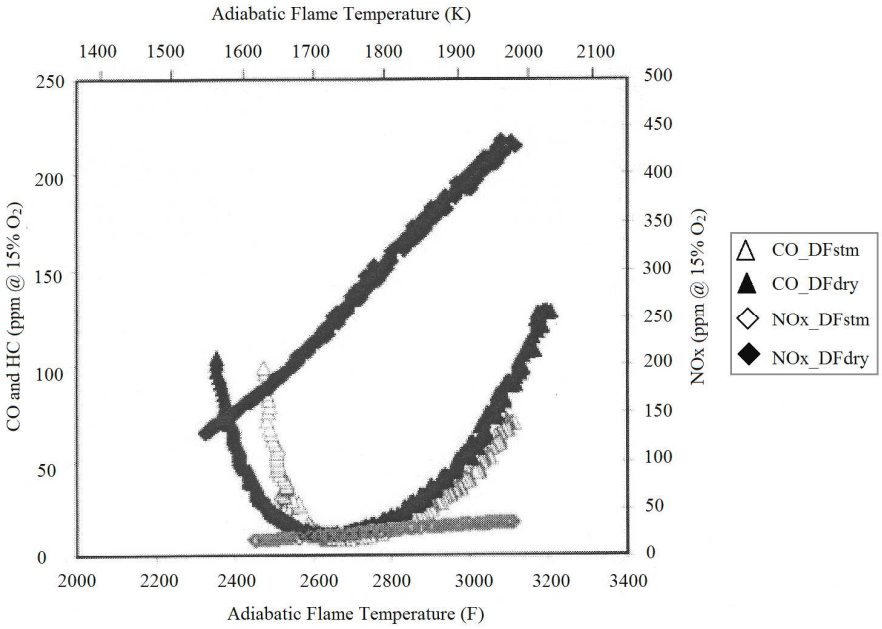

Figure 31. Graphical presentation of test results [36]

In the case of the first plate shown in **Figure 31**, the effect of pressure on combustibility limits is that as the pressure gets higher in the combustion chamber, the lean burn limit may be lowered. In the second and third plates of **Figure 31**, it is clear that the presence of water vapour raises the lean combustibility limit in the combustion chamber.

We know that the combustion in a reciprocating combustion ignition engine is a mixture of premixed and diffusive combustion. Whereas in the turbine combustor presented in this article is primarily premixed, we can nevertheless translate some physical effects. These effects are:

- The presence of water vapour in the air charge raises the limit of lean combustibility. This is attributed to the increase in the specific heat of the charge, necessitating a richer air / fuel mixture for combustion. In a premixed-combustion phase of a reciprocating compression ignition engine, this might be translated as an increase in ignition delay.

- The presence of water vapour increases the specific heat capacity of the charge assuming the same equivalence ratio. This would be in part the reason for a decrease in NOx emissions as dictated by the Zeldovich mechanism, since this mechanism comes into play in the hot combustion products.

- A second chemical effect of the presence of water vapour is noted in the literature which acts on all three NOx production mechanisms; namely Zeldovich, N_2O and Fenimore or “prompt” NO mechanism. All three reactions are modified by a reduction in the quantity of O radicals present. This reduction in the quantity of O radicals is linked firstly to the increase in equivalence ratio for the same flame temperature, thus reduction in O_2 molecules. The presence of water molecules at combustion temperatures promotes the $O + H_2O \leftrightarrow 2OH$ reaction further reducing the number of O radicals present which further reduces the NOx production rate. In addition, the presence of OH radicals promotes the oxidation of hydrocarbon radicals thus reducing the “prompt” NO production.

- Nazha et al. [27] did tests on a 2.5 litre diesel engine of the same type as Ladommatos et al. [22]. The tests performed were of EGR, intake manifold water injection and the use of water/fuel emulsion. The combined effects of these three were also investigated. In general, with intake manifold WI of 1:1 water/fuel ratio, a reduction in 60% of NOx was noted with a negligible increase in PM emission although the PM emission rate increased at high load. For the EGR, a 50% decrease in NOx was noted although the smoke production rate increased by twice at high loads. For a 10% water/fuel emulsion, a reduction in NOx was noted with a slight increase in PM emissions. Further tests were performed with advanced injection timing of 3°. The aim was to evaluate the effect, if any, on the efficacy of the aforementioned emissions reduction techniques.

  Advancing the injection timing by 3° increases the NOx production rate by twice at low load to thrice at full load with a maximum decrease of 10% in the smoke number.

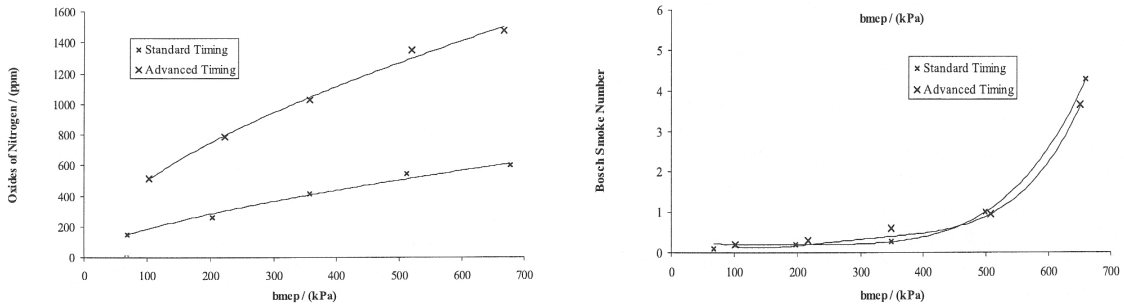

Figure 32. Effect of injection timing on smoke number and NOx production [27]

In **Figure 33**, tests results are presented for manifold and emulsion water injection. In the case of the manifold water injection, a BMEP of 5.8 bars was maintained with water injection rates varying from 0 to 2.75 water / fuel ratio. In the case of the emulsion water injection, the water injection rate was varied between 0 and 20% water / fuel ration in steps of 5% each. In the case of emulsion injection however, two different engine load levels were tested. One was 5.8 bars as for the intake water injection, whereas a lower load of 2 bars was also tested.

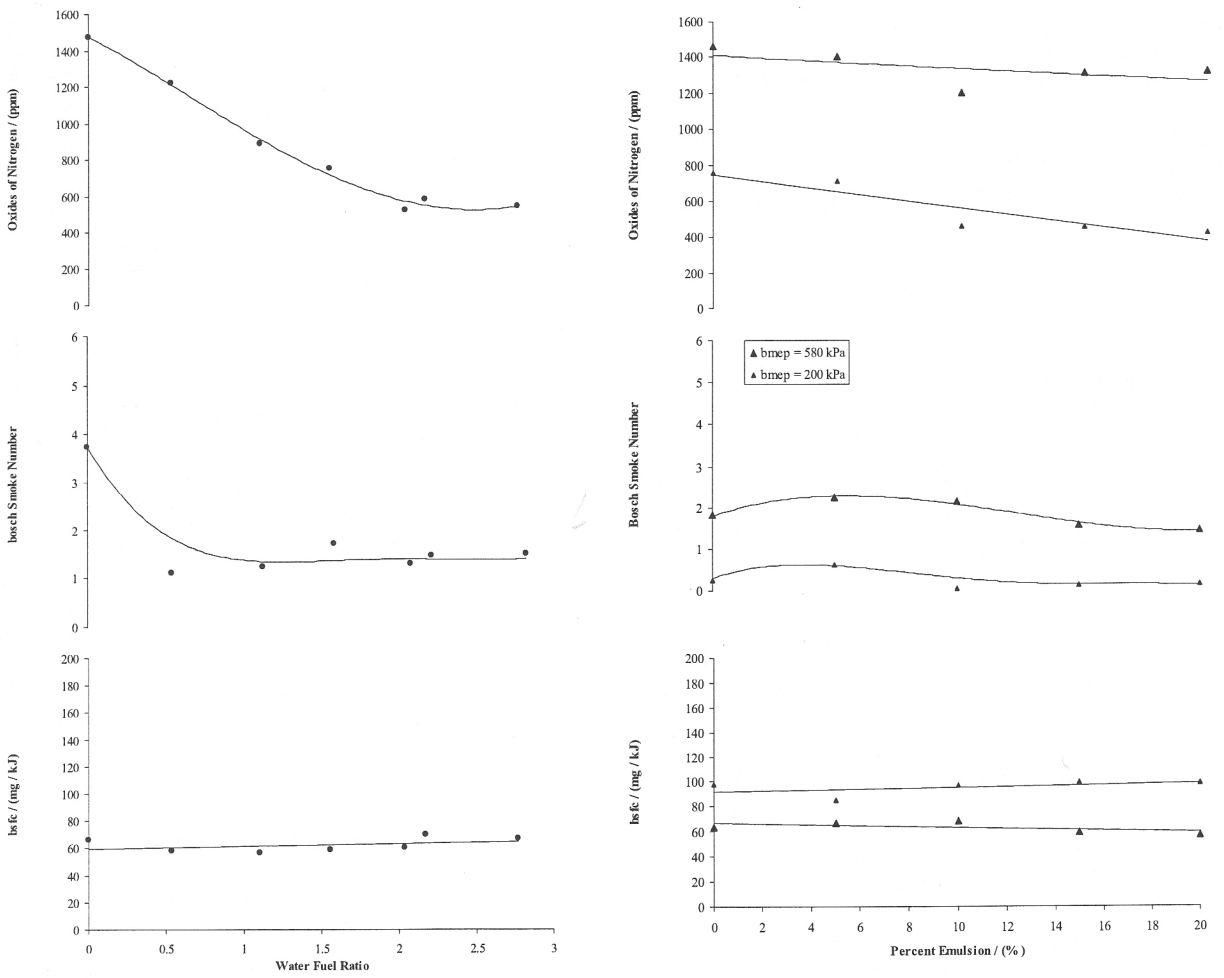

Figure 33. Comparison of emissions and BSFC values for manifold WI and emulsion WI [27]

For the intake manifold water injection, as the water/fuel ratio is increase from 0 to 2.5, we see that the BSFC marginally increases, the Bosch smoke number drops from 3.8 to around 1.5 at 1:1 water/fuel ratio and then remains constant. NOx production rate drops from 1500 ppm to just under 600 ppm at a water/fuel ratio of 2:1 after which it remains constant.

In the case of the emulsion injection, BSFC seems to increase slightly at the 2.0 bar BMEP load, while for 5.8 bar BMEP, remains steady. The Bosch smoke number in this case rises slightly, and then at higher water/fuel ratios, settles down to near original levels. There is very little decrease in NOx formation rate at high load, while at low load, a NOx reduction of around 30% is noted at 20% water/fuel ratio.

The authors note a negligible increase in BSFC for the manifold and emulsion WI while a reduction in NOx production rates of upto 60% are claimed (for the higher load BMEP f 5.8 bars). They do note however a slight increase in smoke. The claimed increase in CO is of 30% from a base value of 300 – 400 ppm and an increase in HC of 30% from a base value of 150 – 200 ppm. The emulsions show a progressive decrease in smoke production at full load but with little reduction in NOx. At part load of 2.0 bars however the reduction in NOx is more evident.

Referencing some other authors for modifications in NOx / PM production levels, it is noted by the authors that their results were at times in close agreement with other research groups, whereas in other cases, the results obtained were markedly different, engine load

levels, emulsion quality and engine types were considered to be the factors responsible for these differences in emission production rates.

A series of tests were done in which results were compared between different WI strategies and EGR to the base configuration. A water/fuel ratio of 1.5:1 was used for intake manifold water injection; a water/fuel ratio of 20% was used for emulsion injection and EGR rate of 16.7% was used. These tests were done for different engine load values varying from a BMEP of 1 bar to 6.5 bars. The results are presented as under in graphical form:

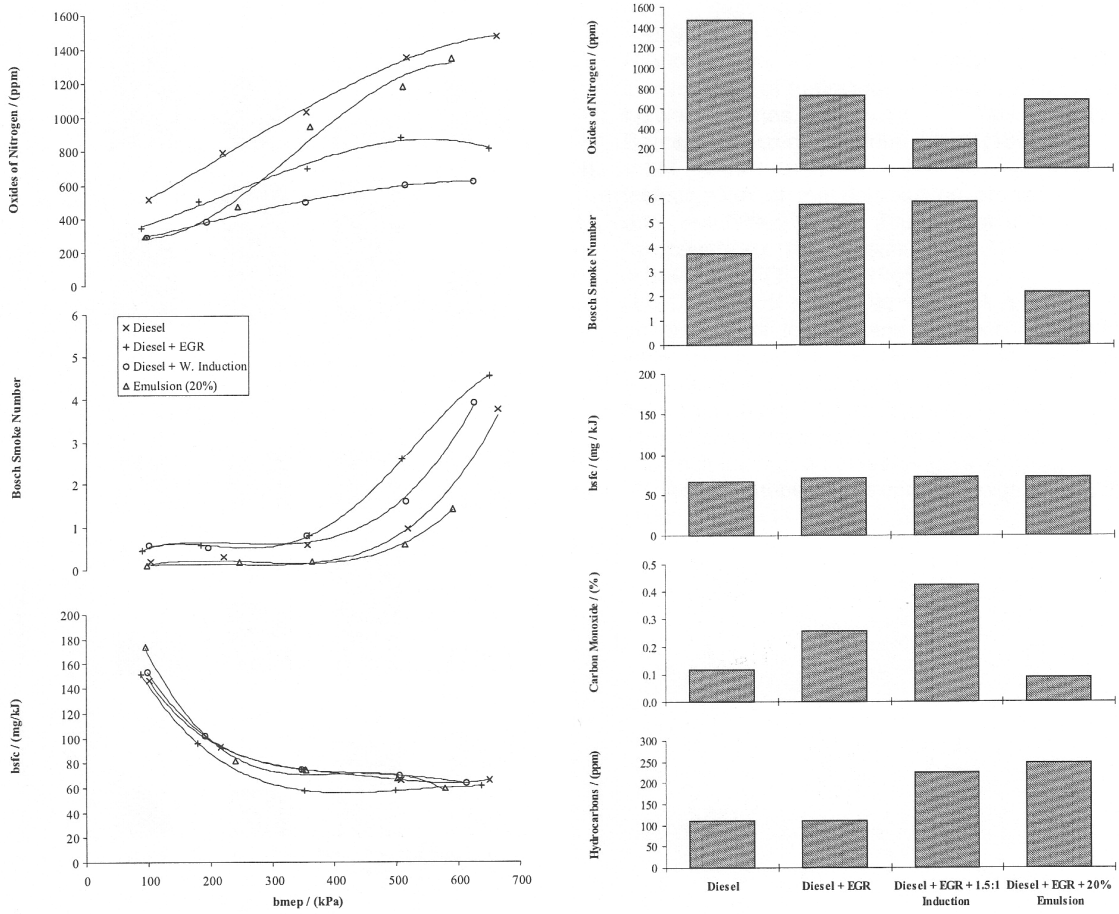

Figure 34. Comparison of Emissions for manifold and emulsion WI, EGR and base configuration [27]

	Diesel	Diesel + EGR	Diesel + EGR + 1.5:1 man. WI	Diesel + EGR + 20% emul. WI
NOx[1]	1500	750	300	750
Red. %	-	50	80	50
BSN[2]	3.8	6	6	2
Red. %	-	-58	-58	47
BSFC[3]	70	70	70	70
Red. %	-	0	0	0
CO[4]	0.12	0.28	0.4	0.08
Red. %	-	-133	-233	33
HC[5]	110	110	240	250
Red. %	-	0	-118	-127

[1] ppm, [2] Bosch Smoke Number, [3] mg/kJ, [4] %, [5] ppm

Table 13. Comparison of results for EGR, Manifold and Emulsion WI and base configuration [27]

The last battery of tests was performed with hot EGR. As noted in the test result **Table 13**, hot EGR was used in parallel with both methods of Water Injection. A noticeable effect of introducing hot EGR was to reduce the ignition delay.

In general, this would have the effect of decreasing premixed burn, reducing NOx and increasing smoke production (this is seen in the tests). Water injection however has a tendency to increase ignition delay due to both reduction in temperature and increase in specific heat of the air charge. Although the increase in ignition delay will have a tendency to increase the NOx production rate, the reduction in temperature would compensate for this and there is a net reduction of overall NOx emissions. In the case of the manifold water injection, the large amounts of water introduced into the engine reduce the temperature considerably, reducing the NOx production rate to a further degree than with emulsion injection.

The effects on the smoke production are a sum of multiple effects. Generally, an increase in ignition delay will reduce the smoke production. However, in the case of EGR, the reduction in available oxygen is detrimental to smoke oxidation, thus the increase in smoke. In the case of water injection, the smoke production rate reduces with emulsion injection, and increases with manifold water injection. In the case of manifold water injection, one can reason that the large quantity of water added to the intake air would increase the specific heat of the intake charge. This would limit the rise in temperature of the charge during combustion, leading to a less “effective” oxidation of smoke, to a limit, negating the advantage of the increased ignition delay. In the case of the emulsion injection however, the water quantity is relatively small, therefore, the increase in specific heat of the charge is negligible. The authors reference works of other researchers in stating that a secondary atomisation is responsible for improved mixing of the fuel with the air charge, thus reducing smoke production.

- Velji et al. [39] have conducted research on water injection on a single cylinder research diesel engine with the following specifications:

Item	Specification
Number of valves	4 – 2 inlet, 2 exhaust
Bore x Stroke (mm)	190 x 120
Engine Speed (RPM)	1500
Compression Ratio	16:1

Table 14. Test engine specifications [39]

The engine is base on a production unit used in stationary and marine applications. Water injection was applied using three methods; emulsion, direct injection into the cylinder and intake manifold injection. The quantity of water injection in relation to the quantity of fuel injected was varied form 0 to 60% (0.6 parts water to 1 part fuel). Unless otherwise noted, results that are presented are presented for full load operation of 20 bars BMEP.

Variations in NOx and Smoke emissions are shown in the graphs below:

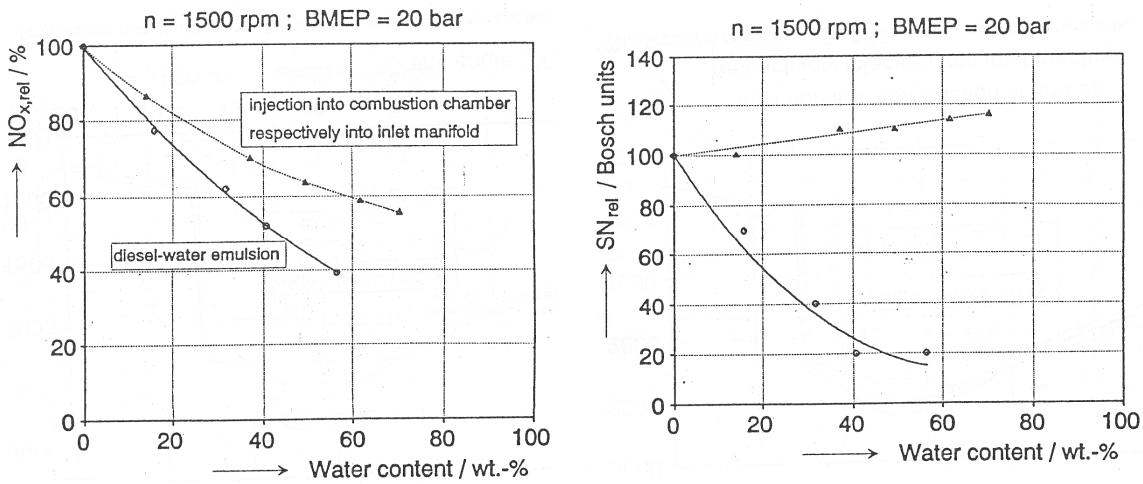

Figure 35. NOx and smoke number variation with varying water injection rates [39]

In general, less water is required in the case of emulsion water injection than with intake manifold water injection. For a 40% NOx reduction, 30% water injection rate required if emulsion is used whereas if direct or intake manifold water injection is used, 60% water injection rate is required.

Using emulsion, the smoke emission drops to 20% of the original value while adding 50% water, while using direct or intake manifold water injection, an increase of 10% in smoke emission is seen with 50% water injection rate.

A two zone combustion model was used to understand the underlying mechanics of why water injection reduces NOx emission rates in diesel combustion. The two zones considered in this model were the pre-flame and post-flame zone. The temperature in the post-flame zone is considered to be the most important factor in determining thermal NO formation. Since 90% of all NOx production is NO and almost all of it is produced in the post-flame zone, it stands to reason that the evolution of temperature in the post-flame zone should be scrutinised closely.

Comparing the temperature profiles in the post-flame zone for intake / direct water injection and for emulsion water injection, it is seen that the temperature reduction is greater when emulsion injection is used. It is considered that in the case of emulsion

injection, the water is present in the zones where the combustion actually takes place, instead of being distributed more or less equally over the whole combustion chamber volume. This presence of water in the appropriate places results in a greater reduction in post-flame temperatures for the same water injection quantity.

The authors have presented two conditions to ensure the highest possible rate of NOx reduction:

- **Injection of water at the right place in the combustion chamber:** The water should be present where there is combustion. This can take place only if the same orifice is used for the injection of water and the fuel. Fuel / water emulsions are one way of achieving this. If water is injected as a mist to the whole of the intake charge, the concentration of water encountered by the fuel jet locally will be relatively low. Therefore, for the same injected water quantity, manifold or direct water injection would be less effective at cooling the combustion, and hence reducing NOx formation.

- **Injection of water at the right time:** NOx production is considered to be at its maximum at the start of the diffusive combustion phase. It is therefore proposed that the water injection take place after the initial ignition delay phase has passed. This would alleviate the problems of increasing combustion delay as water injection rate is increased.

According to the authors, the reduction in smoke may be in part due to the water in the fuel / water emulsion breaking up the spray into smaller droplets. This would mean that the air / fuel ratio in the fuel jet at the start of combustion is nearer stoichiometric (leaner than in case of pure diesel injection) which then results in lower smoke emission. A further reason could be the increase in concentration of OH radicals owing to the presence of water at high temperature. The higher concentration of OH radicals is beneficial to the oxidation of soot in the flame front. The rise in smoke production levels in the case of manifold and direct water injection may be attributed to the decrease in temperature at the start of combustion.

In the case of fuel efficiency, CO and HC emissions, the following results are stated:

- Fuel efficiency is insignificantly influenced by water injection

- In the case of emulsion water injection, CO production is reduced, whereas for the manifold and direct water injection, the CO production rate increases with increasing water injection rate.

- HC emissions rise with rising rates of water injection, with emulsion water injection again influencing HC emissions less than manifold and direct water injection. The HC emissions on the base configuration being so low, the increase for the operating point and water injection rates can all but be neglected.

As noted at the start of the discussion for this paper, the results presented to this point were for full load operation of 20 bars BMEP. Here, some remarks are made for low and part load operation:

- As in the case of the full load operation, the variation in fuel consumption is insignificant for the range of water injection rates considered.

- NOx emissions reduction is the same as at full load.
- In the case of the emulsion water injection, the reduction in smoke emission is similar to full load.
- In the case of the manifold and direct water injection, the increase in smoke emission is proportionally greater than at full load.
- At BMEP of less than 10 bars, the increase in CO emission is quite noticeable, while HC emissions also rise.
- At loads lower than 30% and with water injection rates greater than 30%, engine misfires are recorded.

- Matheaus et al. [34] have conducted tests using Lubrizol's PuriNOx^{TM} Water Injection emulsification product. 4 different fuel/water blends were used. The blends are further explained later in this section. The engine used for testing was Caterpillar 3176 truck engine using 1998 emissions calibration. The injection system is based on a cam driven electronic unit-injector type system capable of a peak injection pressure of 2000 bar with a ramped injection rate. The turbo-charged, aftercooled 4-valve per cylinder engine was considered state of the art for the 1998 year models. Some specifications are given in the table presented below:

Parameter	Value
Number of cylinders	6
Bore	125 mm
Stroke	140 mm
Connecting Rod Length	225 mm
Displacement	10.3 L
Compression Ratio	16.0
Injector Hole size x number of holes x included angle	8 x 0.18 mm x 147°
Swirl Ratio	0.7

Table 15. List of engine parameters used in the tests performed by Matheaus et al. [34]

As concerns the intake air conditions, the temperature set point was at 25° ± 1.7°C, while the humidity was set at 75 ± 5 grains of H2O per lb of dry air – which corresponds to 10.71 ± .71 grammes of H2O per kilogramme of dry air, while the pressure was set at 100 ± 1 kPa (absolute). The temperature of the charge-cooled air was kept at 35°C.

Using the weighting factors used in **Table 16**, an average of the 8-mode emissions data may be calculated, which is representative of the US Heavy Duty – Federal Transient test Procedure (HD-FTP). An example of this calculation, for NOx is shown in **Equation 38**:

$$NOx\left[\frac{g}{hp \cdot hr}\right] = \frac{\sum_{i=1}^{8} W_i NOx_i [g/hr]}{\sum_{i=1}^{8} W_i P_i} \quad \textbf{38}$$

Here, W_i is the weighting factor for each mode (i) listed in **Table 16**, and P_i is the engine output power for each mode. The speed and load points of the AVL 8-mode steady state engine emissions test procedure is presented in **Table 16** [34].

	Weight	Percent	RPM	Percent	Nm
1	0.3501	0	600	0	36
2	0.0634	11	732	25	237
3	0.0291	21	852	63	751
4	0.0334	32	984	84	1304
5	0.0840	100	1800	18	250
6	0.1045	95	1740	40	576
7	0.1021	95	1740	69	994
8	0.0734	89	1668	95	1438

Table 16. Eight-mode Speed and Load conditions [34]

As stated earlier, four types of fuel were used; a baseline Diesel Fuel 2, and three Water / Fuel emulsions. Of these three, the first was the standard formulation of PuriNOx™, the second formulation, CE PuriNOx™, contained the entire PuriNOx™ package plus an additional water based additive (less than 1%) that was designed to improve the combustion quality and thus emissions quality. The third was the SP PuriNOx™ also contains the same additive, but it does not contain the 2-ethylhexyl nitrate that was included in the original PuriNOx™ blend. A summary of the weighted emissions results calculated using **Eq. 38** is presented:

Weighted Emissions [g/(hp-hr)]	Test Fuels			
	DF2	PuriNOx™	CE PuriNOx™	SP PuriNOx™
HC	0.153	0.196	0.118	0.142
CO	0.608	0.865	0.522	0.602
NOx	3.792	3.055	3.312	3.262
NOx + HC	3.945	3.252	3.430	3.404
PM	0.039*	0.033*	0.026*	0.025*
*The weighted PM values are not representative of performance of the engine and fuels on the US HD-FTP, but they should provide a measure of the relative changes between fuels, under steady-state operation				

Table 17. Summary of Weighted Emissions Date [34]

Weighted Emissions [g/(hp-hr)]	Test Fuels			
	DF2	PuriNOx™	CE PuriNOx™	SP PuriNOx™
HC	-	28%	-23%	-7%
CO	-	42%	-14%	-1%
NOx	-	-19%	-13%	-14%
NOx + HC	-	-18%	-13%	-14%
PM	-	-16%	-34%	-36%

Table 18. Changes in the Weighted Emissions Relative to the Baseline DF2 [34]

Fuel	Weighted BSFC [g/(hp-hr)]	Net Heat of Combustion [kJ/kg]	BS Energy Consumption [kJ/(kW-hr)]	Compared to Baseline Diesel
Diesel	224.5	43080	9670	-
PuriNOx™	280.4	34229	9599	-0.7%
CE PuriNOx™	283.5	33941	9621	-0.5%
SP PuriNOx™	279.8	34064	9532	-1.4%

Table 19. Weighted Fuel and Energy Consumption [34]

The weighted brake-specific energy consumption was calculated for each fuel in the same manner as weighted emissions, using **Eq. 38**. The units are kJ/(kW-hr). The brake specific fuel consumption (BSFC) does not provide an accurate assessment of the PuriNOx^{TM} fuel consumption savings because of the water content. The presence of water in the emulsion can be taken into account by multiplying the BSFC by the net heat of combustion, which will give the Brake Specific Energy Consumption (BSEC). These values are presented in **Table 19**. A negative number will signify a reduction in relative value for the fuel type considered. Thus in the case of the BSEC considered, the SP PuriNOx^{TM} gives the best energy consumption savings of 1.4%.

As the heat of combustion is lower for the emulsion mixture as compared to the Diesel Fuel 2, the injection period is increased to compensate. This retards the centroid of the injection rate meaning that the total diesel injection timing is retarded as well. In the case of **Figure 36**, we see that the End Of Injection (EOI) is delayed by around 6° in the case of the emulsion as compared to the Diesel Fuel. The centroid of the injection profile however is shifted by 3.5° for the Mode 8 (**Table 16**) operating condition.

To investigate the influence of differences in the phasing of the combustion processes between DF2 and PuriNOx^{TM} fuel on the engine performance and emissions, two alternative timing strategies were employed (not for CE PuriNOx^{TM} or SP PuriNOx^{TM}). The first strategy was to retard the base injection of the DF2 so that the centroid of the injection would match that of the centroid of the injection profile using the emulsified fuel. In the second case, the injection of the PuriNOx^{TM} emulsion was advanced to match the centroid of the injection profile using the DF2 fuel.

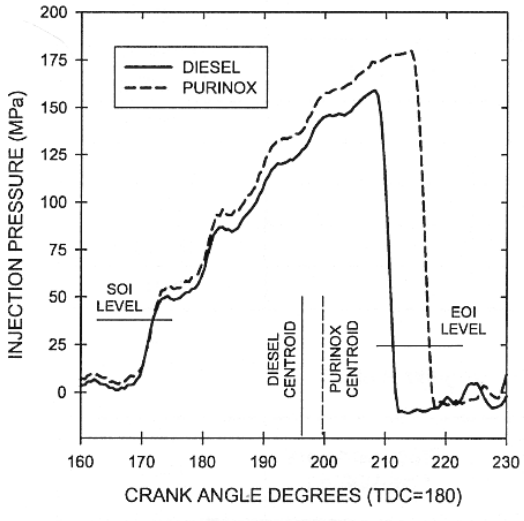

Figure 36. Injection pressure traces for base diesel and PuriNOx^{TM} at 20% for mode 8 [34]

The results thus obtained are presented as:

Weighted Emissions [g/(hp-hr)]	Test Fuels		Percent Change = (PuriNOx™ - Diesel) ÷ Diesel x 100%
	Diesel (Fuel A – Test 1)	PuriNOx™ (Fuel B – Test 2)	
HC	0.153	0.174	13%
CO	0.608	0.728	20%
NOx	3.792	3.446	-9%
NOx + HC	3.945	3.620	-8%
PM	0.039*	0.026*	-32%*
*The weighted PM values are not representative of performance of the engine and fuels on US HD-FTP, but they should provide a measure of the relative changes between fuels, under steady state operation only.			

Table 20. Timing of PuriNOx™ advanced [34]

Weighted Emissions [g/(hp-hr)]	Test Fuels		Percent Change = (PuriNOx™ - Diesel) ÷ Diesel x 100%
	Diesel (Fuel A – Test 2)	PuriNOx™ (Fuel B – Test 1)	
HC	0.155	0.196	26%
CO	0.627	0.865	38%
NOx	3.510	3.055	-13%
NOx + HC	3.665	3.252	-11%
PM	0.039*	0.033*	-17%*
*The weighted PM values are not representative of performance of the engine and fuels on US HD-FTP, but they should provide a measure of the relative changes between fuels, under steady state operation only.			

Table 21. Timing of DF2 retarded [34]

A reduction in a relative value is indicated by a negative value in percentage, while a relative increase is indicated by a positive value in percentage [34]. As can be seen in both cases, the combustion efficiency has a tendency to reduce in the case of the PuriNOx™ mixture as evidenced by the increase in the HC and CO production rates. The CE PuriNOx™ and SP PuriNOx™ formulations showed improved combustion efficiency with lower HC and CO emissions. The NOx emissions reductions were not as large for CE and SP PuriNOx™, but the PM emission reductions were higher.

The following table shows the change in exhaust gas temperature (EGT) due to the DF2 and the PuriNOx™ mixtures.

AVL Mode	1	2	3	4	5	6	7	8
Base	99	205	453	585	276	375	467	553
PuriNOx™	98	201	431	557	263	360	450	541
CE PuriNOx™	103	207	430	553	263	360	447	539
SP PuriNOx™	112	212	425	554	267	362	451	541

Table 22. Comparison of EGTs for various Emulsions compared with straight diesel [34]

In reference to the above table, we see that for higher loads (points 3, 4, 6, 7 and 8), the EGT is reduced when using any of the PuriNOx™ products. For the lower load points (1, 2 and 5) the temperature are either nearly the same, or higher. We can assume from other reasearch that the shift in injection timing has caused the lower load temperatures to go up, while the presence of water in the fuel (and the ensuing increase in specific heat) has reduced EGTs at higher loads.

In summary, the results quoted for Purinox^{TM} 20% water / fuel emulsion by the authors are as follows:

1. NOx emissions reduced by 19% compared to base DF2
2. PM emissions reduced by 16% compared to base DF2
3. With the same start of injection, for both fuels, the energy consumption for the emulsion was 0.7% less than that for base DF2.
4. The CO emissions increased by 42% compared to baseline
5. Combustion improvers can modify the combustion so as to reduce all emissions, however, the tradeoff between NOx and CO-HC-PM emissions.

In light of the data presented, it is important to note that due to weighting of the data, the higher load points' data 6, 7 and 8 are more significant. It is for this reason that the authors of the research article have not included point 1 in the calculation of the weighted emissions. The mechanisms by which water emulsions affect the engine out emissions are likely to be rather complex, at the same time affecting fuel injection rates, spray formation and penetration, ignition and the combustion processes. Some mechanisms are presented below:

- Water is likely to reduce the temperature of the diffusion flame through phase change-cooling and through diluent effects of the vapour-phase water. This reduced diffusion flame temperature is likely to reduce NOx formation rates.
- The water may also act as a diluent in the fuel jet where soot is being formed, thereby reducing the formation rate of soot.
- The presence of supplementary water may affect the chemical kinetics mechanisms of the soot formation and oxidation.
- The presence of water in a fuel emulsion jet may vary the penetration of the said fuel jet. Water having a higher latent heat of evaporation may aid the fuel jet to penetrate further into the hot air charge. This would increase the entrainment of the air charge by the fuel jet.
- The water may affect the stabilisation of the lifted diffusion flame surrounding the combusting diesel jet. The lift-off length of the fuel jet has a significant effect on the soot formation rate. This may lead to a decrease in soot formation for higher load conditions, which have significant fractions of mixing-controlled combustion.

On the following page, a graphical representation of the obtained results presented in **Figure 37** shows the NOx, HC and PM emissions in specific units (g/hp-hr). We see that for high load point 6, 7 and 8, the emulsions reduce NOx emissions as compared to base diesel fuel. In cases of low load and low RPM (high load low-RPM point 3) the NOx emissions are more or less the same between the base diesel and emulsions. In the case of PM production however, except for point 8, all loaded points produced less PM. Especially point 3, which is a medium load low speed point. This point characteristically produces large amounts of PM with base diesel. With emulsion however, the PM production is reduced by around 70%.

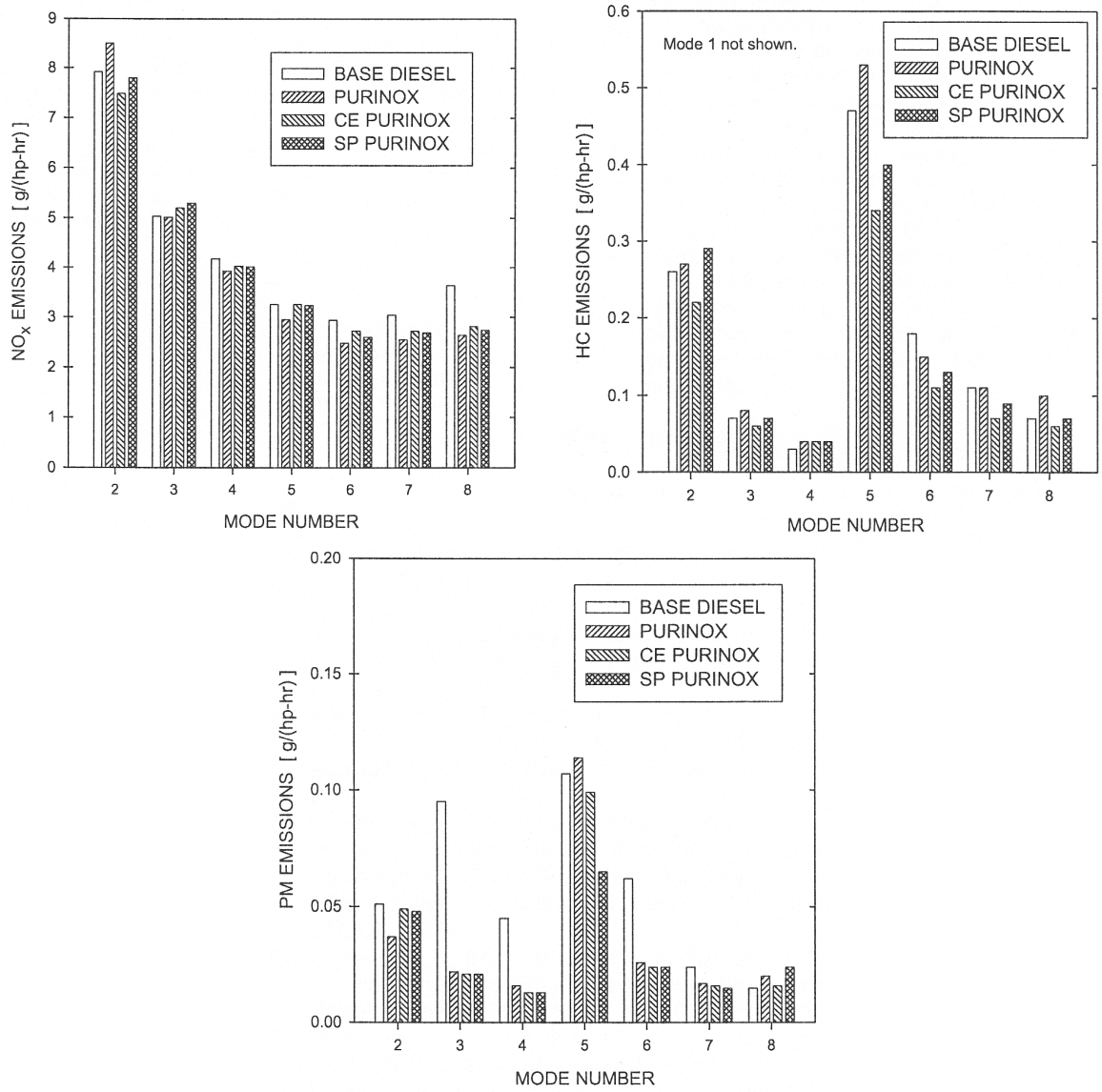

Figure 37. Graphical representation of results of different PuriNOx^{TM} blends for NOx, HC and PM emissions [34]

- Ghojel et al. [51] have conducted test on a HINO industrial 4-cylinder 4 stroke cycle direct injection diesel engine. The engine produces a maximum of 240 N-m of torque at 2400 RPM. The Fuel / water emulsion contains 13% water by mass. The engine testing has been performed at 150 N-m or torque which would place the engine operating condition in the mid- to high- load range.

  To keep the engine power similar in the case of the emulsion and straight diesel fuel injection, the injection parameters were modified from base settings. These settings are adjusted for two different power levels at two different engine speeds and are listed in **Table 23**:

T, Nm	N, RPM	P, kW	Diesel			Emulsion 13%		
			Φ_{inj}, deg	Φ_d, deg	σ, mg	Φ_{inj}, deg	Φ_d, deg	σ, mg
150	1800	28.26	-8.2	8.6	28.5	-6.9	9.9	35.8
200	1800	37.68	-9.1	10.2	36.8	-7.8	12.1	46.0
150	2200	34.54	-6.9	10.3	30.4	-5.0	11.9	37.4
200	2200	46.05	-7.7	12.5	38.6	-6.6	15.4	47.1

Φ_{inj} = Start of Injection, Φ_d = Injection Duration, σ = Mass Injected per stroke

Table 23. Injection system parameters [51]

Figures for NOx and HC emissions and BSFC are presented in the table below:

Ppm	RPM	Diesel		Emulsion		% Reduction	
		150 Nm	200 Nm	150 Nm	200 Nm	150 Nm	200 Nm
NOx	1800	845	1246	582	863	31.12	30.74
	2200	674	873	420	618	37.69	29.21
HC	1800	304	284	38	29	87.50	89.79
	2200	136	96	32	37	76.47	61.46

Table 24. NOx and HC emissions [51]

We see that across the board, we have a roughly 30 percent decrease in NOx production rate at low and high loads and at low and high engine speeds. In the case of PM emissions production rate, we see a nearly 90 percent reduction rate at 1800 RPM while at high RPM; a higher engine load reduces the NOx reduction.

T, Nm	N, RPM	P, kW	Diesel		Emulsion 13%	
			BSFC g/kWh	Brake th. Efficiency %	BSFC g/kWh	Brake th. Efficiency %
150	1800	28.26	217.8	36.73	273.6	36.83
200	1800	37.68	211.0	37.92	263.7	38.22
150	2200	34.54	232.4	34.43	285.9	35.25
200	2200	46.05	221.3	36.15	270.0	37.33

Table 25. Fuel consumption and thermal efficiency variations [51]

- Bertola et al. [52] have studied the effects of water injection on common-rail injected diesel engines. They have chosen to study effects of emulsion injection, with emulsion injection rates of 13, 21 and 30 percent of water to fuel ratios. The engine in question is a 4 cylinder DI diesel engine with a high pressure common rail fuel injection and EGR.

  A few disadvantages are noted however by the authors: 1. Due to the presence of water in the combustion zone, an increase in the ignition delay is noted. 2. Increase in combustion noise and retarded combustion are noted.

The specifications of the engine used for the tests are outlined below:

Engine Type	LIEBHERR D 924 Ti-E A4 4-cylinder 4-Stroke Turbocharged Direct Injection Diesel
Bore	122 mm
Stroke	142 mm
Compression Ratio	17.2
Displacement	6.64 litre
Number of Valves per Cylinder	2
Turbocharger	KKK (Turbine K27.52 – 15.22)
Max. Power Output	183 kW at 2100 RPM
Max. Torque	1060 Nm at 1540 RPM
Max. Speed	2100 RPM
Max. BMEP	20 bar
Swirl	0.65 (Tippelmann)

Table 26. Engine specifications [52]

The fuel tests were conducted with three fuel emulsions and a reference diesel fuel. The properties of the four fuels are given in the following table:

	Water Content $m_W/(m_D + m_W)$ [%]	**Lower Heating Value [MJ/kg]**	**Density [kg/m^3]**	**Stoichiometric Air/Fuel Ratio [kg/kg]**
Reference diesel	0	43.14	819	14.64
Emulsion 13%	12.89	37.98	851	12.98
Emulsion 21%	20.89	34.96	862	12.38
Emulsion 30%	30.17	32.54	871	11.77

Table 27. Fuel properties [52]

Engine operating conditions during the test regime are listed as follows:

Operating Conditions	**Engine Speed [RPM]**	**Engine Load BMEP [bar]**
A25	1250	5
A50	1250	10
A75	1250	15
A100	1250	20

Table 28. Engine operating conditions [52]

In general, the authors note a decrease in NO emissions of which the reduction in thermal NO, they consider that the decrease is due mainly to the reduction of peak flame temperature. In addition to the reduction in NO emissions production, the authors note a decrease in PM emissions across the board for various engine types studied in various research articles. There are a number of reasons stated by the authors: 1. Improvement of air entrainment by the fuel spray. 2. Micro-explosions of the water droplets in the fuel spray (which improves mixing). 3. Increase in presence of OH radicals which is linked to the increase in soot oxidation attributed to the increase in OH radical production.

To maintain a constant power output, and keeping in mind the different energy content of the fuels used as given in **Table 27**, two different injection strategies are put in place to compare the performance results:

Injection strategy A: Constant injection pressure. This results in longer injection duration as the quantity of water in the fuel / water emulsion increases. The quantity of fuel injected into the combustion chamber stays constant.

Injection strategy B: Constant injection duration. This results in a higher injection pressure as the quantity of water in the fuel / water emulsion increases. The quantity of fuel injected into the combustion as in the case of the injection strategy **A** remains constant.

The emissions performance of the test engine is presented in the following tables for each emission type separately – the tests have been grouped into low-load and high-load tests where low-load is represented by the operating points A25 and B25 while the high-load operating points are represented by the operating points A75 and B75:

	Base diesel		**Emulsion 13%**		**Emulsion 21%**		**Emulsion 30%**	
	Val.	**Red. %**	**Val.**	**Red. %**	**Val.**	**Red. %**	**Val.**	**Red. %**
A25	5	-	3.6	28	2.4	52	1.8	64
A75	1.6	-	1.2	25	0.5	69	0.9	44
B25	5	-	2.2	56	1.4	72	0.8	84
B75	1.6	-	1.1	31	0.3	81	0.6	62

Table 29. Test values of opacity for varying emulsion ratios with respect to engine operating parameters [%][52]

	Base diesel		**Emulsion 13%**		**Emulsion 21%**		**Emulsion 30%**	
	Val.	**Red. %**	**Val.**	**Red. %**	**Val.**	**Red. %**	**Val.**	**Red. %**
A25	6	-	5.2	13	4.8	20	4.4	27
A75	7.6	-	6.5	14	5.9	22	5.4	29
B25	6	-	6	0	5.9	1.7	5.9	1.7
B75	7.6	-	6.9	9.2	6.5	14.5	6.6	13.2

Table 30. Test values of NOx for varying emulsion ratios with respect to engine operating parameters [g/kWh] [52]

	Base diesel		**Emulsion 13%**		**Emulsion 21%**		**Emulsion 30%**	
	Val.	**Red. %**	**Val.**	**Red. %**	**Val.**	**Red. %**	**Val.**	**Red. %**
A25	220	-	216	1.8	217	1.4	218	0.9
A75	207	-	210	-1.4	210	-1.4	211	-1.9
B25	220	-	214	2.7	216.5	1.6	219	0.5
B75	207	-	208	-0.5	209	-0.9	209	-0.9

Table 31. Test values of BSFC for varying emulsion ratios with respect to engine operating parameters [g/kWh] [52]

The results obtained from this study are that using emulsion injection, an appreciable decrease in the emissions of soot and NOx is noted. This decrease in the emissions rate is for the most part inversely proportional to the ratio of water to fuel in the emulsion. With these decreases in emissions rates, a negligible decrease in fuel consumption is noted.

There are however, differences to be noted when comparing the two different methods of injection; that is to say, whether the emulsion was injected at a constant duration, or at a constant pressure. When the emulsion is injected at constant pressure, the injection duration is increased. It has been noted that the decrease in NOx emission rate is decreased across the board when fuel is injected at a constant pressure. However, due to the increased

injection and combustion duration, the BSFC is increased to a greater degree as compared to the injection at constant duration. In the case of the constant-duration injection, the decrease in NOx is less marked; however, the decrease in soot emissions is much more marked. This is accompanied with the fact that the BSFC increases only slightly, both for the low load and high load conditions.

- Kegl et al. [31] have conducted test on a truck engine to compare two different methods of water injection; the first in which the water is injected into the air stream during aspiration and the second in which the water is injected directly in the cylinder via the injectors in the form of a fuel / water emulsion. The first system has been divided into three variants however, and they are listed below:

    - **Multipoint injection into the intake manifold** – This system is similar to the fuel injection system found in indirect multipoint injection spark ignition engines. It comprises of one injector per cylinder each of which is fired when the intake valve is open and closed before the intake valves closes.

    - **A mono-point injection before the turbocharger** – A simple arrangement where the water spray flowing into the turbocharger is dispersed into droplets and evenly mixed with the intake air.

    - **A mono-point injection after the turbocharger** – A relatively simple arrangement similar to the outlined above. There are plenty of choices for the positioning of the injector in the intake stream; both in terms of direction and in terms of position along the intake tract.

    - **Fuel / water injection directly into the combustion chamber** – The emulsion in question is composed of fuel, water and a surfactant to enhance the stability of the emulsion. In this research article, the authors have evaluated the fuel / water ratio relative to the volumes of the two components. The authors make reference to the fact that due to the presence of water droplets in the fuel jet, during combustion, micro-explosions can be witnessed due to the sharp evaporation of the said water droplets under the influence of high temperature.

  The engine used in the test is a four-cylinder air cooled Direct Injection diesel truck engine with a displacement of 7118 cm^3 with a maximum power output of 150 kW and 315 Nm. Concerning the torque output, the measurement point given in **Figure 38** shows a BMEP of 14 bar, which corresponds to a torque output of 793 Nm. The 315 Nm note could be a misprint and the engine actually produces either 815 or 915 Nm or torque. Tests on the four water injection systems were performed to evaluate the effectiveness of each system and study the effects. Here, results are presented for the change in percentage of NOx and PM emissions for water / fuel volume ratios of 5, 10, 15 and 20 percent. The engine operating conditions are given in the legend for each set of test graphs (the graphs are drawn in the order:

    i. Multipoint

    ii. Monopoint after TC

    iii. Monopoint before TC

    iv. Water / Diesel emulsion

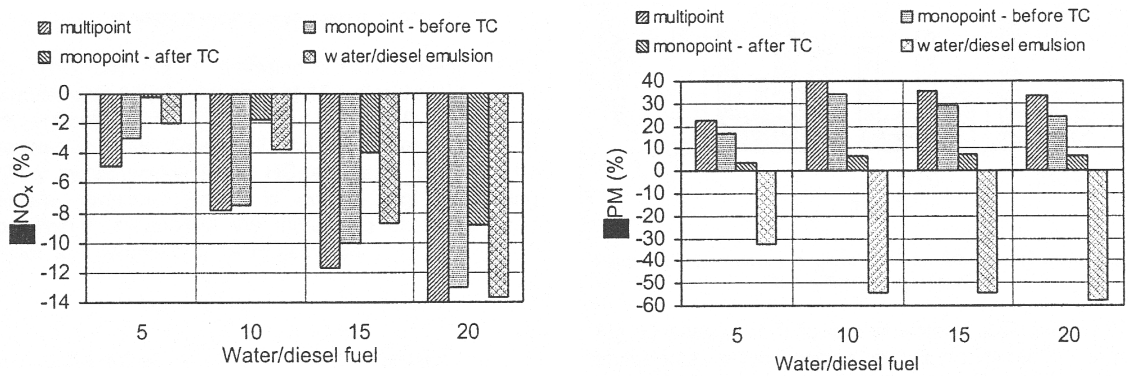

Figure 38. NOx and PM reduction rates for the operating point:
N = 1300 RPM, BMEP = 14 bar, BSFC = 210 g/kWh [31]

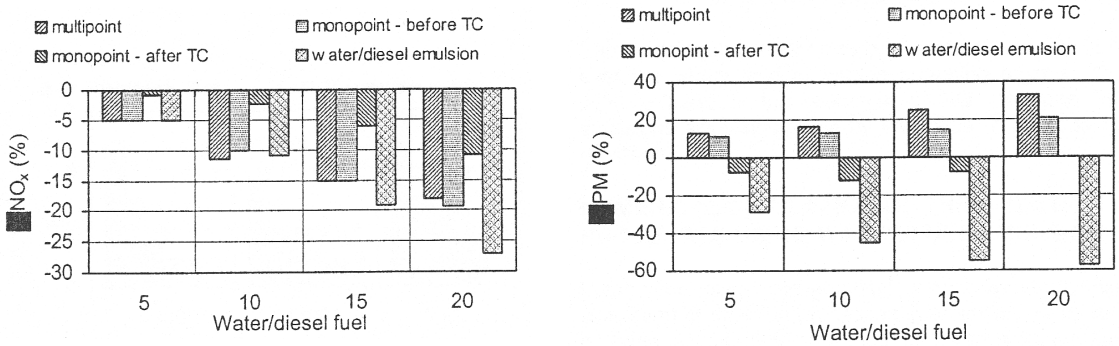

Figure 39. NOx and PM reduction rates for the operating point:
N = 2150 RPM, BMEP = 14 bar, BSFC = 230g/kWh [31]

As can be seen from the results of the test, the water / fuel emulsion is clearly the best compromise to reduce NOx and PM emissions. It has to be noted that at low speed (1300 rpm – as shown in **Figure 38**), multipoint water injection into the intake manifold is marginally better performing as concerns the NOx emissions reduction performance. However, the trade-off in the PM reduction rate for the water / fuel emulsion is such that the reduction in PM can compensate for the lower reduction in NOx emissions. The results shown for NOx and PM reduction show a decrease in performance for the monopoint injection after turbocharger. The authors have not given any reasons why this may be the case.

If we rank the three water injection techniques using injectors, we see that the multipoint system is the most effective at reducing NOx, followed by the monopoint before turbocharger and the monopoint after the turbocharger. On the other hand, for PM increase, the least increase in PM is incurred using the monopoint after the turbocharger, while the monopoint before the turbocharger produces slightly more PM while the multipoint produces the most of the three. The authors have not supplied a plausible reason why this may be.

Seeing that the water / fuel emulsion is generally the most effective at reducing PM and NOx emissions, a further study was performed to broaden the scope of results for varying water injection ratios, engine speeds and engine loads. In the following tests, engine speeds of 1300, 1700 and 2100 RPMs are used. The water injection ratios are of 0, 10 and 15 percent water / fuel by volume. BMEP values are of 5 and 8 bars. The series of graphs from left to right are:

i. Diesel, 8 bar BMEP

ii. 10 percent water / diesel, 8 bar BMEP

iii. 15 percent water / diesel, 8 bar BMEP

iv. Diesel, 5 bar BMEP

v. 10 percent water / diesel, 5 bar BMEP

vi. 15 percent water / diesel, 5 bar BMEP

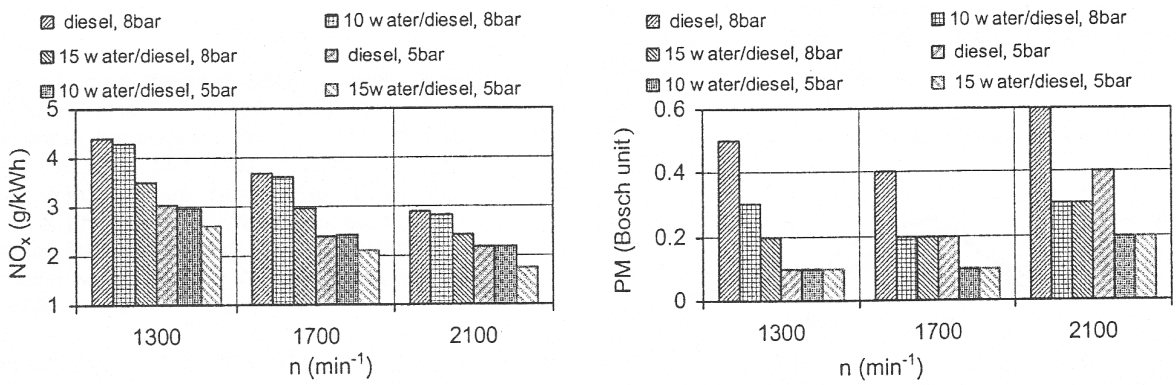

Figure 40. NOx and PM emissions reduction percentages [31]

Judging the values presented by Kegl et al. [31], it is clear that emulsion injection is better than other means of water injection at all the studied load and RPM values and is effective at even low water / fuel ratios.

- Musculus et al. [53] have studied the effects of water in a fuel / water emulsion on the injector spray and combustion characteristics in a Direct Injection diesel engine. Their tests were performed using two fuels, the first being straight N° 2 diesel fuel named D2 and the other a Fuel / Water emulsion with quantity of water being 20% by mass named W20 in the literature.

  Analyses and measures taken of the fuel jet have shown that at the operating conditions noted, the emulsion showed an increase in liquid length of 40-70%. Combined with lower temperatures and / or pressures in the combustion chamber, it is entirely possible that the fuel jet may strike a combustion chamber wall or piston crown, leading to increased PM, HC and CO emissions because of poor mixing.

  Using the natural chemiluminiscence of the diesel spray, the researchers have shown that the ignition delay of the emulsion is 30 – 60 % greater than that for pure diesel and that the ignition occurs 30 – 40 % downstream in the jet. As a result of this, considerably greater mixing occurs for the emulsion, leading to an increase in the air / fuel ratio for the initial premixed burn, which should decrease the soot formation during the initial premixed burn. The diffusion flame lift-off for W20 was consistently 20-60% longer than that for D2 at the tested operating conditions. This increase in the lift-off length allows increased entrainment of air in the fuel jet leading to leaner mixtures being formed during the mixing controlled combustion phase. This should decrease the production of soot during combustion assuming that there is no fuel impingement on the combustion chamber walls or the piston crown.

The tests were performed on a single cylinder engine with optical access, based on a Cummins N-series direct injection, 4-stroke cycle diesel engine. The specifications of the original engine are presented in **Table 32**:

Engine base type	Cummins N-14, DI diesel
Number of cylinder	1
Cycle	4 stroke
Number of intake valves	2
Number of exhaust valves	1*
Combustion chamber	Quiescent, direct injection
Bore	139.7 mm
Stroke	152.4 mm
Bowl width	97.8 mm
Displacement	2.34 litres
Connecting rod length	304.8 mm
Piston pin offset	None
Geometric compression ratio	10.7:1
Simulated compression ratio	16:1
Fuel injector type	Cummins CELECT^{TM}
Design	Closed nozzle, unit injector
Number of hole x diameter [mm]	8 x 0.194
Length / diameter of holes [l/d]	4.1
Angle of fuel-jet axes from firedeck	14°

* In this optically accessible engine, one of the two exhaust valves of the production cylinder head was replaced by a window and periscope

Table 32. Engine and injector specifications [53]

For all operating conditions, cylinder pressure, fuel injector pressure, and injector needle lift data were digitized and recorded at half Crank Angle Degree (CAD) increments. The Apparent Heat Release Rate (AHRR) was calculated from ensemble-averaged pressure data using and air-standard first-law analysis [1].

Although ignition reactions have been considered to occur before the zero crossing of the AHRR, in this article, the Start Of Combustion (SOC) is defined as the time of the first zero-crossing after the pre-combustion AHRR depression due to fuel evaporation. The ignition delay is defined as the time between the Start Of fuel Injection (SOI) and SOC in CAD. The premixed burn fraction was defined as the fraction of the integrated AHRR that occurred between the SOC and the location of the minimum in AHRR between the premixed burn spike and the mixing controlled burn.

The averaged needle lift data accompanied with AHRR data for both fuels is presented in the following **Figure 41**. The thin line represents the needle lift, while the shaded areas represent the AHRR for the two fuel types. The area bounded by the dotted line is the W20 AHRR, whereas the area bounded by the solid line is the D2 AHRR. The integrated values of AHRR and the gross Indicated Mean Effective Pressure (gIMEP) measured in kPa are also shown in the small tables accompanying the graphs.

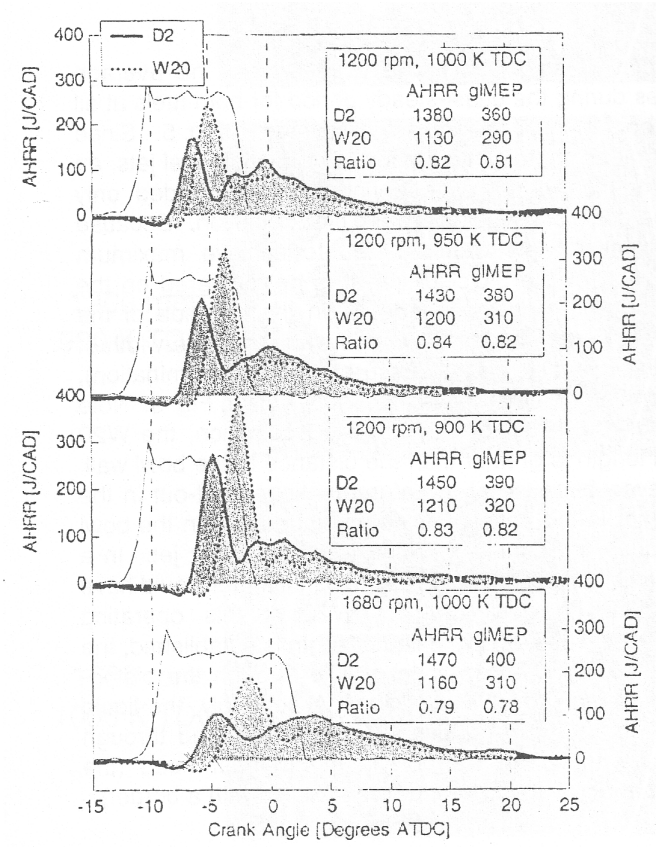

Figure 41. Needle lift, AHRR, integrated AHRR, and gross IMEP [53]

For all three operating points of 1200 RPM, the ignition delay for W20 was consistently greater than for D2 by ca. 40%, leading to greater premixed burn fractions. At the 1680 RPM operating point, the ignition delay is even greater, going to 65% over that of D2. As a result the energy released during the premixed burn for the 1200 RPM operating points was 50% greater than that of D2 and almost twice that for the operating point at 1680 RPM. This result is consistent with the increased ignition delay observed with W20. Although, the total fuel energy content for W20 is only 83% that of D2, the longer ignition delay results in significantly greater premixing of fuel and air prior to ignition, resulting in a much greater premixed burn fraction. In the following table, the operating points are listed with different test results.

Operating Condition	**1**		**2**		**3**		**4**	
Fuel	**D2**	**W20**	**D2**	**W20**	**D2**	**W20**	**D2**	**W20**
Engine Speed [RPM]	1200		1200		1200		1680	
Motored TDC Air Temperature [K]	1000		950		900		1000	
Motored TDC Air Density [kg/m^3]	16.6		16.6		16.6		16.6	
Intake Air Temperature [K]	426		405		383		426	
Intake Air Pressure [kPa]	189		180		171		189	
Actual Start Of Injection [CAD ATDC]	-11.5		-11.5		-11.5		-10.5	
Duration Of Injection [CAD]	9.5		9.5		9.5		12	
Peak Injection Pressure [MPa]	82		82		82		115	
Mean Injection Pressure [MPa]	71		71		71		88	
gIMEP [kPa]	360	290	380	310	390	320	400	310
Ignition Delay [CAD]	3.1	4.4	3.7	5.4	4.6	6.5	3.5	5.8
Integrated AHRR [J]	1490	1230	1570	1320	1610	1330	1650	1320
Premixed Burn Fraction [%]	26	48	32	58	39	71	21	50

Table 33. Experimental Matrix [53]

The article goes on to explain the affect the cylinder combustion mechanism has on engine-out emissions, and their difference when using either W20 or D2 as a fuel. Musculus et al. [53] have conducted tests on a Caterpillar 3176 engine, the type used by Matheaus et al. [34] to compare different formulations of a 20% water/fuel emulsion. The results for the W20 are presented in the following table, with the change in emission production shown as a percentage difference.

AVL Mode	**Weight**	**Load [%]**	**Speed [%]**	**TDC Density [kg/m^3]**	**TDC Temperature [K]**	**Premixed Burn Fraction [%]**	**Predicted Liquid Length [mm]**	**Change in Modal Emissions from D2 [%]**			
								HC	**PM**	**CO**	**NOx**
1	0.350	0	Idle	19	816	98.5	54	140	580	230	-48
2	0.063	25	11	19	814	89.4	54	1	-27	7	-7
3	0.029	63	21	23	835	13.2	45	22	-77	-65	0
4	0.033	84	32	34	835	4.1	36	54	-65	-74	-6
5	0.084	18	100	24	835	42.7	45	12	7	46	-9
6	0.104	40	95	27	835	10.8	38	-18	-58	14	-16
7	0.102	69	95	19	835	3.8	31	-2.5	-32	24	-16
8	0.073	95	89	16	835	1.5	28	42	-30	180	-28

Table 34. Steady state emissions test results for W20. (negative values for percentages indicate decrease) [53]

The flame lift-off length for W20 is in all cases longer than that for D2 for all operating conditions, after the diffusion flame is established. There is more cycle-to-cycle variation as well. In both cases (D2 and W20), the lift-off length is observed to advance upstream as soon as the diffusion flame is established. This result is compared to that obtained by Higgins and Siebers [10], who have shown that the flame lift-off length reduces as the in-

cylinder temperature rises. It is entirely plausible that the flame lift-off may be affected by either the entrainment of hot products into the jet, or by the rise in the bulk temperature of the in-cylinder gases. The entrainment effect is hard to quantify, however, the increase in bulk temperature of the in-cylinder gases can be estimated from the in-cylinder pressure measurement. Since the W20 ignition is delayed in comparison to that of D2, the reduction in flame lift-off length is phased later for W20 than for D2. Comparisons of lift-off lengths and other flame parameters are outlined in the following **Table 35**:

Operating Condition		**1**	**2**	**3**	**4**
Engine Speed [rpm]		**1200**	**1200**	**1200**	**1680**
TDC Air Temperature [K]		**1000**	**950**	**900**	**1000**
Average Lift-Off [mm]	D2	9.2	9.9	12.9	10.3
	W20	**11.5**	**13.4**	**21**	**12.8**
Upswirl Lift-Off [mm]	D2	11.3	11.5	15.8	11.8
	W20	**13.5**	**16.5**	**25.3**	**16.4**
Downswirl Lift-Off [mm]	D2	7.1	8.3	10.2	8.7
	W20	**10.1**	**10.7**	**16.7**	**9.2**
Assymetry [%]	D2	23	16	22	15
	W20	**17**	**23**	**20**	**28**
Φ_{AF} at Lift-Off	D2	16.5	14.6	12.5	13.7
	W20	**10.2**	**8.4**	**5.5**	**8.3**
Φ_{OX} at Lift-Off	D2	16.5	14.6	12.5	13.7
	W20	**6.5**	**5.8**	**4.3**	**5.8**

Table 35. Quasi-steady flame lift-off parameters

The average lift-off length is the average of all flame lift-off lengths over the quasi-steady ignition period. The upswirl and downswirl lift-off lengths are due to the swirl present in the combustion chamber, which also results in the asymmetry of lift-off lengths. The equivalence ratio Φ_{AF} (Air/Fuel) and Φ_{OX} (Oxygen) for the D2 fuel is the same since there is no diluent, whereas in the case of the W20, water acts as the diluent which reduces the equivalence ratio when reasoned in terms of available oxygen.

In view of the experimental and model results, the authors are of the opinion that fuel water emulsions have the capability to reduce PM and NOx production at the same time. The NOx benefit is more or less present at almost all operating conditions owing to the reduction in flame temperature. Improvements in PM are achieved through physical processes of increased fuel / air pre-mixing in both the premixed burn and the mixing-controlled combustion phases. This enhanced fuel / air mixing however is accompanied by an increase in the ignition delay, which may increase the engine noise output. In addition to this, the reduction in PM value at high and medium load operation may be countered by high PM, HC and CO production rates at low load, where the fuel spray may impinge on the in cylinder surfaces.

- A report written by Fleetway Inc. [18] for the Transportation Development Centre of Transport Canada gives general values for the comparison of NOx reduction for different technologies. These technologies vary from physical changes in the engine to exhaust after-treatment systems:

Method	NOx red. %
Primary	
Retarded Fuel Injection	2-3
Reduced Scavenge Air (two strokes)	5
Common Rail Injection	20
EGR (Exhaust Gas Recirculation)	50
WaCoReG (Water Cooled Rest Gas)	70
WIS (Simple Charge Air Water Injection System)	30
CASS (Combustion Air Saturation System)	10-30
HAM (Humid Air Motor)	50-80
DWI (Direct Water Injection)	20-50
FWE (Fuel – Water Emulsions)	10-50
Secondary	
SCR (Selective Catalytic Reduction)	75-95
Wet Scrubber	15
Non(Thermal Plasma	90

Table 36. Average NOx reduction values for different emissions control systems [18]

	Relative NOx Reduction	Effect on PM Emissions	Variability of Water Addition	Effect on Cold Start	Lubricating oil Dilution	Expense
Inlet Manifold Water Injection	-	--	+	none	--	-
DWI – Separate Nozzle	-	--	++	none	-	--
Diesel Fuel / Water Emulsion	+	++	--	-	-	-
Stratified diesel – water – diesel injection	++	++	++	none	none	--

Table 37. Evaluation of different Water Injection systems [18]

The effects of water have been divided into three main types according to the authors; dilution, thermal, and chemical effects. If the water is injected as a liquid, a supplementary effect due to the evaporation will also be included.

The authors take great pains to differentiate between the dilution effects and thermal effects of water injection. According to them, some definitions of the thermal effect account for not only the increase in the specific heat of the air / water mixture, but also the addition of mass of water in the combustion chamber. In this case, the dilution effect would only consider the dilution effect of the increase in mass of water in the reacting species which would modify the combustion reactions. Other definitions of the thermal effect consider only the increase of the specific heat capacity of the gases and include the increase in diluent (water) mass in the dilution effect.

Different literature surveys were done by the authors to clarify the effect of water vapour, CO_2 and other diluent gases on the production of NOx. It was determined that the most

important effect was the dilution effect on the peak flame temperature which then reduced the NOx emissions. For water, the thermal effect (increase in specific heat) was not insignificant, resulting in 15% of the total NOx reduction. The chemical effects however, for the tests under consideration were small.

They clarify that the working definition of dilution effect would account for both the differences in concentration and the extra mass and increased heat capacity for the non-oxygen gas which do not actively take part in the combustion. Even if the total heat capacity of the gases in the cylinder has not significantly changed, diluting the intake air with diluent shifts some of the heat capacity from the oxygen to the non-oxygen gases which do not actively take part in the combustion. The decrease in the proportion of oxygen in the gas mixture for the same overall specific heat capacity means that the peak flame temperatures are reduced, thus the reduction in NOx emission production rates.

The authors refer to the works of Ladommatos et al. [22]. While their studies suggest that the chemical effect of adding water is negligible, the type of engine used for their studies was an automotive high speed direct injection diesel engine, and hence the chemical effect may not be negligible in the case of slow speed marine engines – the target of the study in this research report. During combustion, water promotes the production of OH radicals through the reaction:

$$\mathrm{O} + \mathrm{H_2O} \leftrightarrow \mathrm{OH} + \mathrm{OH} \quad \textbf{39}$$

And inhibits OH consumption through the reaction:

$$H_2 + OH \leftrightarrow H + H_2O \quad \textbf{40}$$

This serves to reduce the concentration of O radicals especially in the flame zone where super-equilibrium concentrations of O are present and increases the concentration of OH.

The thermal NO mechanism is the most sensitive to temperature, therefore the dilution effect will be the most significant for reducing thermal NO since it results in a decrease in the peak flame temperatures. Based on numerical studies of coaxial diffusion air / methane flames, adding water to the air side is more effective than adding water from the fuel side. In the case of counterflow diffusions flames, a similar effect is noted. A greater quantity of water can be present in the flame zone if it is added from the air side.

The N_2O and prompt NO mechanisms are much less sensitive to temperature than the thermal NO mechanism. The N_2O and prompt NO mechanisms are affected to a greater degree by dilution than the thermal NO mechanism. The chemical effect of water on the prompt NO mechanism is mainly a result of increased OH. OH promotes the oxidation of hydrocarbon radicals and therefore inhibits the prompt NO inhibition reactions such as:

$$CH + N_2 \leftrightarrow HCN + N \quad \textbf{41}$$

The chemical effect on the N_2O mechanism can arise from reductions in O radicals. The NO formed via this mechanism forms rapidly in the flame zone where super-equilibrium O concentrations occur. Any reductions in the in flame zone O concentration levels will suppress the initiation reactions such as:

$$O + N_2 + M \leftrightarrow N_2O + M \quad \textbf{42}$$

The absolute value of the super-equilibrium concentration of O in the flame zone decreases as water in the flame zone increases. However, the decrease is less than the equilibrium concentration in the post flame gases. This implies that the relative contribution of NO

from the N_2O will increase compared to the thermal NO as the quantity of water increases in the flame zone.

1.3.3. Résumé of Effects of Water Injection on combustion and emissions:

The effects of WI on diesel engine combustion can widely be divided into the following groups:

a. Thermal effects

b. Dilution

c. Chemical effects

These effects are identified according to the physical change they bring to the combustion, and are identified below, giving a consolidated view of the results of various researchers presented in the previous sub-section.

1.3.3.1. Thermal Effects:

In the case of manifold water injection, evaporation cooling may take place reducing the temperature of the inlet air charge. This increases the density of the charge and potentially the air mass flow into the engine. For a diesel engine, this would mean more air available for the fuel.

The decrease in temperature of the intake charge also reduces the starting temperature when fuel is injected. Generally, a reduction in temperature has a tendency to increase the ignition delay, the lift-off length, the liquid length and the proportion of fuel that will burn in premixed combustion. Siebers et al. [9] note that the decrease in temperature increases the lift-off length which in turn decreases the equivalence ratio at the lift-off length thus reducing the propensity to soot.

A second phase of the thermal effect happens inside the cylinder. In this case, the presence of water vapour causes a rise in the specific heat quantity of the intake charge. This usually results in lower combustion temperatures and lower NOx emissions [18, 24, 26, 28, 29, 30, 3, 31, 32, 33, 34, 37, 39, 52, 53]. It has been found that the rise in specific heat capacity of intake air charge is higher for water vapour than for CO_2 when compared on a mass basis [22].

Water injection may increase the specific heat capacity of the intake air charge. An increase in the intake air charge specific heat may increase the ignition delay of the fuel jet. In actual fact, the change in specific heat capacity with the introduction of CO_2 or H_2O vapour has been found to be rather minor [22].

In the case of in-cylinder water injection, the water droplets reduce flame temperatures due to evaporation thus reducing NOx emissions [18, 23, 26, 27, 3, 31, 32, 33, 34, 39]. Even if the water evaporates during the compression process, the temperature of the charge in the combustion chamber as fuel is injected will be lower as compared to dry air.

In the case of emulsion injection, Matheaus et al. [34] propose that the temperature of the diffusion flame is likely to reduce resulting in a reduction in the formation rates of NOx emissions. In addition, the reduction of temperature in the core of the fuel jet during the soot

formation process is likely to reduce the soot formation rates [34]. These effects have been confirmed by various other researchers and research groups [27, 3, 31, 33, 39, 51, 52, 53]

1.3.3.2. Dilution Effects:

Introducing an inert medium (gas or liquid) to a combustion mixture will reduce the concentration of oxygen per unit volume or mass of charge.

The dilution effect in general reduces NOx production. When dilution takes place, the fuel jet has to take in a greater volume of air charge since the lower proportion of oxygen in the air charge causes the combustion process to slow down, and the fuel jet continues to entrain the air charge for a longer period of time. This results in a greater mass of gas for the same fuel quantity which has a tendency to reduce the peak flame temperature [18, 26, 27, 3, 32, 34, 47, 48] thus reducing thermal NOx emissions.

In the case of an emulsion, the air entrainment is similar to that of neat fuel jet in the same air charge. The overall air / fuel ratio in the jet will however be higher since in the same volume of emulsion, a lower quantity of fuel is present. This will potentially reduce the PM production rate [3]. The quantity of gas entrained per unit mass of fuel being increased, the specific heat capacity of the gas mixture will have increased and potentially, the NOx production rate may be decreased.

Emulsions tend to have longer ignition delay periods as compared to neat diesel fuel [16]. It has been seen that as the water/fuel ratio is increased, the ignition plume becomes less luminous, indicating a reduction in sooting. This is verified by the overall soot formation rate at exhaust. The phenomenon of micro-explosions as described earlier promotes the mixing of the air/fuel jet and is considered to increase the volume of air mixed in the plume. This would presumably limit the peak flame temperatures and limit NOx formation rates.

Emulsions can also cause an increase in the in-cylinder penetration of the fuel jet [18, 26, 3, 33, 34, 39, 52, 53]. The high latent heat of vaporisation of water increases the time required for vaporisation, thus increasing the entrainment of air by the liquid fuel jet. A secondary effect of this may be that the fuel jet touches the cylinder walls. In addition to this, the lift-off length is changed significantly as well. In general, it increases as the ratio of water to fuel increases. An increase in lift-off length is credited with decreasing the soot formation rate as well [34].

In the case of emulsion injection, micro-explosions may be apparent in the fuel spray that decrease the size of fuel spray droplets further, increasing the energy transfer between the compressed air charge and the fuel. These micro-explosions also have been noted to improve the oxidation of hydro-carbons, reducing the emissions of PM [23, 27, 3, 32, 34, 52, 53].

1.3.3.3. Chemical Effects:

Due to the generation of heat during combustion, certain diluents may dissociate to form more reactive specie that can aid in the reduction of certain pollutant emissions. In the case of water vapour, the dissociation of H_2O into H and OH radicals has been tested experimentally to reduce soot formation for a pre-mixed laminar flame [25]. For water vapour addition in a diesel engine, Ladommatos et. al [22] have conducted experiments to isolate chemical effects of water vapour. Their findings indicate an increase in PM emissions with the addition of water vapour in the intake charge. The intake charge was prepared such that thermal and

dilution effects on the combustion would be negligible. CO_2 on the other hand, seemed to reduce PM emissions.

It appears that the formation of NO is suppressed in the presence of OH radicals [50]. These OH radicals are formed by thermal decomposition of H_2O during combustion. This is in addition to the suppression of NO formation by limiting the peak flame temperature.

The bibliographic study produced in this chapter shows us the complexity of the diesel combustion and recall the principal processes. NOx and solid particle production have especially been given attention.

In the second part, the experimental and numerical work related to the use of water injection for reduction of pollutant emissions has been condensed and analysed. The following assessments can be made:

- ✓ *First and foremost, it appears that a multitude of technologies exist. Water can be injected in the intake manifold, directly into the cylinder via a separate injector, via the same injector as a stratified mixture, or even as an emulsion.*
- ✓ *In all cases, a drop in NOx emissions is observed, however for the same technology, the relative reduction varies from one case study to the other*
- ✓ *As for the effect of water injection on PM emissions and the efficiency (specific consumption) of the engine, results vary both in a qualitative and quantitative manner with respect to the manner in which water has been injected, and for the same technology, from one case study to the other.*
- ✓ *The engine load seems to play an important role in the obtained results, but for the most part, studies are made on engines at higher values of load. In addition, they concern large displacement industrial or stationary engines, or in some cases, automotive powerplants of relatively older technology.*
- ✓ *In the end, some of the analyses presented are not conclusive, and it would seem that there are a multitude of effects of water injection, thermal effects, chemical, dilution etc.*

In light of these elements of the study, it would be interesting to perform a detailed study on a modern automobile diesel engine to try and separate the different effects of water injection and to make a comparison with a traditional means of engine out pollutant emissions control system – exhaust Gas Recirculation (EGR). Water injection via the intake is considered for study, for reasons of simplicity. The planned limits of water injection are however much higher than those used traditionally to better define the limits of the process.

L'étude bibliographique menée dans ce chapitre a permis de monter la complexité de la combustion Diesel et d'en rappeler les principales étapes. Une attention particulière a été portée à la formation des espèces polluantes NOx et particules solides.

Dans un deuxième temps, les travaux expérimentaux et numériques relatifs à l'utilisation de l'injection d'eau pour réduire les émissions polluantes des moteurs Diesel ont été recensés et analysés. On retiendra :

- ✓ *Il apparaît tout d'abord que plusieurs technologies existent : l'eau peut être injectée dans l'air d'admission, directement dans le cylindre à l'aide d'un injecteur spécifique ou d'un injecteur eau / gazole commun, ou bien encore en émulsion avec le carburant.*
- ✓ *Dans tous les cas une baisse des émissions de NOx est observée, mais pour une même technologie, la diminution relative varie d'une étude à l'autre.*
- ✓ *Concernant les effets de l'eau sur les émissions de PM et le rendement du moteur (consommation spécifique) les résultats varient quantitativement et parfois qualitativement en fonction du mode d'introduction de l'eau, et pour une même technologie, d'une étude à l'autre.*
- ✓ *La charge du moteur semble jouer un rôle important dans les résultats obtenus, mais la plupart des études s'intéressent surtout aux charges élevées. En outre, elles concernent le plus souvent des moteurs industriels ou utilitaires, ou bien encore des moteurs automobiles de conception ancienne.*
- ✓ *Enfin, l'analyse des résultats est parfois partielle alors qu'il apparaît que les effets de l'eau sont multiples : effet thermique, dilution, effet chimique,…*

Au vue des ces éléments bibliographiques, il semble intéressant d'effectuer une étude détaillée, sur un moteur automobile récent en tentant de séparer les différents effets de l'injection d'eau et en comparant au moyen de dépollution à la source traditionnel, à savoir la recirculation des gaz d'échappement (EGR). Le mode d'introduction de l'eau retenu est l'injection dans l'air d'admission, pour des raisons de simplicité technologiques, mais les quantités d'eau envisagées sont plus importantes que celles traditionnellement utilisées afin de cerner les limites du procédé.

2. CHAPTER 2 : Experimental setup and modelling tools

Ce chapitre a pour but de présenter les outils expérimentaux, théoriques et numériques qui seront utilisés par la suite pour étudier l'injection d'eau à l'admission d'un moteur Diesel automobile. Il est divisé en deux grandes parties.

La première partie concerne le dispositif expérimental. Elle comprend tout d'abord une description du moteur de série modifié qui a été utilisé, puis une présentation détaillée du système d'injection d'eau, avec les évolutions successives développées spécifiquement pour cette étude. Enfin, les principales caractéristiques des instruments de mesure - notamment des analyseurs d'émissions polluantes - et du système d'acquisition sont fournies, ainsi que les incertitudes de mesure associées.

La deuxième partie concerne le développement d'outils numériques d'analyse destinés à évaluer où se produit l'évaporation de l'eau injectée sous forme liquide. Quelques éléments théoriques sur la description thermodynamique du changement de phase et l'air humide sont tout d'abord rappelés. Puis, plusieurs situations sont analysées : mélange et évaporation dans le répartiteur d'admission, évaporation dans le cylindre pendant la phase d'admission et enfin évaporation pendant la phase de compression. Enfin, les résolutions numériques mise en œuvre sont rapidement exposées.

This chapter presents the experimental, theoretical and numerical tools which will be used to study intake water injection on an automotive diesel engine. It is divided into two parts.

The first part concerns the experimental setup. The basic specifications, modifications and developments made to the engine are discussed. A detailed presentation of the water injection system is then given including the successive modifications made specifically for this study. Finally, the principal characteristics of the measurement system – specifically the emissions analysers – and the acquisition system are given, as well as the associated measurement uncertainties.

The second part concerns the development of numerical tools for the analysis of the evaporation of water in liquid form in the engine cycle. At the beginning, thermodynamic principles of water in its liquid and vapour form are recalled. These principles will eventually be used to define the evaporation of water during different phases of the engine cycle. Different scenarios are then analysed: mixing and evaporation in the intake manifold, evaporation in the cylinder during intake into the engine cylinder, and finally, evaporation during compression. At the end, a summary of the resolution of numerical processes is presented.

2.1. Experimental setup:

The experimental setup consists of the basic engine test bench, of which the details are noted in the following text, a Low Pressure Exhaust Gas Recirculation System (LP EGR) system that was developed at the laboratory, and finally the Water Injection system. Details of each are presented in the following paragraphs:

2.1.1. Test Engine:

The engine used on the test bench is a 2.0 litre HSDI automobile diesel engine. This engine has already been used for an earlier PhD thesis [12] on the effect of composition of intake charge on the combustion and emissions of an automobile diesel engine. The specifications of the test engine are presented as under:

Displacement (cc)	1998
Emissions control standard	EURO 4
Architecture / layout	4 cylinder inline
Bore x stroke (mm)	85 x 88
Valves / cylinder	4
Compression ratio	18:1
Minimum – maximum engine speed	750 – 5100 RPM
Maximum power at RPM	100 kW at 4000 RPM
Maximum torque at RPM	320 Nm at 1750 RPM
Turbocharging	Variable Geometry Turbine – chargecooler
EGR system	Cooled high pressure EGR
Injection system	Common rail, piezoelectric injectors, 2^{nd} generation
Injector orifices	7
Injector orifice diameter (mm)	0.150
Maximum injection pressure (bar)	1600
Combustion chamber	Re-entrant bowl-in-piston

Table 38. Engine characteristics

The original chargecooler has been installed to cool down the air charge after the turbocharger compressor. Unfortunately, to be effective, the chargecooler needs a large amount of airflow, similar to that encountered when installed at the front of a moving vehicle. Since the airflow in the engine test room is rather weak, another cooling system was devised which consists of spraying the chargecooler core with cool cooling water. To control the intake charge temperature, a solenoid valve is put in line with the cooling spray circuit. The cooling water flow is tailored to meet the required intake charge air temperature. The photos shown here are of the engine before the installation of the water injection system.

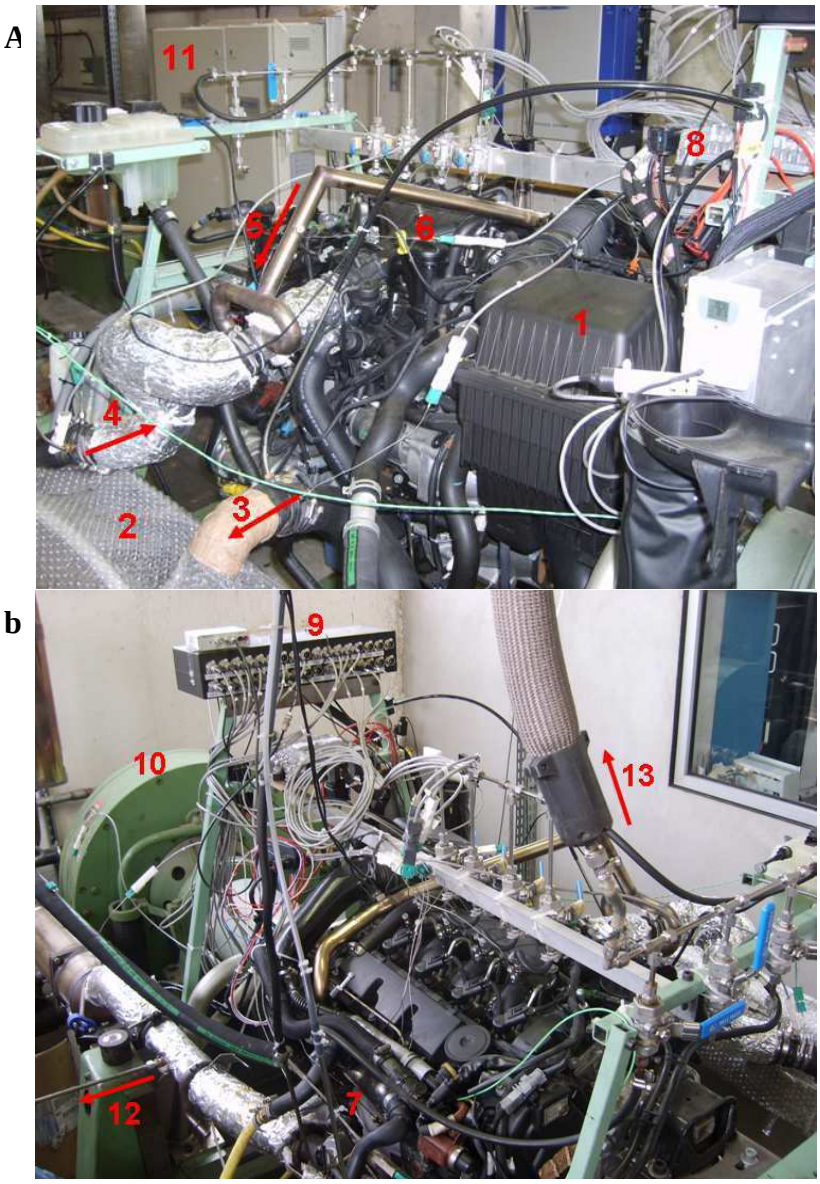

1	Air filter
2	Chargecooler
3	Turbocharger outlet
4	Chargecooler outlet
5	EGR Loop (aft of EGR cooler)
6	Intake manifold
7	Exhaust manifold
8	Electronic Control Unit
9	Data Acquisition Unit
10	Dynamometer brake
11	Fuel Consumption Measurement
12	Probe for smoke measurement
13	Heated conduit for emissions analysis

Figure 42. Details of the engine on the test bench **a.** Intake side **b.** Exhaust side

LP EGR System: An LP EGR loop has been added on the engine, originally equipped with a High Pressure (HP) EGR loop. The recirculated gases are taken downstream of the DPF to avoid the recirculation of soot into the compressor. To avoid uncontrolled condensation downstream the introduction of recirculated gases which may damage (by corrosion) or foul the compressor blades and the intercooler, a large LP EGR cooler is used to maintain the EGR temperature T_{egr_LP} under 50°C, to remove water from recirculated gases. These are thus dry and free of PM. Condensed water is separated by gravity and collected in a catch tank. An exhaust valve has been added to control exhaust back pressure and thus permit high rates of exhaust gas recirculation using the LP EGR loop.

As mentioned in the last section, the intake air temperature T_2' is controlled separately, allowing control over the temperature T_2" of inlet gases after mixing with EGR and water injection, independent of EGR rate.

2.1.2. Water Injection System:

The Water Injection system that is running on the engine test bench at this moment is actually the fourth generation of the system. In this section, the evolution of the water injection system shall be presented.

The basic requirements of a water injection system were defined from the start and are listed as:

1. Accuracy and precise metering of a known mass flow rate of water into the engine intake manifold
2. Good quality of spray – that is to say, that the water should be atomised to a mist fine enough that it floats in air and can easily follow the contours of the intake manifold
3. Maintenance of good quality of the atomised water mist over a wide range of fluid mass flow rates
4. The system should limit modifications to the base engine to a minimum

In addition to these basic criteria, some additional, secondary, but no less important criteria were decided upon to increase the quality of the system.

1. Safety measures incorporated so that the engine may not get damaged if the system malfunctions
2. Possibility of interfacing to the engine test bench electronics
3. Monitoring of as many parameters as possible, to enhance the quality of measurements – air and water pressures, air and water mass flow rates, and water temperature.

Keeping in mind the basic requirements of the system, the system evolved, with each evolution changing the sources of fluid pressures, injector constructions and measurement strategies for the various parameters.

First Generation – The first generation of the water injection system consisted of petrol injectors of the type used in port fuel injected spark ignition engines. These injectors were supplied fluid pressure directly from the tap, wherein the water pressure was measured at all times. The mass flow rate was not measured directly; it was only estimated using the injector duty cycle and the water supply pressure. Unfortunately, there were a few factors due to which the precision of the system was considered to be rather poor and it was not pursued further:

1. Poor atomisation of water – seeing that the pressure was rather low (of the order of 4-5 bars) and the only atomisation process in effect was hydraulic, the quality of atomisation was rather poor. To improve the atomisation quality, fine plastic meshes were added to the injector noses to facilitate droplet break-up. While this worked to break the jet up into finer droplets, a lot of the water jet stayed on the mesh, and would dribble from the injector nose.
2. Rusting of injector pintles – the injectors were not designed to be used with pure water. After a few hours of working, the injector pintles would jam, rendering the injector useless.

3. Absence of real-time water flow rate measure – In the absence of a closed-loop control, the mass flow rate of the injectors was based on the pressure of the water supply and the duty cycle of the injectors. Since the water supply is off the fresh tap water supply, there are variations in pressure over the course of the test day. Therefore, the injectors would have to be calibrated for different pressures. In addition, as stated earlier, the fact that the injectors slowly rust over time and jam, the duty cycle of the injector flow is an unknown factor.

In view of the above, SI engine petrol injectors were quickly abandoned as a viable means of controlled water injection for the test bench.

Second Generation – To alleviate some of the problems of the 1st generation system, it was decided that since a higher pressure can improve atomisation of water, a redesigned system with a much higher pressure than 3 bars be devised. A prototype system was developed using a Kärcher high-pressure water pump, the type that is used for pressure washing. In consideration of the high water injection pressure (in the region of 80 to 100 bars), a special nozzle holder was made to enable the user to change different nozzles while guaranteeing the absence of leaks and securely holding the nozzle in place. The injector nozzle used for this system was a common rail diesel injector nozzle. The injector was chosen for the small size of its orifices and also due to the fact that it was a multi-orifice injector, thus forming a mushroom of water jets when in operation. This system was considered to be unsuitable for the water injection test bench due to the following reasons:

1. **Variation of water flow rate** – In this system, the flow rate could not be varied since the injector would run at full open all the time. One way to vary the flow rate would be to reduce pressure. However, seeing that the water flow rate varies as a square root of the fluid pressure, the variation in pressure would have been too great for a relatively small variation in flow rate.

2. **Spray pattern** – Direct injection diesel injectors are not designed to atomise fuel. Fuel gets sprayed out of the injector orifices as a steady stream which is then broken up with friction against the air in the combustion chamber. While this type of jet works perfectly in a diesel engine, for a water injection system, it is not suitable. Hence the requirement for an atomising injector nozzle.

In general, the difficulty in precisely varying the water flow rate while maintaining a sufficiently fine atomised water jet was what rendered this system unsuitable for use as a viable water injection system.

Third Generation – This system is based on an air-assist water injection nozzle. The water is passed radially through two concentric, smooth discs. This stretches the water out into a thin film. These plates have concentric holes in the centre from which high pressure air is passed. This high pressure air breaks the film of water into a fine mist which is fine enough to be able to follow the intake manifold inner profiles without wetting the walls too much. The system consists of a special injector whose details are shown in **Figure 43** and **Figure 44**:

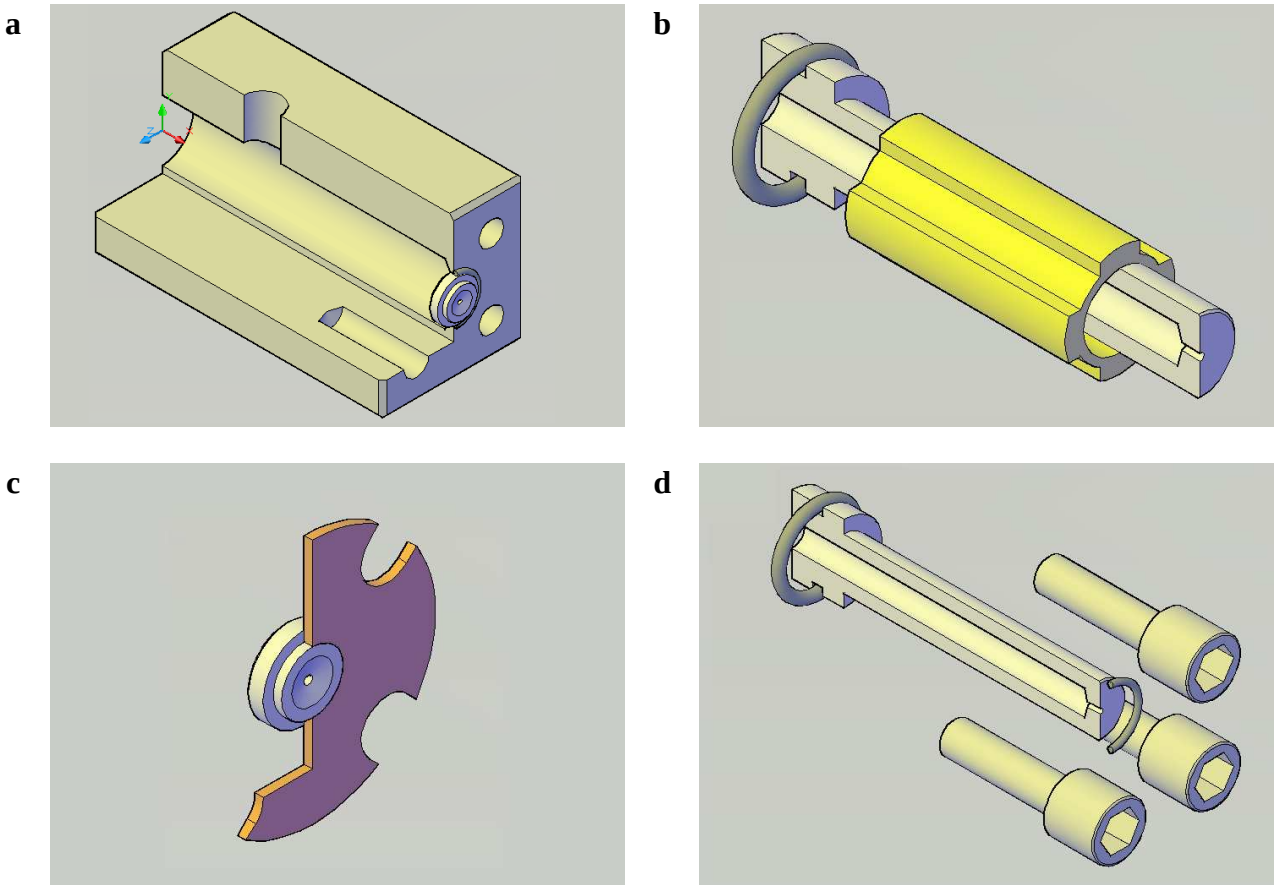

a. Injector body with nose cone and O-ring seal
b. Injector core with support (yellow) and O-ring seal
c. Injector nose cone with nose plate
d. Injector core with both O-ring seals and nose plate bolts

Figure 43. Parts of the water injection nozzle

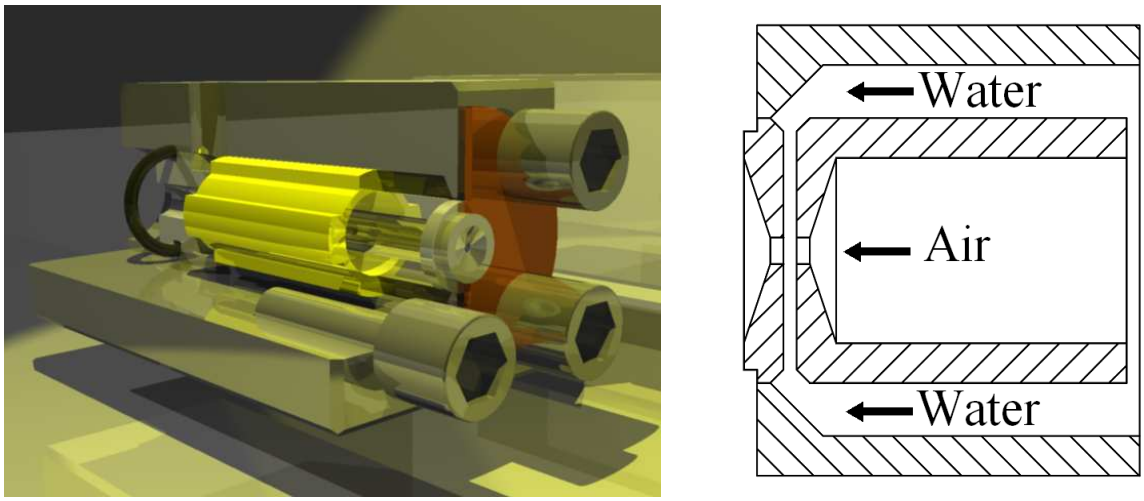

Figure 44. CAD drawing and simplified functional drawing of the air assisted water injector

Construction details:

1. The injector body is a mono-block aluminium bar stock with the requisite diameter of holes drilled directly into it. The axial holes are for the injector outlet and air supply, while the transverse hole is for the water supply.

2. The injector core is taken from a petrol injector. It is the main body of the injector nozzle without the pintle. This part gives us the entry for the high pressure air and the nose of the nozzle gives us one of the two smooth discs required to generate the thin water film. The injector core centring bushing is made from a length of vinyl tubing with axial grooves cut into the outer periphery to allow the passage of water.

3. The nose plate comprises of the retainer and the nose of an injector core. This gives us the second surface to generate our thin water film. With the rubber o-ring, we can tighten the retaining bolts more or less to increase or decrease the gap between the two smooth surfaces, thereby giving us more or less flow rate range. A steel nose plate holds the injector nose in place with the help of four allen bolts.

4. Four allen bolts are used to hold the injector nose and nose plate in place. The bolts tighten the nose plate against a rubber O-ring giving a water and air tight seal, while also giving a certain "tuneability" to the injector by varying the distance between the injector core and injector nose. The rear O-ring on the injector core prevents the water – which is outside the core – mixing with the water – inside the core. **Figure 44** shows the functioning of the injector, and the assembled component.

The WI system comprises of the following components:

- *Kärcher* K2.01 High Pressure water pump
- 8 Bar Air Compressor
- *Parker Pneumatic* 8 Bar Air Pressure Regulator
- *Radiospares* Turbine Flowmeter
- Competition variable fuel pressure regulator
- *K-type* thermocouples
- Electromagnetic solenoid valve

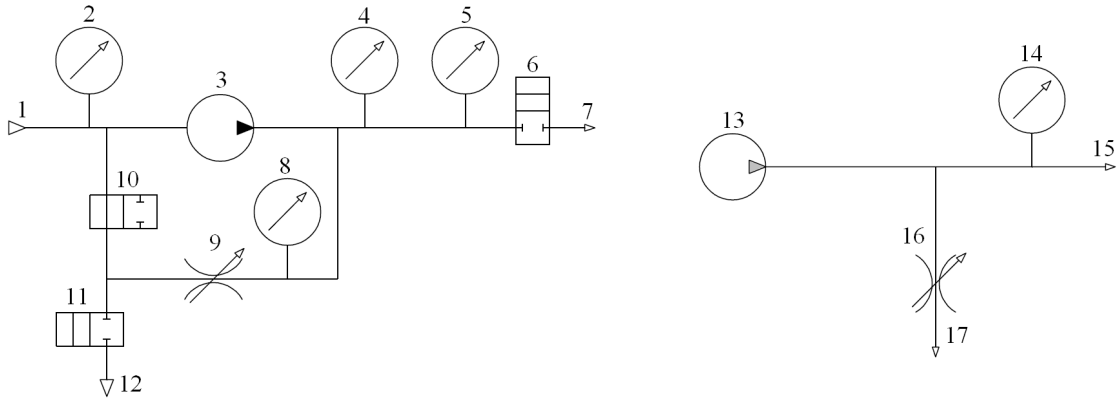

1 Water inlet from tap
2 Turbine mass flow meter
3 Kärcher high pressure water pump
4 Temperature measurement
5 Turbine mass flow meter
6 Solenoid valve – Normally Closed (N/C)
7 Connection to water injector nozzle
8 Pressure measurement
9 Variable pressure regulator
10 Ball valve – Normally Open (N/O)
11 Ball valve for purging system – Normally closed
12 Discharge
13 Air compressor
14 Pressure measurement
15 Connection to water injector nozzle
16 Variable section orifice (ball valve)
17 Discharge

Figure 45. Schematic of the water supply (left) and air supply (right) sub-systems of the water injection system

The size of droplets depends on the water flow rate; an increase in flow rate increases the size of the water droplets. The following photographs show the quality of the mist during system operation.

Figure 46. Spray quality of the injector (left) and the air/spray mixer (right)

And finally, **Figure 47** shows the system mounted on the engine test bench, with the control post outside the test cabin to allow adjustments to be made to the system flow rate and pressure.

a

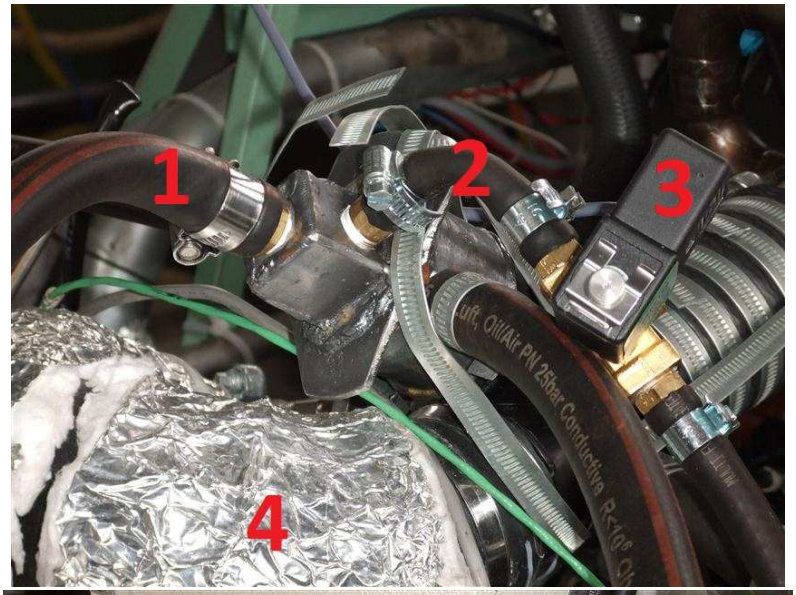

b

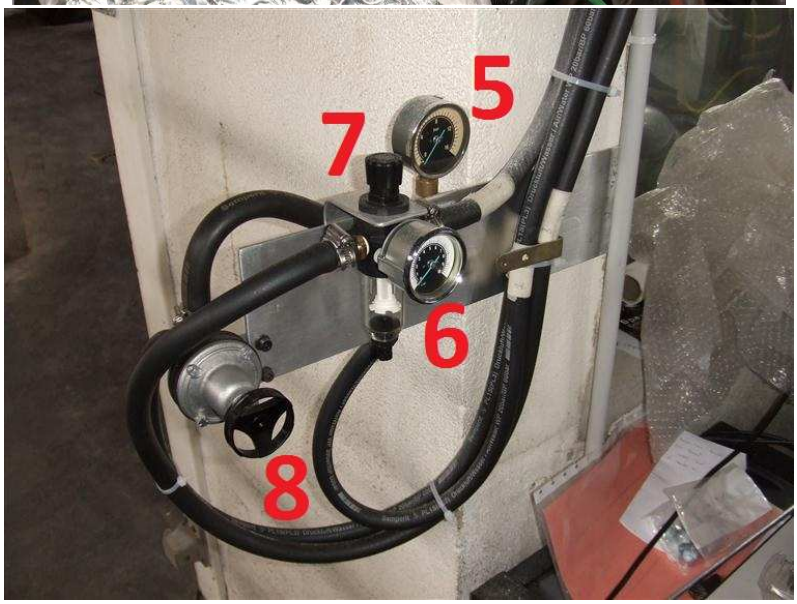

1	Air supply
2	Water supply
3	Water supply safety / cut-off solenoid
4	Post charge cooler air intake pipe
5	Water pressure gauge
6	Air pressure gauge
7	Air pressure regulator
8	Water pressure regulator

Figure 47. Installed water injector a. on the engine at the intake b. water injector pressure / flow rate control post

With reference to **Figure 45** and **Figure 47**, a list of how the system is used is given below:

1. Before the engine is started, the WI system purged with fresh water by closing valve **10** and opening valve **11** (**Figure 45 a**). This forces water from the water supply **1** (**Figure 45 a**) to pass through the whole circuit.

2. The air compressor is started; the air supply is however not connected to the WI nozzle. The valve **16** (**Figure 45 b**) is adjusted to achieve between 5 and 6 bars of air pressure shown on barometer **14** (**Figure 45 b**).

3. The engine is started and stabilised at the operating point of interest.

4. With the engine stabilised and air line for the WI nozzle unconnected, the base reading for air flow is taken.

5. As the air injection line **15** (**Figure 45 b**) is attached to the WI nozzle, air is bled into the air intake tract of the engine. The air pressure in the air line is left to stabilise and

the bleed valve **16** may need to be adjusted to bring air pressure back to between 5 and 6 bars.

6. Since a part of the air going into the intake tract is being fed by the air line from the external air compressor, the air mass flow meter will show a drop in air flow rate. In reality, since the manifold pressure and temperature and engine RPM remain the same, it can be surmised that the real air flow rate into the engine remains the same.

7. The water feed line **7** (**Figure 45 a**) is connected to the WI nozzle.

8. Water pressure in increased using the variable pressure regulator **8** (**Figure 47 b**) until water flow is achieved (minimum of 3 kg/hour and maximum of 21 kg/hour) measured by the turbine flow meter **5** (**Figure 45 a**)

9. As water pressure is increased, the air pressure in the WI air supply line increases – **14** (**Figure 45 b**). This is due to the fact that as the water flow rate increases, the cross-sectional area in the WI nozzle available to the airflow is reduced. An assumption has been made that the air flow rate of the positive displacement compressor **13** (**Figure 45 b**) remains stable independent of discharge pressure. Seeing that the air flow cross section at the bleed valve **16** (**Figure 45 b**) remains the same, the net air flow pressure increases due to the decrease in total air flow discharge cross-sectional area. As a result, more of the air will flow out of the bleed valve **16** (**Figure 45 b**). This reduction of airflow at the WI nozzle is taken into account using pressure ratios and measured air flow rates.

10. After the test session is completed, first the WI water pressure is reduced to zero, and the safety solenoid **3** (**Figure 47 b**) is cut-off. The engine is then put under load, while the intercooler cooling system (**Figure 48**) is deactivated. The aim is to increase the air flow rate and temperature to dry the insides of the intake tract and the engine itself. During the drying process, the temperatures at the entry to the intake valves $\mathbf{T_{2''}}$ will remain relatively low, since water evaporation will keep the thermocouples cool. As soon as the tract is dray however, there will be a marked increase in temperature to around 80-110°C depending upon the engine operating point. The engine is run at this point for a little while longer and then the engine speed is reduced to idle.

11. All parameters in the ECU are returned to base values, and the water and air connections are disconnected from the engine while the engine is running at idle. The engine is then run at idle for 10 minutes to cool down the turbocharger and the exhaust system and then it is shut off.

12. The air compressor is shut off, and the air bled out.

13. The water pump **3** (**Figure 45 a**) is shut off, the mains supply **1** (**Figure 45 a**) is cut-off, and the circuit is emptied via the discharge valve **12** (**Figure 45 a**).

2.1.3. Instrumentation and measurement uncertainties:

2.1.3.1. Instrumentation:

The engine is mounted to an Eddy Current engine dynamometric brake that can be controlled for a specified Torque or RPM value.

A Pierburg PLU 4000 fuel flow measurement system is used that measures fuel flow rate along with the fuel temperature – which is regulated.

Interfacing to the engine ECU is achieved by an ETAS ES690 interfacing unit along with INCA®. The unit along with the software allows the operator to measure, show or download various engine operating parameters of which some examples are;

1. Air flow rate into the engine
2. Intake air temperature
3. Ambient air pressure
4. Manifold air pressure
5. Fuel rail pressure
6. EGR valve position
7. Turbocharger Nozzle Guide Vanes actuator position
8. Injector injection events
9. Engine RPM
10. Coolant temperature

The air flow rate going into the engine may be measured via different devices, such as a venturi, a Pitot tube, a Karmann anemometer (measures frequency of vortex shedding), a vane type anemometer or a hot wire anemometer. In general, the higher the precision of a measuring device, the narrower its operating range, as in the case of the venturi. In the case of an internal combustion engine, a relatively high accuracy of air mass flow measurement is required over a wide operating range. For that, the hot-wire or hot-film air mass flow meter is considered to be suitable since it is generally attributed a 1% precision over the whole measured scale. The air flow rate is measured at the exit of the air filter housing. The air flow rate from the air flow meter was compared to the air flow rate measured from the air/fuel ratio given by the 5-gas analyser and the fuel flow rate given by the PLU 4000. The relative difference between the two measurement techniques stays under 3%. This difference remains the same even while using EGR or WI. The EGR valve is in closed loop with relation to its opening percentage. The Variable Nozzle Turbine guide vanes are driven with a pneumatic actuator, and the position of the guide vanes is also in closed loop. The outlet pressure of the diesel injection pump is regulated by a solenoid valve on the high pressure pump stage. As concerns the measurement of real fuel-injected quantity, the injection quantity of 1.0 to 2.0 mg/stroke during the pre-injection stage is considered to be correct, the remainder of the injection quantity (the main injection) is measured from the total fuel consumption rate given by the PLU 4000. The cyclic variations in injected mass per injector is considered to be

cancelled out over a finite number of cycles (for example 50, 100 etc.), and the variations of injected fuel quantity between the four cylinders is negligible. The SOI given by the ECU is the electrical signal for opening the injection nozzles. In reality, there is a lag of a few hundred µs* between the injector command signal and the real SOI.

* The actual value depends on the type of injector and is given by the injector manufacturer.

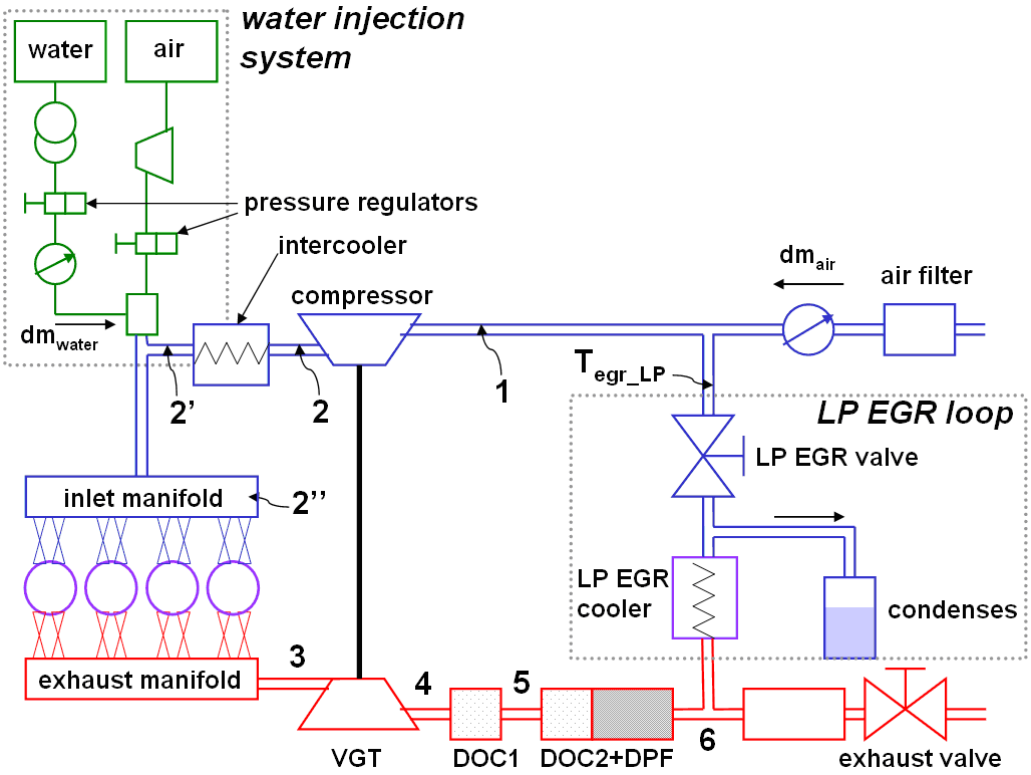

Figure 48. Nomenclature of the test engine with the WI and LP EGR system, with numbered measurement points

A specific instrumentation was installed on the engine to measure various parameters. The following test parameters are measured on the test engine using a data acquisition system running under Labview® v. 7.1:

- The temperature and pressure of gases at various points in the intake and exhaust system – the temperatures being measured by K-type shielded thermocouples of 1mm diameter, and piezo-resistive relative pressure sensors of the HCX range from SensorTechnics®. The measuring range of the sensors was chosen such that the precision of measurement is maximised. The pressure range used is 2 bars relative on the intake side and 5 bars relative on the exhaust side:
    - 1 – engine inlet, before compressor
    - 2 – compressor outlet, before chargecooler
    - 2' – chargecooler outlet, before WI
    - 2" – After WI
    - 3 – engine exhaust port, before turbocharger turbine

- 4 – turbocharger turbine outlet, before DOC
- 5 – after DOC, before DPF (FAP)
- 6 – after DPF (FAP)
- EGR – recirculated exhaust gases, post EGR cooler, before mixing with fresh air

In addition to this the temperatures of the intake and exhaust gases are measured at all times separately for each cylinder.

- The atmospheric temperature and pressure are measured respectively, with the help of a silicon-based LM35AZ temperature sensor and a piezo-resistive HCX absolute pressure sensor by SensorTechnics®.

- An HIH-4000 sensor measures the relative humidity of the air that is aspirated by the engine in the test cell. It is positioned at the opening of the intake tract that leads into the air filter.

- The turbocharger rotational speed is measured using a Pico-Turn inductive sensor by ACAM, which is mounted directly to the compressor volute. As soon as a compressor blade passes in front of the inductive sensor, there is a variation in the inductance level of the sensor. This change in the value of inductance is picked up by the acquisition system which converts the signal into a frequency signal proportional to the rotational speed of the turbocharger. The system is capable of measuring a rotational speed between 200 and 350 000 RPM.

- Real-time in-cylinder pressure measurement is done with the help of a piezo-electric 6055 sensor by Kistler. The signal from this sensor is amplified by a charge amplifier also provided by Kistler. The start of the data acquisition is performed with the help of an incremental angular encoder which is used as a reference for the start and end of the pressure signal sampling. The angular encoder is mounted at the front side of the crankshaft and has a resolution of 1000 points every 360°. The measurement step is thus 0.36° per increment on the encoder.

- Labview® is a software that allows us to easily acquire and analyse data retrieved from the measurement system by the data acquisition system. In addition to this, the software allows us to visualise the incoming data in real-time on floating graphs that update data values according to the refresh rate of the data acquisition system. Using this function, it is easy to see the stabilisation of operating parameters of the engine so that tests can be performed.

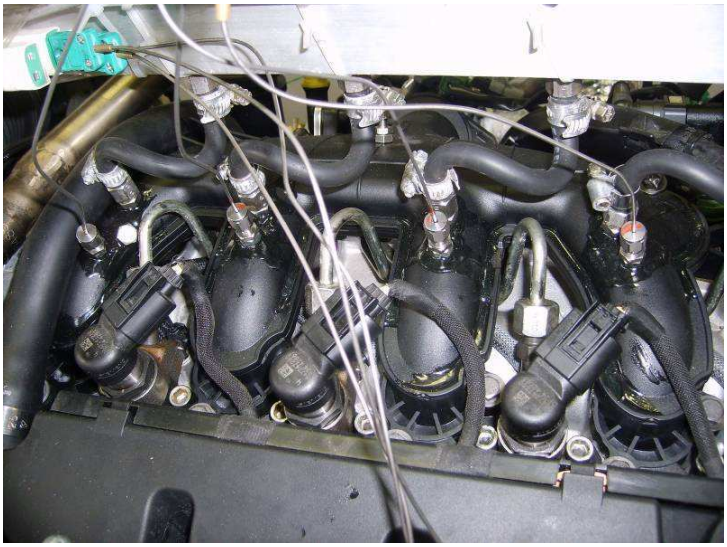

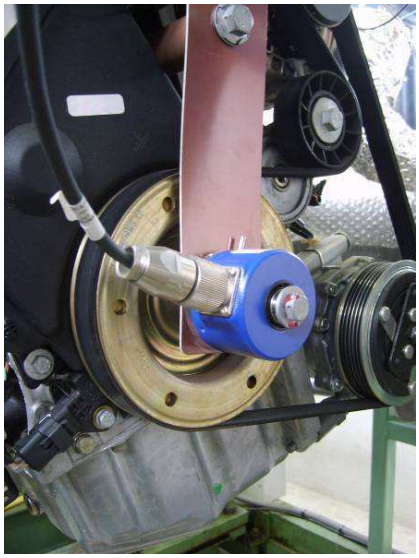

a) Instrumented intake manifold **b)** Angular encoder

Figure 49. Detailed photographs of intake manifold and the angular encoder

The compositions of the intake and exhaust gases are measured with a Siemens gas analyser bench, which comprises the following elements:

- An ECOPHYSICS® CLD 700EL machine is used to measure the NOx emissions. This machine functions by chemiluminescence of NO with Ozone O_3.
- A SIEMENS® ULTRAMAT 23 for measuring the concentrations of CO2, CO and O_2 with the help of an NDIR (Non Dispersive InfraRed) sensor.
- A SIEMENS® FIDAMAT 5E for measuring total unburnt HCs using the FID (Flame Ionisation Detection) method.

In the case of the CLD 700EL, the gas to be analysed is mixed with ozone in excess. There is a reaction between the ozone and the NO, which leads to chemiluminescence. The intensity of this chemiluminescence is proportional to the concentration of NO in the sample. A second sample of the NO is sent into a catalysing oven which converts all NO_2 to NO. This second volume contains only NO, which undergoes the same mixing with ozone and the resulting intensity of chemiluminescence is measured. The difference between the two intensities of chemiluminescence gives the ratio of NO_2 and NO in the original NOx sample.

In the case of the ULTRAMAT 23, an infrared beam is passed through the analysed gas. The frequencies in the absorption spectrum are analysed, each frequency of the absorption spectrum corresponds to a specific gas species. In addition to this, the NDIR sensor has a relatively narrow spectrum.

The FIDAMAT 5E works by passing the gas sample through a hydrogen-fuelled flame. The energy from the hydrogen flame releases electrons from the gas sample. These electrons are then captured by electrodes, and are measured with the help of a high gain amplifier. The current is thus proportional to the number of carbon atoms present in the organic bonds of the sample gas.

A heated gas line (at 160°C) is put in place between the measurement point and the gas analyser to avoid condensation of water vapour during gas transfer. Once the gas sample has reached the analyser, it is condensed in a refrigeration section to dry the gas.

All of the apparatus which constitutes the gas analyser is recalibrated after a half a day of tests (4 – 5 hours) using sample gases of known constitution. The constitution of gases is chosen to minimise the measurement error in the gas analyser. At the end of the tests, the gas analyser is again recalibrated to check for any deviation from true. The experiments are considered valid if the deviation for CO_2, CO and NOx are lower than 0.5% and 5% for HC. Measurement points that have been drilled into the intake manifold (**Figure 49 a**) allow us to analyse the gases entering into each cylinder. The reason this measure is taken for each cylinder is that originally, the engine was provided with a HP EGR system which injected exhaust gases into the intake manifold via a T-connection. Due to the perpendicular flow of intake air and EGR, the cylinder-to-cylinder variation of injected EGR mass was rather significant. With the installation of the LP EGR system and its associated EGR mixer, the disparity has been reduced to an order of the precision of the measuring equipment [12]. Also aiding the mixing of the exhaust gases in this case is that the mixing of the intake air and LP EGR gases is done further upstream of the intake manifold. The gas analyser measures and analyses gas composition over a period of time, thus the values are averaged. In reality, the pulsating nature of the gas flows in the intake manifold would vary the air/EGR mix ratio over time, this effect is reduced by the use of an EGR mixer, and by the addition of exhaust gases into the intake air further upstream as compared to the original setup. The EGR rate for each of the cylinders is given by:

$$X_{EGR\_cyl_i} = 100 \cdot \frac{X_{CO_2\_a\_cyl_i}}{X_{CO_2\_e}} \qquad \textbf{43}$$

Analysis of the exhaust gases (CO_2, O_2, HC, CO, NOx) is achieved by taking gas samples at the turbocharger exit before the DOC. While at the intake side, a system of solenoid valves allows us to take gas samples from one of the four cylinders or from the exhaust. As for the PM measurement, an AVL 415S smoke meter is used, and it is fed exhaust gases before the DPF as shown in **Figure 42 b**. The smoke meter passes the smoke sample through a special filter paper, and the darkening of the filter paper is compared to the reference values and a BSN value is given to the smoke sample. Also, it is assumed that the deposition of PM on the internal walls of the exhaust system before the DPF is negligible, thus the PM concentration measured by the smoke meter is the real value.

The values of NOx and PM obtained from the measurement devices are then converted to g/h or g/kWh values in accordance with the documentation supplied. Here, we present the method to convert emissions from ppm to g/h.

Volume flow rate of exhaust gases: Since the engine always runs with a lean mixture, the exhaust gases consist of a mixture of stoichiometric exhaust products and unused air. In addition to this, the volume flow rate of the "wet" exhaust gases (including water vapour from the combustion reaction) is given by:

$$\dot{V}_{exh\_wet} = \dot{m}_f \cdot \left[\frac{1 + (A/F)_{st}}{\rho_{exh\_prod}} + \frac{(\lambda - 1) \cdot (A/F)_{st}}{\rho_{air}} \right] \qquad \textbf{44}$$

In which case ρ_{exh_prod} = 1.33 kg/m3 is the density of the exhaust products of a stoichiometric mixture, and ρ_{air} = 1.293 kg/m3 is the density of air at STP (273K and 760mm Hg). By the same way, the volumetric flow rate of dry exhaust gases is given by:

$$\dot{V}_{exh\_wet} = \dot{m}_f \cdot \left[\frac{\left(1 + \left(A/F\right)_{st}\right) \cdot \sigma}{\rho_{exh\_prod}} + \frac{\left(\lambda - 1\right) \cdot \left(A/F\right)_{st}}{\rho_{air}} \right] \quad \textbf{45}$$

Where σ is the mass of dry exhaust products in 1 kg of non-condensed exhaust product gas (for diesel, this value is of 0.924).

Emissions of PM in g/h: The documentation of the AVL 415S smoke meter gives the relation between the FSN (Filter Smoke Number) and the concentration of particulates in mg/m3:

$$PM\left(mg/m^3\right) = \frac{1}{0.405} \cdot 5.32 \cdot FSN \cdot \exp\left(0.362 \cdot FSN\right) \quad \textbf{46}$$

Since the smoke meter measures the smoke index using non-condensed gases, the particulate emissions in g/h is given by the following equation:

$$PM\left(g/h\right) = 10^{-3} \cdot PM\left(mg/m^3\right) \cdot \dot{V}_{exh\_wet} \quad \textbf{47}$$

Emissions of NOx in g/h: From experience, we know that the NOx emissions of en engine depend on the humidity of intake air. The NOx production reduces as humidity increases. Consequently, measuring the humidity of intake air is important so that corrections may be made to the NOx production rates. For this purpose, an empirical formula is used (directive 91/441/CEE). The correction factor is written thus:

$$Coeff_{NOx} = \frac{1}{1 - \left(0.0329 \cdot \left(\left(621.1 \cdot \frac{P_{vap}}{P_{dry}} \right) - 10.71 \right) \right)} \quad \textbf{48}$$

Where P_{vap} and P_{dry} are the vapour pressure and the pressure of dry air respectively, given in mmHg, calculated using the following:

$$P_{vap} = P_{sat} \cdot \frac{RH}{100} \quad \textbf{49}$$

$$P_{sat} = 4.56 + \left(0.345 \cdot T_{db}\right) + \left(9.36 \cdot 10^{-3} \cdot T^2{}_{db}\right) + \left(2.52 \cdot 10^{-4} \cdot T^3{}_{db}\right) + \left(13.235 \cdot 10^{-7} \cdot T^4{}_{db}\right) + \left(2.43 \cdot 10^{-8} \cdot T^5{}_{db}\right) \quad \textbf{50}$$

$$P_{dry} = P_{atm} - P_{vap} \quad \textbf{51}$$

Where P_{sat} is the saturated vapour pressure at the dry-bulb temperature (or wet-bulb, since at saturation, both wet-bulb and dry-bulb temperatures are the same), and the RH is the relative humidity of the intake air.

The NOx emissions can then be corrected thus:

$$NOx_{corr}\left(ppm\right) = Coeff_{NOx} \cdot NOx\left(ppm\right) \quad \textbf{52}$$

By convention, the molar mass is equal to that of NO_2. The NOx analyser measures after drying the exhaust sample, therefore, the corrected NOx emissions expressed in g/h are given by:

$$NOx(g/h) = \frac{M_{NO_2} \cdot NOx_{corr}(ppm) \cdot \dot{V}_{exh\_dry}}{10^3 \cdot V_m} \quad \textbf{53}$$

Where V_m is the molar volume of gas, equal to 22.4 L/mol at STP.

In the same manner, the emissions of CO, HC, CO_2 and O_2 are given by:

$$CO(g/h) = \frac{M_{CO} \cdot CO(ppm) \cdot \dot{V}_{exh\_dry}}{10^3 \cdot V_m} \quad \textbf{54}$$

$$HC(g/h) = \frac{M_{HC} \cdot HC(ppm) \cdot \dot{V}_{exh\_dry}}{10^3 \cdot V_m} \quad \textbf{55}$$

$$CO_2(g/h) = \frac{M_{CO_2} \cdot CO_2(ppm) \cdot \dot{V}_{exh\_dry}}{10^3 \cdot V_m} \quad \textbf{56}$$

$$O_2(g/h) = \frac{M_{O_2} \cdot O_2(ppm) \cdot \dot{V}_{exh\_dry}}{10^3 \cdot V_m} \quad \textbf{57}$$

2.1.3.2. Measurement uncertainties:

In this section, a means of determining the measurement uncertainties is presented. These uncertainties would help us to determine the maximum possible error associated to any one measured variable. For this, we shall use the differential method of error propagation based on the Taylor theorem [12]. The maximum probable uncertainty of a function f(x1, x2, x3,…, xn) is given by:

$$u(f(x_1, x_2, x_3, ..., x_n)) = \sqrt{\sum (c_i \cdot u(x_i))^2} \quad \textbf{58}$$

Where c_i are multiplier coefficients. If "f" is a function of sum of variables x_i, the following equation may be used:

$$u(f(x_1 + x_2 + x_3 + ... + x_n)) = \sqrt{\sum (u(x_i))^2} \quad \textbf{59}$$

if "f" is a function of products of the variable x_i, the following equation may be used:

$$u(f(x_1 \cdot x_2 \cdot x_3 \cdot ... \cdot x_n)) = f(x_1 \cdot x_2 \cdot x_3 \cdot ... \cdot x_n) \cdot \sqrt{\sum \left(\frac{u(x_i)}{x_i} \right)^2} \quad \textbf{60}$$

The precision and relative errors are given in …

After the calculations, we obtain the maximum relative error "ε_r" for the different measured variables which are taken from measurements, and are noted as:

$\varepsilon_r(X_{EGR})$: 1.4%
$\varepsilon_r(NOx(g/h))$: 1.5%
$\varepsilon_r(PM(mg/m^3))$: 6.27%
$\varepsilon_r(PM(g/h))$: 6.36%

$\varepsilon_r(CO_2(kg/h))$: 1.5%
$\varepsilon_r(O_2(kg/h))$: 1.1%
$\varepsilon_r(CO(g/h))$: 1.5%
$\varepsilon_r(HC(g/h))$: 1.5%
$\varepsilon_r(\lambda)$: 1.05%
$\varepsilon_r(Q_{exh\_wet})$: 1.1%
$\varepsilon_r(Q_{exh\_dry})$: 1.1%
$\varepsilon_r(H_2O\text{-}WI)$: 3%

It is important to keep in mind that the measurement precision for NOx is 4 times higher as compared to that for the measurement of PM (6.36% against 1.5%). Below, a table of precisions for different sensors and equipments is given:

	Measurement range	Precision	Relative error (%)
Temperatures (K-type thermocouple)	0 – 1000 °C	± 1 °C	± 0.75
Atmospheric temperature	-60 – 150 °C	± 0.2 °C	± 0.1
Pressure – relative measurement sensor HCX 5 bar	0 – 5 bar	± 5 mbar	0.8
Pressure – relative measurement sensor HCX 2 bar	0 – 2 bar	± 2 mbar	0.3
Pressure – relative measurement sensor HCX 1 bar	0 – 1 bar	± 1 mbar	0.25
Air mass flow rate	0 – 1000 mg/stk	± 5 mg/stk	1
Fuel consumption rate	0.05 – 23 kg/h	± 37 g/h	± 0.16
Relative humidity	0 – 100 %	± 3.5 %	± 3.5
Turbocharger speed	0 – $3.5x10^5$ rpm	± 200 rpm	± 0.06
Cylinder pressure (range of 0 – 200 bars)	0 – 200 bar	± 1 bar	1
Cylinder pressure (range of 0 – 100 bars)	0 – 100 bar	± 0.5 bar	1
NOx	0 – 1000 ppm	± 5 ppm	1
Smoke	0 – 10 FSN	± 0.1 FSN	2
CO_2	0 – 20 %	± 0.1 %	1
O_2	0 – 25 %	± 0.025 %	0.2
CO	0 – 1000 ppm	± 5 ppm	1
HC	0 – 400 ppm	± 2 ppm	1

Table 39. Range of measurement, precision and relative error for each measuring instrument

2.1.4. Engine operating points:

This study has been performed on four operating points. These points are listed in the following table and are labelled A to D. The engine RPM, mean torque, and BMEP are given below. For the most part, points B and C are used a fair amount during the tests, since these points are fairly representative of medium and high load operations on road. Also, these points give a relatively high flexibility for modifications in the engine operating parameters.

Point	Engine speed (rpm)	Mean torque (Nm)	Mean BMEP (bar)
A	1511	44	2.8
B	1664	110	6.9
C	2052	150	9.4
D	2000	198	12.5

Table 40. Test points

2.2. Description of Numerical Model and its Development

In this section, the development of a numerical model shall be presented in detail. The numerical model shall be broken down into parts to facilitate explanation and implementation as a computer code. The model can be broken down into the following parts based on functions performed:

- Determination of conditions and properties of the working gas up until the point where it enters the cylinder, during the intake period, compression, combustion and expansion.
- Determination of the quantity of water in liquid form that enters the cylinder after initial mixing and evaporation in the intake manifold.
- Using signals given for cylinder pressure and taking into account the properties of the working gas; the Rate of Heat Release may be calculated (ROHR).
- Using the ROHR, ignition delays and combustion rates may be calculated.

Using these values, the changes in pollutant emission rates may be correlated.

2.2.1. Definitions of Properties of Air and Water (vapour and liquid)

In general, calculations for engine cycles only use properties of perfect gases to define the working fluid. In the case of water injection however, there shall be the existence of water in liquid and vapour form to contend with. Assuming that air and water are at different temperatures and that the air is not saturated with vapour, there shall be an energy transfer. This energy transfer will cause a change in the temperature of the mixture. In addition as a result of the mixing of air and water, the overall properties such as specific heat and density of the air / water will change. This shall play an important role during the calculations of the ROHR.

In this sub-section, a few basic concepts of evaporation and gas mixtures will be presented. Then, energy transfer as a result of mixing of water and air shall be explained.

2.2.1.1. Laws of Partial Pressures

In a mixture of ideal gases, each ideal gas has a pressure that is equal to the pressure it would exert if it were alone in the volume. The total pressure of the mixture of gas is the sum of partial pressures of all the gases in the volume. Dalton's Law of partial pressure is stated thus:

> *"The total pressure exerted by a gaseous mixture is equal to the sum of the partial pressures of each individual component in a gas mixture"*

This empirical law was observed by John Dalton in 1801 and is related to the ideal gas laws. Mathematically, it is stated thus:

$$P_{total} = \sum_{i=1}^{n} P_i \qquad \textbf{61}$$

Here, $\boldsymbol{P_i}$ is the partial pressure of each gas. It is assumed that the gases do not react with each other.

In a mixture of ideal gases, the mole fraction of each gas can be determined from the partial pressure of each gas.

$$X_i = \frac{P_i}{P} = \frac{n_i}{n} \quad \textbf{62}$$

2.2.1.2. Vapour Pressure

By definition, Vapour Pressure is the pressure exerted by a vapour in equilibrium with its non-vapour state, be it solid or liquid. For the case of water injection at the temperatures under consideration, it will be equilibrium of pressure of vapour with its liquid phase.

Often, the term is used to describe a liquid's tendency to evaporate. It is a measure of the tendency of molecules and atoms to escape from a liquid or a solid. A liquid's atmospheric pressure boiling point corresponds to the temperature at which its vapour pressure is equal to the surrounding atmospheric pressure – or as we learnt from the earlier section, total pressure of its surrounding gases – and it is often called the **normal boiling point**.

The higher the vapour pressure of a liquid at a given temperature, the lower the normal boiling point of the liquid. As an example, at 30°C, ethanol has a vapour pressure of 10.460 kPa while water has a vapour pressure of 7.4 kPa at the same temperature. Ethanol boils at a temperature of 78.4 °C as opposed to 100°C for water at atmospheric pressure.

2.2.1.3. Humidity values

There are various methods of expressing values of presence of water vapour in air. Some are presented below:

1. **Humidity Ratio** – also called the Mixing Ratio, is expressed as a ratio between mass of water vapour $\boldsymbol{m_v}$ and mass of dry air $\boldsymbol{m_d}$ at a specified pressure. It is a standard axis used on psychrometric charts for psychrometric calculations. Mathematically, it may expressed as:

   $$HR = \frac{m_v}{m_d} \quad \textbf{63}$$

   It is a dimensionless quantity as such, however, for the sake of simplicity; the values are expressed in terms of kg/kg or g/kg.

2. **Specific Humidity** – is defined as a ratio of mass of water vapour to mass of wet air i.e. with water vapour. Mathematically, it is defined as:

   $$SH = \frac{m_v}{m_a} \quad \textbf{64}$$

   Or, if we wish to relate to Humidity Ratio, we may do it such:

   $$SH = \frac{HR}{1 + HR} \quad \textbf{65}$$

   $$HR = \frac{SH}{1 - SH} \quad \textbf{66}$$

3. **Relative Humidity** – is defined as a ratio of the vapour pressure of the water vapour in air to the saturation pressure at the same temperature. It is normally expressed as a percentage and is mathematically stated as:

$$RH = \frac{P_{(H_2O)}}{P_{sat\,(H_2O)}} \times 100\% \qquad 67$$

2.2.1.4. Thermodynamic Processes during evaporation

In this subsection, the thermodynamic processes that take place right after WI are detailed. This section is divided into three further parts: In the first part, the analytical relations for the thermodynamic processes of a general case of water / water spray mixing are detailed. In the second part, these analytical relations are applied to WI thermodynamic processes in the intake manifold and the engine cylinder. In the third part, the adaptation of these basic analytical relations is made so that calculations may be performed numerically.

If the intake air charge is not saturated with water vapour when water is added to the stream as a spray, some of the injected water will evaporate. The resulting dry air / water mixture will have a certain temperature, mass, volume and pressure after the evaporation process has been completed. Of this mass, we can define the fractions of dry air and water in its different forms:

m : Total mass of the air / water mixture
m_a : Mass of dry air
m_w : Mass of water
m_v : Mass of water as vapour
m_l : Mass of water as liquid

After evaporation, there are two possibilities; one that some of the injected water is evaporated. Or two, all of the water is evaporated. Let us look at both cases separately:

Some of the injected water mass is evaporated: In the case that all of the water is not converted to water vapour, the water vapour will be present in the saturated vapour state, with the remainder of the water mass at the saturated liquid state.

By definition, the total pressure of the intake wet air is a sum of the partial pressures of all gases present. The partial pressure of the dry air sample can be determined using the perfect gas laws. The partial pressure of vapour on the other hand, is the saturation pressure at the average temperature of the wet air sample at thermodynamic equilibrium.

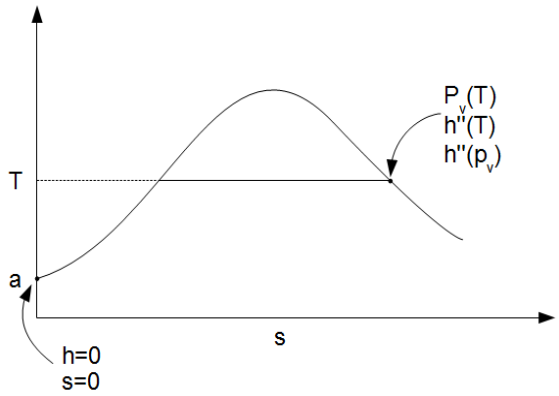

Figure 50. Definition of the state of vapour at temperature "T"

Solving for the water vapour properties, we proceed with calculations as follows:

$$P_v \cdot V = m_v \cdot R_v \cdot T \qquad 68$$

$$m_v = \frac{P_v \cdot V}{R_v \cdot T} \quad \textbf{69}$$

The above assumptions are made assuming that p_v is relatively insignificant as compared to the dry air partial pressure. A schematic of the mixing of water and dry air to make a mixture of water, saturated vapour and water spray with change of temperature from $\boldsymbol{T_i}$ to $\boldsymbol{T_f}$ is shown below:

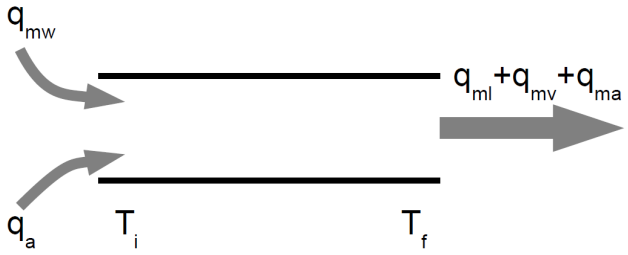

Figure 51. Mixing of water and dry air

$$H_v = m_v \cdot h''(T) \quad \textbf{70}$$

From **Eq. 69**, we get:

$$H_v = \frac{P_v \cdot V}{R_v \cdot T} \cdot h''(T) \quad \textbf{71}$$

For a mixture of gases, the total pressure is the sum of partial pressure of all the constituent gases. Continuing onto properties of dry air, we shall start with the partial pressure:

$$P_a \cdot V = m_a \cdot R_a \cdot T \quad \textbf{72}$$

$$m_a = \frac{P_a \cdot V}{R_a \cdot T} \quad \textbf{73}$$

Definition of enthalpy for air is as shown below:

$$H_a = m_a \int_{T_a}^{T} C_{pa}(T) dt \quad \textbf{74}$$

Where;

T : Final temperature of mixture
T_a : Initial temperature of air sample before heat transfer

Assuming that the value of $\boldsymbol{C_{pa}}$ does not change over the period of $\boldsymbol{T_a}$ to $\boldsymbol{T}$, **Eq. 74** could be simplified to:

$$H_a = m_a C_{pa}(T - T_a) \quad \textbf{75}$$

Solving **Eq. 75** for $\boldsymbol{m_a}$ we get:

$$H_a = \frac{P_a \cdot V}{R_a \cdot T} \cdot C_{pa}(T - T_a)$$

$$H_a = \frac{\gamma}{\gamma - 1} \cdot \frac{P_a \cdot V}{T} \cdot (T - T_a) \quad \textbf{76}$$

For water in liquid form, we can define enthalpy by the following relation:

$$H_l = m_l C_w (T - T_a) \quad \textbf{77}$$

Adding enthalpies for water vapour and liquid, and air, we get the following relation:

$$H = \frac{P_v \cdot V}{R_v \cdot T} \cdot h''(T) + \frac{\gamma}{\gamma - 1} \cdot \frac{P_a \cdot V}{T} \cdot (T - T_a) + m_l C_w (T - T_a)$$

Or,

$$H = m_a \cdot C_{pa} \cdot (T - T_a) + m_v \cdot h''(T) + m_l C_w (T - T_a) \quad \textbf{78}$$

Bringing **Eq. 78** to per unit mass of air, we get the following relation:

$$h = C_{pa} \cdot (T - T_a) + \frac{m_v}{m_a} \cdot h''(T) + \frac{m_l}{m_a} C_w (T - T_a) \quad \textbf{79}$$

Seeing that:

$$m_l = m_w - m_v$$

We can change **Eq. 79** thus:

$$h = C_{pa} \cdot (T - T_a) + \frac{m_v}{m_a} \cdot h''(T) + \frac{m_w - m_v}{m_a} C_w (T - T_a) \quad \textbf{80}$$

We know that $p_v \cdot V = m_v \cdot R_v \cdot T$ and $P_a \cdot V = m_a \cdot R_a \cdot T$, thus:

$$\frac{m_v R_v}{m_a R_a} = \frac{P_v}{P_a}$$

$$\frac{m_v R_v}{m_a R_a} = \frac{P_v}{P - P_v}$$

$$\frac{m_v}{m_a} = \frac{R_a}{R_v} \cdot \left(\frac{P_v}{P - P_v} \right)$$

$$h_{(T,P,\frac{m_w}{m_a})} = C_{pa} \cdot (T - T_a) + \frac{R_a}{R_v} \cdot \left(\frac{P_v(T)}{P - P_v(T)} \right) \cdot h''(T) + \left(\frac{m_w}{m_a} - \frac{R_a}{R_v} \cdot \left(\frac{P_v(T)}{P - P_v(T)} \right) \right) \cdot C_w (T - T_a) \quad \textbf{81}$$

All of the injected water mass is evaporated: Eq. 81 expresses a general form of enthalpy in a mixture of dry air, water vapour and liquid. In case of complete evaporation of water, two situations can exist:

Only saturated vapour: In this case, the values of enthalpy, specific volume, and vapour pressure are all taken from steam tables:

$$h = C_{pa} \cdot (T - T_a) + \frac{m_v}{m_a} \cdot h''(T) \quad \textbf{82}$$

Superheated vapour: In this case, as in the previous case, steam tables are used as reference for different vapour properties:

$$h = C_{pa} \cdot (T - T_a) + \frac{m_v}{m_a} \cdot h_{vap}(T) \quad \textbf{83}$$

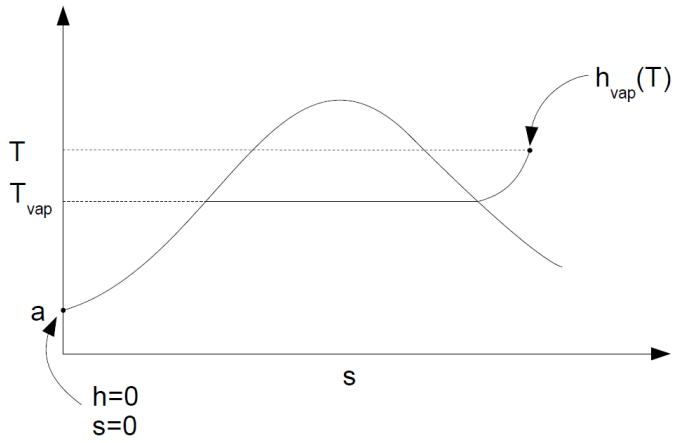

Figure 52. Superheated vapour properties

Application of thermal transfer to intake manifold and engine cylinder: In this section we shall apply what we have learned above to the actual case of WI where water is added to the intake stream after the intercooler. During the WI process, water is added in a fine spray to the intake air charge after the turbocharger compressor. The humidity of air is measured beforehand at the inlet to the air filter. After the intake air undergoes compression and cooling via the intercooler, the relative and specific humidity of the intake air are known. Water is injected into this compressed, cooled air charge.

This air / water mixture will stabilise after a certain time undergoing a thermal transfer between each other or with the system boundaries – in this case, the intake manifold. This mixture will then enter the engine cylinder during the intake phase where it will undergo further thermal transfers from the metal boundaries such as the intake valves, intake ports, combustion chambers, piston tops and cylinder walls and from the residual gases remaining from the last engine cycle. At the end of the intake stroke, the intake valves will close, entrapping the air / water / residual gas mixture and the compression stroke will commence. We may divide the WI thermal analyses into two distinct zones:

1. WI air / water mixing and associated thermodynamic processes in the intake manifold.
2. Air / water mixture thermodynamic processes in the engine cylinder during the intake process.
3. Air / water mixture thermodynamic processes in the cylinder during mixture compression.

WI air / water mixing and associated thermodynamic processes in the intake manifold: As stated earlier, the process starts from the intake manifold. Here, the WI system injects water at a determined, measured mass flow rate. Air mass flowing into the intake manifold is also measured. For a thermodynamic energy balance, we shall make the following hypotheses:

1. The system is an open adiabatic system
2. The thermodynamic processes will take place at constant pressure.

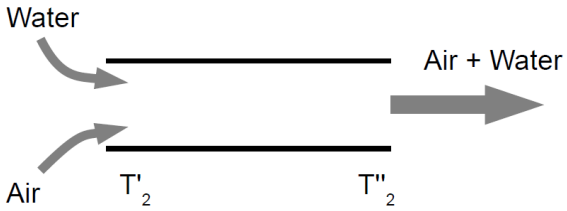

Figure 53. Adiabatic and isobaric mixing of air and water streams in intake manifold

From the first law of thermodynamics, we know that:

$$h_2'' - h_2' = w + q \qquad \textbf{84}$$

Where;

h_2'' : Enthalpy of mixture post at outlet of intake manifold
h_2' : Enthalpy of mixture post at inlet of intake manifold
w : Work produced by mixture
q : Heat transferred to mixture

Knowing that there is no generation of work, and that the process is assumed to be adiabatic, ***w*** and ***q*** terms are null and the total enthalpy of the air / water mixture remains constant from inlet to outlet of the intake manifold.

Air / water mixture thermodynamic processes in the engine cylinder during the intake process: Now we shall treat the in-cylinder processes. A simplified diagram of the aspiration of a saturated air and water mixture is shown in **Figure 54**:

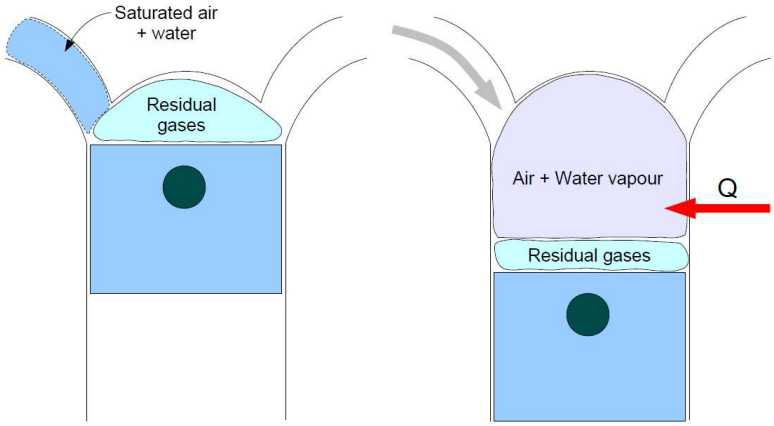

Figure 54. Simplified diagram of processes during aspiration of air and water mixture

Going by the first law of thermodynamics, we can write:

$$dU_{cyl} = \delta W + \delta Q + dm_i \cdot h_i \qquad \textbf{85}$$

Integrating the above equation we get:

$$U_2 - U_1 = -\int P \cdot dV + Q + h_i \cdot \int dm_i \qquad \textbf{86}$$

Where;

dU_{cyl}	:	Change in internal energy of the in-cylinder charge
δW	:	Work produced by the working fluid
δQ	:	Heat transfer to the fluid from the cylinder walls
dm_i	:	Element of intake air charge (water + air)
h_i	:	Intake charge enthalpy
P	:	Total pressure of in-cylinder charge (measured)
dV	:	Variation of cylinder volume (calculated from geometry and crank angle)
$\int dm_i$	:	Mass flow rate of intake charge into the cylinder

Estimation of final temperature at the end of the intake stroke can be done by the following relations. We know that the total volume of the cylinder is taken up by the air, water and residual gases. Thus:

$$V_{cyl} = V_{air} + V_{vap} + V_{rg} \quad \textbf{87}$$

Expanding the above equation, we get:

$$V_{cyl} = \frac{m_{air} \cdot R_{air} \cdot T}{P_{cyl}} + m_{vap} \cdot \upsilon_{vap}(P,T) + \frac{m_{rg} \cdot R_{rg} \cdot T}{P_{cyl}} \quad \textbf{88}$$

Where;

V_{cyl}	:	Total cylinder volume
V_{air}, V_{vap}, V_{rg}	:	Volume taken up by air, vapour and residual gases respectively
m_{air}, m_{vap}, m_{rg}	:	Mass of air, vapour and residual gases (measured, measured, calculated)
R_{air}, R_{rg}	:	Molar gas constants of air and residual gases (measured, calculated)
P_{cyl}	:	Total cylinder pressure (measured)
$\upsilon_{vap}(P,T)$	:	Specific volume of vapour (tables – measured)

In view of the preceding calculations, **Eq. 88** can be developed further as shown below:

$$U_2 - U_1 = -\int P \cdot dV + Q + h_i(m_a + m_w) \quad \textbf{89}$$

$$U_2 - U_1 = -P \cdot V_{cyl} + Q + h_i \cdot m_i \quad \textbf{90}$$

$$U_2 - U_1 = \left[U_a(T_f) - U_a(T_i)\right] \cdot m_a + \left[U_v(T_f) - U_v(T_i)\right] \cdot m_v + \left[U_r(T_f) - U_r(T_i)\right] \cdot m_r - \left[m_{wl} \cdot U_{wl}(T_i)\right] \quad \textbf{91}$$

Where subscripts;

a	:	Air
v	:	Vapour
wl	:	Water liquid
r	:	Residual gas
f	:	Final
i	:	Intake

Eq. 91 gives us the state of each of the components that make up the in-cylinder charge; air, residual gases, water vapour and liquid water. In the upcoming section, we shall first adapt these basic equations to allow solution using numerical methods, and then, various properties of the intake charge will be determined, such as temperature, specific heat etc.

Air / water mixture thermodynamic processes in the cylinder during mixture compression: Seeing that the compression of the air / residual gas and water mixture is a non-flow process, the first equation of thermodynamics will take the following form:

$$dU = dQ - dW \quad \textbf{92}$$

This shall be modified and the equation will take the form:

$$\frac{d}{dt}\cdot\left(U_a + U_w + U_l\right) = \frac{d}{dt}\cdot\left(Q_a + Q_w + Q_l\right) - \frac{d}{dt}\cdot\left(W_a + W_w + W_l\right) \quad \textbf{93}$$

Here the properties of air and residual gases are combined using the Keenan and Kayes gas models. The resulting gas is indexed in the equations as “air”. Developing the left hand side of **Eq. 93** we get:

$$\left[m_a\cdot\frac{du_a}{dt} + u_a\cdot\frac{dm_a}{dt}\right] + \left[m_v\cdot\frac{du_v}{dt} + u_v\cdot\frac{dm_v}{dt}\right] + \left[m_l\cdot\frac{du_l}{dt} + u_l\cdot\frac{dm_l}{dt}\right] \quad \textbf{94}$$

For water vapour, the following relation can be used:

$$h = u + P\cdot\upsilon \quad \textbf{95}$$

Or;

$$\frac{dh}{dt} = \frac{du}{dt} + P\cdot\frac{d\upsilon}{dt} + \upsilon\cdot\frac{dP}{dt} \quad \textbf{96}$$

Using **Eq. 96** while solving **Eq. 94**, we get:

$$\left[m_a\cdot\frac{du_a}{dt} + u_a\cdot\frac{dm_a}{dt}\right] + \left[\left(m_v\cdot\frac{dh_v}{dt} + h_v\cdot\frac{dm_v}{dt}\right) - \left(P_v\cdot\frac{dV_{cyl}}{dt} + V_{cyl}\cdot\frac{dP_v}{dt}\right)\right] + \left[m_l\cdot\frac{dh_l}{dt} + h_l\cdot\frac{dm_l}{dt}\right] \quad \textbf{97}$$

Solving for the right hand side of **Eq. 93** we get:

$$\frac{d}{dt}\cdot\left(Q_a + Q_w + Q_l\right) - \frac{d}{dt}\cdot\left(W_a + W_w + W_l\right) = \frac{dQ_{tot}}{dt} - \frac{dV_{cyl}}{dt}\cdot\left(P_a + P_v\right) \quad \textbf{98}$$

Where:

$$Q_{tot} = Q_a + Q_v + Q_l \quad \textbf{99}$$

Combining **Eq. 98** and **Eq. 97**, we get:

$$\frac{dQ_{tot}}{dt} - \frac{dV_{cyl}}{dt}\cdot\left(P_a + P_v\right) = \begin{array}{l}\left[m_a\cdot\frac{du_a}{dt} + u_a\cdot\frac{dm_a}{dt}\right] + \left[m_l\cdot\frac{dh_l}{dt} + h_l\cdot\frac{dm_l}{dt}\right] \\ + \left[\left(m_v\cdot\frac{dh_v}{dt} + h_v\cdot\frac{dm_v}{dt}\right) - \left(P_v\cdot\frac{dV_{cyl}}{dt} + V_{cyl}\cdot\frac{dP_v}{dt}\right)\right]\end{array} \quad \textbf{100}$$

Where;

$\frac{du_a}{dt}$: $= C_{va}\cdot\frac{dT}{dt}$

$\frac{dh_v}{dt}$: $\approx C_{pv}\cdot\frac{dT}{dt}$ or $f(T)$ if saturated, or $f(T, P_v)$ if superheated

$\frac{dh_l}{dt}$: $\approx C_l\cdot\frac{dT}{dt}$ or $f(T)$ if saturated, and null if superheated

After substitutions and simplifications and solution for dT/dt, **Eq. 100** can be then written in its final form as:

$$\frac{dT}{dt} = \frac{\frac{dQ_{tot}}{dt} - u_a \cdot \frac{dm_a}{dt} - \left(h_l \cdot \frac{dm_l}{dt} + h_v \cdot \frac{dm_v}{dt} \right) + \left(V_{cyl} \cdot \frac{dP_v}{dt} - \frac{dV_{cyl}}{dt} \cdot P_a \right)}{\left(m_a \cdot C_{va} + m_v \cdot C_{pv} + m_l \cdot C_{pl} \right)} \qquad \textbf{101}$$

The quantities and variables used in **Eq. 101** are explained in the following table:

$\frac{dQ_{tot}}{dt}$	:	Total heat transfer in the system from the working fluid to the surroundings. Can be estimated / calculated using the Hohenberg heat transfer model for heat transfer between cylinder walls and the working fluid.
u_a	:	Internal energy of air
$\frac{dm_a}{dt}$	:	Change in entrapped air mass. This could be used to define blow-by in the engine. For the present case, this has been neglected
h_l	:	Enthalpy of water in its liquid state. This can be determined from steam tables using cylinder temperature as a reference
$\frac{dm_l}{dt}$	:	Change in the mass of liquid water. This can be defined as a result of blow-by and conversion of liquid water to vapour. As stated above that the blow-by is neglected, this will signify only reduction of liquid water mass for conversion to vapour
h_v	:	Enthalpy of water vapour. Again, this is determined using steam tables, and is defined for temperature in saturated conditions, and pressure and temperature if it is superheated
$\frac{dm_v}{dt}$	:	Change in mass of water vapour. Again, assuming zero blow-by, this will be equal in magnitude but negative in sign to $\frac{dm_l}{dt}$
V_{cyl}	:	Total volume of engine cylinder. Combines swept volume and clearance volume and is defined as a function of engine geometry, crank / conrod lengths and crank angle.
$\frac{dP_v}{dt}$	:	Change in vapour pressure as a function of a change in temperature and specific volume. Can be estimated by making an assumption of $P_v \cdot \upsilon_v = k_v T$, where k_v can be calculated at different points in the steam table.
m_a	:	Mass of air
C_{va}	:	Specific heat at constant volume calculated using the Keenan and Kayes model
m_v	:	Mass of water vapour
C_{pa}	:	Simulated values of Specific heat at constant pressure calculated from steam tables
m_l	:	Mass of water in liquid form
C_{pv}	:	Specific heat of water as a function of mixture temperature, taken from the steam tables

In the next sub-section, we shall see how the aforementioned equations are resolved. The resolution of these equations is specifically done numerically.

2.2.2. Numerical solution of thermal transfer relations for WI:

For a liquid to transform into a gas, latent heat of energy is required to complete the transformation. In a gas / atomised liquid mixture, this energy is taken from the air. This in turn brings down the average temperature of the mixture. For a case where a water spray is injected in the air stream, the heat transfer would be considered, for simplicity's sake, to proceed in the following fashion:

- Mixing of the air and atomised water
- Transfer of heat between liquid water and air.
- Evaporation of liquid water using the heat transfer from the liquid water / air mixture.
- Assuming satisfactory mixing and a sufficiently long time duration, the evaporation of the atomised, liquid water would continue until the combined effect of mixture cooling and increase in the content of water vapour would bring about saturation.

Thermodynamically, the above processes would proceed as under;

1. **Transfer of heat between liquid water and air** – The thermodynamic equation that dictates the heat transfer between air and water at the moment when both are mixed would be expressed as under;

$$m_w(h_w - h_m) = m_a C_{pa}(T_m - T_a) \quad \textbf{102}$$

The equation may be modified thus;

$$m_w C_w(T_w - T_m) = m_a C_{pa}(T_m - T_a) \quad \textbf{103}$$

Where ;

$$C_w = \frac{ha - hw}{Ta - Tw} \quad \textbf{104}$$

$$m_w C_w(T_w - T_m) \approx m_w(h_w - h_m) \quad \textbf{105}$$

$$C_{pa} = \frac{C_{pTa} + C_{pTm}}{2} \quad \textbf{106}$$

The final result that is obtained for mean temperature of the liquid water and air mixture is;

$$T_m = \frac{m_w C_w T_w + m_a T_a C_{pa}}{m_a C_{pa} + m_w C_w} \quad \textbf{107}$$

The variables used are;

m_w	:	Mass of water in the volume
m_a	:	Mass of air in the volume
T_a	:	Initial temperature of air
T_w	:	Initial temperature of water
T_m	:	Final temperature of mixture
h_w	:	Specific enthalpy of water at T_w
h_a	:	Specific enthalpy of water at T_a
C_w	:	Specific heat of water

C_{pa} : Specific heat of air
C_{pTa} : Specific heat of air at T_a
C_{pTw} : Specific heat of air at T_w

2. **Evaporation of water taking in heat from the air / liquid water mixture** – For the sake of simplicity for numerical analysis, the general thermodynamic equation that dictates such a heat transfer has been divided into two parts;

The initial phase – where the air is considered to be dry, without presence of water vapour. Here, the mass of water is reduced by a small amount of $\Delta \boldsymbol{m_w}$ which corresponds to the quantity of water that is converted into vapour. Thus, the thermodynamic equation for this energy transfer would be;

$$\left((m_w - \Delta m_w)C_w + m_a C_{pa}\right)\left(T_{mold} - T_{mnew}\right) = \Delta m_w h_{fg} \qquad \textbf{108}$$

Where the variables used are;

m_w : Mass of water in the volume
Δm_w : Mass of water evaporated
T_{mold} : Initial temperature of air / water mixture
T_{mnew} : Final temperature of air / water mixture after evaporation
h_{fg} : Latent heat of water

The second phase – where the air is considered to be a mixture of air and vapour. Here, the heat required for evaporation is given by air, liquid water and the previously mixed vapour mass.

This system of addition of water vapour into the mixture lends itself well to numerical treatment since it is iterative in nature. The thermodynamic equation for this energy transfer would be;

$$\left((m_w - 2\Delta m_w)C_w + m_a C_{pa} + \Delta m_w C_{pv}\right)\left(T_{mold} - T_{mnew}\right) = \Delta m_w h_{fg} \qquad \textbf{109}$$

Since $\boldsymbol{C_{pv}}$ itself is not defined, an approximation is performed using steam tables for saturated vapour using values for enthalpy $\boldsymbol{h_g}$ and temperature $\boldsymbol{T}$. The estimated value of $\boldsymbol{C_{pv}}$ comes out to around 2.1 ~ 2.6 kJ/kg-K depending upon temperature. As for the value of $\boldsymbol{h_{fg}}$ of water, it too can be found from the steam tables usually under the heading of $\boldsymbol{H_{fg}}$. The value of this varies from just over 2500 kJ/kg to nought. Again, the value depends on temperature of the mixture. As temperature rises the value of $\boldsymbol{H_{fg}}$ or $\boldsymbol{LH}$ declines.

Referring to **Eq. 109**, we can see that the form of the equation is an iterative progression from **Eq. 108**. This can be defined in a more general form as under;

$$\left((m_w - i\Delta m_w)C_w + m_a C_{pa} + (i-1)\Delta m_w C_{pv}\right)\left(T_{mold} - T_{mnew}\right) = \Delta m_w LH \qquad \textbf{110}$$

Where the value of the iteration index $\boldsymbol{i}$ changes from $\boldsymbol{1}$ to $\boldsymbol{n}$. The value of $\boldsymbol{n}$ is defined by a numeric check that stops the iterations if the relative humidity of the mixture reaches a certain predefined limit.

3. **Attainment of a target saturation limit** – Taking over from the previous sections and corresponding equations, we can calculate the final temperatures and humidity ratios of the mixture given the following data;

m_w : Mass of water in the volume
m_a : Mass of air in the volume
T_m : Temperature of mixture of air and water vapour

P_t : Total Pressure of mixture
RH_1 : Initial relative humidity of the air / water vapour mixture
RH_2 : Relative humidity to be targeted
HR : Humidity Ratio

As defined in **Eq. 67**, the relative humidity of the air / vapour mixture is defined as a ratio of the partial pressure of the existing vapour in the mixture to the saturation vapour mixture. Calculating the vapour pressure in the mixture may be done using the law of partial pressures. Given the mass, temperature and total pressure of the gas mixture, we shall be able to determine the specific volumes of each component. The ratio of specific volumes for air and water vapour is the Humidity Ratio of the mixture expressed in kg/kg of vapour in dry air. Numerically, the calculation shall commence by a first iteration where the variable $\boldsymbol{H_{rel\_1}}$ is used to determine the humidity ratio as shown below;

$$P_v = P_{vsat} \cdot RH_1 \quad \textbf{111}$$

$$P_a = P_t - P_v \quad \textbf{112}$$

$$\nu_a = \frac{RT_m}{P_a} \quad \textbf{113}$$

$$HR = \frac{\nu_a}{\nu_v} \quad \textbf{114}$$

After the initial Humidity Ratio is determined, the change in relative humidity can be easily followed as water mixed with the air. Numerically, this is done by progressively adding fractions of water $\Delta \boldsymbol{m_w}$ as defined earlier. At each step of water addition, the temperature of the air / vapour mixture drops as a result of evaporative cooling. At this point, the humidity ratio ***at saturation for that total pressure and temperature*** is determined. The real humidity ratio is then checked using the equation;

$$HR = \frac{m_v + n\Delta m_w}{m_a} \quad \textbf{115}$$

Where $\boldsymbol{n}$ is the $\boldsymbol{n}^{\text{th}}$ iteration of the program or loop. If the value of $\boldsymbol{HR}$ is still under limits, the next iteration of addition of $\Delta \boldsymbol{m_w}$ is then performed. This process is repeated until the limit of humidity ratio is reached. In the case of tests performed on the engine, varying degrees of humidity were achieved. In cases where only cooling was desired, humidity was kept below 100%, on other cases, saturated vapour and water spray were made to enter the engine.

2.2.2.1. Definition of properties of air and water during different phases of the cycle

In the previous section, various terms have been defined with respect to the properties of vapour and how to calculate them given ambient conditions. In this section, the changes in air / water vapour mixture properties at the following steps in the engine cycle will be discussed;

- Mixing of water spray in the intake tract and the conditions of the air, water vapour and liquid water spray after mixing.
- Aspiration of the air / vapour / water mixture via the intake port into the cylinder and mixing with the residual gases.

- Compression, combustion and expansion phases of the engine cycle – determination of air charge properties.

Inclusion of residual exhaust gases to the intake air charge will be treated later on in this section, while the interaction of water with air shall be treated presently.

2.2.2.2. Usage of vapour and air property tables:

During the course of the calculations of mixture properties, it was necessary to know the values of different properties of air and water – both in its vapour and liquid forms to understand their interaction with each other. For this, tables and equations were used.

In the case of air, the properties were determined for the most part from mathematical relations. Be they estimations using perfect gas laws, or using empirical equations such as the Keenan and Kayes model. In some instances, tables were used as well.

In the case of vapour properties, tables were almost exclusively used since there are no perfect equations to correlate Temperature and Pressure with different vapour properties such as enthalpies, specific volumes and internal energies. Two different types of tables were used to determine water and water vapour properties; ones for saturated vapour and ones for superheated vapour. In the following section, the tables and the operations required to determine different properties will be presented.

1. **Property tables of saturated vapour** – By definition, *a saturated vapour has the minimum amount of energy needed to stay in the vapour phase*. Taking temperature as a reference, a saturation state at a certain temperature will have a certain pressure, a certain internal energy, enthalpy, specific volume and entropy. In effect, a saturated vapour state may be defined by either a temperature or pressure. Saturation state tables are therefore defined as either pressure or temperature tables. A part of an example saturated *temperature* steam table is presented below;

P bar	T °C	υ m^3/kg	h_{fg} kJ/kg	h_f kJ/kg	h_g kJ/kg
0	0,0061097	206,30	2499,3	0,00	2499,3
1	0,0065668	192,70	2496,8	4,23	2501,0
99	0,97796	1,7300	2257,8	414,44	2672,2
100	1,0136	1,6730	2255,3	418,67	2674,0
101	1,0504	1,6190	2252,8	422,85	2675,6
233	29,560	0,06772	1799,1	1003,56	2802,7
373	218,30	0,004100	269,5	1968,21	2237,7
374	220,94	0,003580	135,6	2030,98	2166,6
374,2	221,36	0,003180	0,0	2098,78	2098,8

Table 41. Saturated water properties table using ***Temperature*** as a reference [70, 72]

A part of an example saturated *pressure* steam table is presented below:

P bar	T °C	υ m^3/kg	h_{fg} kJ/kg	h_f kJ/kg	h_g kJ/kg
0,02	17,5	66,16	2458,3	73,279	2531,623
0,04	28,9	34,88	2431,6	121,141	2552,739
1,00	99,6	1,70	2256,3	416,930	2673,259
1,02	100,1	1,67	2254,9	419,273	2674,206
1,04	100,7	1,64	2253,6	421,549	2675,116

Table 42. Saturated water properties table using ***Pressure*** as a reference [71]

It is worth noting that as the temperature rises, the latent heat h_{fg} of water reduces. Thus, as temperature rises, it becomes "easier" to evaporate water, or to put it another way, during evaporation; water will require less energy from the ambient gases and will cool them less. The energy required to heat water in its liquid form needs to be calculated. In addition, energy will be required to evaporate water in accordance with its latent heat value at that temperature. Both these energies will then give us the saturated vapour enthalpy at that temperature, h_g. This maximum value of h_g is found between 230 and 237 °C, while the corresponding saturation pressures would be between 28 and 31.78 bar.

When saturated vapour properties are required by different computer programs, a linear interpolation between predefined data points is performed.

2. **Property tables of superheated vapour** – By definition, *a superheated vapour is at a higher temperature than its boiling point at that pressure.* To define different state properties, enthalpy, entropy, internal energy, entropy etc., it is imperative to use both temperature and pressure as references. For each state property, a two-dimensional is defined in terms of pressure on one axis and the temperature on the other. Since superheated vapours are not limited in terms of temperature or pressure, pressures higher than 212 bar and temperatures higher than 374°C can be obtained / defined.

   In our case, where in-cylinder processes are investigated, definitions of state properties at high temperatures are a must. As a reference, superheated vapour tables defined to a temperature of 3000K are used. An example of a superheated vapour table for internal energy is presented **Table 43**;

Pressure	0,000611	0,01	0,05	0,1	0,2	0,3
Temperature	Specific enthalpy					
0	2502,1	0	0	0	0	0
45,81	2586,9	2584,7	0	0	0	0
50	2594,7	2592,6	0	0	0	0
81,33	2653,3	2652,1	2645,9	0	0	0
99,63	2687,8	2686,8	2681,8	2675,5	0	0
100	2688,5	2687,5	2682,5	2676,2	0	0
120,23	2726,8	2726,1	2722	2716,7	2706,7	0
133,55	2752,1	2751,6	2748	2743,4	2734,5	2725,3
143,63	2771,4	2770,8	2767,7	2763,6	2755,5	2747,2

Table 43. Superheated vapour table for enthalpy [73]

Here, the pressure is defined in MPa and the temperature is defined in degrees Celsius. The zeroes in the table in the diagonal direction are the states where water exists as liquid, and the superheat steam table is undefined for those conditions.

To calculate a state property from the given table, linear interpolation in two dimensions is required. The choice for linear interpolation is done due to the following reasons;

- Unavailability of sufficient data points near the points for minimum pressure and minimum temperature.
- The relative error between using a linear or a 3rd or higher order interpolation at well-populated axes (e.g. at 143.63 °C) is relatively small, thus, a linear interpolation can be performed.
- The tables themselves have been developed using linear interpolation to fill in various intermediate data points.

The two-dimensional linear interpolation of the data variables can be performed using Cartesian coordinates and can be done in a square or a triangle to find the intermediate value. In the computer program, three sub-functions are used; one for linear interpolation using square coordinates, and two for linear interpolation using triangular coordinates. Mathematical equations are presented in the following section on how to perform such interpolations.

Linear interpolation using square coordinates – An example table and graphical representation of the interpolation are presented. In this case, the value of the variable ***H*** is to be calculated given the values of ***P*** and ***T***.

Enthalpy	**P_1**	**P_2**
T_1	h_1	h_2
T_2	h_3	h_4

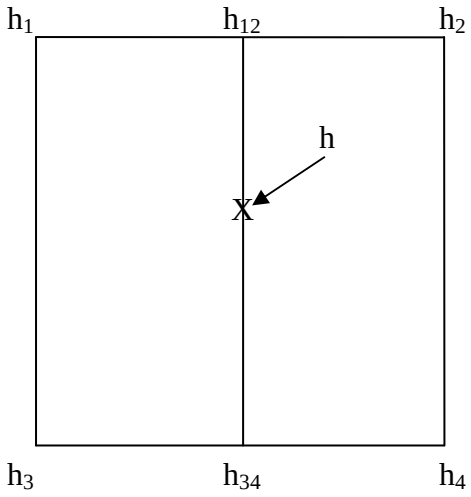

Figure 55. Interpolation using Cartesian coordinates for a square

Here, we shall have two coordinates, ***x*** and ***y***, which will give us the relative position of the variable ***H*** in the figure on the right. We shall use the values of Pressure and Temperature as ***P*** and ***T*** respectively in the equations which are shown thus;

$$x = \frac{P - P_1}{P_2 - P_1} \quad \textbf{116}$$

$$y = \frac{T - T_1}{T_2 - T_1} \quad \textbf{117}$$

$$h_{12} = x(h_2 - h_1) + h_1 \quad \textbf{118}$$

$$h_{34} = x(h_4 - h_3) + h_3 \quad \textbf{119}$$

$$h = y(h_{34} - h_{12}) + h_{12} \quad \textbf{120}$$

Linear interpolation using triangular coordinates – This type of interpolation is used where only three values are present in the vapour property table. The calculations that are required to be done in this case are slightly more involved as compared to the last case however, as we shall see. As before, ***H*** is to be determined given values of ***P*** and ***T***.

Enthalpy	**P_1**	**P_2**
T_1	h1	h_1
T_2	h_2	h_3

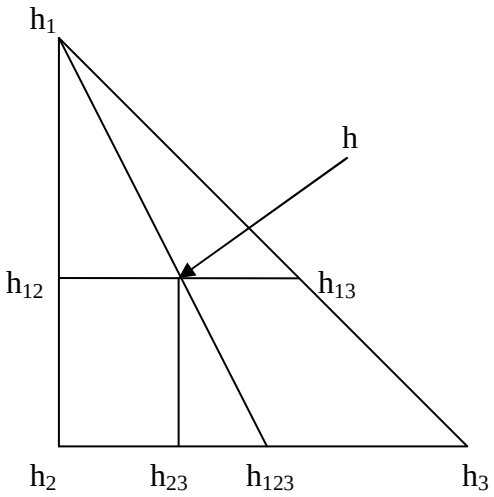

Figure 56. Interpolation using Cartesian coordinates for a triangle

Using various laws of triangles, we obtain the following mathematical equations. **Eqs. 118** to **120** can be re-used here;

$$h_{23} = x(h_3 - h_2) + h_2 \quad \textbf{121}$$

$$h_{13} = x(h_3 - h_1) + h_1 \quad \textbf{122}$$

$$h_{123} = \frac{h_{23}(h_2 - h_1) + h_2(h_2 - h_{12})}{h_{12} - h_1} \quad \textbf{123}$$

$$h = \frac{h_{12} - h_1}{h_2 - h_1}(h_{123} - h_2) \quad \textbf{124}$$

The engine that has been used in the study is a modern diesel automotive engine, of 2 litres displacement, 4 cylinders, turbocharged, equipped with common rail fuel injection, and it conforms to EURO IV emissions standards. It has been extensively modified, notably by the addition of a controlled-temperature low pressure EGR system.

The water injection system has been developed specifically for this thesis. Several evolutions of the system were necessary to get to a point where the system could inject large quantities of water (up to 5 times the injected fuel mass) while assuring a spray quality of the injected water similar to a fog. The water is injected at around 5 to 7 bars of pressure, with air at high pressure being injected in parallel to atomise the water spray. The instrumentation that has been installed has very low measurement uncertainties, which allow us to reliably analyse small variations in consumption and pollutant emissions production.

The water that is injected after the turbocompressor and the chargecooler mixes with the intake air and there is an exchange of energy, according to an open, isobaric and adiabatic thermodynamic process. The produced mixture then enters the cylinders during the intake phase. At this stage, it is not possible to neglect the heat transfers that take place between the metallic walls of the cylinder and the residual gases and the intake charge. As the intake valves close and the piston rises to compress the air / water charge, there are further heat transfers between the intake charge and the metal surfaces of the cylinder, combustion chamber and piston crown. At each step of the intake process, the injected water may evaporate either partially or completely depending on the level of saturation reached at that specific temperature, volume and pressure of the intake charge.

Le moteur retenu pour cette étude est un moteur Diesel automobile récent, de 2 litres de cylindrée, suralimenté, doté d'une injection à rampe commune et satisfaisant à la norme Euro 4. Il a été largement modifié, notamment par l'ajout d'un système EGR basse pression et des dispositifs de contrôle de différentes températures.

Le système d'injection d'eau à l'admission a été développé spécifiquement pour cette étude. Plusieurs évolutions ont été nécessaires pour aboutir à un système permettant d'injecter de grandes quantités d'eau (jusqu'à 5 fois le débit de carburant) tout en assurant une pulvérisation très fine de type brouillard. L'eau est injectée sous quelques bars de pression, l'introduction simultanée d'air comprimé au niveau de l'injecteur facilitant la pulvérisation. L'instrumentation mise en place conduit à des incertitudes de mesure réduites qui permettent d'analyser des variations assez faibles d'émissions polluantes ou de rendement.

L'eau injectée dans le circuit d'admission en aval du turbocompresseur et de l'échangeur de refroidissement d'air de suralimentation se mélange à l'air d'admission et échange de l'énergie avec lui, suivant un processus en système ouvert qui a été modélisé comme adiabatique et isobare. Le mélange ainsi produit pénètre ensuite dans les cylindres pendant la phase d'admission. Il n'est alors plus possible de négliger les échanges de chaleur qui ont lieu au niveau des parois et par mélange avec les gaz résiduels. Enfin, lorsque les soupapes d'admission se ferment, commence une phase de compression, en système fermé mettant là aussi en jeu des échanges de chaleur à travers les parois. A l'occasion de ces étapes successives, l'eau liquide injectée peut se vaporiser partiellement ou totalement, suivant que la saturation est atteinte ou pas.

3. CHAPTER 3: Numerical and experimental study of water injection

L'analyse théorique esquissée dans la deuxième partie du chapitre précédent a montré que l'injection d'eau liquide dans le circuit d'admission d'un moteur à combustion interne pouvait donner lieu à des situations variables concernant l'évaporation de l'eau.

L'objet de ce chapitre est de s'appuyer sur les modèles développés et exposés dans le chapitre 2, pour évaluer les caractéristiques thermodynamiques du mélange air/eau depuis l'injection de l'eau liquide jusqu'au début de la combustion. Il s'agit en particulier de tenter de déterminer l'état de l'eau et la température du mélange. Cette analyse est menée pour les conditions effectivement testées expérimentalement et présentées en détail dans le chapitre 4, mais au-delà, pour une plus large gamme de conditions qu'il est possible de rencontrer au sein d'un moteur, afin de déterminer les paramètres d'influence et les situations les plus favorables. Aussi, ce chapitre est divisé en trois parties, correspondant aux étapes successives rencontrées dans le moteur :

- ✓ *La première partie traite de l'injection d'eau liquide et du processus de mélange avec l'air dans le circuit d'admission.*
- ✓ *La deuxième partie décrit l'évolution du mélange air-eau pendant la phase d'admission dans les cylindres.*
- ✓ *Enfin, la troisième partie concerne la phase de compression, une fois les soupapes d'admission fermées, et l'évaluation du dégagement de chaleur pendant la combustion.*

The theoretical analysis outlined in the second part of the last chapter has shown that water injection in the intake system of an internal combustion engine may give rise to different situations as concerns evaporation of water.

The purpose of this chapter is to use the models developed and shown in the last chapter, to evaluate the thermodynamic properties of the air / water mixture as it is injected into the engine from injection to combustion. The aim is to try and determine the state of water and the temperature of the mixture. The analysis is performed not only for test points that have been experimentally measured on the test engine – which are discussed in Chapter 4 – but also for a wider range of operating conditions, which may be encountered in engine operation, to determine the influencing parameters and conditions conducive to optimal evaporation. This chapter has been divided into three parts, corresponding to steps observed in succession in an engine operation:

- ✓ *The first part deals with the injection of liquid water in the intake manifold and the mixing process in the intake air circuit.*
- ✓ *The second part describes the evolution of the air / water mixture during the intake phase into the cylinders.*
- ✓ *The third and final part concerns the compression phase, after the closing of the intake valves, and the evaluation of the heat release during combustion.*

3.1. WI analysis for intake manifold:

On the test engine, the water injector is mounted between the intercooler outlet and the intake to the engine. The temperature at the intercooler exit can be controlled using a water cooling system on the intercooler core. Thus, even at high boost pressures, the charge temperature can be cooled down significantly.

Thermodynamically, the mixing of the air and the water spray are considered to be adiabatic in nature, meaning that all the energy required for the evaporation of the water spray will be provided by the air / water vapour mixture. This can be explained by the fact that the difference in temperature between the walls of the admission tract and the air charge is relatively minor. As a general case during the tests, the temperature of the water spray is always lower than the pressurised air charge.

The results obtained from the calculations provide us different theoretical scenarios in which final mixture temperatures and vapour / liquid fractions are given for water when mixed with intake air charge. In general, three different conditions can be attained after the WI has interacted with the intake air charge:

Air charge with vapour at saturated conditions and water suspended in the air charge in liquid form: In general, this condition is the easiest to achieve. In this situation, as water is injected into the air charge, the water droplets interact with the air charge – undergoing a heat transfer directly from water droplets to air and if air is not saturated with water vapour, said water droplets evaporate in contact with the air undergoing further heat transfer.

Air charge with water vapour in the superheated condition: After WI, if all of the water has been evaporated and the relative humidity of the resulting water / air vapour charge are still less than 100 %, the vapour will be in a superheated state.

Air charge with water vapour in the saturated condition: After WI, if all of the water has been evaporated and the relative humidity of the resulting air / water charge is a 100 %, the vapour will be in a saturated state.

3.1.1. Physical parameters dictating the condition of intake air charge:

After introduction of water injection in the intake air charge, thermodynamic processes take place which bring about a change in the temperature and saturation of the air / water / vapour mixture. The final temperature of the mixture and state of the air / water mixture will depend upon various factors. The most significant of these factors are:

- Initial ambient humidity
- Boost pressure of the air charge in the intake manifold
- Temperature of the air charge prior to water injection in the intake manifold
- Initial temperature of the injected water spray in the intake manifold
- Mass ratio of the air charge and the WI sample

Using these inital known conditions, a numerical code developed in MATLAB® was used for the calculations of water vapour and liquid masses. The same code calculates the temperature

of the intake air charge using the equations described in **Chapter 2** earlier while using the following numerical process:

- Definition of initial conditions (as defined above and detailed later in **Table 44**)
- Calculation of quantity of vapour present in air based on the ambient atmospheric conditions. Separation of intake air into dry air and vapour components.
- Calculation of initial air / water mixture temperature after mixing in the intake tract (without evaporation).
- Calculation of temperature of air / vapour / atomised water mixture by progressively evaporating water.
- During evaporation and cooling, the relative humidity of the charge is verified at each iteration and the loop is stopped when it reaches saturation.

To numerically calculate these states, the computer code takes data corresponding to the following input parameters listed in **Table 44**:

T	:	Ambient temperature of intake air
T_w	:	Initial temperature of injected water
T_{air}	:	Temperature of air in the intake manifold after intercooler
P_{boost}	:	Air (Boost) pressure in the intake manifold
RH_i	:	Initial relative humidity
m_a	:	Mass of air sample in the mixture
m_w	:	Mass of water sample in the mixture

Table 44. Parameters used for calculation of air / water / vapour states

Ambient temperature "T": The specific humidity of an air / vapour mixture varies greatly with the temperature. The ambient temperature and the ambient pressure are used to determine the initial specific humidity of the air charge. This value of specific humidity will be used after the compression of the air charge to measure the relative humidity at that state of pressure and temperature.

Temperature of injected water "T_w": The temperature of the injected water in the air charge plays a major role in the final temperature and saturation level of the air / vapour charge in the intake manifold. Assuming the case where the air charge is initially unsaturated, when water is injected into the compressed air stream, it will evaporate, taking heat away from the air / water mixture. This has the effect of reducing the temperature of the air / vapour mixture. A higher initial temperature of the injected water will result in a higher final temperature of the air / water vapour mixture. If we inject water with the aim to obtain a saturated air / water vapour mixture, we will have a higher specific humidity for the air / vapour charge if the initial temperature of the injected water is higher, since the water will aid in heating up the air charge.

Initial temperature of the boost air "T_{air}": The initial temperature of the boost air will have similar effects to that of T_w, in that a higher temperature for the same pressure will result in a higher final specific humidity value.

Boost pressure: As we increase total charge pressure, for the same initial relative humidity and constant temperature, the specific humidity reduces. As mixture pressure is increased for

the same mass of air charge at the same temperature, it follows that the volume of the charge has reduced. Seeing that the temperature remains the same, the specific volume of the vapour remains the same, as does its vapour pressure. The reduction in volume occupied by the air / vapour charge results in a smaller mass of vapour. Thus, as the total pressure increases at constant temperature, for a given charge with a predefined specific humidity ratio, the relative humidity increases.

Initial relative humidity 'RH_i": The initial relative humidity, in conjunction with ambient temperature and pressure, will give us a value of initial specific humidity. This will indicate whether the air charge is saturated or not in the intake manifold.

Mass of air and water injection samples "m_a", "m_w": The ratio of water / air mass is an important factor for the final temperature of the air / water mixture. This, in conjunction with the air and water stream temperatures, will give us the temperature and mass of the vapour and liquid water in the air / water mixture. In general, when the ratio of water / air is increased, the final temperature of the mixture tends to approach the temperature at which the water was initially injected.

3.1.2. Study of the scope of effects of WI on compressed air charge:

In this sub-section, a range of values is given to each physical parameter which may have an effect on the water injection process. The results that are of interest are the final vapour mass and the final mixture temperature. The range of values for each parameter is given below:

T	:	20°C
T_w	:	15 and 90°C
T_{air}	:	30, 70, 110 and 150°C
P_{boost}	:	3 bars
RH_i	:	0, 50 and 100%
m_a	:	1 kg
m_w	:	0.1, 0.3 and 0.5 kgs

Table 45. Values of parameters of water injection

With reference to **Table 44** and **Table 45**, the ambient temperature of air is taken as 20°C, the temperature of water for injection is taken as 15 and 90°C. The temperature of 90°C for the water injection is comparable to that used in Munter's HAM (Humid Air Motor) sytem [18]. The manifold air charge temperature is taken as between 30 and 150°C with steps of 40°C each. The boost pressure is taken as 3 bars. The highest intake air temperature, i.e. 150°C corresponds closely to a 3 bar compression with 75% adiabatic compression efficiency (which analytically yields ~165°C). The ambient air humidity at 20°C is taken as 0, 50 and 100%. The mass of air charge (wet, at any of the relative humidity levels) is taken as 1 kg. The mass of injected water is taken as 0.1, 0.3 or 0.5 times that of the intake air charge mass.

In the following part, we shall see the effect of water injection on the final air / vapour / liquid mixture temperature and constitution. In general, as temperature of air and / or water is increased, the evaporation of water is increased. Also, if the intial vapour mass in the air charge is high, the final vapour mass will be higher than for a sample of air that was dryer before WI.

Here, six graphs are shown. These graphs are divided in three sets of two graphs each. Each set comprises of graphs for injected water temperature at 15°C and 90°C. The three sets are divided by ratio of injected water mass to air charge mass of 0.1, 0.3 and 0.5. Each graph shows the post WI intake air charge temperature and the final water vapour mass per

kilogramme of dry air (specific humidity). The dashed lines represent temperature, the dotted solid lines represent specific humidity in kg of water vapour in the air charge (1 kg mass) and the solid lines represent the remaining water in liquid form in the air charge. For each of the two measured parameters, there are three lines, coloured black, red and orange. These lines represent the different initial humidity ratios of 0%, 50% and 100% measured at atmospheric conditions (1.01325 bars and 20°C). Referring to **Figure 57**:

a.

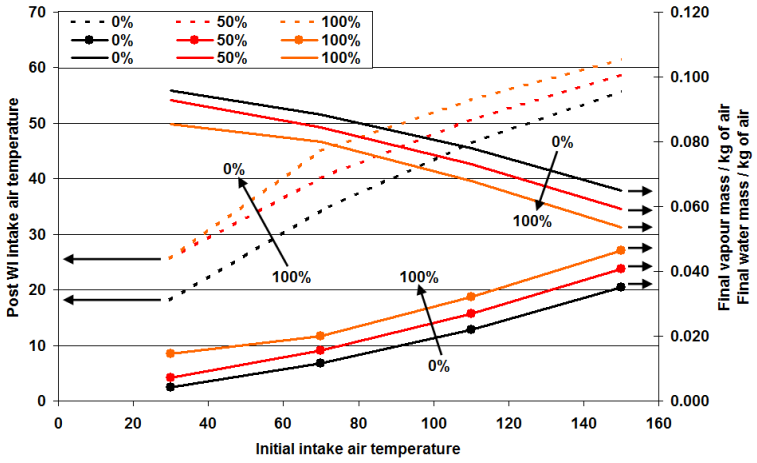

b.

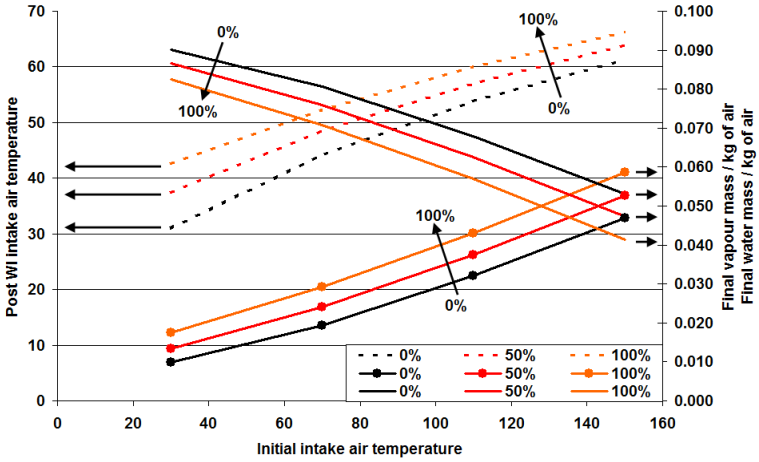

Figure 57. Graph for water to air mass ratio of 0.1 and injected water temperature of **a.** 15°C and **b.** 90°C

From **Figure 57**, we can see that the relatively low mass of the injected water in relation to the mass of air charge means that around half of it is evaporated. Due to the evaporation of water, the temperature of the air and liquid water drop. In the case of **Figure 57 a.**, we see that the final temperature of the mixture varies between 55.7 and 61.5 °C (for relative humidity of 0 to 100% and initial air charge temperature of 150°C) whereas in the case of **Figure 57 b.**, the temperature varies between 61.4 and 66.3 °C. This shows that a 75°C difference of injected water temperature resulted in only around 5°C difference in the final air charge / water vapour / liquid mixture. If we injected even less water, such that all of it were evaporated, the difference in final mixture temperature would have been even closer.

The reason this is so is that the latent heat of evaporation of water at these temperature / pressure ranges (15°C – lowest for injected water – to 150°C – the highest for initial air charge temperature) is of the order of 500 to 600 times greater than the specific heat of liquid water. The higher the temperature, the higher the specific heat of water and the lower the latent heat of evaporation, hence the ratio tends to drop in value as the temperature rises. It is

due to this reason that the final temperature of the air / water vapour mixture is relatively insensitive to the intial temperature of the injected water.

If however, the mass of the injected water were increased, the aforementioned statement would no longer be true. The limit of evaporation is determined by the saturation pressure of the water vapour. The larger quantity of water in liquid form can thus have a larger influence on the final mixture temperature. We shall see this exact effect in the following graphs, the first set of two for water / air ratio of 0.3 and the second set of two for water / air ratio of 0.5:

a.

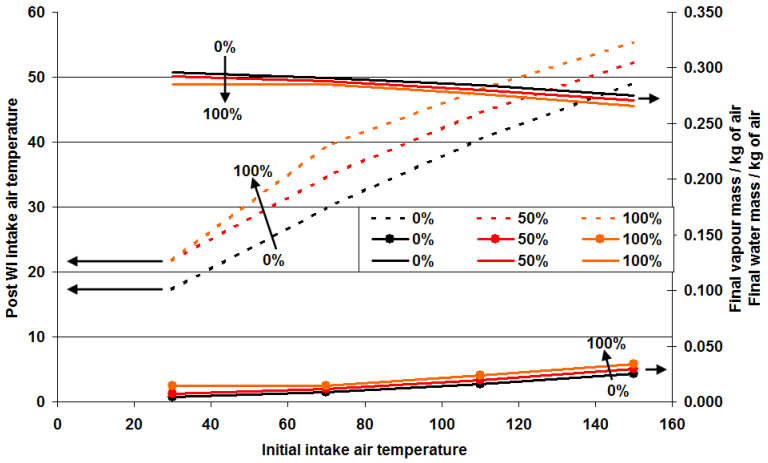

b.

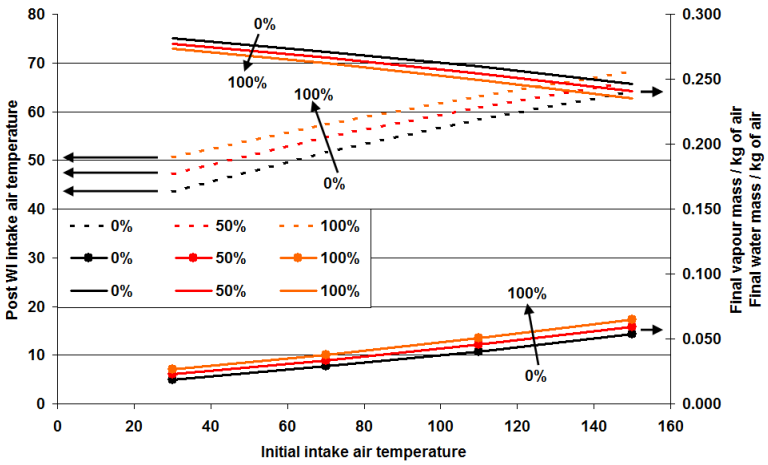

Figure 58. Graph for water to air mass ratio of 0.3 and injected water temperature of **a.** 15°C and **b.** 90°C

a.

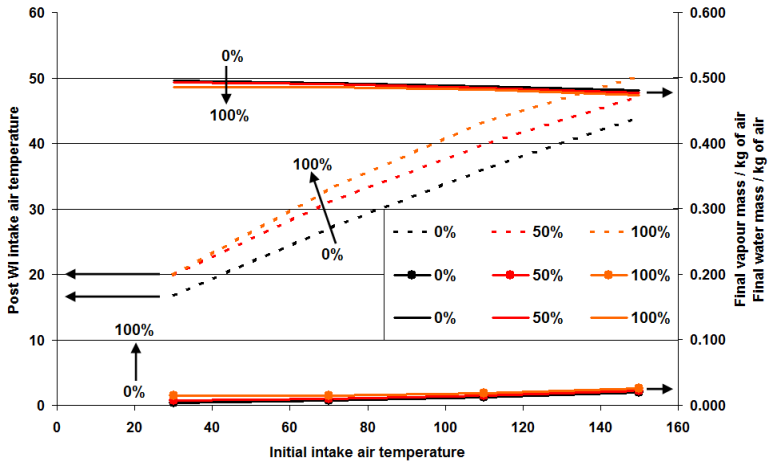

b.

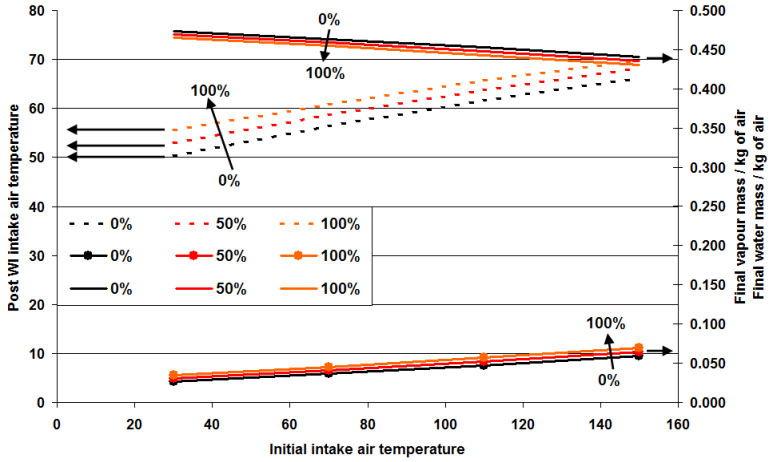

Figure 59. Graph for water to air mass ratio of 0.5 and injected water temperature of **a.** 15°C and **b.** 90°C

Comparing the graphs shown in **Figure 58** and **Figure 59** as compared to **Figure 57**, we can see that a lot of the injected water remains as liquid. In addition to that, the influence of injected water temperature on the final air / vapour / water mixture is much more marked as the ratio of injected water mass to air charge mass increases.

In the case of the water / air ratio of 0.3 given in **Figure 58 a.**, for 15°C injected water temperature, the final mixture temperature varies between 49.2 and 55.4°C (for relative humidity of 0 to 100% and initial air charge temperature of 150°C). In **Figure 58 b.**, for 90°C injected water temperature, the final mixture temperature varies between 64.2 and 68.3°C. This shows that a 75°C difference of injected water temperature resulted in around 13 to 15°C difference in the final air charge / water vapour / liquid mixture.

We shall see that for **Figure 59**, this influence of injected water temperature is even more marked owing to the fact that the water / air ratio is of 0.5. Again, referring to **Figure 59 a.** and **b.**, we see that the influence of water injection gives a variation of between 44.1 and 50.3°C for the 15°C water injection, and between 66.3 and 69.9°C for the 90°C water injection. This brings the influence of water injection temperature to around 20°C.

Earlier in this section, a comparison with the Munter's HAM system [18] was made where water is injected via a humidification tower which is placed between the intake air compressor and the engine. Water that is pre-heated with waste engine heat is sprayed from nozzles at the top of the column into the air flow entering from the bottom. An amount of water far in excess

of that required to saturate the air is supplied. Only 5% to 10% of the water sprayed into the tower evaporates. Water that does not evaporate into the air is collected at the bottom and re-circulated.

By definition of the sytem's functioning, it is clear that the ratio of injected water mass to the air charge mass is much higher than that used in the earlier simulations. And it is for this reason that the air / vapour charge will be at 90°C when it enters the engine cylinders. The excess liquid water spray is collected and recirculated for further water injection.

3.1.3. Comparison of real and measured post WI air / water charge temperature:

In this subsection, we will compare post WI air charge temperatures measured using experimentation and from calculations based on known physical initial parameters. After water injection, the resulting air / water charge may be found in two broadly defined states:

1. Undersaturated air / vapour mixture.
2. Saturated air / vapour mixture with excess of liquid water.

There is a third case, where the air and water vapour are at a saturated state with no liquid water present. This case however is very difficult to achieve, and has not been studied here.

Undersaturated air / vapour mixture: Here, the temperature and pressure of the air / water vapour mixture dictate that the vapour exists in a superheated state. There is only dry air and water vapour in the mixture. No water exists in the liquid form in the charge mixture. The WI process proceeds in the following manner:

1. Air charge is compressed by the turbocompressor
2. The air charge is heated during the compression phase
3. The air charge is cooled down via the chargecooler
4. Water is injected into the hot air charge
5. Water evaporates completely in the air charge cooling down the mixture

Here, we shall perform a comparison of the experimental and calculated data. A test point of interest is test point C which is outlined in chapter 4 of this document. The characteristics of this operating test point are presented in **Table 46**:

Points		Measured	Calculated
Injected water temperature	**℃**	22.4	
Measured air mass flow rate	**mg/cp**	803.5	
Ambient Relative Humidity	**%**	74	
Ambient temperature	**℃**	22.2	
WI mass flow rate of water	**mg/cp**	13.3	
Post I/C air charge temperature	**℃**	91	
Manifold pressure	**mbar**	1800	
Patm	**mbar**	1013	
Temperatures:			
Post WI manifold air charge temperature	**℃**	46.2	52.2
Cylinder 1 intake air temperature	**℃**	55.8	52.2
Cylinder 2 intake air temperature	**℃**	53.2	52.2
Cylinder 3 intake air temperature	**℃**	48.8	52.2
Cylinder 4 intake air temperature	**℃**	50.5	52.2
Post WI relative humidity in the intake manifold	**%**		57.1

Table 46. Table comparing measured test point temperatures with those calculated using numerical code

In this table, we see the physical parameters of the boosted charge air in the left column and the results from the numerical code in the right column. We see a good agreement between the measured and calculated values. We do note a tendency of the charge temperature to rise between the manifold and each cylinder intake; this may be considered to be due to the backflow of hot gases during the intake valve opening interval [12].

Saturated air / vapour mixture with excess of liquid water: Here, the temperature and pressure of the air / water vapour mixture dictate that the vapour exists in a saturated state with a surplus of water existing in the liquid state. The air charge mixture is composed of dry air, water vapour and water in suspended liquid form. The WI process proceeds in the following manner:

1. Air charge is compressed by the turbocompressor
2. The air charge is heated during the compression phase
3. The air charge is cooled down via the chargecooler
4. Water is injected into the hot air charge
5. Water evaporates partially in the air charge cooling down the mixture, while a remainder of the injected water mass remains suspended in the air / water vapour mixture.

Here, we shall perform a comparison of the experimental and calculated data. Four test points as defined in **Table 40** have been used in this experiment, and all of those are outlined below:

Points		A	B	C	D
Injected water temperature	**℃**	18.6	23	24.4	24.7
Measured air mass flow rate	**mg/stk**	512.3	538.9	579.9	743.8
Ambient Relative Humidity	**%**	51	44	49	76
Ambient temperature	**℃**	16.3	20.1	25.3	18.6
WI mass flow rate of water	**mg/stk**	31.9	52.5	60.9	87.4
Post I/C air charge temperature	**℃**	31.2	30	60	31
Manifold pressure	**mbar**	1108.4	1182.3	1347.7	1650.1
Patm	**mbar**	985.5	992.8	993.7	986.6
Temperatures:					
Post WI manifold air charge temp	**℃**	22.1	26.6	36.3	29.8
Cylinder 1 intake air temperature	**℃**	22.2	27.0	37.0	30.4
Cylinder 2 intake air temperature	**℃**	22.9	26.9	36.8	29.8
Cylinder 3 intake air temperature	**℃**	21.1	25.1	34.9	28.0
Cylinder 4 intake air temperature	**℃**	21.2	25.1	34.9	28.1
Water / air mass ratio		0.06	0.1	0.1	0.1
Calculated post-WI charge temp (cylinders 1 – 4)	**℃**	17.8	19.1	29	25.4
Post WI relative humidity in intake manifold	**%**	100	100	100	100

Table 47. Table comparing measured test point temperatures with those calculated using numerical code

Referring to temperatures calculated in **Table 47**, we see that they are slightly lower than those measured. The difference of 3 – 7°C may be due to the assumptions made for the numerical calculation and/or to experimental uncertainties. However, the fact that the water / air mass ratio never exceeds 0.1, we can safely state that the temperature of water does not greatly influence the final temperature of the air / water / vapour mixture.

As a matter of interest, the comparison of measured vs. calculated post-WI manifold temperatures is made for point C. This point is chosen since it has the greatest number of test points and the spread of available experimental data is good.

Water injection quantity	kg/h	0	5	9	13	17	21
Injected water temperature	℃	24	24	24	24	24	24
Measured air mass flow rate	mg/stk	880.1	873.7	860.5	854.3	851.1	845.1
Ambient Relative Humidity	%	68	65	54	52	46	41
Ambient temperature	℃	21.6	22.8	24.9	25.5	23.1	23.9
WI mass flow rate of water	mg/stk	0	20.3	36.5	52.2	68.4	84.9
Post I/C air charge temperature	℃	30	30	30	30	30	30
Compressor outlet pressure	mbar	1800	1800	1800	1800	1800	1800
Patm	mbar	1023	1022	1021	1020	1017	1016
Temperatures:							
Post WI manifold air charge temp	℃	29.2	27.3	28.8	30.0	28.8	29.2
Cylinder 1 intake air temperature	℃	30.2	27.5	29.0	30.0	28.7	29.1
Cylinder 2 intake air temperature	℃	30.2	27.5	29.1	30.4	29.1	29.6
Cylinder 3 intake air temperature	℃	28.4	25.8	27.5	28.8	27.4	27.9
Cylinder 4 intake air temperature	℃	28.7	25.9	27.6	28.8	27.4	27.9
Water / air mass ratio		0.000	0.023	0.043	0.062	0.082	0.102
Post WI relative humidity in intake manifold	%	71.5	100	100	100	100	100
mvin – intake vapour mass	mg/stk	9.6	9.8	9.1	9.1	6.9	6.4
mvf – final vapour mass	mg/stk	9.6	10.8	10.3	10.2	8.9	8.6
mw – residual liquid water mass	mg/stk	0	19.3	35.3	51.1	66.4	82.7
Calculated post-WI charge temp (cylinders 1 – 4)	℃	30	26.9	26.4	26.3	24.3	23.8
Post-WI ΔT (T_{meas} - T_{calc})	℃	-0.8	0.4	2.4	3.7	4.5	5.4

Table 48. Variation of post-WI intake manifold air charge temperature, and difference between measured and calculated values in function of injection flow rate.

We see in **Table 48** that as the mass injected quantity of water is increased, the difference in temperature between the measured and calculated values increases, varying from close to zero to around 5°C. The calculated post WI temperature decreases from 26.9°C to 23.8°C when the WI mass flow rate is increased from 5 to 21 kg/h, because the supplemental liquid water even if does not evaporate (the final vapour mass slightly decreases when WI is increased) tends to cool down the mixture. On the other hand, the measured post WI manifold air charge temperature and the various cylinder intake temperatures do not seem to follow such a tendency, varying only slightly between 27°C and 30°C.

These discrepancies between calculation and measurements could be explained by the following points:

- ✓ The calculation relies on the assumption of an adiabatic mixing. However, it can be estimated that some heat transfer happens between the charge air and the surrounding air through the wall of the intake tract. The intensity of this transfer obviously depends on the temperature difference between charge air and outside air (which is usually at a lower temperature, thus causing heat losses to the charge air) and may also be influenced by the water content of the charge air (the convective transfer being enhanced by the presence of water).
- ✓ Another assumption of the calculation is that water evaporates until saturation is reached (equilibrium state). It may be possible that evaporation kinetic is such that the equilibrium reached at the point where temperature measurements are done. Water vapour may also condensate locally due to cold spots.

- ✓ An eventual back flow from the cylinders through the intake valves is not taken into account in the calculation. It may modify (increase) the temperature measured in the intake ducts, near the intake valves.
- ✓ The measurement uncertainties obviously concern measured temperature, but also influence calculated temperatures, since the calculation relies on measured values (water and air mass flow, post I/C air temperature, water temperature, compressor outlet pressure,...).

3.2. WI analysis during the intake process.

In this section, we shall make a comparison of different scenarios during the intake of the air charge into the cylinder. To stay coherent with reality, we shall be using one real-world operating point shall for this study, where the intake air charge will vary from having no water injection, to four levels of WI rate.

After the air water mixture has been formed, it passes via the intake valves into the cylinder. Unlike the intake tract, where the air / water flow was considered to be adiabatic, there will be considerable heat transfers between different metallic surfaces and the charge. This is due to the fact that the charge flow is forced to follow a path that is in close proximity with hot metal parts. This would result in the heating up of the charge air going into the cylinder. For this, various scenarios are proposed for calculation of the physical state of the intake charge during the intake process:

1. In the case of “dry” air intake (with or without WI, but all water is evaporated in the intake tract before entry into cylinder), the intake charge will undergo heat transfer with the residual gases and the metallic surfaces comprised of the cylinder and piston walls and valvegear.

2. In the case of “wet” air intake (with WI, where some water is present in suspended liquid form on entry into cylinder), residual gases and the cylinder walls transfer heat to the whole mixture and help in evaporation of the liquid water until:

    i. All the water is evaporated and the vapour goes superheated.

    ii. The air / water vapour charge is saturated and liquid water is left behind to be evaporated during either the compression or combustion phases of the engine cycle.

According to the mass ratio of air charge and injected water, initial humidity, intake manifold pressure etc., we may either find ourselves in a situation where all the water is evaporated in the intake, or some liquid is left in the intake charge which will subsequently evaporate during the closed part of the cycle.

The calculations needed to determine the physical parameters of the air charge inside the cylinder would include the following:

1. **Mass of air and injected water** – This is already defined in the test data sheets. The water injection system in essence consists of a constant mass-flow air compressor, a relief valve and the air-assist water injection nozzle as detailed in **sec. 2.1.2**. Generally, the relief valve is adjusted to give a certain “leakage” of air to the atmosphere to maintain a constant pressure in the line in conjunction with the water injector. In absence of this relief valve, the compressor would always trip or shutdown

as the maximum supply air pressure of 5 – 6 bar is reached, thus causing the air pressure to fluctuate undesirably.

The water flow rate is controlled by its pressure using a pressure regulator. As the water flow rate increases, the effective orifice size for the air flow becomes smaller. This causes a change in the compressed air flow into the engine and increases the line pressure of the compressed air supply. The change in the pressure of the compressed air supply is monitored and is correlated using the following steps:

- A baseline measure of air mass flow into the engine is taken using no air injection.
- For the same engine control settings, a second measure of air mass flow rate into the engine is taken with the air supply for the water injection system turned on.
- The difference of the two engine air flow rates is correlated with the air supply pressures to correct the air flow into the engine during water injection.

Since the flow characteristics of the compressor are unknown, the calculation of variation of air flow rate into the engine has been simplified somewhat. The system is treated as a network of two orifices in parallel. For the first orifice, the flow section will remain constant; this orifice is the pressure relief orifice which will stabilise the pressure of the high pressure air line. For the second orifice, the flow section will change, in reality due to change in flow rate of water – the greater the flow rate, the smaller the effective flow section for air. A difference in air flow is taken for the baseline and for compressed air injection. This difference is added to each air flow measure using water injection.

The ratio of air flow through an orifice (the relief valve) is proportional to the square root of the pressure difference between the inlet and outlet of an orifice. The pressure measured in the air supply line is relative. Therefore, the ratio of air flow between the baseline and measured point is the square root of their respective relative pressures. We have assumed for this exercise that the air flow rate from the compressor between 5 and 6 bars does not vary (fixed-displacement compressor), therefore, any increase in the air line pressure will result in an increase in air flow from the bleed orifice to the atmosphere and will result in less air flow into the WI system. And hence, less air will be added to the intake air charge measured by the air flow meter. This correction factor is defined as:

$$\Delta m_c = \Delta m_b \sqrt{\frac{P_m}{P_b}} \qquad \textbf{125}$$

Δm_c	:	Air mass flow rate correction to be added to measured value
Δm_b	:	Difference in mass flow rate of air for baseline measure
P_m	:	Pressure of injected air at measured point
P_b	:	Pressure of injected air at baseline point

As a point of interest, the measured and corrected air flow rates for the operating point given in **Table 52** are shown here for reference:

		1	2	3	4
Measured water injection rate	Kg/h	3.0	9.0	16.9	20.9
WI air line pressure	bar	5.8	6.1	6.5	6.6
Measured air flow into engine	mg/stroke	865	849	840	834
Air mass flow correction	mg/stroke	12	11	11	11
Corrected air mass flow	mg/stroke	877	860	851	845
Percentage correction	%	1.4	1.3	1.3	1.3

Table 49. Air correction section from **Table 52**

2. **Total pressure inside the cylinder at the end of the intake stroke** – As it stands, the actual instantaneous pressure inside the cylinder when the intake valve closes could not be measured. For the sake of simplicity, the final pressure in the cylinder at the end of the intake stroke at BDC was considered to be equal to the air charge pressure in the intake tract.

3. **Residual gas mass in the cylinder** – The calculation of the residual gas mass in the cylinder depends on the following factors [56]:

    - Engine speed
    - Temperature of exhaust gases at the end of expansion stroke
    - Pressure of inlet and exhaust gases
    - Valve overlap factor (OF) [56]
    - Compression ratio
    - Composition of exhaust gases – presence or otherwise of water injection and fuel / air equivalence ratio λ

    The temperature of the exhaust gases at TDC on the exhaust stroke is assumed to be equal to the temperature of exhaust gases in the exhaust manifold. This assumption is made on the basis that for the test engine in question, it was not possible to instantaneously measure the temperature of the gases inside the cylinder. Seeing that the exhaust gas temperature sensor sees the flux of hot gases passing by almost continuously over it during the exhaust gas phases, the temperature read by this sensor was considered to be the average temperature of exhaust gases at the end of the exhaust stroke.

    As with the exhaust gas temperature, the pressure of the exhaust gases at TDC on the exhaust stroke is assumed to be equal to the pressure of exhaust gases in the exhaust collector. Same is the case for the intake gases. Cylinder pressure is measured using a piezo-resistive pressure sensor which measures pressure as a relative quantity. Therefore after each measure, it is impossible to know the exact pressure of the charge in the clearance volume at the end of the exhaust stroke.

    The valve overlap factor in a cylinder influences the residual mass entrapped in the clearance volume of a cylinder very directly. The difference between the pressures in the exhaust and the intake collector would cause a non-negligible flow of gases across the combustion chamber. In case the gas flow is from the intake to the exhaust, this will help in the scavenging operation to maximise the concentration of fresh air in the cylinder. The valve overlap factor is defined as:

$$OF = \frac{D_i \cdot A_i + D_e \cdot A_e}{V_d} \quad \textbf{126}$$

In the above expression, $\boldsymbol{D_i}$ and $\boldsymbol{D_e}$ are the inner seat diameters of the intake and exhaust valves and $\boldsymbol{V_d}$ is the displacement volume of the engine. The quantities $\boldsymbol{A_i}$ and $\boldsymbol{A_e}$, which have dimensions of length time crank angle (degrees), are areas under the valve-lift/crank-angle curves defined by the following:

$$A_i = \int_{IVO}^{IV=EV} L_i \cdot d\theta \quad \textbf{127}$$

and

$$A_e = \int_{IV=EV}^{EVC} L_e \cdot d\theta \quad \textbf{128}$$

Where $\boldsymbol{L_i}$ and $\boldsymbol{L_e}$ are the intake and exhaust valve lifts, ***IVO*** and ***EVC*** denote Inlet Valve Opening and Exhaust Valve Closing crank angles respectively, ***IV=EV*** denotes the crank angle degree where the inlet and exhaust valve lifts are equal. The value for the ***OF*** has a dimension of crank angle degree per unit length. As a reference, an intake and exhaust valve profile is given below compared to the test engine at valve overlap:

a

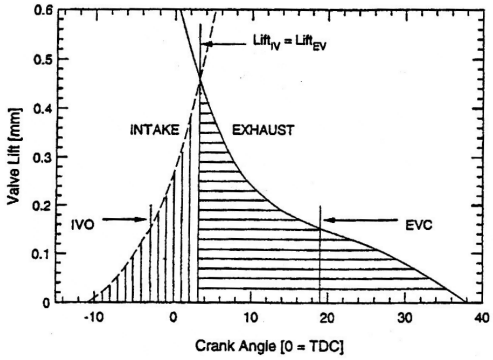

b

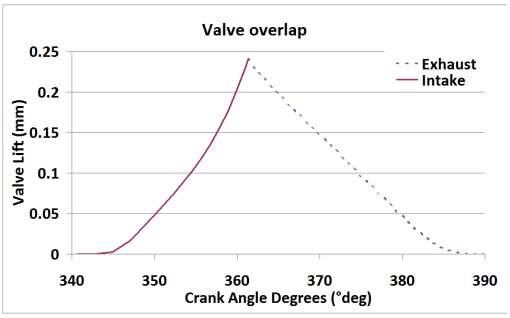

Figure 60. Valve lift diagrams from **a.** literature [56], **b.** test engine.

The intake and exhaust valve lift profiles give us the effective valve flow area which can be used in conjunction with the differential in the intake and exhaust pressure to produce a gas flow either towards the intake or towards the exhaust. The direction of gas flow would depend on the relative difference in pressures.

As per the residual gas model developed by Heywood et al. [56] and used by others [54, 55], in the case of the test engine, we have the following values for the valve events:

IVO	:	340.65°
IVO=EVC	:	361.35° @ 0.24 mm lift
EVC	:	393.06°
A_i	:	1.55 °-mm
A_e	:	2.76°-mm
OF	:	0.223°/m

Table 50. Valve overlap event values

The average flow area would then be defined as;

$$Av, mean = \frac{\pi V_s OF}{\Delta\theta} \quad \textbf{129}$$

$A_{v,mean}$: Mean valve overlap area (metre^2)
$\Delta\theta$: Valve overlap period (degrees)

Using values calculated earlier, the flow area comes out to

$$Av, mean = 6.7\times10^{-6}\, m^2 \quad \textbf{130}$$

To determine the residual gas mass fraction, the following simplified equation is used;

$$x_r = C_1 \cdot \frac{OF}{N} \cdot \left(\frac{P_e}{P_i}\right)^{\frac{\gamma+1}{2\gamma}} \cdot \sqrt{|P_e - P_i|} + C_2 \cdot \Phi \cdot \frac{(P_e/P_i)^{1/\gamma}}{r_c} \quad \textbf{131}$$

Where;

x_r : residual gas mass fraction
N : engine speed in revolutions per second
P_e : exhaust gas pressure
P_i : intake gas pressure
Φ : fuel equivalence ratio
r_c : compression ratio of engine
γ : ratio of specific heats
C_1, C_2 : non-dimensional proportional constants of 1.266 and 0.632 [54, 56]

A comparison of residual gas masses was performed using relations defined in [12]. The results of the residual gas mass fractions were similar. It has to be said that the overlap factor of the test engine is very small and may be a contributing factor of why there is not so much cross flow during the overlap period. The composition of the exhaust gases can be determined using the water injection rate and the air / fuel ratio.

4. **Temperature of the charge in the cylinder** – the temperature of the charge in the cylinder is calculated indirectly. Using the pressure, entrapped mass of aspirated and residual gases and cylinder volume, the ideal gas laws are used to calculate the in-cylinder temperature at the end of the intake stroke. As described earlier, the pressure at the end of intake stroke is considered to be equal to that found in the intake tract.

   In the case where EGR is used, only a direct calculation is needed to estimate in-cylinder temperature. However, if water injection is used, the process of calculation of in-cylinder temperature is iterative in nature. This is due to the fact that the values of vapour pressure vs. temperature are tabulated and that during calculation, a check needs to be made at each step to see if the air / water mixture reaches saturation. In the event that saturation is reached, it is assumed that the water remains in liquid form until the compression and/or combustion furnishes enough energy to the mixture to evaporate it. In general, if the temperature is higher than the saturation temperature of the air / water mixture, all the water is assumed to be in vapour form. Mathematically, this is the sequence of calculations that will have to be performed:

   - Calculation of initial temperature of air and residual gas
   - Addition of water vapour to the air / residual gas mixture
   - Monitoring the state of saturation

The operating point **C** as defined in **Table 40** is chosen, and the operating parameters with certain important physical characteristics of the engine are reiterated in the table below:

Parameter	Units	Value
P_{boost}	mbar	1800
T_{boost}	°C	30
φ	ratio	1.89
m_{ac}	mg/stk	880
RH_i	%	68% @ 21.6°C
$T_{exhaust}$	°C	491
$P_{exhaust}$	mbar	2413
$V_{clearance}$	m^3	$2.9374x10^{-5}$
V_{swept}	m^3	$4.9936x10^{-4}$

Table 51. Physical parameters of the test engine and operating point ***C*** without WI

Here, results from calculations outlined in **section 2.2** are used. The fact that water may or may not exist in vapour form depends on the mass of the water to be vaporised. For a given pressure and volume of the combustion chamber, and a given mass of air and vapour, we can determine the charge temperature. If that temperature is such that the vapour exists in the superheated form, we may say that the water may be evaporated at the end of the intake phase. If however the resultant temperature is too low for the water to exist in vapour state (given its partial pressure and specific volume) we can say that the water will ***not*** have vaporised at the end of intake and will evaporate during the compression or combustion phases of the cycle. Following this, the results of the calculations are presented.

The first case is where there is only air charge entering the cylinder. No WI is present. The first calculation will be to determine what temperature the dry air charge will have to be at BDC to fill up the total volume of the cylinder at the intake manifold air pressure. The total air charge mass in the total volume of the cylinder is thus a sum of the intake air charge and the residual gases. The temperature thus obtained from measurements is:

$$T_{mixture} = 90.3°C$$

The second calculation was performed to see what the final mixture temperature would be after a heat transfer between the hot residual gases and the cool intake air mixture. The temperature comes out to the following value:

$$T_{mixture} = 48.0°C$$

This means that 42.31°C of the rise in temperature of the mixture of the intake air charge and the residual gases can be attributed to the heat transfer from the cylinder walls during the intake phase. From calculations, this value of transferred heat comes out to:

$$dQ = 39 Joules$$

Now, we shall introduce water injection into the same air charge. This engine operating point ***C*** is obtained experimentally, and for all test points, the air/water mixture in the intake manifold is saturated, with water present in liquid form. The nominal WI rates are 3, 9, 17 and 21 kg/h of mass flow. The measured and calculated parameters are noted in **Table 52**:

Parameter	Units	Case 1	Case 2	Case 3	Case 4
P_{boost}	mbar	1800	1800	1800	1800
T_{boost}	°C	27	29	30	30
T_{water}	°C	20	20	20	20
φ	ratio	1.88	1.85	1.83	1.82
m_{ac}	mg/stk	877	860	851	845
m_w	mg/stk	12.2	36.5	68.4	84.9
$m_{ac}+m_w$	mg/stk	889.2	896.5	919.4	929.9
RH_i	%	68% @ 21.9°C	54% @ 24.9°C	46% @ 23.1°C	41% @ 23.9°C
$T_{exhaust}$	°C	481	465	444	435
$P_{exhaust}$	mbar	2364	2370	2420	2440
$V_{clearance}$	m^3	2.9374×10^{-5}			
V_{swept}	m^3	4.9936×10^{-4}			
$T_{nonevap}$	°C	92	95	96	98
T_{evap}	°C	81.4	65	62	62
$\Delta H_{nonevap}$	J	59	67.4	75.5	82
ΔH_{evap}	J	77.2	120.6	194	199.7
ΔH_{rg}	J	14.7	14.2	14.8	14.4

Table 52. Physical parameters of the test engine at operating point ***C*** with WI

Where:

P_{boost} : Boost pressure in the intake manifold
T_{boost} : Temperature of air in the intake manifold
T_{water} : Temperature of injected water
φ : Air / Fuel equivalency ratio
m_{ac} : Mass of air charge in cylinder with each intake stroke
m_w : Mass of injected water in cylinder with each intake stroke
RH_i : Initial ambient Relative Humidity
$T_{exhaust}$: Temperature of exhaust gases (at TDC)
$P_{exhaust}$: Pressure of exhaust gases in clearance volume
$V_{clearance}$: Clearance Volume of cylinder
V_{swept} : Swept volume of cylinder
$T_{nonevap}$: Temperature of air charge in cylinder at BDC in the absence of evaporation
T_{evap} : Temperature of air charge in cylinder at BDC after evaporation
$\Delta H_{nonevap}$: Heat transfer between intake air charge and cylinder walls + residual gases in the absence of evaporation
ΔH_{evap} : Heat transfer between intake air charge and cylinder walls + residual gases in the presence of evaporation
ΔH_{rg} : Heat transfer between intake air charge and residual gases

Each of these measured points will have two calculated temperatures at the end of the intake stroke. The first temperature is calculated assuming that none of the injected water is evaporated. The only vapour existing in the air charge is the atmospheric vapour and the vapour from the residual gases – of which, one part is from combustion and the second part is from the water injected during the previous cycle.

The second temperature is calculated assuming that all the injected water is converted to water vapour in the cylinder during the intake stroke. This is true for the first three points, whereas for the fourth test point, 70mg of water was evaporated, leaving behind 14.9 mg of

water in liquid form. In point 3 and 4, the injected water brings the air charge to saturation at the end of the intake stroke.

Three values of enthalpy changes are given in the table. The first one "$\mathbf{\Delta H_{nonevap}}$" is the heat transfer from the cylinder walls to the intake air charge heating the air / vapour / water charge without evaporation of injected water. The increasing final "non-evaporation" temperature and increasing total mixture mass ($\mathbf{m_{ac}+m_w}$) from Case 1 to 4 entails an increase in the value of heat transfer. Calculation of "$\mathbf{\Delta H_{nonevap}}$" requires initial and final temperatures ($\mathbf{T_{boost}}$ and $\mathbf{T_{nonevap}}$), masses of air, atmospheric vapour and injected liquid water, and the specific heats of the same.

$$\Delta H_{nonevap} = \left(m_{ac} \cdot C_{pa} + m_{vap} \cdot C_{pv} + m_w \cdot C_w\right) \cdot \left(T_{nonevap} - T_{boost}\right) \quad \textbf{132}$$

The second one "$\mathbf{\Delta H_{evap}}$" is the heat transfer required from the cylinder walls to the intake air / water / vapour charge with evaporation of injected water.

$$\Delta H_{evap} = \left(m_{ac} \cdot C_{pa} + m_{vap} \cdot C_{pv} + m_w \cdot C_w\right) \cdot \left(T_{evap} - T_{boost}\right) + m_w \cdot h_{fg} \quad \textbf{133}$$

The third one "$\mathbf{\Delta H_{rg}}$" is the potential available heat transfer between the hot residual gases at the end of blowdown and the intake air charge.

$$\Delta H_{rg} = \left(m_{rg} \cdot C_{prg}\right) \cdot \left(T_{exhaust} - T_{mixture}\right) \quad \textbf{134}$$

Please not that the values of the different final temperatures are calculated implicitly as outlined earlier.

As can be seen from the **Table 52**, the heat transfer via the cylinder walls could potentially be from five to fifteen times as great as the adiabatic heat transfer between the residual gases and the intake air charge. The heat transferred to the intake air charge via the cylinder walls / metallic surfaces is given in **Table 53**:

Parameter	Units	Point 1	Point 2	Point 3	Point 4
$dQ_{nonevap}$	J	44.3	53.2	60.7	67.6
dQ_{evap}	J	62.5	106.4	179.2	185.3
dQ_{evap} -$dQ_{nonevap}$	J	18.2	53.2	118.5	117.7
dm_{wf}	mg	9.6	33.3	64.2	65.6
$m_w x\ h_{fg}$	J	22.1	76.6	147.7	150.9

Table 53. Heat transfer from the cylinder walls and other metallic surfaces to the intake air charge

Where:

$dQ_{nonevap}$: Heat transferred to intake air charge by cylinder walls in the absence of evaporation

dQ_{evap} : Heat transferred to intake air charge by cylinder walls with evaporation of injected water charge

dm_{wf} : Total mass of water evaporated during intake of the air charge into the cylinder

$dm_{wf} x\ h_{fg}$: Latent heat of evaporation of the injected water mass

Two graphs are presented in **Figure 61** to give an idea of heat transfer and final temperature. In this graph, the solid lines represent calculated final temperature at the end of the intake stroke, while the dotted lines represent the calculated heat transferred to the intake charge as a function of evaporation of the injected water mass. The red dot is the calculated reference value of temperature for the dry air intake, while the black dot is the calculated reference value of heat transfer for the dry air intake.

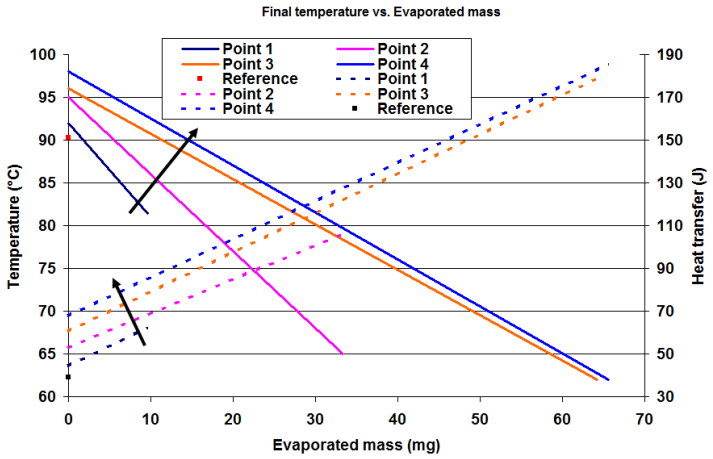

Figure 61. Calculated values of temperature and heat transfer for different WI rates

We see that as we progress from case 1 to 4, the temperature of the intake charge does not vary among the four test cases. The difference in temperature is due to the difference in air charge mass in the cylinders. However, as we progress along the x-axis, we see that as the evaporated mass increases, the final intake charge temperature drops. Case 3 is at the limit of saturation, while case 4 is saturated with water still existent in the liquid form. For the heat transfer, the values of heat transfer correspond very closely the mass of water that is to be evaporated. The difference in starting temperature shown on the graph (at 0 mg evaporated mass) is due to the fact that as WI quantity is increased, the mass of air charge progressively decreases, since part of the space is taken up by the water in the case of increasing WI quantity. For the same cylinder pressure, the temperature at the starting point (0 mg evaporation) will be higher for each successive WI measuring point. The arrows show the increasing WI quantity.

The aim of this section was to attempt the determination of the physical state of the injected water during intake into the engine cylinder. The undetermined factor is the heat transfer between the air charge and the metal structure of the engine cylinder. Unlike the calculations performed in **section 3.1**, which were for the most part considered to be adiabatic in nature, and some inevitable “real-world” adjustments aside, were much easier to perform, the calculations proposed and presented in this section try to take into account all possibilities of heat transfer. It has been attempted to define the outer limits of what is and what is not possible as concerns the evaporation (or otherwise) of water when it is taken in liquid form into the cylinder along with the saturated (at intake conditions) air / vapour charge. It has been observed that in most cases, the conditions in the engine cylinder permit the injected water in liquid form to completely evaporate. In a few cases however, there is no possibility of water to evaporate at the end of the intake stroke. The analysis of what happens to the air / vapour / water charge will then be performed during the compression / combustion stage which is outlined in the next section. The same operating points outlined in this section have been used to maintain coherence in the analyses.

3.3. WI analysis during the compression / combustion process:

In the previous sections, an analysis was performed to estimate the thermodynamic processes taking place during the intake process of an engine. In **section 3.1**, we calculated post WI intake air temperatures and saturations based on different parameters such as air flow rates, temperatures, WI flow rates and charge pressures. These analyses were then used to try and predict the temperatures of a test case.

In **section 3.2**, analyses were performed to estimate the final air charge temperature in the presence and absence of WI. This analysis gave us a range of temperatures that may exist at the end of the intake stroke and indicated whether it is possible to evaporate the injected water completely or not. It was noted (and shown in **Table 52**) that up to operating point 3, it is possible to evaporate all of the injected water mass. Operating point 4 however, shows that a part of the injected water will exist as liquid at the end of the intake stroke.

This section is divided into two parts. In the first part, we shall simulate a compression using more or less the same air mass as given in **Table 52**. The difference is that we will only have saturated air, and no water in liquid form shall be present in the air charge when compression starts. Referencing **Table 52**, which will be operating point 3. Three compressions will be performed:

1. Adiabatic compression
2. With heat transfer using Hohenberg's model [58] with:
    a. Cylinder walls at normal operating temperature.
    b. Cylinder walls at ambient temperature.

In the second part, the thermodynamic processes will be analysed from the end of the intake stroke (BDC) to the end of compression (TDC) and then during the combustion process for a real cycle given for operating points given in **Table 52** will be performed.

3.3.1. Comparison of theoretical vs. real pressure profile

Here, the cycle is considered to have entered the "closed" phase, that is to say, the mass of charge entrapped in the cylinder is considered to be constant. From the last series of calculations, we obtain the composition and initial temperatures and pressures of the intake charge. Using the pressure trace obtained from the tests, and using the variation in volume with respect to crank angle, the temperature of the gas charge in the cylinder is estimated.

Seeing that the wall temperature is higher than charge temperature at the start of the compression and lower at the end of the compression, there will be a transfer of heat between the entrapped gas charge and the walls of the combustion chamber and cylinder during the compression stroke. Hohenberg's heat transfer model [58] is used to estimate heat transfer and correct the Rate Of Heat Release diagram.

$$h_{loss} = 130 \cdot V_{cyl}^{\ -a3} \cdot P_{tcyl}^{\ a1} \cdot T_{cyl}^{\ -a2} .\left(PV + 1.4\right)^{a1} \quad \textbf{135}$$

$$dQ_{loss} = \frac{h_{loss} \cdot S_{cyl} \cdot B \cdot \pi \cdot \left(T_{cyl} - T_{cw}\right) \cdot N \cdot 1000}{60} \quad \textbf{136}$$

Where:

h_{loss}	:	Thermal transfer coefficient
V_{cyl}	:	Total cylinder volume (clearance and swept volume combined)
P_{cyl}	:	Total cylinder pressure
T_{cyl}	:	Cylinder temperature
PV	:	Piston Velocity
S_{cyl}	:	Piston stroke length (uncovered cylinder wall)
B	:	Bore diameter
T_{cyl}	:	Temperature of in-cylinder gases
T_{cw}	:	Temperature of cylinder wall
N	:	Engine speed in rpm
$a1,a2,a3$	:	Empirical coefficients

The pressure signal from the in cylinder pressure measurement is used in conjunction with the composition of the compressed gas charge to determine the temperature of the in-cylinder mixture at each point in the engine cycle.

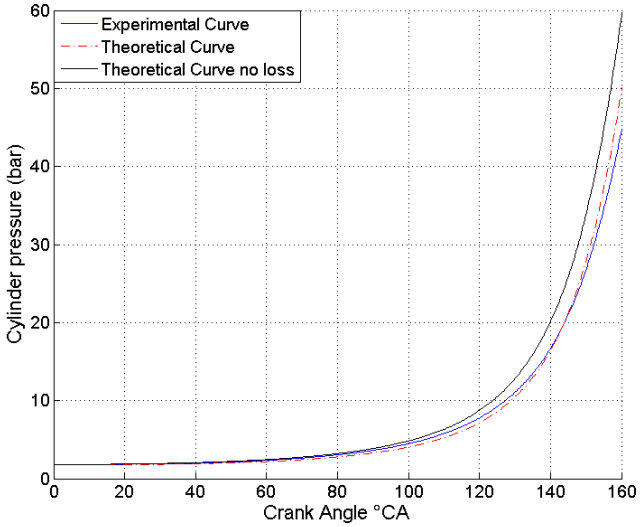

Figure 62. Comparison of real, and theoretical pressure curves

3.3.2. Calculation of SOC, premixed combustion ratio and ROHR:

The injector opening / closing signals are given by the ECU (Electronic Control Unit) of the engine. The actual opening / closing of the injector fuel pintle for this particular engine are delayed by 270 μS. This translates to a delay in crank angle in degrees which varies according to engine speed. This delay is added to the injector opening and closing signal to estimate the physical fuel injection period.

$$SOI_r = SOI + \frac{IOD \cdot N \cdot 360}{6 \cdot 10^7} \qquad \textbf{137}$$

Where;

$\boldsymbol{SOI}$, $\boldsymbol{SOI_r}$	:	Start Of Injection (indicated), Start Of Injection (real) in degrees
$\boldsymbol{IOD}$	:	Injector Opening Delay in ms
$\boldsymbol{N}$	:	Rotational speed of engine in RPM

After the initial delay is calculated, the fuel flow profile is calculated. This calculation is performed based on a model defined by actual injector flow profiles defined by the manufacturer, who have specific test benches designed to calibrate the fuel injection model from real measured data. In general, the profile is defined by **Figure 63**:

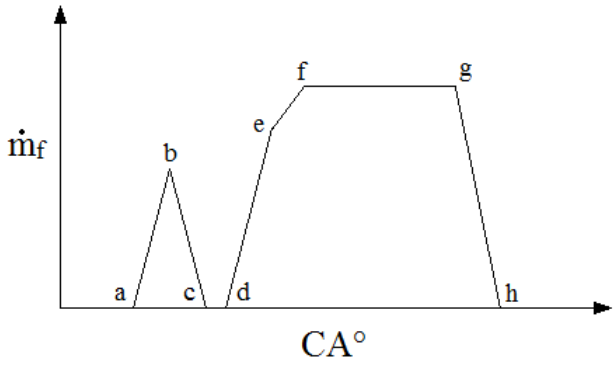

Figure 63. Idealised "real" fuel injection profile

The slopes **a-b**, **b-c**, **d-e**, **e-f**, and **g-h** are all defined by empirical relations given by the engine manufacturer. The line **f-g** is when the injector is 100% open. The injection rate profile given by **a-b-c** refers to the pre-injection event. In this case, the fuel injector pintle remains in the "ballistic" mode and never opens to the full extent.

In the case of the profile **d-e-f-g-h**, we can see a reference to the main injection event. This profile starts with the opening **d-e** similar to **a-b**, however, at point **e**, the opening rate slows down until the injector is completely open at **f**, from here, the injector is at 100% flow rate until point **g,** where electrical power to the injector is cut off and the hydraulic forces show their effect and close the injector pintle from **g-h**.

Using an extension of calculation from the last section, we can calculate the acceleration of combustion. When the acceleration of combustion passes 200 MWatts / second, the combustion "proper" is said to have been established. The delay between the SOI (Start Of Injection) and the SOC (Start Of Combustion) will dictate the amount of fuel that is burnt in pre-mixed combustion. The profile of injection, which is defined using **Figure 63**, is used to calculate the premixed fuel combustion for SOI and SOC values for both pilot and main injections.

3.3.3. Example test point measurement and result (including ROHR):

In this section of the chapter, an example test point has been taken. This example test point is similar to the test point given in **Table 52**. The difference is that to ensure the intake of water in vapour form into the cylinder, intercooling was not used. As water was injected, the charge is cooled while evaporating the atomised water. The calculations thus performed consist of obtaining the following data:

1. Real-time cylinder pressure curve in its raw and filtered form
2. Engine and test bench data obtained from the ECU and pressure / temperature sensors via LabVIEW®
3. Emissions data obtained via the Pollutant Emissions test benches

Real-time cylinder pressure measurement: The data recovered from the in-cylinder pressure measurement in its original form has quite a bit of noise due to, among other factors, mechanical resonance of the engine parts. The operating point in question is shown in the table below, with the engine operating conditions given below:

Engine speed	*tr/min*	2045	Pexhaust' - P. exh out turbine	*mbar*	1118
Brake torque	*N.m*	142.6	Pexhaust - P. exh out engine	*mbar*	2345
Temperature of injected water	℃	24			
Measured fuel flow rate	*mg/stk*	30.81	**VALUES MEASURED BY ECU**		
Measured air flow rate	*mg/stk*	809	Ambient temperature – $\mathbf{T_{amb}}$	℃	21.0
Humidity	*%*	38.0	Ambient pressure – $\mathbf{P_{atm}}$	*mbar*	1012
Ambient temperature	℃	20.3	Intake manifold temperature – $\mathbf{T_{boost}}$	*mbar*	60.0
WI rate at intake	*mg/cp*	13.2	Measured turbo boost pressure – $\mathbf{P_{boost}}$	*mbar*	1800
TEMPERATURES - PRESSURES			Total fuel flow rate ECU – $\mathbf{m_{f\_tot}}$	*mg/stk*	31.8
Texhaust – T. exh engine out	℃	505	Pilot fuel flow rate – $\mathbf{m_{f\_pilot}}$	*mg/stk*	2.0
Texhaust' - T. exh turbine out	℃	397	SOI pilot – $\mathbf{SOI_{pilot}}$	*°V*	-16.80
Texhaust_1 - T. exh cyl 1	℃	470	DOI pilot – $\mathbf{DOI_{pilot}}$	*ms*	0.19
T exhaust_2 - T. exh cyl 2	℃	472	Main injection flow rate – $\mathbf{m_{f\_main}}$	*mg/stk*	29.8
T exhaust_3 - T. exh cyl 3	℃	467	SOI main – $\mathbf{SOI_{main}}$	*°V*	1.99
T exhaust_4 - T. exh cyl 4	℃	481	DOI main – $\mathbf{DOI_{main}}$	*ms*	0.72
Tturbo - T. air out compresseur	℃	106	Water/Air ratio	*kg/kg*	0.016
Tboost' - T. air out chargecooler	℃	99	Water/Fuel ratio	*kg/kg*	0.430

Table 54. Engine operating point with temperature, pressure and flow rate data

Using the values defined in table **Table 54**, we shall first of all determine if the injected water has all been evaporated. To determine that, we shall use the values given by the following variables;

Temperature of injected water	℃	24	T2'	℃	99
Measured air flow rate	*kg/stk*	809	Tamb	℃	21.0
Humidity	*%*	38.0	Patm	*mbar*	1012
Ambient temperature	℃	20.3	Tboost	℃	60
WI rate at intake	*mg/stk*	13.2	Pboost	*mbar*	1800

Using the ambient temperature and pressure values with the given relative humidity, it is possible to determine if all of the injected water was evaporated in the intake or not. The methodology to perform this test has already been explained earlier in **Section 2.2.1.4**.

The next step, given the properties of the intake air, we shall acquire the in-cylinder pressure signal from the data acquisition system, and then perform signal conditioning operations as shown in **Figure 64**:

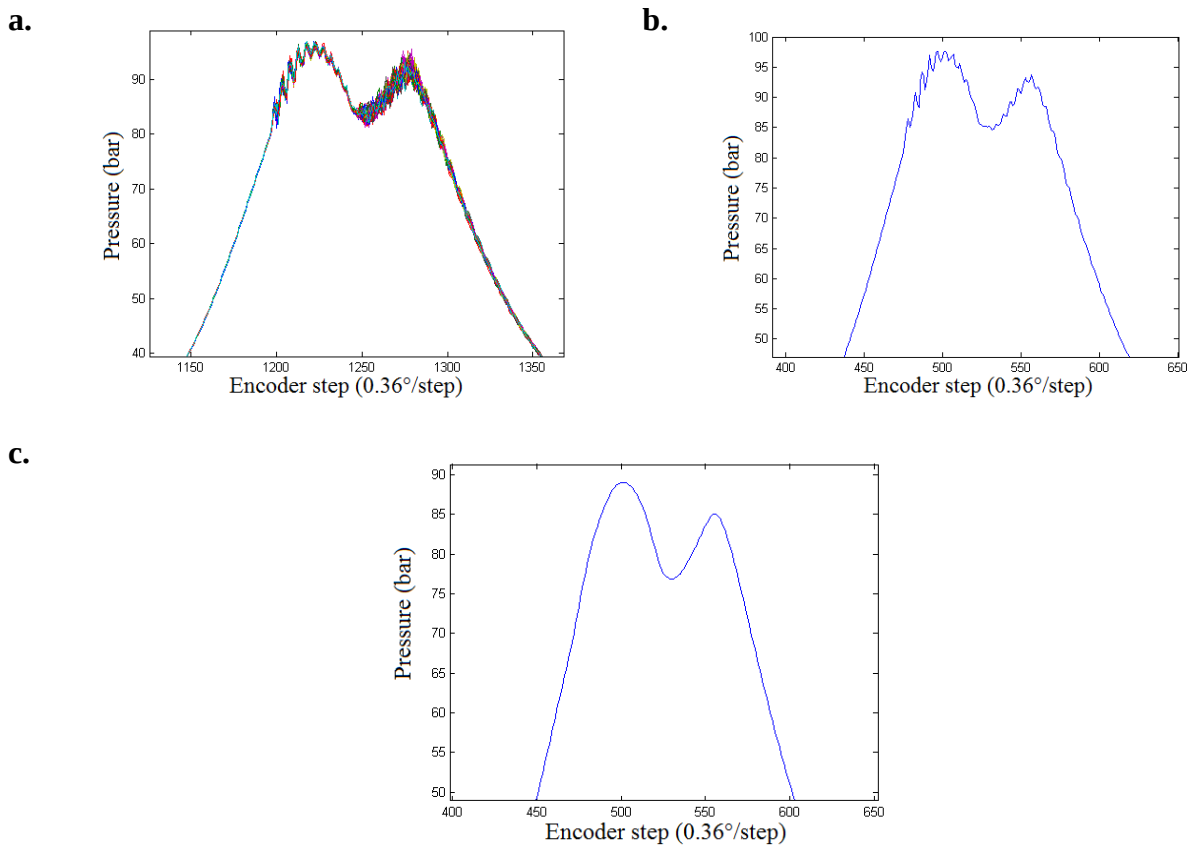

Figure 64. Conditioning of in-cylinder pressure signal acquired from the data acquisition system

Following are the operations performed during the signal conditioning phase;

a. Acquire 60 cycles over the same engine operating point.

b. Average the signal over the 60 cycles (number of cycles per sample may be varied according to need).

c. Filter the signal and reference it to the intake manifold average air pressure (although the intake manifold air pressure changes due to the flow fluctuations and pressure variations introduced by the intake valves, it is the best reference available).

With the obtained filtered pressure curve, we may thus proceed to measure the following curves:

1. In-cylinder temperature
2. Heat loss from the cylinder walls
3. Cumulative Heat Release
4. ROHR
5. Combustion acceleration
6. SOC

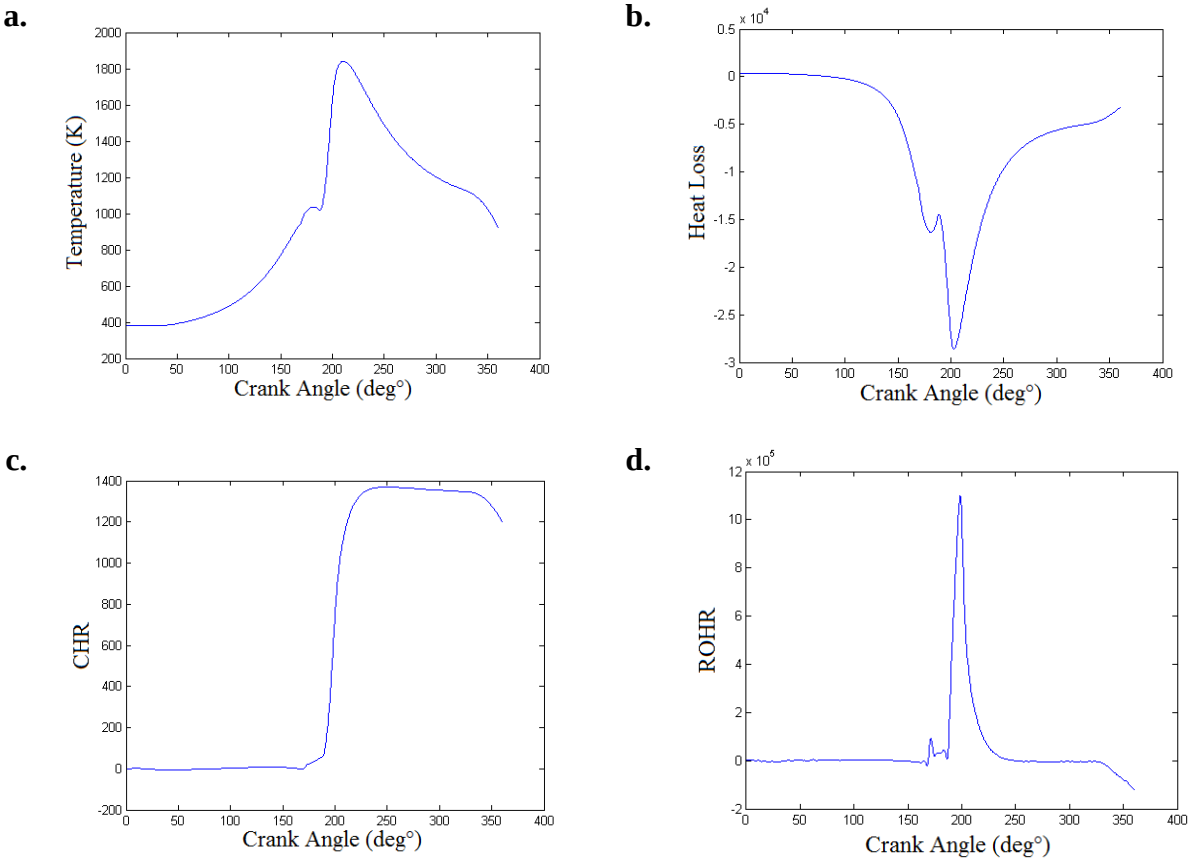

Figure 65. a. In cylinder temperature, **b.** Heat loss from cylinder walls, **c.** Cumulative Heat Release **d.** ROHR

In all of the curves represented in **Figure 65**, the abscissa is the crank angle degrees with 180° being TDC. **Figure 65 c.** gives us an estimate of the thermal energy generated inside the combustion chamber. To verify, the product of the injected fuel mass and the LHV of diesel fuel should equal the cumulative heat release.

$$CHR = LHV \times m_f \qquad \textbf{138}$$

$$CHR = \left(43\times10^{6}\, J/kg\right)\times\left(31.8\times10^{-6}\, kg\right)$$

$$CHR = 1367.4J$$

Where;

CHR	:	Cumulative Heat Release
LHV	:	Lower Heating Value
m_f	:	Mass of fuel injected

The calculated value was 1369.3 Joules – a 0.14% difference.

From the ROHR diagram; we can also calculate the combustion acceleration which will indicate the SOC. This may be used to determine the ratio of fuel that burns in a premixed mixture, before the start of, quasi-stable, diffused combustion:

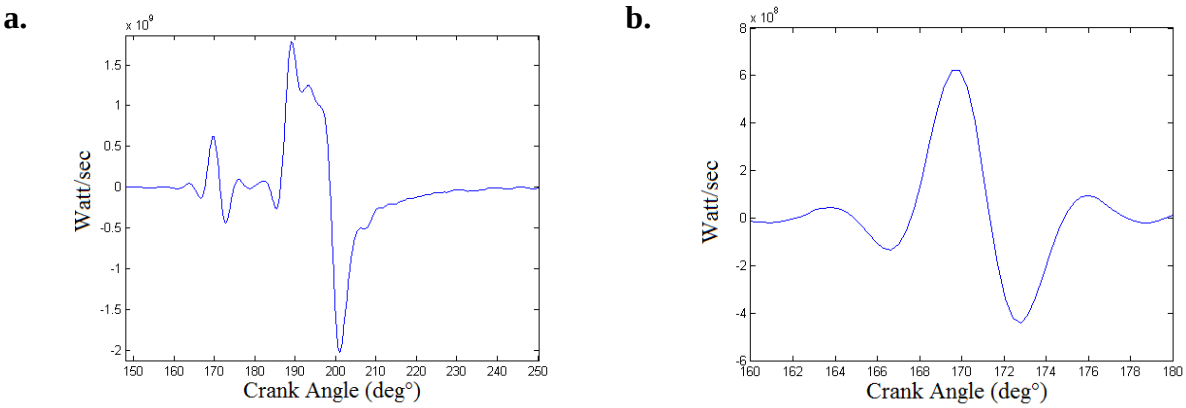

Figure 66. a. Combustion acceleration for the pilot injection and the main injection **b.** Focus on pilot injection

Referring to **Figure 66**, we see the overall profile of combustion acceleration in part **a.** where the value of combustion acceleration is provided over the whole "closed cycle" – that is to say when the valves are closed and the compression and combustion / expansion phases of the engine cycle are considered. In part **b.**, we see a part of the curve which focuses on the pilot injection. As stated earlier, a value of 200 MW/s was considered a starting point for combustion. From this value onwards, combustion is said to have been initiated. As mentioned earlier and given by **Eq. 137**, the real SOI is calculated with the help of the engine operating parameters given in **Table 54**. With the value of the real SOI obtained, the mass of fuel that burns in the premixed combustion can be determined.

Using the same calculation processes that were used to calculate the different pressure, temperature and heat transfer curves from **Figure 64** to **Figure 66** for the operating points given in **Table 52**. Essentially, apart from the water injection quantities and post-intercooler temperatures, the operating parameters defined in **Table 54** hold true. The presentation of the graphs will be different to the ones presented above since we shall be seeing four different curves with magnified zones to show detail.

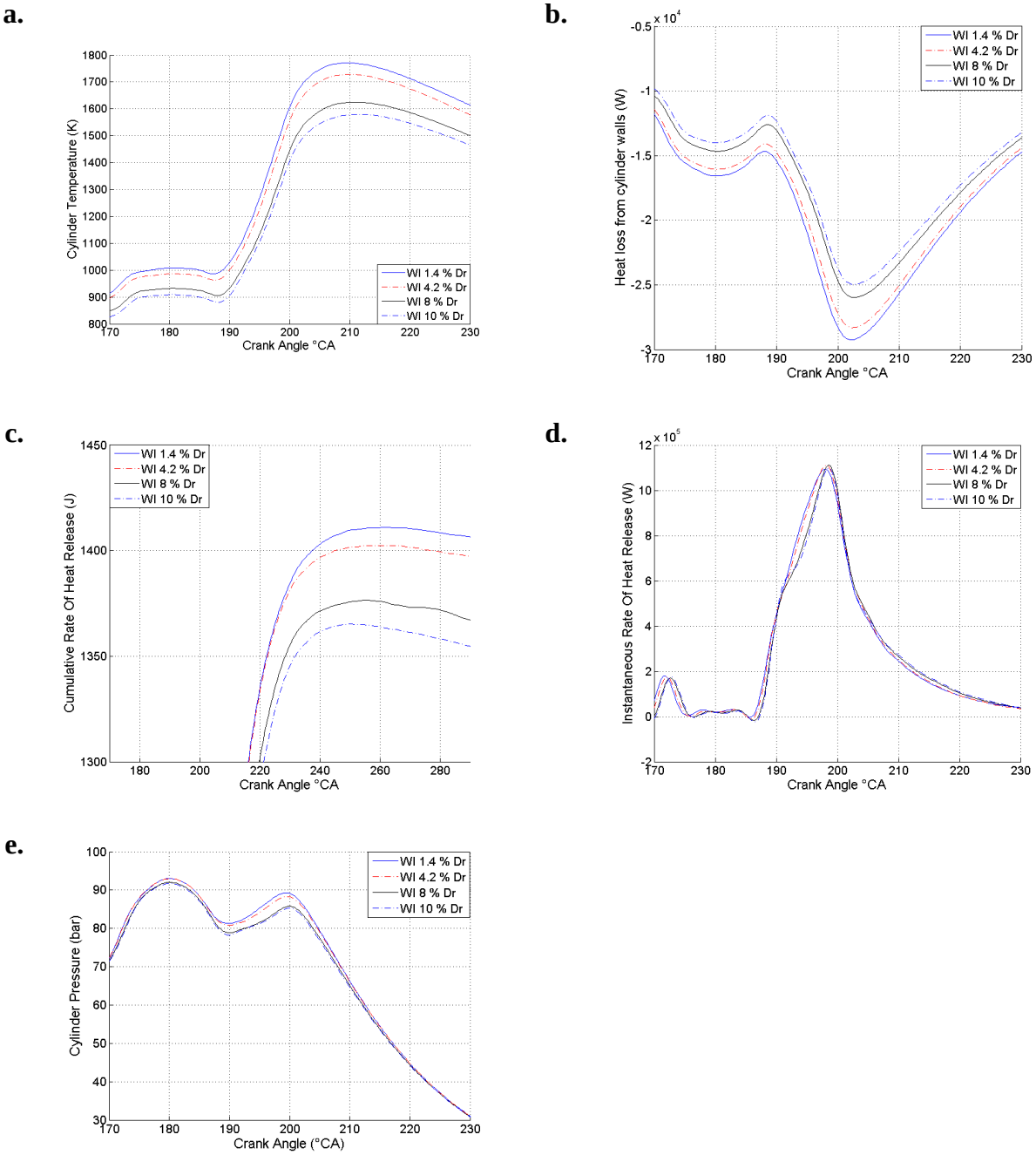

Figure 67. a. In cylinder temperature, **b.** Heat loss from cylinder walls, **c.** Cumulative Heat Release, **d.** ROHR, **e.** Total cylinder pressure

Referencing to **Figure 67 a.**, we see that we lose around 200 K in peak bulk cylinder temperature when injecting water from 3 kg/h (dilution ratio Dr = 1.4%) to 21 kg/h (Dr = 10%). In comparison to the temperature given in **Figure 65.**, we lose around 40 K for the same water injection quantity. The difference being that for the latter, water evaporates after entry into the combustion chamber.

Referencing to **Figure 67 b.**, we see a reduction in heat transfer to the cylinder walls at TDC, which would seem logical given that the air / water charge was cooler for the higher WI rates and that the adiabatic index **γ** for water vapour is lower. The strength of heat transfer could be

increased in the presence of vapour however, if the heat transfer coefficient of vapour is found to be higher than that of dry air. Owing to the greater proportion of water vapour in the intake charge, we could have a net increase in the value of the heat transfer coefficient.

Referencing to **Figure 67 c.**¸ we see that the cumulative ROHR has reduced from 1410 Joules to 1365 Joules. From **Table 52**, we see that the final intake air / water charge temperature at BDC for points 3 and 4 were similar. So it would stand to reason that the difference between the two points here for their cumulative ROHR would be due to the presence of water at BDC for point 4. If the remaining liquid mass of 14.9 mg were to be evaporated at room temperature, it would account for about 34.5 Joules of difference. The difference here is of around half that. It could be possible that a part of the required heat was provided by the cylinder walls during compression as well. The remaining liquid water was evaporated by the high temperature of the combustion process.

Referencing to **Figure 67 d.**, we see that the injected water quantity has a relatively minor bearing on the form of the instantaneous ROHR. This could be explained by the fact that the operating point is of a moderate load, and the high boost pressure may help in stabilising the combustion.

Referencing to **Figure 67 e.**, we see that for increasing WI rate, the peak cylinder pressure drops by around 1.5 bars near TDC and around 4 bars at the peak of instantaneous Rate of Heat Release (just before 200° crank angle) with increasing WI rate. The translation of dilution ratio and WI injection rate in kg/h is given below:

WI rate	Case 1	Case 2	Case 3	Case 4
kg/h	3.0	9.0	16.9	20.9
mg/stk	12.2	36.5	68.4	84.9
Dr	1.4	4.2	8.0	10.0

Table 55. Correlation between different values of WI rate and their measurement techniques.

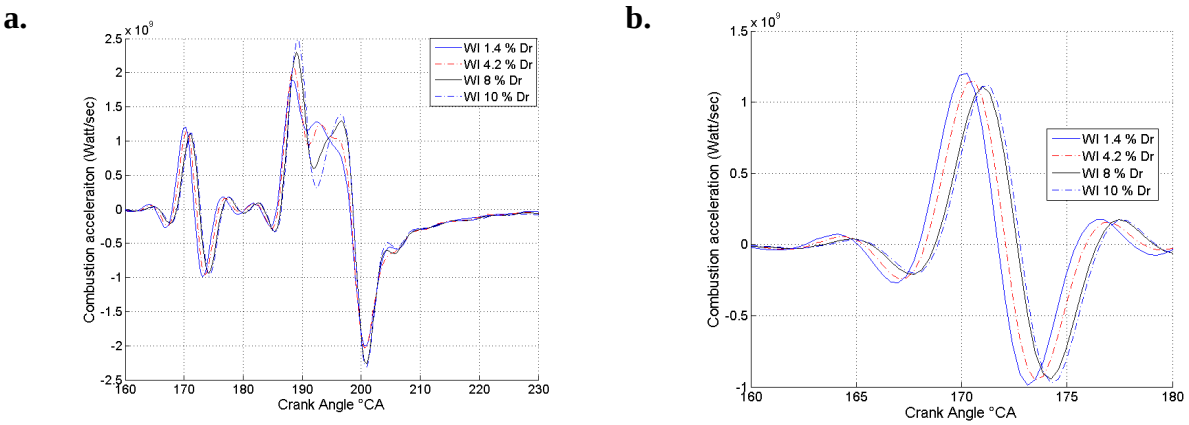

Figure 68. a. Combustion acceleration for the pilot injection and the main injection **b.** Focus on pilot injection

Referring to **Figure 68**, we see the overall profile of combustion acceleration in part a. where the value of combustion acceleration is provided over the whole "closed cycle" – that is to say when the valves are closed and the compression and combustion / expansion phases of the engine cycle are considered. In part b., we see a part of the curve which focuses on the pilot injection. As stated earlier, a value of 200 MW/s was considered a starting point for combustion. From this value onwards, combustion is said to have been initiated. For all operating points, we see that the pilot injection crosses the 200MW/s limit, thus there is not

failure of combustion of pilot injection. Also, the delay in combustion is of the order of a few degrees, falling into the precision limits of the rotary encoder (**section 2.1.3.1**).

At the end of **section 3.2**, it was stated that for case 4, it was impossible that the injected water be evaporated completely at the end of the intake stroke. In this section, the compression and combustion process were both analysed using the same engine test points to determine experimentally the state of the gas in the cylinder. An attempt has been made to determine the evaporation of water vapour and the state of the air / vapour charge in general during the compression / combustion phase. Data for heat release during the combustion phase has been used as a tool to determine the energy potentially imparted to the liquid water for evaporation. From the quantities of liquid water calculated in **section 3.2**, the measured differences in CHR have been in good agreement with the predicted / calculated results. The results show the magnitude of the heat transfer between the hot combustion products and the injected water, and it is within the correct range of values. However, the exact value of heat transfer and its profile according to the crank angle has not been determined.

The numerical analysis performed in this chapter has helped to clarify the possible evolutions of condition of water injected into the air intake circuit of an internal combustion engine.

The injected water and air are mixed in the intake manifold. Water may completely or partially evaporate during mixing as a function of conditions of vapour saturation. The primary effect of this evaporation is the marked reduction in the intake charge temperature. A parametric study was performed to show the influence of injected water temperature and the different parameters of air (pressure, temperature, humidity) before mixing, on the quantity of water evaporated and the final temperature after mixing. The comparison of calculated values of temperatures and those which were measured show that the proposed hypotheses (most importantly the adiabatic nature of the mixing process), are not completely verifiable, yet allow a good approximation of the actual situation.

When saturation is achieved, and the injected water stays in a liquid form in the intake, the intake of the air / water mixture into the cylinder may cause evaporation of a part of the liquid due to heat transfer from the combustion chamber and cylinder valves and the residual gases. Quantities of water and air measured directly from the experiments confirm the presence of this evaporation and show also that the transfer of heat between the air charge and the cylinder walls is affected more or less in relation to the quantity of liquid water present in the intake charge. It is therefore not possible to use classic modelling of thermal transfer processes to predict the evaporation of water in the phase of air / water intake.

Finally, in the case of presence of water present in liquid form in the engine cylinders after the closing of the intake valves, it seems that the rise in temperature of the gas charge in the cylinder due to compression and the transfer of heat from the cylinder walls lead to a supplementary evaporation during the compression phase of the engine cycle.

In addition, the numerical tools allowing the calculations of thermodynamic properties of the air / vapour / residual gas charge have been presented. These allow the correction of heat release diagrams when combustion takes place in an air charge having water vapour. The impact of water injection on engine combustion will be analysed in the forthcoming chapter.

L'analyse numérique menée dans ce chapitre a permis de clarifier les évolutions possibles de l'eau injectée sous forme liquide dans le circuit d'admission d'air d'un moteur à combustion interne.

Au niveau du circuit d'admission, l'air et l'eau se mélangent, l'eau pouvant s'évaporer partiellement ou complètement en fonction des conditions de saturation. Cela a pour effet de diminuer la température à l'admission, parfois de façon très importante. Une étude paramétrique a permis de montrer l'influence de la température de l'eau et des caractéristiques de l'air (température, pression, hygrométrie) avant mélange sur la quantité d'eau évaporée et sur la température finale après mélange. La comparaison des valeurs de température calculées avec des mesures montre que les hypothèses retenues (notamment l'adiabaticité) ne sont pas parfaitement vérifiées mais permettent d'obtenir une bonne approximation de la situation réelle.

Lorsque la saturation est atteinte et que de l'eau reste à l'état liquide dans le circuit d'admission, le processus d'admission dans les cylindres peut conduire à l'évaporation d'une partie de l'eau, grâce à la chaleur apportée par les parois du cylindre et par le mélange avec les gaz résiduels provenant du cycle précédent. La mesure expérimentale des quantités d'air et d'eau confirment l'existence de cette évaporation et montrent aussi que la quantité de chaleur échangée par l'air avec les parois du cylindre est largement affectée par la présence d'eau en plus ou moins grande quantité. Il n'est donc pas possible d'utiliser les modélisations classiques de transfert thermique pour prédire l'évaporation de l'eau pendant la phase d'admission.

Enfin, dans l'éventualité où de l'eau liquide est présente dans le cylindre à la fermeture de la soupape d'admission, il apparait que l'augmentation de température liée à la compression et la chaleur transmise par les parois au mélange gazeux présent dans le cylindre permettent une évaporation supplémentaire pendant la phase de compression.

Par ailleurs, les outils numériques mis en place permettant d'évaluer les propriétés thermodynamiques d'un mélange air/vapeur d'eau/gaz résiduels ont été présentés, rendant possible l'évaluation correcte des dégagements de chaleur liés à la combustion en présence d'eau. L'impact de l'injection d'eau sur la combustion seront ainsi analysés dans le chapitre suivant.

4. CHAPTER 4: Experimental study of the influence of water injection on combustion, pollutant emissions, and engine performances

Ce chapitre présente les résultats expérimentaux obtenus avec le dispositif décrit au chapitre 2. Quatre points de fonctionnement différents, représentatifs d'un usage en propulsion automobile (charges faibles à moyennes) sont étudiés. Pour chacun d'entre eux, plusieurs débits d'eau, couvrant l'intégralité des possibilités du système d'injection, sont testés.

La réduction de la température de l'air d'admission étant le premier effet de l'injection d'eau, cet effet est étudié séparément de façon à l'isoler. L'influence de l'injection d'eau sur la combustion (délai d'inflammation, dégagement de chaleur) est ensuite détaillée. Puis l'impact de l'injection d'eau sur d'autres paramètres du moteur comme la température de fin de compression, l'évolution de la pression dans le cylindre, la consommation spécifique ou les émissions de CO.

Ces éléments sont ensuite utiles pour interpréter les évolutions des émissions polluantes (NOx et PM) en fonction du débit d'eau injecté. Une comparaison est également établie avec l'EGR, moyen traditionnel de dépollution à la source en propulsion automobile, avec des comparaisons en fonction du taux de dilution. Enfin, des essais sont menés pour évaluer si les effets de l'injection d'eau et de l'EGR peuvent se cumuler lorsque ces deux techniques sont utilisées simultanément.

This chapter presents the experimental results obtained with the system outlined in Chapter 2. Four engine operating points, representative of operating points in automotive propulsion (part and low to high load) are studied. For each of these operating points, a multitude of water injection quantities, covering all possibilities of the injection system are tested.

The reduction of the intake air temperature being the first and foremost effect of water injection is studied separately. The influence of water injection on combustion (ignition delay, heat release), is then detailed. Then, the impact of water injection on other parameters of the engine like temperature at the end of compressions, in-cylinder pressure evolution, specific consumption and CO production are studied.

These elements are thus useful for the interpretation of the evolutions of emissions pollutants (NOx and PM) in function of the injected water quantity. A comparison is then done using EGR – which is a traditional means of controlling engine-out emissions – based on the dilution ratio is a comparison parameter. And finally, tests have been performed to see if the effects of EGR and WI combine when they are used simultaneously.

4.1. Results of WI on combustion and engine parameters:

In this section, we shall consider test results only with WI being active.

4.1.1. Influence of WI on intake temperature:

Historically, WI was used to reduce intake temperatures in turbocharged spark ignition engines and in gas turbines to reduce post-compressor air temperatures. In a turbocharged engine, the intake air temperature rises due to the compression of air as it passes through the compressor blades. This heating is not entirely adiabatic since the blades themselves are heated via the turbine shaft and the turbine which is exposed to the hot exhaust gases. This heating up of intake air reduces the mass air flow into the engine, which will potentially reduce the power output of the engine. To increase the density of the intake air charge, a chargecooler is fitted to most turbocharged engines.

In this section, a test was performed by which the cooling of the intake charge was performed via the WI system. The properties of air in the atmosphere and post-compressor are known. Using basic psychrometric calculations, the final air / water vapour mixture temperature can be determined along with its composition. The test point used was test point C. The test parameters are presented in the table below:

Configuration	**C1**	**C2**	**C3**
Cooling method	-	intercooler	WI (3kg/h)
P_2'' (mbar)	1800	1800	1800
T_2'' (°C)	91	60	60
NOx (g/kg fuel)	**27.1**	**24.6**	**17.8**
PM (g/kg fuel)	**0.28**	**0.26**	**0.35**
Rel. NOx reduction	**-**	**9%**	**34%**
Rel. PM increase	**-**	**-8%**	**26%**
λ	**1.78**	**1.86**	**1.82**

Table 56. Comparison of cooling effects of WI and the chargecooler

The value of ***λ*** in **Table 56** changes slightly in relation to each operating point since the mass of ingested air varies slightly. In the case of operating point ***C2***, we see that we have marginally more air as compared to operating point ***C3***, this can be explained by the fact that water vapour has taken place of the air thus reducing oxygen concentration in the air / fuel charge.

The ROHR curves are given in **Figure 69**. As can be seen the difference between the three ROHR curves is very slight. Since a pilot injection is used during these tests, it has been seen that the main combustion is mostly diffusive in nature with less than 3% of injected fuel burning in a premixed combustion, owing to the short ignition delay before SOC. For this operating point, the influence of intake air temperature on the ROHR between 91 and 60°C is negligible. The reduction of temperature will theoretically increase air / fuel mixing due to an increase in air density. This is due to the act that the same volume of air entrained by the fuel jet has a greater mass. This can be partly compensated for by a slower spray penetration, so that the speed of diffusive combustion increases only very slightly. Normally, the speed of the diffusive combustion should reduce for the case where WI is used, however if reference is made to **Table 56**, we see that the level of dilution is very slightly changed (of the order of 2%). A greater WI injection rate would without doubt change the dilution of the air / fuel charge to such an extent that changes in ROHR would be noticeable.

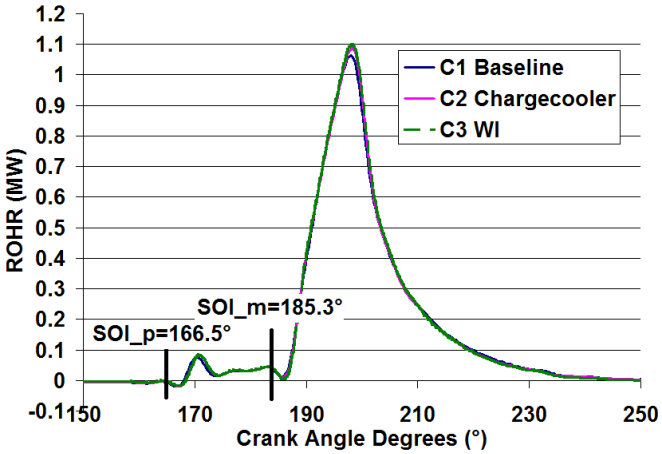

Figure 69. ROHR diagram for comparison of intake cooling via chargecooler or WI

Looking at pollutant emissions, again with reference to **Table 56**, we can see that with reference to the base configuration given by ***C1***, the NOx emission rate has been reduced by 34% with the use of WI (***C2***). The reduction obtained with intake air cooled by the chargecooler (***C3***) amounts to only 9% from baseline. It can be surmised that of the total NOx reduction via WI, 26% is by the cooling effect of WI (as given by ***C2***) and 74% is by other effects of WI such as dilution. Considering PM emissions, a 26% increase in emissions is observed between the baseline (***C1***) and the WI (***C2***) configurations. On the other hand, the same intake temperature reduction obtained via the chargecooler (***C2***) can reduce PM emissions rate by 8%. This would mean that the potential PM reduction effects of cooling the intake charge are overcompensated for by other effects of WI which give rise to an increase in PM emission rate. Some effects are:

- A decrease in flame temperature which results in a decrease of soot oxidation at the jet periphery.
- Variation in the global AFR that would influences soot oxidation.
- Variation of flame lift-off length and corresponding AFR, in addition to the core spray temperature that both affect the soot production rate in the core spray [8, 59, 61, 62].

Local experiments in the combustion chamber (on a Diesel engine with optical access) would help us understand the various effects of WI on PM production and oxidation in the combustion chamber during the course of injection and combustion. The relative part of effects of air charge cooling on the production of PM and NOx are indicative in nature and may vary depending upon operating conditions and WI flow rate.

In the following section, the influences of WI on the four different operating points shall be considered. In this section, the intake temperatures for all test points shall be kept the same.

4.1.2. Influence of WI on combustion:

4.1.2.1. Influence of WI on ignition delay (ID):

The rate of heat release (ROHR) curves for operating points A to D are given in **Figure 71**. The influence of WI on ignition delay for main injection is given in **Figure 70**. As depicted in both figures, the very first effect of WI on combustion is the increase in ignition delay. This agrees with previous researches [27, 29]. This influence can be observed for both pilot and

main injection as shown in **Figure 71**. The greater the quantity of water being used, the greater would be the ignition delay. As an example, for operating point B, the ignition delay is increased from 0.24 ms to 0.86 ms while increasing the dilution ratio from 0% to 10.2% (**Figure 70**). This evolution can be explained easily by the cooling effect of water since air temperature is known to have a major influence on ignition delay. **Figure 72** shows the in-cylinder average temperature deduced from the in-cylinder pressure measurement and bulk gas properties, for operating points B and D (medium-low and high load). WI reduces the in-cylinder temperature at SOC for operating point D of about 260 K for the maximum water flow rate, 21 kg/h corresponding to the highest dilution ratio in **Figure 72**. In the case of operating point B, the maximum reduction in cylinder temperature seen was of the order of 240 K with a WI rate of 11 kg/h. Water may also have a chemical and/or diluting effect on the ID. To study such effects, combustion with WI should be compared to combustion without WI but with the same in-cylinder temperature at SOI. This was performed above in the section dealing with intake charge cooling using WI. However, with the little amount of water, no noticeable effect of water on ID (except for cooling effect) was observed. A comparison with a higher WI rate would be probably more interesting. It is on the other hand difficult to perform practically because it would require a very low air temperature at cylinder inlet (T_2") which is difficult to attain with a traditional chargecooler as found on the present engine test bench.

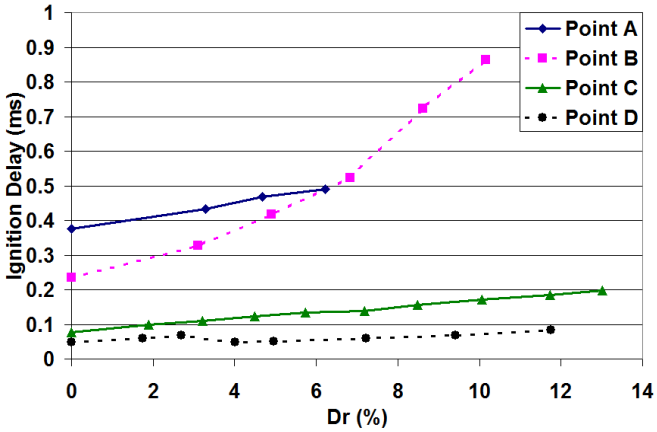

Figure 70. Ignition delay for main combustion of operating points A through D in milliseconds.

4.1.2.2. Influence of WI on ROHR:

The increase in ID has a direct influence on combustion: the proportion "***r***" of fuel injected during ID rises in value while increasing WI rate. A consequence of which is an increase in the premixed part of combustion. For instance, for operating point A, ***r*** is increased from 40% to 57% while increasing the dilution ratio from 0% to 6.2%. The higher the engine load, lower will be the ratio ***r*** (for a given dilution ratio). For the highest load tested here (operating point D), ***r*** rises from 3% to 4% while increasing the dilution ratio from 0% to 11.8%. The first peak of heat release is little delayed but becomes higher with moderate amounts of WI. This is very noticeable at low load, when injection duration is shorter and thus premixed part has a greater relative importance (operating points A and B, see **Figure 71 a** and **b** respectively). However, when in-cylinder temperatures become too low, premixed combustion speed may decrease due to chemical reactions which are slowed down, resulting in a decrease of the total ROHR (premixed and diffusion combustions). This can be observed for operating point A (see **Figure 71 a**), as well as for operating point B when large amount of WI are used (dilution ratio above 6.8%, see **Figure 71 b**).

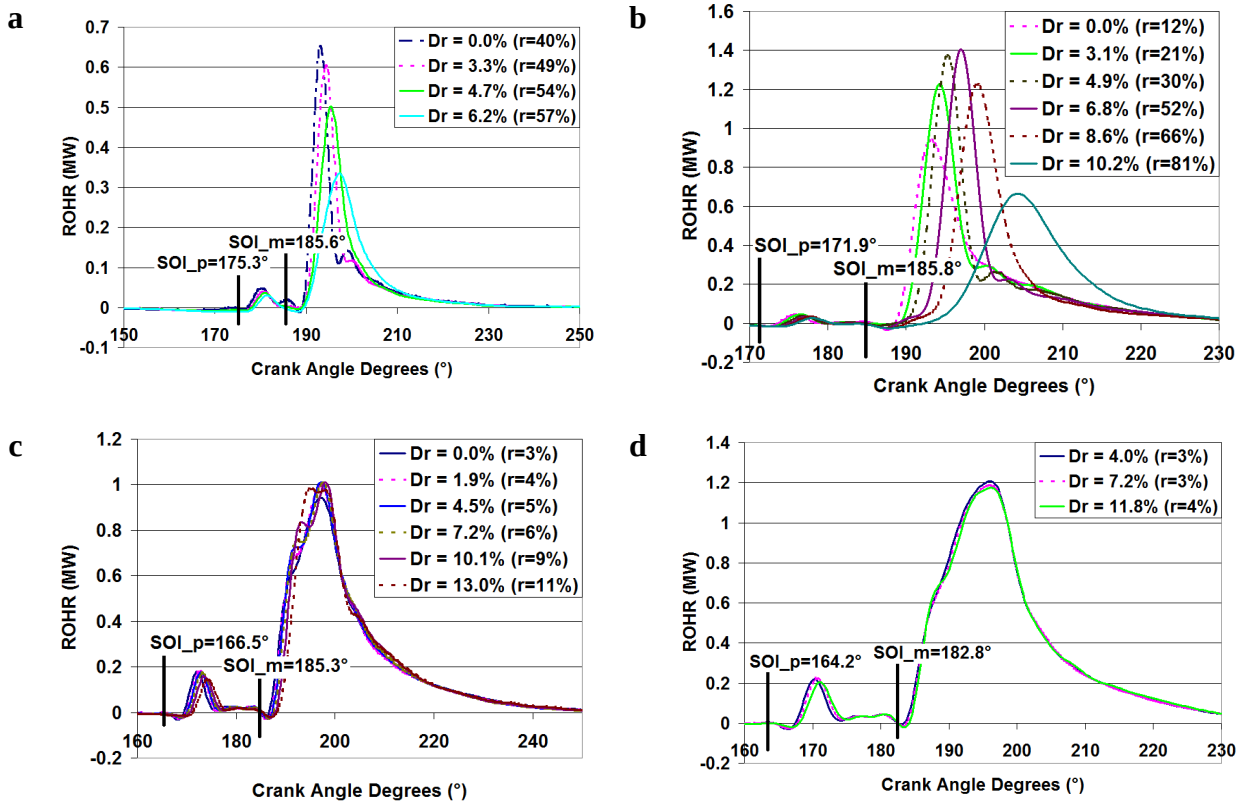

Figure 71. ROHR diagrams for all four operating points A through D

At higher loads, the combustion is almost purely diffusive, the proportion of fuel injected during ID being very low. In these cases, the influence of WI on ROHR is negligible. Here, the diffusive combustion speed is controlled by the amount of air entrained by the fuel spray per unit time. When WI is used, the spray entrains a water/air mixture instead of pure air, so that a decrease in combustion speed could be expected (due in part to, for example, reduction in oxygen concentration and presence of a diluent). Such a decrease is observed for diffusive combustion with EGR when EGR rate is increased at constant boost pressure [47, 48]. In the case of constant boost pressure, the EGR gases replace air, this leads to a decrease in the mass of entrapped fresh air. In the case of WI however, water does not replace air but is added to it: even if boost pressure is kept constant, the cooling effect produced by water vaporisation increases the density of gases entrapped in the cylinder. In other words, when WI is used, assuming that fuel spray entrains the same volume of gas per unit of time than without WI, this volume contains a greater mass of gas (air & water vapour) and almost the same mass of air, so that combustion speed does not change noticeably.

4.1.2.3. Influence of WI on in-cylinder temperature:

Here we shall discuss in-cylinder average temperature after SOC (**Figure 72**). As the amount of WI increases, the in-cylinder gas temperature reduces. It may be noted here that the temperature difference between WI and the reference case increases during combustion (it may of the order of over 200 K against around 100 K at SOC), especially at high dilution ratio (high rates of WI). There can be several explanations for this. First, the trapped mass increases with WI rates, thus the in-cylinder heat capacity is greater. This is achieved by the evaporation of water spray in the intake at IVC while boost is kept constant. Modifications in ROHR due to delay in combustion also alter the evolution of in-cylinder temperature. A third reason appeared during analysis of ROHR over the course of a cycle. In order to ensure a correct cumulative heat release it was found that it is necessary to increase heat losses at

cylinder walls (all the more since a higher WI rate is used). **Figure 73** depicts the calculated cumulative combustion gross heat release while varying WI rate for operating point B. The final value decreases with WI whereas CO, HC and PM emissions show that combustion efficiency is not noticeably altered. This means that the calculation of combustion heat release is underestimated, which in turn can be attributed to an underestimation of heat losses (gross combustion heat release is equal to net heat release (from in-cylinder pressure measurement) plus heat exchange at the wall (estimated with a model)). Two elements could explain an increase of heat losses at cylinder wall when WI is used and the water flow rate is increased:

- As outlined earlier, WI has a cooling effect during water vaporisation which may decrease wall temperature during inlet and at the beginning of compression stroke, which in turn would increase the heat exchange when in-cylinder temperature becomes higher than wall temperature, in particular during combustion and expansion stroke.
- Water vapour has a much higher convective coefficient than air; that could justify a more intense heat exchange between in-cylinder gas content and the wall.

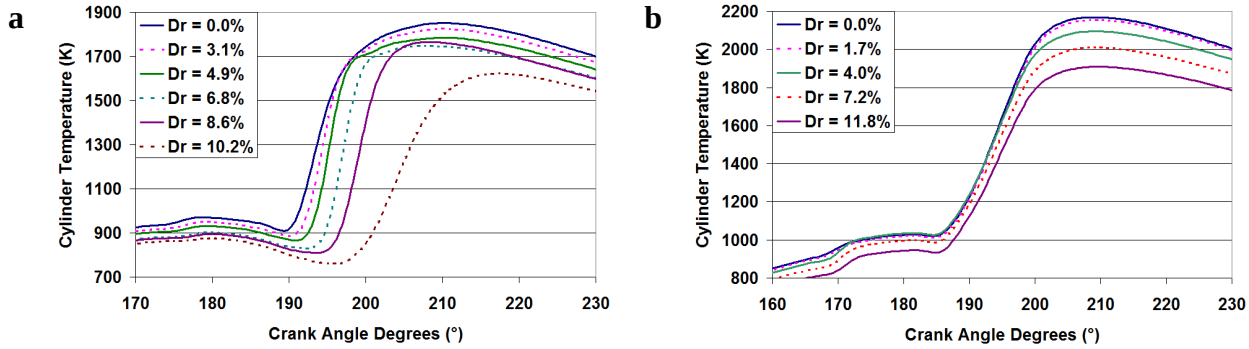

Figure 72. In-cylinder bulk gas average temperature for operating points B and D

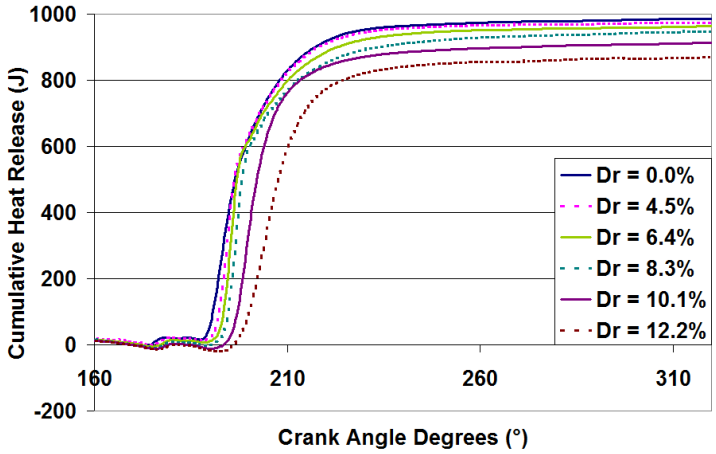

Figure 73. Cumulative Heat Release curves for different values of WI rates for operating point B

4.1.2.4. Influence of WI on in-cylinder pressure and engine BSFC:

When WI modifies the ROHR to a measurable extent, it follows that in-cylinder pressure traces are also altered. As a result of this, the engine torque is reduced when the combustion is delayed (the injected fuel mass kept constant). As depicted in **Figure 75**, this engine global thermal efficiency reduction is very marked at low and middle load conditions (operating points A, B, and C). For operating point A (refering to **Figure 75 a**), the WI rate is limited by combustion stability (for a dilution ratio above 6.2%, corresponding to a water flow of 6

kg/h). The combustion quality greatly deteriorates with production of large amounts of CO and HC in addition to rough running and evidence of misfired cycles. The engine efficiency is decreased from 28.0% to 23.3% while increasing dilution ratio from 0% to 6.2%. on the other hand, at higher loads, WI has very little influence on ROHR and thus on in-cylinder pressure (referring to **Figure 74 b** for operating point D).

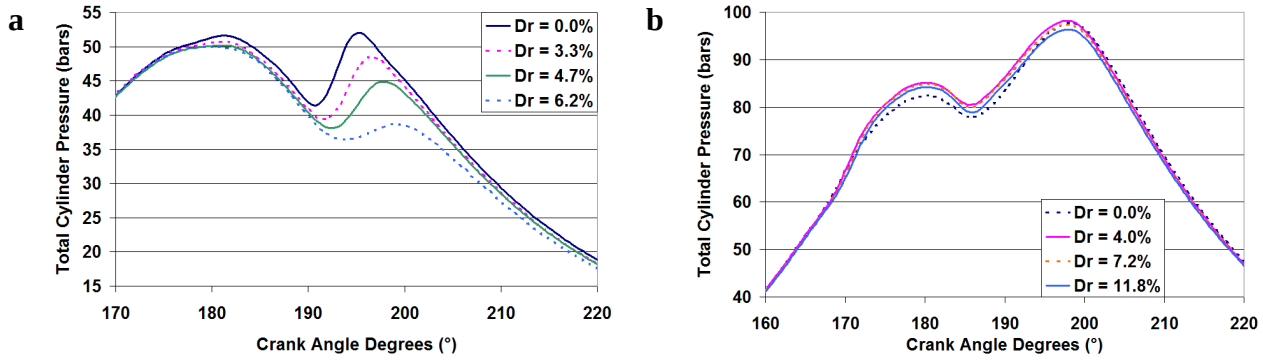

Figure 74. Total cylinder pressure traces for Points A and D with a variation of WI rates (Dilution ratio)

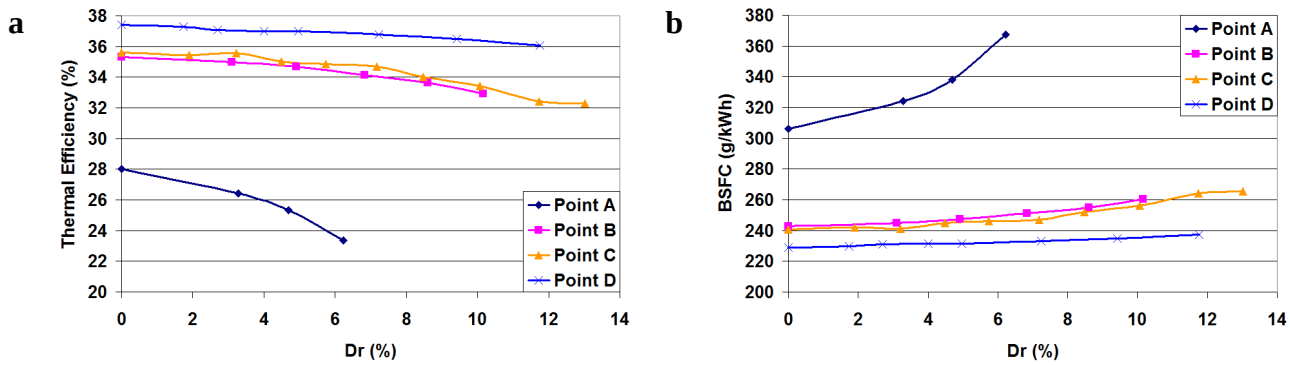

Figure 75. Thermal efficiency and BSFC curves for all operating points in relation to Dilution Ratio

4.1.2.5. Influence of WI on CO emissions:

The influence of inlet WI on CO emissions upstream of the DOC is given in **Figure 76**. It can be seen that the increase of the dilution ratio results in a corresponding increase in CO emissions rate entering into the DOC. This may affect the oxidation rate of CO by the DOC as seen downstream of the DOC. This may come about not only due to the increase in the CO production rate, but also via a reduction in the EGT.

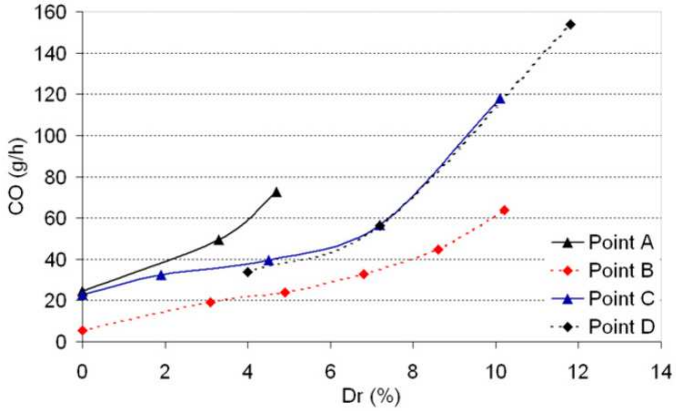

Figure 76. Comparison of points A through D for CO production in g/h

As a reference **Figure 77** is presented which outlines the EGT rate corresponding to each operating point relative to the dilution ratio while using WI. It is clear that as WI rate is increased, the EGT goes down. This may affect the final CO emissions (downstream the DOC) if the DOC is unable to oxidize a higher CO flow rate. Furthermore, the decrease of exhaust gas temperature induced by WI may reduce the conversion efficiency of the DOC. The impact of WI on CO and hydrocarbon emissions as well as their after-treatment in the DOC should be further investigated before any industrial application.

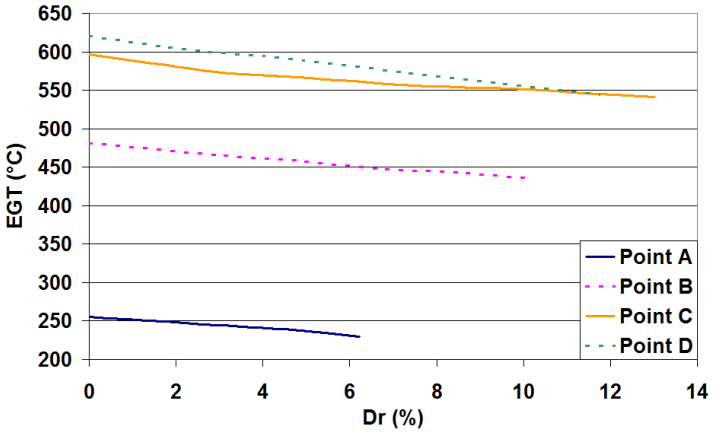

Figure 77. Figure outlining the evolution of EGT (T3) with respect to dilution ratio with WI

4.2. Influence of WI on pollutant emissions and comparison with LP EGR:

In this section, a comparison is made between WI and EGR. Different tests were performed on the test bench and were aimed at trying to get the different parameters such as intake temperature, dilution ratio, boost pressure, air mass flow rate etc. comparable between WI and EGR groups of tests. The aims of this were to isolate the different effects that modify combustion and emission production rate. In addition to the aforementioned comparison in combustion performance, supplementary effects were noted as well, such as turbocharger performance, physical effects on the engine etc.

The following subsection will deal with the comparison of effects of WI and EGR on combustion, and from there on, will progress to emissions performance with respect to NOx and PM and lastly will recount miscellaneous effects on the test engine.

4.2.1. Comparison of WI and EGR on combustion:

Figure 78 shows a comparison of WI and EGR effects on ROHR for the same dilution ratio, for operating points A and B. We can see that both EGR and WI cause ID to increase. In the case of EGR, this increase can be attributed to the dilution effect. In effect, O_2 density decreases and heat produced by the initiation reaction of combustion is absorbed by a larger mass of gas, thus the temperature increase encountered is smaller. The in-cylinder gas temperature at SOI is not significantly modified when compared to the reference case, since the inlet gas temperature (T_2") remains the same.

In the case of WI on the other hand, as said before, the main effect on ID should be the decrease in gas temperature at SOI, due to the WI cooling effect. The result is that the ignition delay increase is more significant with WI than with EGR (for the same Dr). However, the

peak heat release due to premixed combustion is not increased (it is even reduced in the case of the operating point A) because lower temperatures tend to reduce chemical reaction rates.

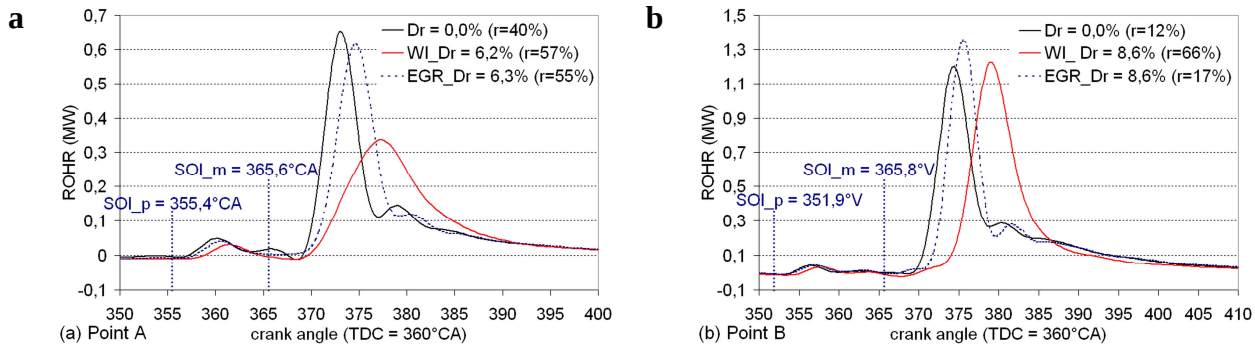

Figure 78. Comparison of operating points A and B for influence of EGR and WI at same dilution ratio

Figure 79 presents a comparison of the in-cylinder bulk temperature for all four operating points. Reference values of Dr are duly noted with each figure. The sub figures **a** through **d** represent operating points A through D respectively.

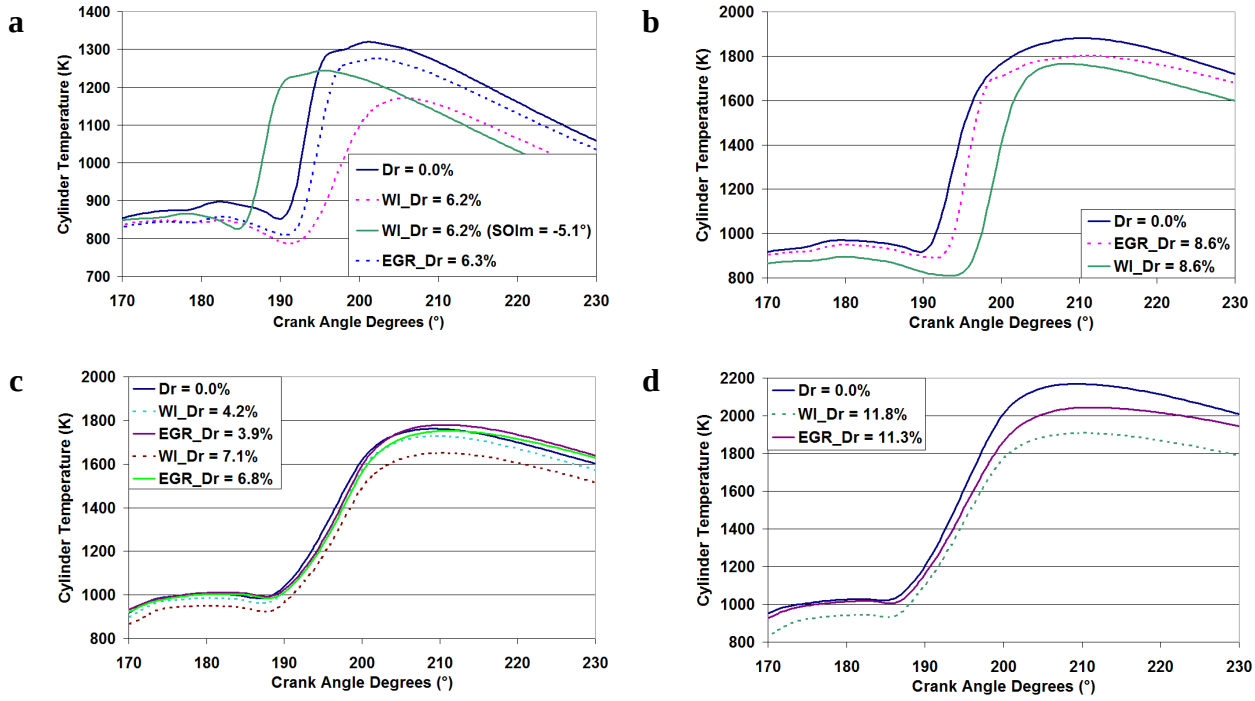

Figure 79. Comparison of in-cylinder bulk temperatures for EGR and WI on operating points A through D

In **Figure 79 a**, we see four curves, the first being for the reference case without dilution of any kind. The second and third curves are for WI, with the third curve corresponding to an operating point where the injection timing was advanced by 5.1° to try to recover lost torque owing to the delayed combustion. The fourth curve is for the case where EGR is used. In this case, all four operating settings produce more or less the same cylinder temperature up until SOC. For curves two and four (corresponding to WI and EGR with base injection settings), things start to diverge near after SOIm. Going through the combustion acceleration diagrams as shown in **Figure 80 a**, it is clear that there is no combustion of the pilot injection for both cases due to a high level of dilution (in fact, even the reference curve without dilution barely reaches the pre-defined minimum limit of 200 MW/s, while with the injection advanced, the fuel is injected too soon to burn in the pilot injection phase).

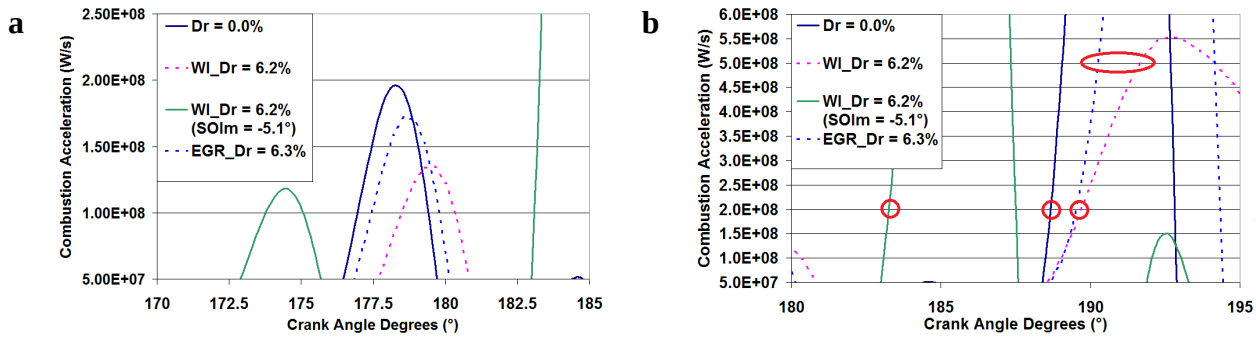

Figure 80. Combustion acceleration values for operating point B with corresponding Dr values.

In the case of the main injection, we can see that the WI operating point with advanced injection has reached the predefined combustion acceleration limit relatively early as shown in **Figure 80 b**. After this we see that the reference point with undiluted intake charge reaches the pre-defined combustion acceleration limit of 200 MW/s around 5° later. It is interesting to note that by advancing the injection timing, we are at the same ID for WI as for the reference (non-diluted) point (seeing that we have advanced the injection timing by about 5°). Afterwards, the combustion acceleration for both EGR and WI diluted operating points proceeds at mostly the same rate until the combustion acceleration limit of 200 MW/s is reached, after which the EGR combustion acceleration rises much more than for WI. This could explain the slower rise in in-cylinder temperature as shown in **Figure 79 a**. On the final in-cylinder temperature curve (**Figure 79 a**), we can see that the peak temperature in the case of WI is of the order of 100K less than that for EGR.

Referring to the in-cylinder bulk temperature graph of operating point B, EGR also leads to lower temperatures during combustion compared to the reference operating point, but to a lesser extent than WI. It seems that the reduction in temperature is only due to dilution, whereas WI seems to reduce the in-cylinder temperature before SOC as can be seen in **Figure 79 b**.

With reference to points C and D for which the in-cylinder bulk temperature evolution is given in **Figure 79 c** and **d**, we see that in both cases, the temperatures before SOC are slightly lower when WI is used and this difference in temperature becomes even more pronounced as the main diffusive combustion takes place.

4.2.2. Influence of WI on PM and NOx emissions:

4.2.2.1. Influence of WI on NOx emissions and comparison with LP EGR:

The influence of WI on NOx emissions is given in **Figure 81** for operating points A to D. As expected, NOx emissions decrease when WI rate increases. This is due to temperature reduction which itself has several causes as discussed in the above section: water cooling effect due to vaporisation, increase of heat capacity due to higher trapped mass, increase of specific heat capacity due to air dilution with vapour, increase of heat losses at the wall, combustion delay due to increase in ID and eventually decrease of chemical reactions rates. Here it should be noted that some effects of WI (such as a possible increase of premixed combustion peak) may have a tendency to increase NOx emissions but are largely overcome by other competing effects.

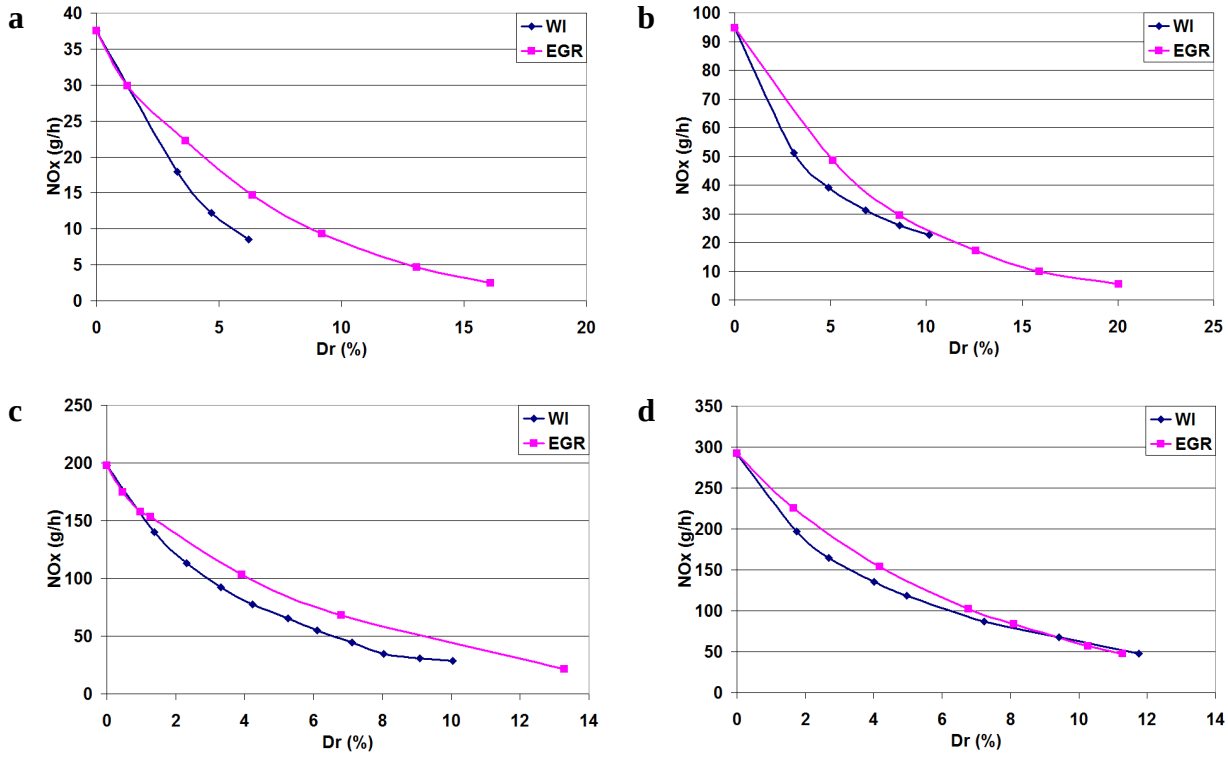

Figure 81. Comparison of NOx emissions rates with WI and EGR for all four operating points

The maximum NOx reduction depends on the maximum WI rate, which is in turn limited by combustion stability. It reaches 77.3, 76.1, 85.4 and 83.8% for operating points A to D respectively, with a corresponding WI rate of 6, 11, 21 and 21 kg/h respectively. The maximum water/fuel mass ratio varies from 2.3 to 4.0 and the water /intake air mass ratio varies from 0.10 to 0.15. NOx emissions obtained with the LP EGR system are plotted on the same figures for a comparison. EGR also causes NOx emissions to decrease. It must be underlined that the nature of diluent (water or dry exhaust gas), which was studied by Ladommatos et al. [22] is not the only difference between the two cases: WI cooling effect leads to lower temperatures before SOC compared to EGR, water is added to air (supplemental) while EGR replaces some air (substitution) and ROHRs are also different. However these differences seem to compensate for each other so that for a given dilution ratio the NOx reductions with EGR and WI are of the same magnitude, generally a little lower with EGR.

4.2.2.2. Influence of WI on PM emissions and comparison with LP EGR:

In the case of PM emissions, the global trend is an increase of emissions of 23%, 141% and 502% using WI for operating points B, C and D (refer to **Figure 82 b** to **d**), thus leading the common trade-off between NOx and PM emissions (reduction in NOx coupled with an increase in PM). This evolution can be explained by the decrease in in-cylinder temperature during combustion which limits soot oxidation. A slight decrease of λ is also observed (of 6.8, 8 and 3%) which may also limit PM oxidation process. PM production (in the core spray) may also be altered by WI, for instance by the increase of premixed part of combustion which generally produces no PM, or by a change in richness at lift-off length that has a strong effect on the PM production rate [25, 60, 63]. But this latter point requires that an optical access be available on the test engine so that the phenomenon may be investigated experimentally. Returning to the figures, we can see that the increase in PM emissions with EGR is much more significant as compared to WI, for a given dilution ratio. Even if the nature of diluent

(water or dry EGR) may play a role [22, 65], a major explanation for the trend between EGR and WI seems to be the difference in global air/fuel equivalence ratio λ. As was stated earlier and seen here in **Figure 82**, for WI, the cooling effect compensates for the dilution effect so that the trapped mass of air does not vary much with WI rate, whereas the recirculated gases replace some of the air when EGR rate increases (substitution EGR). This is because EGR is performed at constant density at engine inlet (boost pressure and inlet air temperature being kept constant). The decrease of λ is likely to limit PM oxidation, thus explaining the higher final emissions. PM production may also be different between WI and EGR, in particular due to differences in temperatures in the core spray or local fuel/air ratio at lift-off length.

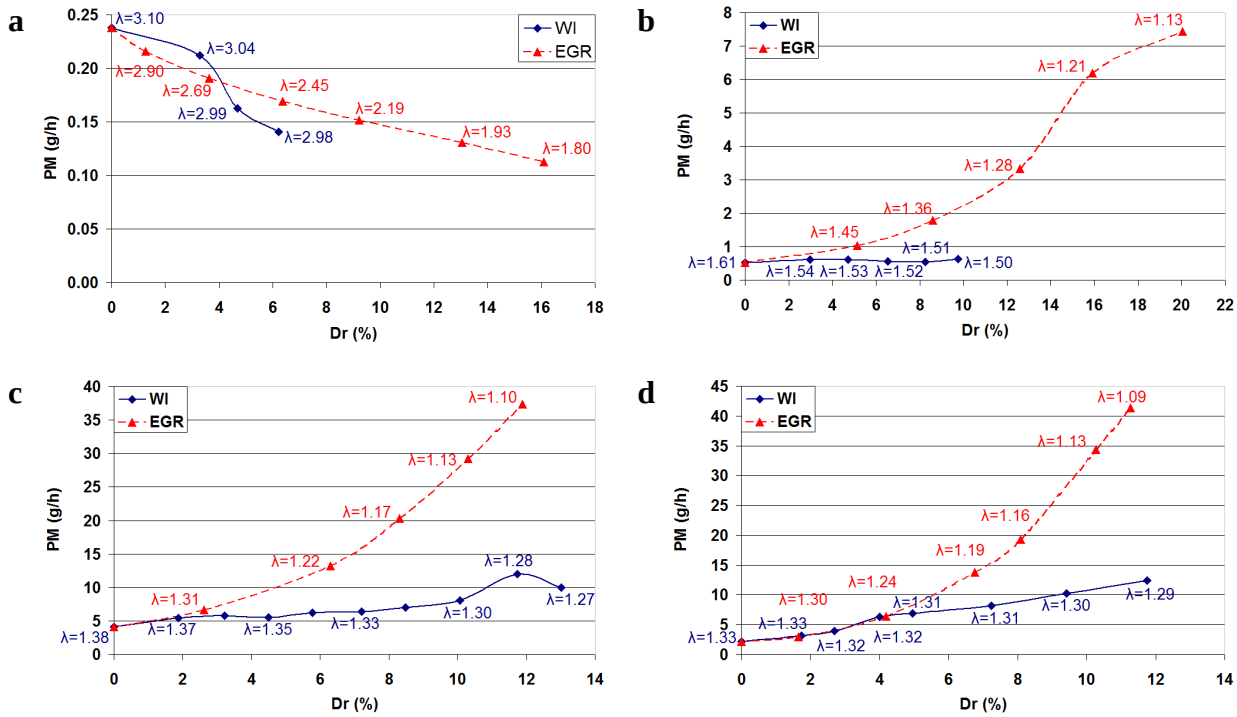

Figure 82. Comparison of PM emission rates for WI and EGR on operating points A-D

A different trend is observed for operating point A (refer to **Figure 82 a**): PM emissions decrease when WI rate is increased. This can be explained by the fact that at low load, combustion temperatures are already low without the presence of WI. The introduction of WI may cause the engine to enter a low temperature combustion (LTC) mode. In that case, a decrease in PM emissions is classically observed while temperatures are decreased (generally with large amount of EGR [48]). The temperatures then become too low for PM to form, so that engine-out emissions can be reduced, although PM oxidation is also drastically reduced. A major drawback is that at these temperatures CO and UHC emissions increase a lot, in addition to the engine BSFC, while combustion efficiency decreases. In this case, PM emissions are similar for both WI and EGR for a given dilution ratio.

4.2.2.3. Influence of WI on NOx – EGR trade-off :

Here, NOx/PM trade-off curves obtained with WI are presented in **Figure 83** for operating points A through D. The corresponding values of BSFC are also presented in addition to the NOx/PM trade-off obtained with LP EGR. For operating point A, a simultaneous reduction of NOx and PM can be achieved, both with WI and EGR. This is due to a particular combustion mode (LTC) as described in the previous sub-section dealing with WI effects on PM emissions. For the other three points, a more classical trade-off is obtained which is much

better with WI than with EGR: this means that for a given NOx level, PM emissions will be lower with WI than with EGR.

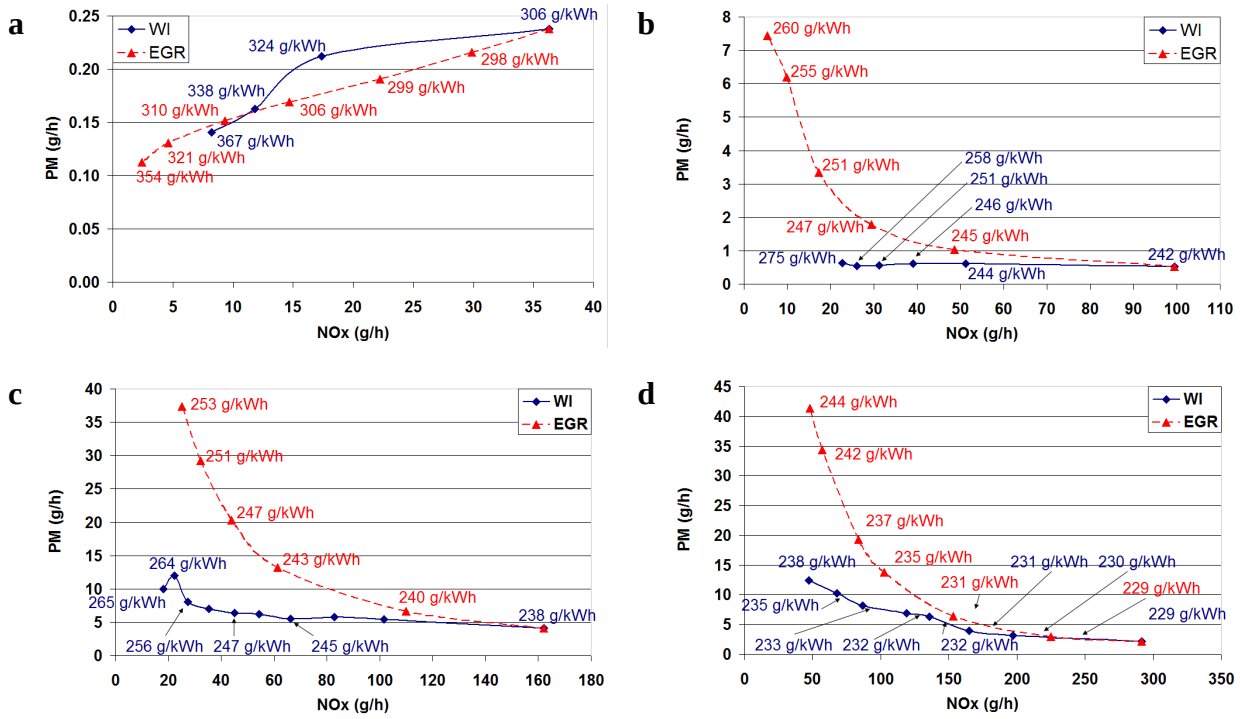

Figure 83. NOx / PM trade-off diagrams for all four operating points A through D

It has been mentioned and proven previously that WI delays combustion. In the absence of injection timing adjustments, this would mean that the combustion reactions are slowed down due to the lower in-cylinder bulk gas temperature. This combustion retarding effect has positive influence on NOx emissions which are reduced (in-cylinder pressure and in-cylinder temperature are lower during combustion). A major drawback on the other hand is an increase in the engine BSFC. This is true for the first three operating points.

In the case of operating point D however, WI is actually beneficial with respect to BSFC in that it reduces it slightly. This may be due to the fact that at such low values of λ, any EGR would cause a rich combustion which is not optimal for torque production. This can be seen in **Figure 82 d** where unlike WI (which is 30% higher than stoichiometric), EGR causes the air/fuel ratio to drop down to only 9% off of the stoichiometric. It can be noted that supplemental EGR (i.e. boost pressure is increased along with EGR rate to keep the A/F ratio constant) can lead to PM emission evolution closer to those obtained with WI, than substitution EGR. However, supplemental EGR has two major differences with WI:

- ✓ The increase in boost pressure causes an increase in pressure during combustion, and in turn changes very important parameters such as flame lift-off length and corresponding richness. Thus an increase in injection pressure is often required [66].
- ✓ The rates of supplemental EGR are limited by the ability of turbocharging system to deliver high boost pressure, in particular at middle and high load conditions [66].

In addition to this, referring back to pressure traces presented in **Figure 74 b**, it is quite clear that WI has very little effect on the phasing of combustion and reacts for the most part to reduce NOx production via a reduction in combustion temperature.

4.3. Study of test points with simultaneous use of WI and EGR

Finally, two test points (**B** and **D** – please refer to **Table 40**) have also been studied with LP EGR used in conjunction with WI. For point **B**, the WI injection rate was fixed at 3.0 kg/h and the EGR rate was varied, while in the case of point **D**, the WI rate was fixed at 6.0 kg/h and the EGR rate varied. The influence of dilution ratio on the NOx production rate is shown in **Figure 84**.

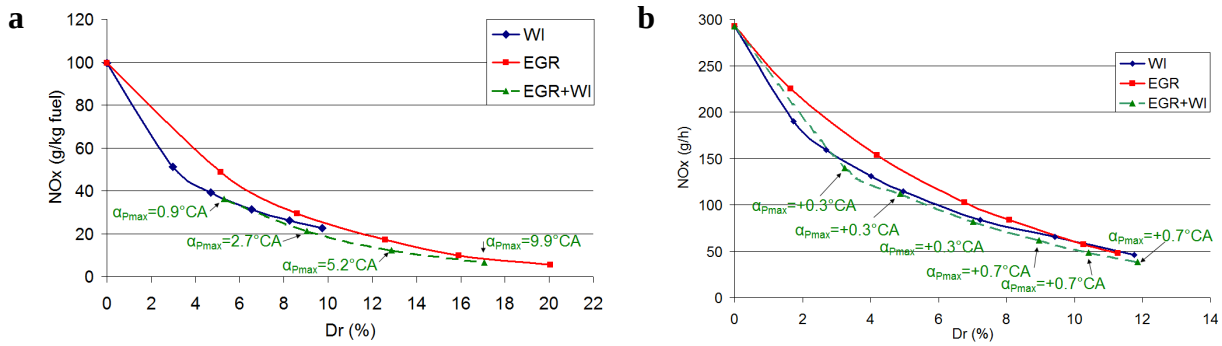

Figure 84. Comparison of NOx emissions for points **B** and **D** with EGR + WI.

We can clearly see that the inclusion of EGR allow us to reduce NOx emissions rates to a greater extent while using EGR and WI for point **B**. The limit for WI rate was determined by misfiring. That is to say, at Dr value of 10% with WI only, the engine was misfiring to such an extent that it was not possible to increase WI rate. However, with the inclusion of EGR, the engine combustion is stabilised, and for the same dilution ratio, we see a marginally better performance for NOx reduction.

In the case of point **D**, shown in **Figure 84 b.**, we see that due to the high engine load, the WI system has achieved its limit before destabilising the engine combustion. As for NOx emissions rates, as with the EGR + WI usage for operating point **B**, we see that NOx reduction is slightly improved as compare to straight WI or straight EGR.

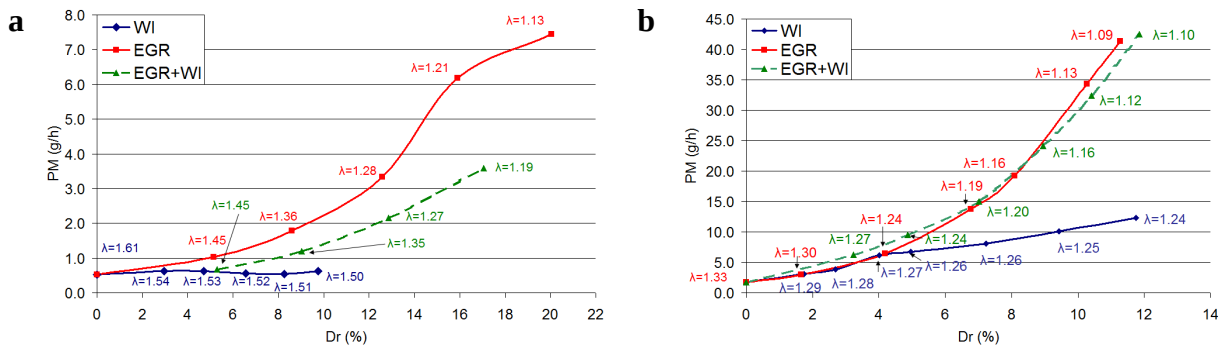

Figure 85. Comparison of PM emissions for points **B** and **D** with EGR + WI.

Figure 85 a. and **b.** show a comparison of PM emissions rates for both point **B** and **D**. In the case of point **B** shown in **Figure 85 a.**, we see that EGR + WI helps mitigate some of the rise of PM emissions when EGR is used. It seems that the use of WI brings down the PM emissions rate to between EGR and WI levels for the same dilution levels. An interesting fact to note here is that for the same dilution ratio, the equivalence ratio with EGR + WI seems to

be almost the same as for EGR, and yet EGR produces more PM emissions. This may have something to do with the greater fuel reaction potential of supplementary OH radicals produced during combustion with WI as discussed in **section 1.3.3.3** and some earlier bibliographic citations.

In the case of operating point **B** as shown in **Figure 85 b.**, we see that comparing EGR and EGR + WI, we see almost the same performance in terms of PM emissions rates with reference to the equivalence ratio. At low EGR rates, the PM emissions rates are higher and at higher EGR rates, the PM emissions fall.

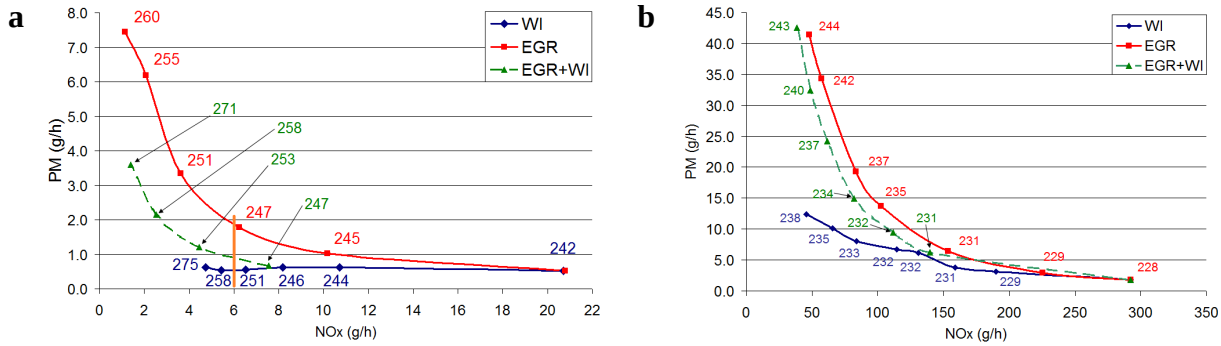

Figure 86. PM / NOx emissions trade-off for points **B** and **D** with EGR + WI.

In **Figure 86**, we see PM / NOx trade-off diagrams with specific fuel consumption values superposed onto the graphs. In the case of operating point **B**, we see that WI clearly affects combustion performance, reducing the efficiency of the engine. For the same NOx performance, EGR + WI is much better than WI alone, and only slightly worse than EGR alone. Taking the example of 6 g/h of NOx emission, BSFC value with EGR is at 247 g/kW-h, with EGR+WI, it is around 250 g/kW-h, while with WI, it is at 254 g/kW-h. At the same time, the PM emissions of the EGR + WI setup is much better as compare to EGR alone (around half in g/h), while not being favourable as compared to WI (30% higher in PM emissions).

In the case of point **D** shown in **Figure 86 b.**, we see that we have a slightly better specific consumption when using WI, this may be due to a slightly greater availability of oxygen which results in a better combustion, and hence a better combustion profile. Otherwise, the difference in fuel consumption between EGR and WI is very narrow.

The effects of inlet WI have been investigated on a modern, small, automotive HSDI Diesel engine. Parts of this study were reported in two publications [67, 68]. The effects of water as vapour and as liquid on combustion have been presented and compared with EGR. Here are the main conclusions:

- ✓ *A large reduction of NOx emissions can be achieved with high WI rates, at low load as well as high load conditions. A water mass of about 60 to 65% of the fuel is needed to obtain a 50% NOx reduction.*
- ✓ *At low load conditions when air excess is naturally high, EGR has the capability to reduce NOx emissions without increasing PM emissions too much. At these conditions, from a practical point of view, EGR seems to have an advantage compared to WI because it does not require a second liquid (water) in addition to fuel. At higher loads, WI has the capability to reduce NOx emissions without a large increase of PM emissions because the air flow rate remains approximately unchanged. At these operating points, NOx emissions cannot be largely decreased by EGR because the air flow rate cannot be reduced without a large increase in PM emissions. Thus, the WI technique has a clear advantage in terms of NOx reduction as compared with EGR at high load.*
- ✓ *A new effect of inlet WI as compared with EGR is the reduction of inlet temperature due to vaporisation, which a consequence is a large decrease of in-cylinder temperature at SOI and during combustion, as well as exhaust temperature (which will have consequences on the design and matching of the turbine and the exhaust after treatment devices).*
- ✓ *However, WI seems to increase heat losses at cylinder wall, which can affect negatively the engine global efficiency.*
- ✓ *The influence of WI on combustion (pilot and main injections) has been also studied and show the same effects as for EGR (increase of ignition delay and consequently of the premixed part of combustion, off-phasing effect on combustion). These effects are much more significant for WI than for EGR for a given dilution ratio. To maintain the cycle efficiency, the readjustment of fuel injection while increasing the dilution ratio is thus higher with WI than with EGR.*
- ✓ *Finally, the simultaneous use of a moderate quantity of EGR and WI give us results which are comparable to either only EGR or only WI in terms of NOx and PM emissions. This could allow the reduction of use of water, all the while drastically reducing the quantity of NOx emissions while keeping the increase of PM emissions in check, compared to EGR only and for the same NOx emission rate.*

Les effets de l'injection d'eau à l'admission d'un moteur Diesel automobile récent ont été étudiés expérimentalement. Les résultats ont donné lieu à deux publications [67, 68]. Les principales conclusions sont données ci-après :

- ✓ *Il apparaît que de larges réductions des émissions de NOx peuvent être obtenues, aussi bien à faible charge qu'à charge plus élevée. Un débit d'eau égal à environ 65% du débit de carburant est nécessaire pour une réduction de 50% des émissions de NOx.*
- ✓ *A faible charge lorsque l'excès d'air est naturellement élevé, l'EGR a la capacité de réduire les émissions de NOx sans que les particules n'augmentent exagérément. Dans ces conditions l'EGR semble plus avantageuse que l'injection d'eau car elle ne nécessite pas de fluide supplémentaire. A plus forte charge l'injection d'eau permet de réduire les émissions de NOx sans trop pénaliser les émissions de particules, car le débit d'air est peu modifié. Elle a alors un avantage clair sur l'EGR (au moins de substitution), qui du fait de la baisse du débit d'air conduit dans ces conditions à des hausses très importante des émissions de particules.*
- ✓ *Un effet spécifique de l'injection d'eau par rapport à l'EGR est la réduction de la température d'admission grâce à la vaporisation de l'eau. Elle a pour conséquence une réduction importante de la température dans le cylindre au début de l'injection de carburant et pendant la combustion, ainsi que de la température d'échappement ce qui peut avoir des conséquences sur les systèmes de post-traitement et sur l'adaptation de la turbine du turbocompresseur.*
- ✓ *Toutefois, l'injection d'eau semble augmenter les pertes thermiques aux parois du cylindre, ce qui peut altérer le rendement global du moteur.*
- ✓ *L'influence de l'injection d'eau sur la combustion (dans le cas d'une injection pilote + principale) a également été étudiée et montre les mêmes effets que l'EGR (allongement du délai d'inflammation et par conséquent de la part de carburant suivant une combustion de type pré-mélange, retardement de la phase de combustion). Pour un taux de dilution donné, ces effets sont beaucoup plus marqués avec l'injection d'eau. Par conséquent le réajustement du phasage de l'injection pour maintenir le rendement de cycle est aussi plus important.*
- ✓ *Finalement, l'utilisation simultanée d'une quantité modérée d'eau et d'EGR conduit à des résultats intermédiaires (par rapport à l'eau seule ou l'EGR seul) en termes d'émissions de NOx et de particules. Cela permet de limiter la quantité d'eau utilisée, tout en réduisant de manière drastique les émissions de NOx et avec une hausse moindre des particules, comparativement à l'EGR seul et pour un même niveau d'émissions de NOx.*

Conclusions and perspectives

The bibliographic study in chapter 1 provides a summary of up-to-date knowledge on the sequence of events that take place in direct injection diesel combustion and on the production of pollutant emissions (NOx and PM). Different means of WI are also dealt with in detail, as well as their effect on combustion and production of pollutant emissions. At times, different results were obtained by different authors, as much as quantitative in nature (relative WI quantity required for a similar NOx reduction), as qualitative (for some, WI caused a drop in PM production rates while for others, an increase was noted).

In the second chapter, the principal tools and elements were presented (diesel engine type, the WI system developed specifically for this thesis, measurement apparatus and their associated measurement precision) and numerical analysis tools were developed. These tools allow analysis of different thermodynamic conditions after the injection of water in liquid form in the intake manifold; evaporation in the intake manifold, evaporation in the cylinder with the intake valves open (open thermodynamic system), or evaporation in the cylinder during compression after the intake valves have closed (closed thermodynamic system).

The numerical tools developed in chapter 2 were then used with the aim to determine the state of water and the temperature of the mixture during different phases of the engine cycle (while mixing in the intake manifold, intake into the cylinders, and then during compression of the mixture). A parametric study has allowed us to show the influence of the initial temperature of water and the initial conditions of air (pressure, temperature, humidity) before mixing on the quantity of water that can be evaporated and the final temperature of the mixture. In addition to this, the closely monitored condition of the state of water and the thermodynamic properties of the air /vapour/liquid/residual gas mixture allows us to calculate the heat release with relatively high accuracy.

At the end, a summary of tests performed on a modified, production DI diesel engine are presented (chapter 4). Different operating points have been tested and quantities of WI going up to 4 times the mass of fuel have been used. The results have been interpreted in part with the help of the tools developed in chapter 2 (especially for the instantaneous heat release rate calculations). An analysis of the experimental results has given us new information on the influence of presence of water in the intake charge on the NOx and PM emissions, on combustion (ignition delay, and instantaneous heat release), as well as the heat transfer to the cylinder walls, the bulk temperature and the gas temperature in the cylinder, the specific fuel consumption, and to a lesser extent, the CO emissions and exhaust gas temperatures. Finally, the exhaust gas recirculation (low pressure EGR) in parallel with WI allows us to drastically reduce the emissions of NOx, while keeping the PM emissions in check (in comparison to EGR only for the same NOx emissions), showing that an intake WI system may be practically viable for the reduction of engine-out NOx emissions.

The presented work shows several paths for further research:

- ✓ *From an understanding point of view, a few questions are left unanswered, for example, what are the chemical effects of WI on the production of particulate matter (production and partial oxidation in the combustion chamber)?*
- ✓ *It would be equally interesting to perform local measures (on an optically-accessible engine or via endoscopy on a production engine) so as to collect information on the effects of water on combustion (lift-off length and associated equivalence ratio, temperature of the flame core etc.)*

- ✓ *It would be additionally interesting to test other modes of water injection, notably as an emulsion with the injected fuel, with the aim to simultaneously reduce the NOx and PM emissions*
- ✓ *From an industrial standpoint, it seems interesting:*
  - *To study the effects of WI on the reliability (problems of corrosion in the intake after the point of WI, problems linked to the exhaust due to condensation, cold starting, contamination of oil in the sump from the engine cylinders etc.)*
  - *For automotive use, it seems to be difficult to imagine an "open" WI system. The reason being that to achieve low levels of NOx, it is shown that the ratio of water to fuel is very often above 1, that is to say, more water is injected than fuel. One way to work around this problem would be to use WI in conjunction with EGR as shown at the end of chapter 4. Another means would be to develop a system to condense the water vapour present in the tailpipe and re-inject it into the engine (closed circuit).*
  - *If we condense water at the exhaust, the heat that is needed to be removed from the exhaust gases could potentially be used to drive a bottoming-cycle power generation system for generation of auxiliary electricity (based on the Rankine or HIM combined cycle), to reduce fuel consumption and increase global efficiency for both automotive and stationary power generation purposes.*

L'étude bibliographique (chapitre 1) a fourni une synthèse des principales connaissances à ce jour sur le déroulement de la combustion Diesel à injection directe et sur la formation des émissions polluantes (NOx et particules). Elle a exposé de manière détaillée les différentes techniques d'injection d'eau, ainsi que leurs effets sur la combustion et les émissions polluantes. Des résultats parfois différents ont été observés par les différents auteurs, d'un point de vue quantitatif (niveau d'eau requis pour avoir une réduction donnée des émissions de NOx) et parfois même qualitatif (baisse des particules observée par certains auteurs, hausse observée par d'autres).

Dans un second chapitre, les principaux outils expérimentaux ont été présentés (moteur Diesel utilisé, système d'injection d'eau développé spécifiquement pour cette étude, appareils de mesure et incertitudes associées) et des outils numériques d'analyse ont été développés. Ceux-ci permettent d'analyser différentes situations thermodynamiques après injection de l'eau sous forme liquide dans l'air d'admission : évaporation dans le répartiteur d'admission ou évaporation dans les cylindres pendant la phase d'admission (système ouvert), évaporation après la fin de l'admission pendant la compression (système fermé).

Les outils numériques développés au chapitre 2 ont ensuite été utilisés pour tenter de déterminer l'état de l'eau et la température du mélange pendant les différentes phases (mélange dans le répartiteur d'admission, admission dans les cylindres, puis compression du mélange). Une étude paramétrique a permis de montrer l'influence de la température de l'eau et des caractéristiques de l'air (température, pression, hygrométrie) avant mélange sur la quantité d'eau évaporée et sur la température finale après mélange. Outre le suivi de l'état de l'eau et des propriétés thermodynamiques du mélange air / eau liquide / eau vapeur / gaz résiduels, un calcul correct du dégagement de chaleur de combustion en présence d'eau est de sorte rendu possible.

Enfin, une synthèse des expériences menées sur moteur Diesel automobile de série modifié a été présentée (chapitre 4). Différents points de fonctionnement ont été testés et des quantités d'eau allant jusqu'à 4 fois le débit de carburant ont été injectées. Les résultats ont

été interprétés pour partie à l'aide des outils développés dans le chapitre 2 (notamment pour le calcul du dégagement instantané de chaleur). Une analyse des résultats a permis d'apporter des informations nouvelles sur l'influence de la présence d'eau dans l'air d'admission sur les émissions de NOx et de particules, la combustion (délai d'inflammation et dégagement instantané de chaleur), mais aussi sur les pertes aux parois du cylindre, la température moyenne et la pression des gaz dans la chambre de combustion, la consommation spécifique de carburant, et dans une moindre mesure sur les émissions de CO et la température des gaz d'échappement. Enfin, la recirculation de gaz d'échappement (boucle EGR basse pression) en parallèle de l'injection d'une quantité modérée d'eau a permis de réduire de manière drastique les émissions de NOx, tout en limitant la hausse des émissions de particules (par rapport à l'emploi de l'EGR seul pour un même niveau d'émissions de NOx visé), montrant un intérêt « pratique » certain pour l'injection d'eau à l'admission d'un moteur pour la maîtrise à la source de ses émissions polluantes.

Les travaux présentés ouvrent plusieurs perspectives de recherche :

- ✓ *Du point de vue de la compréhension, certaines questions restent en suspend, comme par exemple quel est l'effet chimique de l'eau sur les particules (formation et oxydation partielle dans la chambre de combustion) ?*
- ✓ *Il serait également intéressant de réaliser des mesures locales (sur moteur à accès optique ou par endoscopie sur moteur de série) afin d'apporter des informations locales quant à l'impact de la présence d'eau sur la combustion (longueur d'accroche de flamme et richesse correspondante, températures de cœur de jet et de flamme,…).*
- ✓ *Il serait en outre intéressant de tester d'autres modes d'introduction de l'eau, notamment en émulsion avec le carburant, dans un but de réduction simultané des émissions de NOx et de particules.*
- ✓ *D'un point de vue industriel, il parait intéressant :*
    - *D'étudier les aspects liés à la fiabilité (problèmes de corrosion à l'admission en aval de l'injection d'eau, mais aussi à l'échappement en cas de condensation de l'eau par exemple lors d'un démarrage à froid, problèmes de contamination de l'huile par de l'eau aux parois du cylindre,…).*
    - *En automobile, il paraît difficilement envisageable d'utiliser de l'eau en système ouvert car le débit d'eau nécessaire pour atteindre de faibles niveaux d'émissions de NOx est important (supérieur au débit de carburant). Une alternative serait d'utiliser des quantités « raisonnables » d'eau en parallèle de l'EGR, comme cela a été montré à la fin du chapitre 4, ou bien d'utiliser un système de condensation de l'eau au niveau des gaz d'échappement et réutiliser cette eau, après traitement (système fermé).*
    - *La condensation de l'eau nécessitant l'abaissement de la température des gaz d'échappement, il parait possible de coupler ce système avec un système auxiliaire de production d'électricité utilisant une partie de la puissance thermique des gaz d'échappement (cycle combiné de type Rankine ou Hirn), dans le cadre d'une application automobile ou stationnaire, et dans le but d'augmenter le rendement global.*

References

1. Heywood, J. B., “Internal Combustion Engine Fundamentals”, McGraw-Hill Book Company, 1988
2. Lilly, L. R. C., “Diesel Engine Reference Book”, Butterworth and Co Publichers Ltd., 1986
3. Hountalas, D.T., Mavropoulos, G.C., Zannis, T.C., Mamalis S.D., “Use of water emulsion and intake water injection as NOx reduction techniques for heavy-duty diesel engines”, SAE paper 2006-01-1414, 2006
4. Health Aspects of Air Pollution with Particulate Matter, Ozone and Nitrogen Dioxide (13-15 January 2003), Report on a WHO Working Group, Bonn, Germany
5. Flynn, P. F., Durrett, R. P., Hunter, G. L., zur Loye, A. O., Akinyemi, O. C., Dec, J. E., Westbrook, C. K., “Diesel Combustion: An integrated view combining, Laser diagnostics, chemical kinetics, and empirical validation”, SAE Paper 1999-01-0509, 1999
6. Dec, J. E., “Diesel Combustion And Emissions Formation Using Multiple 2-D Imaging Diagnostics”, Diesel Engine Emissions Reduction (DEER) proceedings, 1997
7. Siebers, D. L., “Scaling Liquid-Phase Fuel Penetration in Diesel Sprays Based on Mixing-Limited Vaporization”, SAE Paper 1999-01-0528, 1999
8. Tree, D. L., Svensson, K. I., “Soot processes in Compression Ignition engines”, Elsevier Sciencedirect Progress in Energy and Combustion Science, 2006.
9. Siebers, D. L., Pickett, L. M., “Soot in diesel fuel jets: effects of ambient temperature, ambient density and injection pressure”, Elsevier Sciencedirect Combustion and Flame, 2004.
10. Higgins, B. S., Mueller, C. J., Siebers, D. L., “Measurement of fuel effects on liquid-phase penetration in DI sprays”, SAE Paper 1999-01-0519, 1999
11. Pickett, L. M., Idicheria, C. A., “Effect of EGR on diesel premixed-burn equivalent ratio”, Elsevier Sciencedirect Proceedings of the Combustion Institute, 2007
12. Maiboom, A., “Etude experimentale et modelisation phenomenologique de l’influence des caracteristiques thermodynamiques et de la composition des gaz d’admission sur la combustion et les emissions d’un moteur diesel automobile”, Ecole Centrale de Nantes, 2007
13. Mellor, A. M., Mello, J. P., Duffy, K. P., Easley, W. L., Faulkner, J. C., “Skeletal Mechanism for NOx chemistry in diesel engines”, SAE Paper 981450, 1998
14. Guillet, R. “Du diagramme hygrométrique de combustion aux pompes à vapeur d’eau”, Elsevier 1998
15. “Systematic Method for selecting the most effective nonionic emulsifier(s) for any given application”, Uniqema Ltd, 2005
16. Park, J. W., Huh, K. Y., Park, K. H., “Experimental study on the combustion characteristics of emulsified diesel in a RCEM”, FISITA World Automotive Congress - F2000A073, 2000
17. Ehrström, M., “Wärtsilä 50DF LNG FSRU power plant exhaust gas emissions”, Wartsila, 2006
18. “NOx EMISSION STUDY: An investigation of water-based emission control technologies”, Fleetway Inc., 2005
19. “Medium speed SFOC-Emissions trade off”, MAN, 2007
20. Wirbeleit, F., Enderle, C., Lehner, W., Raab, A., Binder, K., “Stratified diesel fuel-water-diesel fuel injection combined with EGR – the most efficient in-cylinder NOx and PM reduction strategy”, SAE paper 972962, 1997
21. Jung, D., Assanis, D. N., “Multi-zone DI diesel spray combustion model for cycle simulation studies of engine performance and emissions”, SAE paper 2001-01-1246, 2001
22. Ladommatos, N., Abdelhalim, S. M., Zhao, H., Hu, Z., “The dilution, chemical and thermal effects of Exhaust Gas Recirculation on Diesel Engine emissions – Part 4: Effects of Carbon Dioxide and Water Vapour”, SAE paper 971660, 1997
23. Lif, A., Holmberg K., “Water-in-diesel emulsions and related systems”, Advances in Colloid and Interface Science - Elsevier, 123-126 (2006), 231-239,, 2006
24. Dickey, D.W., Ryan, T.W. III, Matheaus A.C., “NOx Control in Heavy-Duty diesel engines – What is the limit?”, SAE paper 980174, 1998
25. Roberts, C.E., Naegeli, D., Chadwell, C., “The effect of water on soot formation”, SAE paper 2005-01-3850, 2005
26. Samec, N., Dibble, R.W, Chen, J.H., Pagon, A. “Reduction of NOx and Soot Emission by Water Injection During combustion in a diesel engine”, FISITA Automotive Congress paper F2000A075, 2000
27. Nazha, M.A.A., Rajukaruna, H., Wagstaff S.A., “The use of emulsion, water induction and EGR for controlling diesel engine emissions”, SAE paper 2001-01-1941, 2001

28. Lanzafame, R., “Water injection effects in a single-cylindre CFR engine”, SAE paper 1999-01-0568, 1999
29. Brusca, S., Lanzafame, R., “Evaluation of the effects of water injection in a single cylinder CFR Cetane engine”, SAE paper 2001-01-2012, 2001
30. Tanner, F.X., Brunner, M., Weisser, G., “A computational investigation of water injection strategies for Nitric Oxide reduction in large-bore diesel engines”, SAE paper 2001-01-1069, 2001
31. Kegl, B., Pehan, S., “Reduction of diesel engine emissions by water injection”, SAE paper 2001-01-3259, 2001
32. Hountalas, D.T., Mavropoulos, G.C., Zannis, T.C., “Comparative evaluation of EGR, Intake Water and Fuel/Water Emulsion as NOx Reduction Techniques for diesel engines”, SAE paper 2007-01-0120, 2007
33. Chadwell, C.J., Dingle, P. J. G., “Effect of diesel and water co-injection with real-time control on diesel engine performance and emissions”, SAE paper 2008-01-1190, 2008
34. Matheaus, A.C., Ryan, T.W., Saly, D., Langer, D.A., Musculus M.P.B., “Effects of PuriNOx™ water-diesel fuel emulsions on emissions and fuel economy in a heavy-duty diesel engine”, SAE paper 2002-01-2891, 2002
35. Selim, M.Y.E., Ghannam, M.T., “Performance and engine roughness of a diesel engine running on stabilised water diesel emulsion”, SAE paper 2007-24-0132, 2007
36. Chen, A.G., Maloney, D.J., Day, W.H., “Humid air NOx reduction effect on liquid fuel combustion”, Journal of Engineering for gas Turbines and Power, ASME, Vol. 126, 69 – 74, 2004
37. Bhargava, A., Colket, M., Sowa, W., “An experimental and modelling study of humid air premixed flames”, Journal of Engineering for gas Turbines and Power, ASME, Vol. 122, 405 – 411, 2000
38. Ishida, M., Ueki, H., Sakaguchi, D., “Prediction of NOx reduction rate due to port water injection in a DI diesel engine”, SAE paper 972961, 1997
39. Velji, A., Remmels, W., Schmidt, R.M., “Water to reduce NOx emissions in diesel engines – A basic study, MTU – Germany
40. Jacobs, T.J., Assanis, D.N., “The attainment of premixed compression ignition low-temperature combustion in a compression ignition direct injection engine”, Elsevier, Proceedings of the Combustion Institute, doi: 10.1016/j.proci.2006.08.113, 2007
41. Genzale, C.L., Reitz, R.D., Musculus M.P.B., “Effects of spray targeting on mixture development and emissions formation in late-injection low-temperature heavy-duty diesel combustion”, Elsevier, Proceedings of the Combustion Institute, doi: 10.1016/j.proci.2008.06.072, 2009
42. Marine Vessel exhaust emissions – Phase II (1998-99) prepared for Transportation Development Centre, Transport Canada 999 Emissions research and Measurement Division Environment Canada
43. Imahashi, T., Hashimoto, K., Hayashi, J.I., Yamada, T. “Research on Nox Reduction for Large Marine Diesel Engines”, ISME Yokohama 1995
44. Srinivasan, R., “Research on exhaust emissions reduction technologies from large marine diesel engines”, Matson Navigation Company Inc.
45. Lövblad, G., Profu, E.F., “Experiences from use of some techniques to reduce emissions from ships”, IVL, Swedish Maritime Administration and the Region Västra Götaland Sweden 2006
46. DeMers, D., Walters, G., “BAE SYSTEMS Guide to Exhaust Emission Control Options” CIMAC Committee, 1999
47. Maiboom, A. Tauzia, X., Hétet, J.F., “Experimental study of various effects of exhaust gas recirculation (EGR) on combustion and emissions of an automotive direct injection diesel engine”, Energy, Vol. 33, 22-34, 2008.
48. Maiboom, A., Tauzia, X., Hétet, J.F., “Influence of high rates of supplemental cooled EGR on NOx and PM emissions of an automotive HSDI diesel engine using an LP EGR loop”, International Journal of Energy Research, 2008.
49. Matsuo O., Noriyuki K., Yujiro T., Kazuyuki N., Koichi Y., “Effects of EGR with a supplemental manifold Water Injection to control exhaust emissions from heavy-Duty Diesel powered vehicles” SAE paper 910739, 1991
50. Zhao, D., Yamashita, H., Kitagawa, K., Arai, N., Furuhata, T., “Behaviour and effect on NOx formation of OH radical in Methane-Air diffusion flame with steam addition”, 130:352-360, Elsevier Sciencedirect Proceedings of the Combustion Institute, 2002
51. Ghojel, J., Honnery, D., Al-Khaleefi, K., “Performance, emissions and heat release characteristics of direct injection diesel engine operating on diesel oil emulsion”, Elsevier ScienceDirect Applied Thermal Engineering, 2006

52. Bertola, A., Li, X., Boulouchos, K., “Influence of Water-Diesel Fuel Emulsions and EGR on Combustion and Exhaust Emissions of Heavy-Duty DI-Diesel Engines equipped with Common-Rail Injection Systems”, SAE paper 2003-01-3146, 2003
53. Musculus, M. P. B., Dec, J.E., Tree, D. R., Daly D., Langer, D., Ryan T. W., Matheaus, A. C., “Effects of Water-Fuel Emulsions on Spray and Combustion Processes in a Heavy-Duty DI Diesel Engine”, SAE paper 2002-01-2892, 2002
54. Giansetti, P., “Contrôle moteur à allumage commandé – estimation / prédiction de la masse et de la composition du mélange enfermé dans le cylinder”, PhD Thesis Université d’Orleans, 2005.
55. Senecal, P. K., Xin, J., Reitz, R. D., “Predictions of Residual Gas Fraction in IC Engines”, SAE Technical Paper Series 962052, 1996.
56. Fox, J. W., Cheng, W. K., Heywood, J. B., “A model for predicting residual gas fration in Spark-Ignition engines”, SAE Technical Paper Series 931025, 1993.
57. Giansetti, P., Perrier, C., Higelin, P., Chamaillard, Y., Charlet, A., Couet, S., “A model for residual gas fraction prediction in Spark Ignition engines”, SAE Technical Paper Series 2002-01-1735, 2002
58. Hohenberg, J. F., “Advanced approaches for heat transfer calculations”, SAE Paper 790825, 1979.
59. Musculus, M. P. B., “On the correlation between NOx emissions and the Diesel premixed burn”, SAE paper 2004-01-1401, 2004
60. Siebers, D. L., Higgins, B, Pickett, L. M., “Flame lift-off on direct-injection diesel fuel jets: oxygen concentration effects”, SAE paper 2002-01-0890, 2002.
61. Pickett LM, Siebers DL. Non-sooting, low-flame temperature mixing controlled DI diesel combustion. SAE paper 2004-01-1399, 2004.
62. Maiboom, A., Tauzia, X., Shah S. R., Hétet, J. F., “New phenomenological six-zone combustion model for direct-injection diesel engines”, Energy and Fuels 2009;23:690e703.
63. Dec, J. E., “A conceptual model of DI diesel combustion based on laser-sheet imaging” SAE paper 970873, 1997.
64. Lif, A., Skoglundh, M., Gjirja, S., Denbratt, I., “Reduction of soot emissions from a direct injection diesel engine using water-in-diesel emulsion and microemulsion fuels” SAE paper no. 2007-01-1076, 2007.
65. Ladommatos, N., Abdelhalim, S. M., Zhao, H., Hu, Z., “Effects of EGR on heat release in diesel combustion”, SAE paper no. 980184, 1998.
66. Maiboom, A., Tauzia, X., Shah, S.R., Hétet, J.-F.,“Experimental study of an LP EGR System on an Automotive Diesel Engine, compared to HP EGR with respect to PM and NOx Emissions and Specific Fuel Consumption” SAE International journal of engines, 2010, Volume 2 (2), pp. 597-610
67. Tauzia, X., Maiboom, A., Shah, S.R., “Experimental study of inlet manifold water injection on combustion and emissions of an automotive direct injection Diesel engine”, Energy 2010;35(9):3628-3639.
68. Shah, S.R., Maiboom, A., Tauzia, X., Hétet, J.-F., “Experimental study of Inlet Manifold Water Injection on a Common Rail HSDI automobile Diesel Engine, compared to EGR with respect to PM and NOx Emissions and Specific Consumption”, SAE paper in SP-2243, SAE international publisher, april 2009.

Web references:

69. http://www.greencarcongress.com/2008/02/european-automo.html
70. www.geajet.com
71. http://www.bewdleytech.eu/download/pressione.pdf
72. http://www.bewdleytech.eu/download/temperatura.pdf
73. http://energy.sdsu.edu/testcenter/testhome/index.html

Résumé

La réduction des émissions polluantes des moteurs Diesel automobile est devenue un enjeu majeur ces dernières années. Le post-traitement des NOx restant complexe et onéreux, la réduction à la source est intéressante. Pour ce faire, il existe certaines techniques classiques comme la recirculation des gaz d'échappement refroidis (EGR). L'objectif de cette thèse est d'évaluer le potentiel de l'injection d'eau à l'admission du moteur, qui est utilisée sur certain moteurs Diesel industriels.
Une étude bibliographique est tout d'abord menée. Après avoir brièvement rappelé l'état de l'art sur la compréhension de la combustion Diesel et des émissions polluantes qui s'y rattachent, une analyse détaillée des travaux précédents est présentée. Les différentes techniques d'injection d'eau sont décrites et comparées, notamment du point de vue de leurs effets sur la combustion et les émissions polluantes.
Le dispositif expérimental est ensuite présenté, en particulier le moteur utilisé, le système d'injection d'eau mis en place avec les différentes étapes de son développement et principaux systèmes de mesure et d'acquisition.
Les équations de thermodynamique régissant le mélange de l'eau liquide avec l'air d'admission puis son éventuelle évaporation sont également établies.
Elles sont alors utilisées pour évaluer en fonction des paramètres d'influence, les quantités d'eau évaporées dans le circuit d'admission du moteur et, le cas échéant, dans le cylindre, lors des phases d'admission et de compression, en particulier dans les configurations testées expérimentalement.
Finalement les résultats expérimentaux obtenus au banc d'essais moteur avec l'injection d'eau sont exposés. L'influence de l'eau et ces différents effets sur la combustion et sur les émissions polluantes sont analysés et comparés à ceux de l'EGR.

Mots-clés :
Injection d'eau, Moteur diesel, Etude Expérimentale, Combustion, Emissions polluantes

Abstract

The pollutant emission reduction of automotive Diesel engine has become a difficult challenge during the last decade. NOx after-treatment is still complex and expensive, thus in cylinder reduction remains of interest. For that purpose, there are some well established technologies, such as exhaust gas recirculation (EGR). The aim of this study is to evaluate water injection at the engine intake, which is already in use on some industrial engines.
First a bibliographic survey is presented. State of the art Diesel combustion and corresponding pollutant emissions descriptions and analyses are summarized. Previous studies on water injection are then detailed: the various techniques of water injection are described and compared, in particular, their effects on combustion and emissions.
The experimental setup is then presented. This includes the engine itself as well as the water injection system with a short history of its development to its present, stable, form. Measurement methods are also explained and detailed.
Following that, thermodynamic relations are developed to describe liquid water mixing with the intake air and its evaporation.
They are used to evaluate the quantities of vaporised water in the intake track and eventually inside the cylinder, during intake and compression strokes.
Finally, the results obtained on the engine test bench with the water injection system are presented. These results are analysed and compared to both baseline operating points and also to low-pressure exhaust gas recirculation. In light of the obtained test results, conclusions are drawn discussing the different effects of water injection on diesel engine combustion and emissions.

Keywords :
Water Injection, Diesel Engine, Experimental Study, Combustion, Pollutant Emissions

Discipline : Sciences de l'Ingénieur